



Decolorisation of Methylene Blue with Sodium Persulfate Activated with Visible Light in the Presence of Glucose and Sucrose

Zawadzki Piotr

Received: 9 October 2019 / Accepted: 5 December 2019 / Published online: 14 December 2019
© Springer Nature Switzerland AG 2019

Abstract The paper presents the results of research on the methylene blue (MB) degradation with sodium persulfate (PDS) activated with visible light (Vis) in the presence of glucose and sucrose. The following test were examined: absence and presence of sugars in concentrations of 50–300 mM, presence and absence of Vis radiation, pH of the model solution (6.0–12.0), identification of free radicals, kinetics of the pseudo-first-order reaction. The degradation of the MB ranges from 58 to 84% depending on the pH of the model solution. The highest degradation degree (about 83–84%) was observed after 90 min of visible light irradiation for the process conducted in the presence of persulfate (6.5 mM) and glucose/sucrose (100.0 mM) at pH = 12.0 (PDS-12/100G/Vis and PDS-12/100S/Vis). The mathematically calculated half-life of MB ($t/2$) has been reduced in the visible-light system irradiated from 111.8 min (PDS in pH = 6.0) to 68.0 min (PDS-6/100S/Vis) and from 58.7 min (PDS in pH = 12.0) to 36.9 min (PDS-12/100S/Vis). Decolorisation of the methylene blue takes place with the participation of three radicals: sulfate $\text{SO}_4^{\cdot-}$, hydroxyl OH^{\cdot} and superoxide $\text{O}_2^{\cdot-}$. The dominant radicals were superoxide radicals. In a slightly acidic environment (pH = 6.0), there were hydroxyl and sulfate radicals. At pH = 12, hydroxyl radicals were mainly responsible for the

degradation of methylene blue. The results of this study showed that method may be an interesting alternative for the treatment of coloured wastewater containing low dye concentrations.

Keywords Methylene blue · Sodium persulfate · Sulfate radical · Visible light · Kinetics

1 Introduction

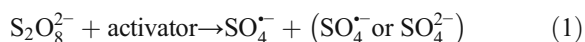
Textile industry is the main source of dyes and generates colour wastewater that can cause serious water pollution. The global production of dyes has been estimated at around 800,000 Mg/year. About 10–15% of this number is lost during various processes in the textile industry and released into the environment as sewage (Hassaan and Nemr 2017). Wastewater containing dyes violates the biological balance of waters, inhibits the processes of biochemical degradation and weakens the transmission of solar radiation. Some of them have an allergenic, mutagenic and carcinogenic effect, as harmful aromatic amines can be released under reducing conditions (Lisiak and Miklas 2007).

A large group of dyes are azo dyes. Azo dyes contain the functional group R-N=N-R' in their structure and constitute a very large group of all colouring agents used. Azo dyes are a triggering factor for histamine, which may exacerbate the symptoms of asthma, as well as cause uterine contractions in pregnant women, resulting in miscarriage. Additionally, in combination

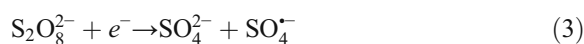
Z. Piotr (✉)
Department of Water Protection, Central Mining Institute, Plac
Gwarków 1, 40-166 Katowice, Poland
e-mail: pzawadzki@gig.eu

with benzoates, they can cause hyperactivity in children. Even for non-allergic persons, they may be the cause of, for example, urticaria (Lisiak and Miklas 2007). This group of dyes includes, for example, methylene blue (MB). Methylene blue is a thiazine dye containing in its molecule a six-membered heterocyclic ring with a sulphur and nitrogen atom (phenothiazine ring). It belongs to the group of cationic dyes. Methylene blue is widely used in the textile, paper, cosmetics, plastics and food industries. Due to the potential hazards for people and high resistance to biodegradation, there is a need to develop technologies for the elimination of methylene blue from water and sewage. The removal of dyes by conventional processes, e.g. activated sludge, does not bring the expected results. Due to low biodegradability, almost 90% of the dyes present in wastewater are not removed in conventional purification processes. Therefore, the degradation of dyes from sewage has aroused considerable interest from researchers around the world. Various physicochemical methods, such as adsorption, precipitation, filtration, ion exchange, electrolysis and advanced oxidation processes, are used for the treatment of colour sewage (Deng and Zhao 2015).

Of all purification methods, advanced oxidation processes (AOPs) seem to be the most promising technology for removing various toxic chemicals from water and wastewater. The common feature of AOPs is the oxidation of organic compounds by producing highly reactive, non-selective, hydroxyl OH^\bullet ($E^0 = 2.80$ V) or sulfate $\text{SO}_4^{\bullet-}$ ($E^0 = 2.70$ V) radicals characterized by high oxidation potential (Herrmann 2005; Ebersson 1987). Currently, more and more papers are devoted to the use of sodium or potassium persulfate to remove organic compounds from water and sewage. Persulfate reacts directly with certain organic compounds, forming sulfate radicals according to the general reaction mechanism (Eq. 1):



The energy transmitted to the persulfate anion by UV light, ultrasound or heat causes the splitting of the peroxide bond and the formation of two sulfate radicals (Eq. 2) (Waldemer et al. 2007). Persulfate can also react with an electron donor from the transition metal to form a single sulfate radical (Eq. 3) (Anipsitakis and Dionysiou 2004).



In order to generate sulfate radicals, persulfate is often subjected to an activation process. Without activation, the persulfate anion will only react with some organic chemicals. The degree of removal of impurities is then smaller than that obtained with the activated persulfate due to the lower oxidation potential of the persulfate anion ($E_0 = 2.01$ V) (Liu et al. 2012). In the presence of an activator, as a result of the reaction of formation of sulfate radicals, effective mineralisation of organic compounds takes place, even to CO_2 and water.

Activation can be achieved by thermal action (Ji et al. 2016; Ahmadi with Ahmadi et al. 2019), photolytic (Zhang with Zhang et al. 2015), sonolytic (Chen 2012) and radiolytic activation (Criquet et al. 2011), as well as by PDS and PMS reactions with magnetic composites of iron oxide (14). The transfer of high-temperature or radiolytic techniques on a technical scale is difficult; therefore, the most common method of activating persulfates is the use of transition metal ions at low oxidation levels, such as Fe^{2+} , Ni^{2+} , Co^{2+} and Ag^+ . Current publications also include laboratory experiments on the development of new methods for the activation of persulfate. Among these techniques, one can distinguish activation at high pH (> 11.0), electrolysis, the use of carbon nanotubes or polymers (polyimides) and ozone. However, there are few papers on the activation of persulfates with visible light (Wang et al. 2019; Watts et al. 2018).

One of the basic catalysts used for the activation of persulfates are transition metal ions at low oxidation levels, such as Fe^{2+} , Ni^{2+} , Co^{2+} and Ag^+ . The price of chemical compounds containing the above metals in their structure (e.g. $\text{FeSO}_4 \times 7\text{H}_2\text{O}$ or $\text{CoSO}_4 \times 7\text{H}_2\text{O}$) is about 11 USD/kg. Currently, materials are sought for, in the presence of which PDS activation is cheaper, yet equally effective. In addition, combinations of methods that will enable the activation of PDS under the influence of visible light are sought. Such materials may be, for example: acids and sugars (Wang et al. 2019; Watts et al. 2018; Ocampo 2009). The price of glucose and sucrose is about 7 USD/kg. Reagent prices were estimated based on www1 2019. The literature review demonstrates that the decontamination process conducted in the presence of PDS is an efficient and effective method of pollutant degradation but expensive chemical

reagents or energy-consuming UV lamps are required. The novelty of the presented study, in comparison with other methods described in the literature, is the possibility of PDS activation with use of non-toxic, pro-environmental reagents (glucose, sucrose) and low-cost solar energy (Vis) with higher process efficiency.

The aim of this study was to perform the degradation of methylene blue using sodium persulfate (PDS) in the presence of glucose and sucrose activated with visible light. The influence of process time, initial pH, dose of oxidants and activators was determined. The radicals participating in the reaction were also identified, and the kinetics of the dye decomposition was analysed based on the pseudo-first-order reaction equation.

2 Materials and Research Methodology

2.1 Materials

Methylene blue with a purity of $\geq 97.0\%$ was obtained from Sigma-Aldrich (Poznań, Poland). The physical and chemical characteristics of the dye are presented in Table 1. The other reagents used during the study came from Avantor Performance Materials Poland S.A. (Gliwice, Poland).

The subject of the research was model solutions prepared on the basis of deionised water with the addition of MB. Methylene blue was introduced into distilled water in the form in which it was supplied. The initial dye concentration for all experiments was in milligrammes per litre. The pH of the model solution before and after the introduction of dye solution was 6.0. Since the pH of the solution is one of the key parameters affecting the oxidation of organic pollutants with $\text{SO}_4^{\cdot-}$ radicals in wastewater or natural water, the study also examined the effect of the initial pH of the solution on

the efficiency of methylene blue degradation. The following pH values were tested: pH = 6.0, pH = 9.0 and pH = 12.0. The pH was corrected with 0.1 mol/L HCl or 0.2 mol/L NaOH from Sigma-Aldrich. The pH of the solution was monitored using a CPC-511 pH metre from Elmetron (Zabrze, Poland).

2.2 Research Methodology

The UV-Vis absorption spectra of methylene blue were tested using a Jasco V-750 spectrophotometer from Jasco in the range from 200 to 700 nm. Figure 1 shows the obtained absorption spectra of methylene blue. The spectra are characterized with three bands: two in the ultraviolet UV range ($\lambda_{\text{max}} = 248.0$ nm and $\lambda_{\text{max}} = 292.0$ nm) and one in the area of visible light Vis ($\lambda_{\text{max}} = 665.0$ nm). In the present study, the range of visible light is the visible light area at $\lambda_{\text{max}} = 665.0$ nm.

The process of methylene blue degradation was carried out in glass reaction vessels containing 100 cm³ of dye at a concentration of 2.0 mg/L. The application of this described method of decolorisation of coloured wastewater containing methylene blue is recommended for the tertiary treatment of wastewater containing low concentration of MB in the range of 1.0–4.0 mg/L (average value about 2.0 mg/L), which treatment in conventional treatment systems has poor effect. The dye concentration was also chosen to avoid the necessity of diluting the sample (which was necessary as part of preliminary tests at higher dye concentrations) in order to maintain the reliability of the results.

The reaction vessels were placed on a magnetic stirrer for proper mixing. Dye degradation was carried out at room temperature (298.0 K) and at atmospheric pressure (1013.0 hPa). An aqueous MB solution with a

Table 1 Physico-chemical characteristics of methylene blue

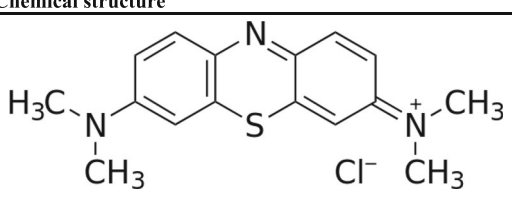
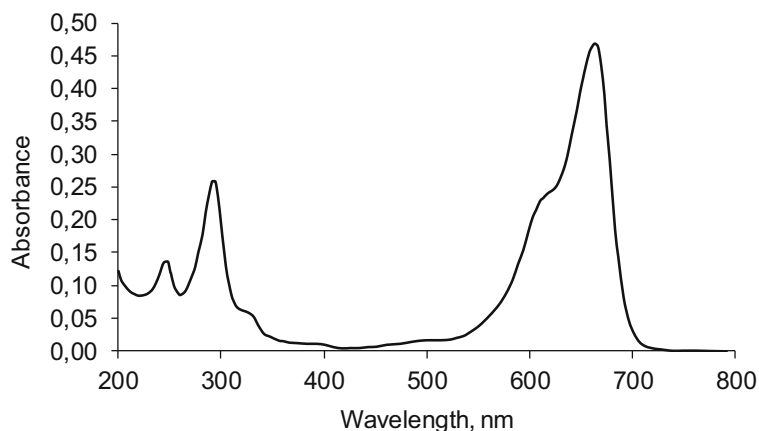
Chemical structure	Physico-chemical properties	
	Molecular formula	C ₁₆ H ₁₈ ClN ₃ S
	Molecular weight [g/mol]	319.85
	Nr CAS	61-73-4
	Water solubility at 25°C [mg/L]	43600.0
	Vapor pressure at 25°C [mmHg]	7.0 × 10 ⁻⁷
	Dissociation constant (pKa) [-]	3.14
	logK _{ow} [-]	5.85
	λ_{max} [nm]	665.0

Fig. 1 Absorption spectra of methylene blue (2.0 mg/L)



concentration of 2.0 mg/L and a set reaction (pH = 6.0, pH = 9.0 and pH = 12.0) containing 6.5 mM $\text{Na}_2\text{S}_2\text{O}_8$ was irradiated with a 10-W tungsten lamp QTH10/M from Thorlabs Inc. (NJ, USA). The lamp emits radiation with a wavelength from $\lambda = 400$ to 2200 nm. For the purposes of the research, the FGS900M filter was used to cut off radiation spectrum bands above 710 nm (Fig. 2). The filter was mounted using a Thorlabs Inc. circular cage system. The lamp emitted radiation from the visible light range. The lamp was placed over the reaction vessel (Fig. 3).

An attempt was made to activate the catalysts by means of Vis radiation in the presence of glucose and sucrose. Variable molar activator concentrations (50.0, 100.0 and 300.0 mM) were used to assess the effect of their different concentrations. The sugar concentration used was several thousand times lower than the lowest literature concentration producing effects (EC_{50}) relative to aquatic plants (algae). The EC_{50} of glucose and

sucrose for algae is $1.9\text{E} + 006$ mg/L (96 h) and $6.02\text{E} + 007$ mg/L, respectively (DHI and PKT Ltd. 2008). All experiments were carried out independently in triplicate. The data presented in the subsequent charts include average values. The degree of MB removal was calculated on the basis of Eq. 4. It takes into account the initial concentration of the impurity and the concentration determined during spectrophotometric analysis. In this way, the dye decomposition during the process was calculated.

$$R(\%) = (C_0 - C_t) / C_0 \times 100 \quad (4)$$

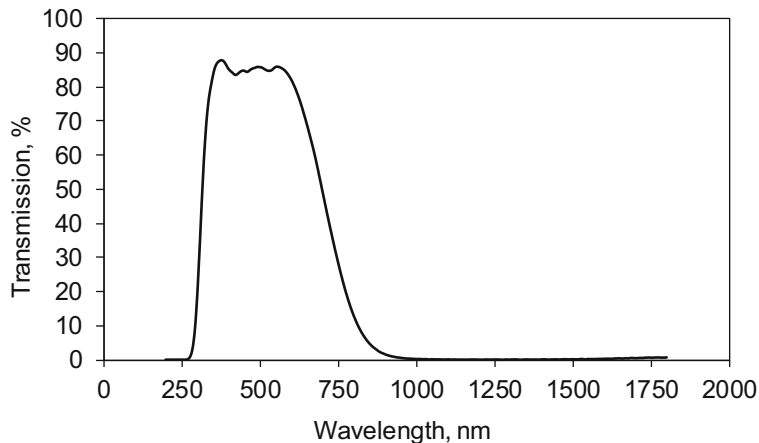
where:

C_t —concentration of the pollutant during time t (mg/L)

C_0 —initial concentration of the pollutant (mg/L)

R —pollution removal rate [%]

Fig. 2 Transmission of FGS900M filter. Source: www2019



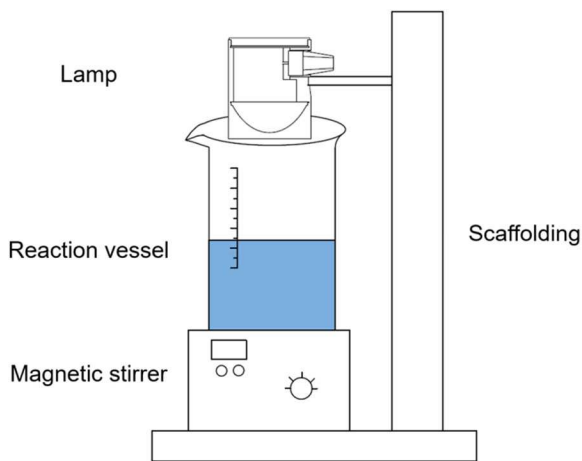


Fig. 3 Test stand for dye degradation subjected to visible light. Own study

The radical scavenger test was used to determine the major radical types involved in dye degradation. The scavengers capture the free radicals present in the mixture and deactivate them, preventing them from reacting with the compounds present in water. The research procedure was carried out similarly to previous studies. Hydroquinone (superoxide radical scavenger), tert-butyl alcohol (hydroxyl radical scavenger) and methanol (hydroxyl and sulfate radical scavenger) were added to the tested samples before the introduction of PDS and/or sugars. Scavengers were always used at the concentration $D_{\text{scav.}} = 50.0 \mu\text{M}$.

Researchers indicate that pseudo-first-order reaction equations of the azo dyes can be used to describe the decolorisation kinetics of most azo dyes (Melgoza et al. 2009; Nunez et al. 2007). The integral form of the pseudo-first-order reaction equation was determined by means of Eq. 6:

$$-\ln\left(\frac{C}{C_0}\right) = kt \quad (5)$$

where:

C_0 —concentration of dye solution before the purification process (mg/L)

C —concentration of dye solution after the purification process (mg/L)

k —reaction rate constant

t —reaction time (min)

Determining the reaction rate constant k makes it possible to calculate the half-life of substrates $t/2$, which is described by Eq. 7:

$$t/2 = \ln(2)/k \quad (6)$$

3 Results of the Research and Discussion

3.1 Choice of Optimum PDS Modification

The first stage of the study was to determine the effect of glucose and sucrose on the degradation of methylene blue without the participation of sodium persulfate. This aim of this stage was to verify whether the addition of sugars does not cause dye degradation. Three different sugar concentrations were tested: from 50.0 to 300.0 mM. The symbols used in the description of the charts along with their explanations are summarised in Table 2. As shown in Fig. 4, running the process in the presence of glucose (a) and sucrose (b) without Vis radiation did not significantly affect MB decolorisation. It was found that after 90 min of the process, the dye decomposition was less than 1%. Regardless of the molar concentration added to the model solution, the dye decomposition was negligible. Also, the sole irradiation of the dye solution with visible light during the period of time tested did not cause degradation of the subjective compound. This is due to the long half-life of the compound in the aquatic environment, which is approximately 24 h (www3 2019).

In model solutions containing the sugars tested and additionally irradiated with visible light, the dye concentration was reduced by 2.0% in the presence of glucose and by 5.0% in the presence of sucrose. The reduction in MB concentration in this case is not significant; however, the reason for this may be, for example, the physical properties of glucose and sucrose. These compounds belong to optically active substances, i.e. they tend to rotate the light plane, which may explain their activity in visible light and low dye decomposition. In the case of glucose, which has two anomers: α and β , the rotation of the α anomer is $+112.0^\circ$, while the β anomer it is $+19.0^\circ$. In turn, the sucrose rotation is $+66.5^\circ$. Higher MB degradation in the presence of sucrose can be attributed to the action of both this sugar and glucose, which is one of the degradation products of

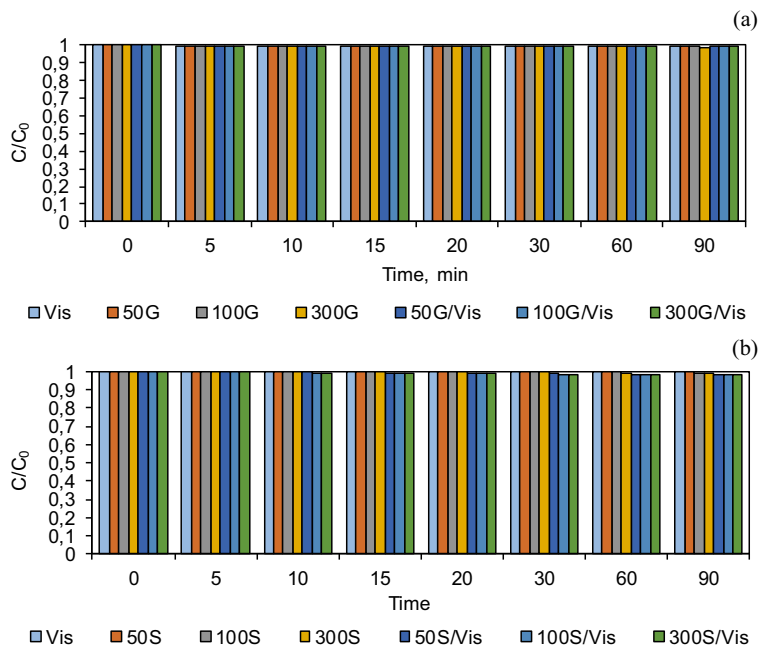
Table 2 Symbols used in tests

Name	Symbol	Name	Symbol
Na ₂ S ₂ O ₈ in pH = 6.0	PDS-6	Na ₂ S ₂ O ₈ + 300 mM glucose	PDS/300G
Na ₂ S ₂ O ₈ in pH = 9.0	PDS-9	Na ₂ S ₂ O ₈ + 300 mM glucose + Vis	PDS/300G/Vis
Na ₂ S ₂ O ₈ in pH = 12.0	PDS-12	Na ₂ S ₂ O ₈ + 50 mM sucrose	PDS/50S
Na ₂ S ₂ O ₈ + Vis	PDS/Vis	Na ₂ S ₂ O ₈ + 50 mM sucrose + Vis	PDS/50S/Vis
50 mM glucose	50G	Na ₂ S ₂ O ₈ + 100 mM sucrose	PDS/100S
100 mM glucose	100G	Na ₂ S ₂ O ₈ + 100 mM sucrose + Vis	PDS/100S/Vis
300 mM glucose	300G	Na ₂ S ₂ O ₈ + 300 mM sucrose	PDS/300S
50 mM sucrose	50S	Na ₂ S ₂ O ₈ + 100 mM glucose in pH = 6.0	PDS-6/100G
100 mM sucrose	100S	Na ₂ S ₂ O ₈ + 100 mM glucose + Vis in pH = 6.0	PDS-6/100G/Vis
300 mM sucrose	300S	Na ₂ S ₂ O ₈ + 100 mM glucose in pH = 9.0	PDS-9/100G
50 mM glucose + Vis	50G/Vis	Na ₂ S ₂ O ₈ + 100 mM glucose + Vis in pH = 9.0	PDS-9/100G/Vis
100 mM glucose + Vis	100G/Vis	Na ₂ S ₂ O ₈ + 100 mM glucose in pH = 12.0	PDS-12/100G
300 mM glucose + Vis	300G/Vis	Na ₂ S ₂ O ₈ + 100 mM glucose + Vis in pH = 12.0	PDS-12/100G/Vis
50 mM sucrose + Vis	50S/Vis	Na ₂ S ₂ O ₈ + 100 mM sucrose in pH = 6.0	PDS-6/100G
100 mM sucrose + Vis	100S/Vis	Na ₂ S ₂ O ₈ + 100 mM sucrose + Vis in pH = 6.0	PDS-6/100G/Vis
300 mM sucrose + Vis	300S/Vis	Na ₂ S ₂ O ₈ + 100 mM sucrose in pH = 9.0	PDS-9/100G
Na ₂ S ₂ O ₈ + 50 mM glucose	PDS/50G	Na ₂ S ₂ O ₈ + 100 mM sucrose + Vis in pH = 9.0	PDS-9/100G/Vis
Na ₂ S ₂ O ₈ + 50 mM glucose + Vis	PDS/50G/Vis	Na ₂ S ₂ O ₈ + 100 mM sucrose in pH = 12.0	PDS-12/100G
Na ₂ S ₂ O ₈ + 100 mM glucose	PDS/100G	Na ₂ S ₂ O ₈ + 100 mM sucrose + Vis in pH = 12.0	PDS-12/100G/Vis
Na ₂ S ₂ O ₈ + 100 mM glucose + Vis	PDS/100G/Vis		

sucrose hydrolysis. Since the hydrolysis of sucrose occurs in an acidic environment, and the pH of the model solution under the tested conditions was pH = 6.0, the

amount of probably generated glucose was so low that MB degradation occurred, but to a very low degree (Clayden et al. 2012; www4 2019; www5 2019).

Fig. 4 The effect of **a** glucose and **b** sucrose on MB (C/C_0) decomposition as a function of time. Decomposition conditions $C_0 = 2.0$ mg/L; $V = 100.0$ cm³; $T = 298.0$ K; pH = 6.0; $t = 0 - 90$ min; molar concentration Na₂S₂O₈ = 0.0 mmol



In the next step, the possibility of PDS activation with glucose and sucrose with and without Vis radiation was investigated. The baseline values against which the effect of sugars were compared was the final MB decomposition in the PDS and PDS/Vis systems (Fig. 5).

It was observed that the decomposition of methylene blue is possible after the addition of $\text{Na}_2\text{S}_2\text{O}_8$ without the addition of catalysts. The degree of dye removal after 90 min of the decolorisation process was determined to be at 44.0%. Possible degradation of impurities, including methylene blue in the PDS system without the use of catalysts is not a novelty (Ahmadi et al. 2019; Hung et al. 2016). It results from the fact that as a result of the decomposition of PDS without the addition of catalysts, radicals can be generated, while the degree of removal of organic impurities without the participation of commonly used catalysts is lower.

Figures 5a and 6a illustrate the impact of process time depending on the different molar concentrations of sugars tested. In general, the effect of reaction time on the degree of dye decolorisation was observed.

Considering all systems, for example after 5 min of reaction time, MB decomposition ranged from 10 to 22%, while after 30 min, its decomposition rate ranged from 27 to 43%. In turn, extending the reaction time to 90 min resulted in a reduction of the initial dye concentration by up to 65% and 58%. This effect was obtained in the PDS/100G/Vis and PDS/100S/Vis systems. The effect of irradiation of the PDS-containing reaction mixture in the presence of glucose and sucrose was also observed by analysing the kinetics of dye decomposition (Fig. 5b and Table 3). Compared with the PDS system ($k = 0.0062 \text{ min}^{-1}$, $t_{1/2} = 111.8 \text{ min}$), the reaction rate constant in the PDS/100G/Vis system increased to $k = 0.0104 \text{ min}^{-1}$ which allowed to shorten the half-life to about 66.6 min. In turn, the increase in reaction rate constant for the PDS/100S/Vis system was $k = 0.0071 \text{ min}^{-1}$, and the half-life was reduced to approximately 87.7 min.

It was also observed that inclusion of the source of Vis radiation after introduction into the model solution of PDS caused an increase in dye decomposition by

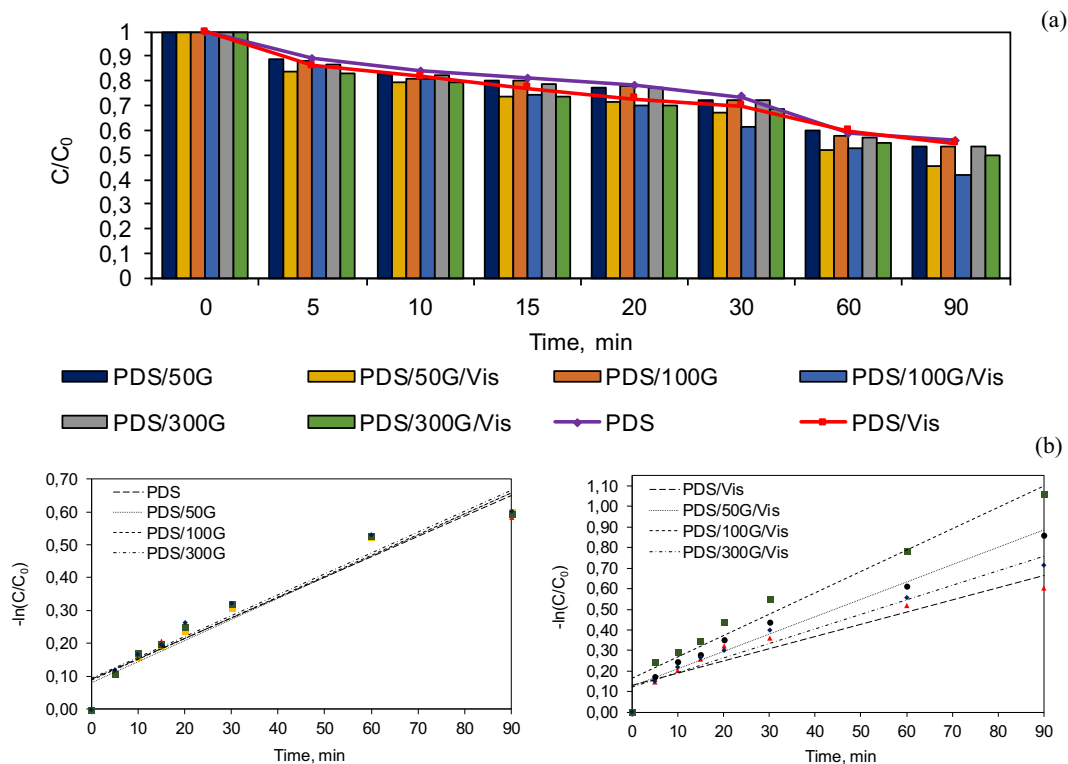


Fig. 5 Effect of glucose addition on **a** MB (C/C_0) decomposition in the presence of $\text{Na}_2\text{S}_2\text{O}_8$ without and with Vis radiation, and **b** reaction kinetics. Decomposition conditions: $C_0 = 2.0 \text{ mg/L}$; $V =$

100.0 cm^3 ; $T = 298.0 \text{ K}$; $\text{pH} = 6.0$; $t = 0\text{--}90 \text{ min}$; molar concentration $\text{Na}_2\text{S}_2\text{O}_8 = 6.5 \text{ mM}$

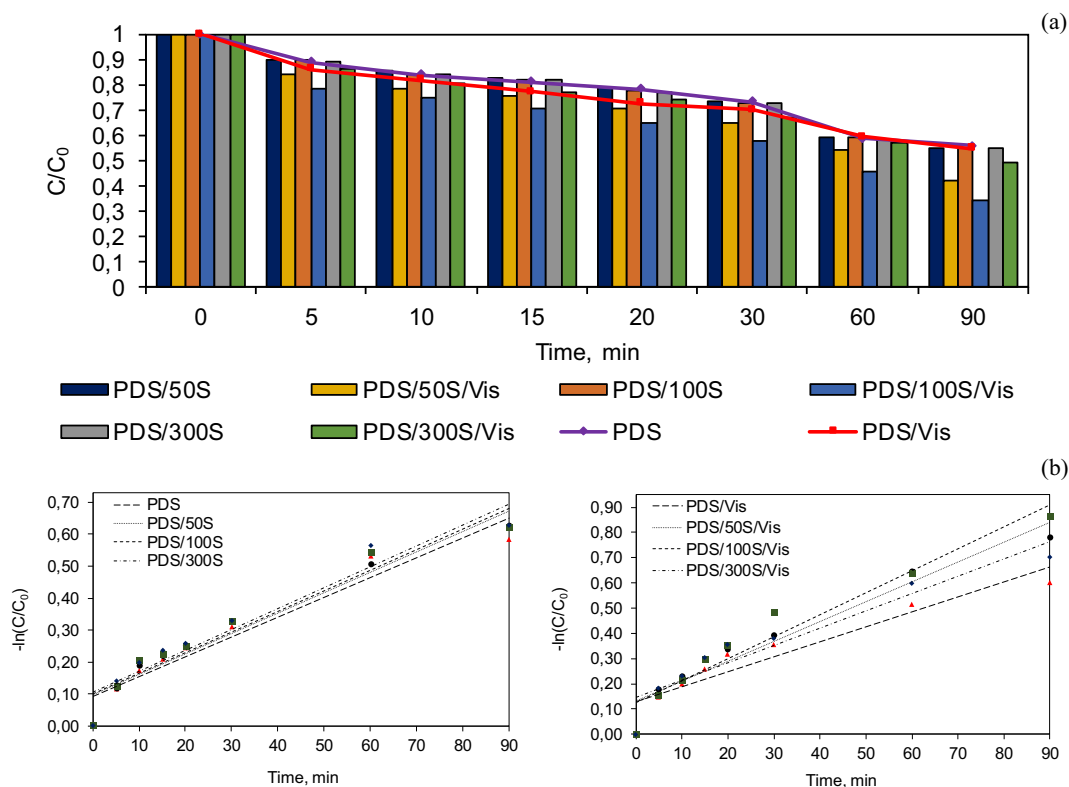


Fig. 6 Impact of sucrose addition on (a) MB (C/C_0) decomposition in the presence of $\text{Na}_2\text{S}_2\text{O}_8$ without and with Vis radiation, and (b) reaction kinetics. Decomposition conditions: $C_0 = 2.0 \text{ mg/}$

$L; V = 100.0 \text{ cm}^3; T = 298.0 \text{ K}; \text{pH} = 6.0; t = 0\text{--}90 \text{ min};$ molar concentration $\text{Na}_2\text{S}_2\text{O}_8 = 6.5 \text{ mM}$

about 5.0% compared with PDS alone (in time from 5.0 to 30.0 min). However, the degree of decolorisation was

not satisfactory. The increase in MB degradation in this system is probably associated with very poor quantum

Table 3 Parameters of pseudo-first-order reaction in tested systems and removal efficiency after 90 min of the process

Process	Efficiency (%)	$k \text{ (min}^{-1}\text{)}$	R^2	$t/2 \text{ (min)}$	Process	Efficiency (%)	$k \text{ (min}^{-1}\text{)}$	R^2	$t/2 \text{ (min)}$
Vis	0.0	0.0001	0.86	6931.5	300S/Vis	2.0	0.0002	0.85	3465.7
PDS	44.0	0.0062	0.93	111.8	PDS/50G	45.0	0.0064	0.95	108.3
PDS/Vis	45.0	0.0059	0.88	117.5	PDS/50G/Vis	48.0	0.0084	0.95	82.5
50G	0.0	0.0001	0.81	6931.5	PDS/100G	45.0	0.0063	0.93	110.0
50G/Vis	1.0	0.0001	0.78	6931.5	PDS/100G/Vis	65.0	0.0104	0.95	66.6
100G	0.0	0.0001	0.89	6931.5	PDS/300G	45.0	0.0064	0.93	108.3
100G/Vis	1.0	0.0001	0.83	6931.5	PDS/300G/Vis	51.0	0.0071	0.93	97.6
300G	1.0	0.0001	0.95	6931.5	PDS/50S	47.0	0.0064	0.94	108.3
300G/Vis	0.0	0.0001	0.85	6931.5	PDS/50S/Vis	44.0	0.0079	0.93	87.7
50S	0.0	0.0001	0.82	6931.5	PDS/100S	46.0	0.0064	0.93	108.3
50S/Vis	2.0	0.0002	0.92	3465.7	PDS/100S/Vis	48.0	0.0087	0.94	79.7
100S	0.0	0.0001	0.90	6931.5	PDS/300S	47.0	0.0065	0.93	106.6
100S/Vis	2.0	0.0002	0.81	3465.7	PDS/300S/Vis	50.0	0.0069	0.90	100.5
300S	1.0	0.0001	0.82	6931.5					

efficiency of sulfate radicals at wavelength $\lambda > 400.0$ nm (Herrmann 2007). One method of activating persulfates is ultraviolet radiation, and the most commonly used wavelength is $\lambda = 254.0$ nm. This is associated with high quantum efficiency of sulfate radicals at this wavelength and the energy input of UV radiation. Partial activation of $\text{Na}_2\text{S}_2\text{O}_8$ may therefore be the result of activation by visible light; however, due to the low activity of $\text{SO}_4^{\cdot-}$ radicals at this wavelength, the activation process was not effective. Research conducted by Herrmann (2007) showed that the quantum efficiency of sulfate radicals decreases with the increase of UV wavelength in the range from 248.0 to 351.0 nm. It can therefore be assumed that at a wavelength $\lambda > 400.0$ nm, the efficiency is so low that the activation of $\text{Na}_2\text{S}_2\text{O}_8$ occurs, but to a very small extent.

As shown in Figs. 5a and 6a, without irradiation of the model solution, activation of $\text{Na}_2\text{S}_2\text{O}_8$ with glucose and sucrose was inefficient. Dye decolorisation when adding pure PDS was approximately equal to the dye degradation process carried out after the sugars were introduced into the solution. The reaction rate constant k (Table 3) in this case was very similar, i.e. for PDS it was $k = 0.0062$, while for glucose and sucrose $k = 0.0064$. For comparison, the reaction rate constant for MB decolorisation with PDS in much higher concentrations (conditions, $V = 250.0$ cm³; $T = 298.0$ K; $C_0 = 10.0$ mg/L; $\text{Na}_2\text{S}_2\text{O}_8 = 1.5$ g/L, pH = 9.0; $t = 3$ – 24 min) carried out by Hung et al. (2016) was $k = 0.040$ min⁻¹.

The effect of Vis radiation on PDS activation has also been noted. Activation of PDS by visible radiation in the presence of glucose and sucrose may result from the probable electron transfer from sugar to PDS and its activation and sugar oxidation to products that are able to activate PDS. It is related to the so-called organic PDS activation with an external carbon source.

In the case of sucrose, PDS activation is probably due to the generation of Krebs cycle compounds during the sucrose degradation process. Krebs cycle compounds are ketone acids (pyruvic acid $\text{C}_3\text{H}_4\text{O}_3$ —the main substrate of the process, acetylacetic acid $\text{C}_4\text{H}_6\text{O}_3$, levulinic acid $\text{C}_5\text{H}_8\text{O}_3$), alcoholic acids (malic acid $\text{C}_4\text{H}_6\text{O}_5$, citric acid $\text{C}_6\text{H}_8\text{O}_7$) and dicarboxylic acids (oxalic acid $\text{C}_2\text{H}_2\text{O}_4$, succinic acid $\text{C}_4\text{H}_6\text{O}_4$). Ocampo (2009) conducted a detailed study on the effects of some Krebs cycle products. The fastest degree of degradation of hexachloroethane (organic chemical compound, chlorine derivative of

ethane) was achieved by activating PDS with ketone acids. Levulinic acid, which has a ketone group located on the third carbon of carboxylic acid, was the most effective compound that activated persulfate. In turn, dicarboxylic acids showed the lowest potential for decomposition of hexachloroethane from all tested compounds of the Krebs cycle. Literature data shows that compounds derived from the Krebs cycle that can activate the persulfates to the greatest extent are compounds from the keto acid group, i.e. compounds containing both a carboxyl ($-\text{COOH}$) and ketone ($\text{C}=\text{O}$ linked to two carbon atoms) group. The ketone functional group causes the most effective activation of persulfate to produce hydroxyl radicals and reducing agents in the system, while organic compounds containing a carboxyl group in their structure activate the persulfates to a small extent.

The results of this study showed that in a neutral pH system (pH = 6.0), PDS activation with glucose and sucrose is possible, whereas the PDS/sucrose system due to the probable presence of Krebs cycle compounds had a higher oxidising potential compared with the PDS system/glucose system. A possible explanation for this behaviour is the electron needed to activate persulfate. In the case of glucose, it comes only from this compound, while the sucrose decomposition leads to the formation of three compounds that can give away the electron needed to activate PDS.

In turn, PDS activation by glucose may result from the activation of persulfate through reduction. In a study conducted by Ahmad et al. (2013), phenoxides and phenols were tested for persulfate activation, with phenols unable to activate PDS. The mechanism of PDS activation by glucose appears to be comparable with the mechanism of activation by phenoxides. The electron from glucose is transferred to the persulfate and activates it, while glucose is oxidised to products that can activate the persulfate (Watts et al. 2018; Ahmad et al. 2013). Although activation of PDS is more effective at high pH, some functional groups such as the carbonyl group accept a negative charge that can activate PDS at a near-neutral pH (as in this study). Based on the results obtained, a concentration of 100 mM was chosen for the optimal molar concentration of glucose and sucrose. In mixtures containing higher concentrations of sugars and exposed to Vis radiation, the degree of decolorisation was lower, which could be due to the capture of radicals by higher glucose concentrations ($k_{\text{OH}\cdot} = 1.5 \times 10^9$) (Buxton et al. 1988).

3.2 Effect of pH

The experiments determined the impact of the initial reaction on the efficiency of dye degradation. Three types of reaction were tested: pH = 6.0, pH = 9.0 and pH = 12.0. The degree of degradation of methylene blue depending on the pH of the solution for various tested systems is shown in Fig. 7. It was found that together with the increase in the reaction pH value, the efficiency of methylene blue removal increases. The highest MB degradation was found at pH = 12.0. The degree of decolorisation in systems containing sugars was almost the same and amounted to 84% for PDS/100G/Vis and 83% for PDS/100S/Vis during the 90-min process. The reduction of the initial MB concentration at this pH after 90 min of reaction for PDS, PDS/100G and PDS/100S was about 69%, 75% and 72%, respectively. At pH = 12.0, activation of Na₂S₂O₈ takes place according to the mechanism of the so-called alkaline activation (Furman et al. 2010). The persulfate hydrolysis produces the HO₂⁻ anion, which then reacts with the persulfate molecule resulting in the sulfate radical and the superoxide radical (Eqs. 7 and 8). The increase in the pH of the reaction medium results in the reaction of the SO₄^{-•} with H₂O or OH⁻ and the production of hydroxyl radicals (Eqs. 9 and 10) (Lei et al. 2015; Furman et al. 2011; Hayon et al. 1972; Norzaee et al. 2017; Huang et al. 2002).

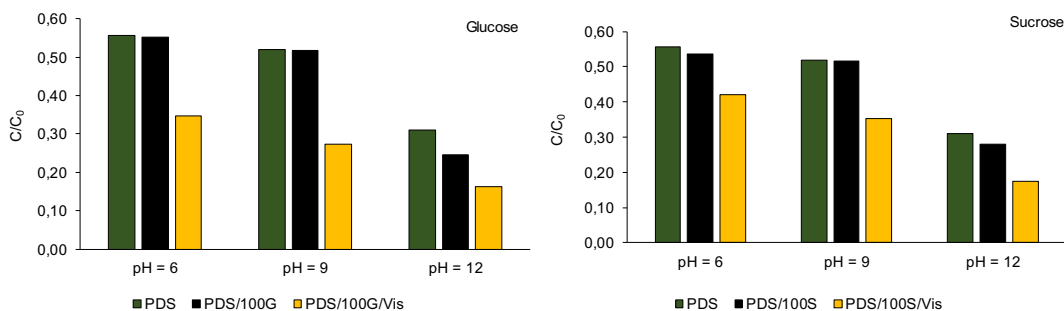
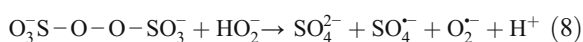
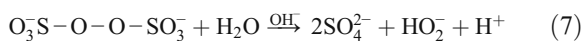


Fig. 7 Impact of the pH of the model solution on the MB (C/C_0) decomposition in the presence of Na₂S₂O₈ in various purification variants. Decomposition conditions: $C_0 = 2.0$ mg/L; $V =$

Based on the analysis of Fig. 7, PDS activation was also observed in the system without Vis irradiation at pH = 12.0 (PDS-12/100G and PDS-12/100S). In these systems, the decrease in initial dye concentration increased from 69% in the PDS-12 system to 75% in the PDS-12/100G system and to 72% in the PDS-12/100S system. Also, the parameters of the pseudo-first-order reaction, summarised in Table 4, have changed. They show an increase in dye decolorisation and a shortening of the half-life from 58.7 min (PDS-12) to about 50 min in PDS-12/100G and PDS-12/100S. The reaction rate constant is $k = 0.0141 \text{ min}^{-1}$ (PDS-12/100G) and $k = 0.0137 \text{ min}^{-1}$ (PDS-12/100S). The reason for this phenomenon may be the form in which glucose and sucrose occur at this pH. The glucose acid (pK_a) strength is $\text{pK}_a = 11.8\text{--}12.3$ (Watts et al. 2018; www6 2019) while sucrose acid $\text{pK}_a = 12.6$ (www7 2019). Thus, at pH = 12.0, glucose was in ionised form and it was its anionic form that could activate PDS. Sucrose, in turn, was only partially present in the form of ions; hence, the lower efficiency of PDS activation, which is confirmed by the analysis of reaction kinetics (Fig. 8). At a pH less than the pK_a of a given sugar, PDS activation occurs only when the solution is irradiated, both for glucose and sucrose. However, at a pH higher than sugar pK_a , activation of PDS is observed not only after switching on the radiation source, but before turning on the Vis lamp. The decomposition of methylene blue is higher for systems containing glucose, since the pH of the solution is higher than the pK_a of this sugar.

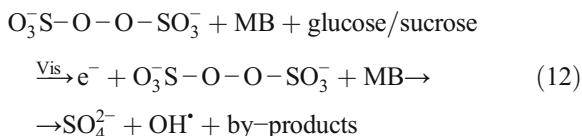
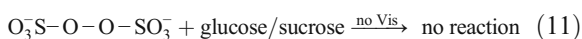
It was also confirmed that the addition of glucose or sucrose to systems with a lower pH than the sugar pK_a , in which no Vis radiation was introduced, does not result in PDS activation. In systems with pH = 6.0 and pH = 9.0, the difference between the PDS system and the

100.0 cm³; $T = 298.0$ K; glucose and sucrose dose, 100.0 mM; $t = 90.0$ min; molar concentration of Na₂S₂O₈ = 6.5 mM)

Table 4 Parameters of pseudo-first-order reaction and removal efficiency in tested systems depending on pH after 90 min of the process

pH	Process	Efficiency (%)	k (min^{-1})	R^2	$t/2$ (min)
6	PDS-6	44.0	0.0062	0.93	111.8
	PDS-6/100G	45.0	0.0063	0.93	110.0
	PDS-6/100G/Vis	65.0	0.0104	0.95	66.6
	PDS-6/100S	46.0	0.0064	0.93	108.3
	PDS-6/100S/Vis	48.0	0.0087	0.94	79.7
9	PDS-9	48.0	0.0066	0.97	105.0
	PDS-9/100G	48.0	0.0067	0.92	103.5
	PDS-9/100G/Vis	73.0	0.0137	0.99	50.6
	PDS-9/100S	48.0	0.0069	0.84	100.5
	PDS-9/100S/Vis	65.0	0.0102	0.94	68.0
12	PDS-12	69.0	0.0118	0.97	58.7
	PDS-12/100G	75.0	0.0141	0.97	49.2
	PDS-12/100G/Vis	84.0	0.0187	0.98	37.1
	PDS-12/100S	62.0	0.0137	0.99	50.6
	PDS-12/100S/Vis	83.0	0.0188	0.99	36.9

systems of PDS with added sugars and without Vis radiation was not significant. This difference was less than 1%. Among the possible reasons, there may be the lack of ionised form of sugars and the probable lack of sugar decomposition in systems not exposed to Vis radiation. Perhaps without an additional stimulus in the form of energy from radiation, electron transfer (whose source is disintegrating sugars) towards PDS is impossible (Eq. 11). In turn, when the pH of the solution is $\text{pH} > 11.0$, i.e. above the pK_a of sugar, irradiation of the solution generates the electron needed to activate PDS (Eq. 12) (Cai et al. 2019):



This can be seen especially when analysing the efficiency of MB decomposition in systems with and without irradiation. The dye decomposes with the inclusion of a radiation source, and the kinetics of decolorisation changes. For example, the reaction rate constant in the PDS-9/100G system is $k = 0.0067 \text{ min}^{-1}$, while in the PDS-9/

100G/Vis system, it increases to $k = 0.0137 \text{ min}^{-1}$, similarly in the case of the PDS-12/100S system ($k = 0.0137 \text{ min}^{-1}$) and PDS-12/100S/Vis ($k = 0.0188 \text{ min}^{-1}$). Also, the authors of other papers have found that the decomposition of impurities increases with increasing pH. Watts et al. (2018) showed that the activation of persulfate was more effective at an alkaline reaction compared with a neutral reaction. Also Li et al. (2017) showed that increasing the pH of the model solution from 8.0 to 12.0 resulted in an increase in benzene degradation by 70%. In turn, Ocampo (2009) investigated the effect of reduced organic compounds, including phenols, catechols and fenoxides. This study also showed the effect of pH on the decomposition of impurities. An increase in the pH of the solution resulted in an increase in the efficiency of nitrobenzene degradation.

3.3 Radicals Scavengers

In order to identify the main active ingredients involved in the MB photo degradation process, tests were carried out using radical scavengers. Tert-butyl alcohol was used in the experiments as the radical scavenger OH^\bullet ($k_{\text{OH}^\bullet} = 5.2 \times 10^8 \text{ M}^{-1} \text{ s}^{-1}$; $k_{\text{SO}_4^{\bullet-}} = \leq 10^6 \text{ M}^{-1} \text{ s}^{-1}$) (Ocampo 2009), while hydroquinone as the $\text{O}_2^{\bullet-}$ ($k_{\text{O}_2^{\bullet-}} = 1.7 \times 10^7 \text{ M}^{-1} \text{ s}^{-1}$) radical scavenger (Rao and Hayon 1975). Due to a similar rate constant of methanol

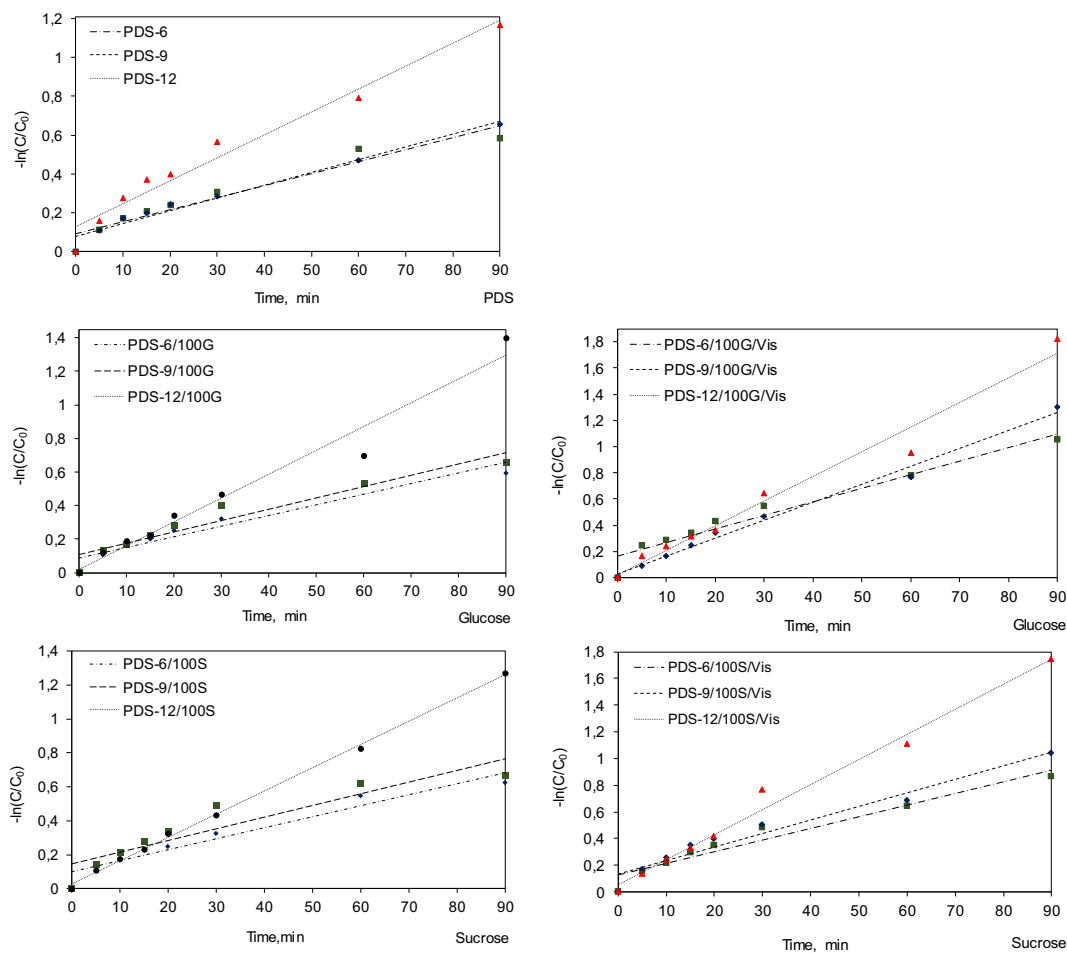


Fig. 8 Kinetics of methylene blue decomposition in various purification configurations. Decomposition conditions: $C_0 = 2.0$ mg/L; $V = 100.0$ cm³; pH = 6.0–12.0; $T = 298.0$ K; glucose and sucrose dose, 100.0 mM; $t = 0.0$ –90.0 min; molar concentration of $\text{Na}_2\text{S}_2\text{O}_8 = 6.5$ mM

reaction with OH^\bullet i $\text{SO}_4^{\bullet-}$ ($k_{\text{OH}^\bullet} = 8.0 \times 10^8 \text{ M}^{-1} \text{ s}^{-1}$ ($k_{\text{OH}^\bullet} = 8.0 \times 10^8 \text{ M}^{-1} \text{ s}^{-1}$; $k_{\text{SO}_4^{\bullet-}} = 1.0 \times 10^7 \text{ M}^{-1} \text{ s}^{-1}$) radicals (Ocampo 2009), this alcohol was used as a scavenger of these radicals to confirm the formation of sulfate radicals. The compounds used are commonly used as radical scavengers by the authors of many papers (Nakarada and Petkovic 2018; Wang and Wang 2018; Azarpira et al. 2019). Scavengers were always used at a concentration of 50 μM .

The influence of individual radical scavengers depending on the pH of the solution is shown in Fig. 9. The rate of degradation of methylene blue is basically inhibited by all scavengers introduced into the system. It is confirmed by the fact that sulfate $\text{SO}_4^{\bullet-}$, hydroxyl OH^\bullet and superoxide $\text{O}_2^{\bullet-}$ radicals are generated during the reaction. As shown in Fig. 9, among the three radical

scavengers, the addition of hydroquinone inhibited methylene blue decomposition reactions to the greatest extent. This phenomenon took place in all systems studied. This indicates the important role of superoxide radicals in the photodegradation reaction of methylene blue. A similar important role of $\text{O}_2^{\bullet-}$ radicals in an alkaline environment was demonstrated by Zhao et al. (2013). The author presents research on mechanisms for the removal of polycyclic aromatic hydrocarbons (PAHs) in different variants of persulfate activation. The main radicals generated during the removal of PAHs under alkaline conditions were superoxide radicals, which subsequently produced some amounts of hydroxyl and sulfate radicals.

However, the high pH of the solution means that the sulfate radicals generated in the system can be converted

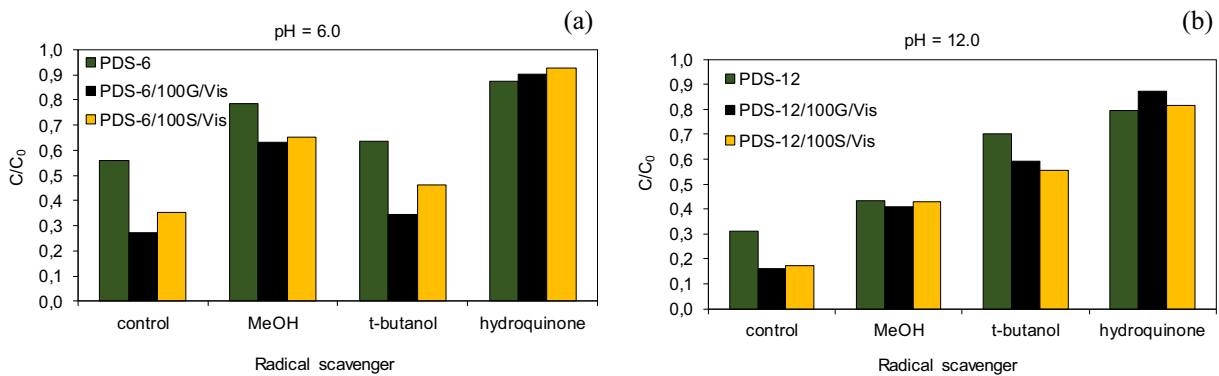


Fig. 9 Decomposition of methylene blue in the presence of various radical scavengers at pH = 6.0 (a) and pH = 12.0 (b). Decomposition conditions: $C_0 = 2.0$ mg/L; $V = 100.0$ cm³; $T =$

298.0 K; glucose and sucrose dose, 100.0 mM; $t = 90.0$ min; molar concentration of $\text{Na}_2\text{S}_2\text{O}_8 = 6.5$ mM)

into OH^\bullet radicals by reaction with O_2^- radicals (Eq. 12, “Section 3.2”). In slightly acidic environment (pH = 6.0), there were hydroxyl and sulfate radicals. The mechanism of their formation is presented in Eqs. 9–

12 (“Section 3.2”). Also, in this case, all tested systems were characterized by the presence of these radicals, although their share in the MB decomposition compared with superoxide radicals was smaller, which is indicated

Table 5 Parameters of pseudo-first-order reaction and removal efficiency in tested systems depending on pH after 90 min of the process

pH	Process	Efficiency (%)	k (1/min)	R^2	$t/2$ (min)
6	PDS-6	44.0	0.0062	0.93	111.8
	PDS-6 + MeOH	22.0	0.0024	0.81	288.8
	PDS-6 + t-butanol	37.0	0.0046	0.90	150.7
	PDS-6 + hydroquinone	12.0	0.0012	0.80	577.6
	PDS-6/100G/Vis	65.0	0.0137	0.99	50.6
	PDS-6/100G/Vis + MeOH	37.0	0.0048	0.94	144.4
	PDS-6/100G/Vis + t-butanol	65.0	0.0111	0.99	62.4
	PDS-6/100G/Vis + hydroquinone	10.0	0.0009	0.80	770.2
	PDS-6/100S/Vis	48.0	0.0102	0.95	68.0
	PDS-6/100S/Vis + MeOH	35.0	0.0043	0.92	161.2
	PDS-6/100S/Vis + t-butanol	54.0	0.0078	0.96	88.9
	PDS-6/100S/Vis + hydroquinone	7.0	0.0008	0.82	866.4
12	PDS-12	69.0	0.0118	0.97	58.7
	PDS-12 + MeOH	56.0	0.0087	0.94	79.7
	PDS-12 + t-butanol	30.0	0.0038	0.91	182.4
	PDS-12 + hydroquinone	20.0	0.0024	0.9	288.8
	PDS-12/100G/Vis	84.0	0.0187	0.98	37.1
	PDS-12/100G/Vis + MeOH	59.0	0.0053	0.89	130.8
	PDS-12/100G/Vis + t-butanol	41.0	0.0013	0.87	533.2
	PDS-12/100G/Vis + hydroquinone	13.0	0.0013	0.87	533.2
	PDS-12/100S/Vis	83.0	0.0188	0.99	36.9
	PDS-12/100S/Vis + MeOH	57.0	0.0088	0.88	78.8
	PDS-12/100S/Vis + t-butanol	45.0	0.0059	0.88	117.5
	PDS-12/100S/Vis + hydroquinone	19.0	0.0019	0.82	364.8

Table 6 Summary of the efficiency of organic pollutant degradation techniques in advanced oxidation processes

Process	Compound	Conditions	Effectiveness	Literature
This study (PDS/glucose-sucrose/Vis)	Methylene blue	Reaction time = 90.0 min Room temperature Initial dye concentration = 2.0 mg/L Persulfate concentration = 0.065 mM Glucose/sucrose dose, 100 mM Volume = 100.0 cm ³ pH = 6.0–12.0	in pH = 6.0 PDS-6/100G/Vis <i>R</i> (%) = 65.0% PDS-6/100S/Vis <i>R</i> (%) = 58.0% in pH = 12.0 PDS-12/100G/Vis <i>R</i> (%) = 84.0% PDS-12/100S/Vis <i>R</i> (%) = 83.0%	–
C _{methanol} -TiO ₂ /AC C _{ethanol} -TiO ₂ /AC C _{dextran} -TiO ₂ /AC	Bisphenol A (BPA)	Reaction time = 45.0 min Initial BPA concentration = 1 mg/L Catalyst dose = 100 mg/L pH = 7.0 Room temperature Volume = 700 cm ³	<i>R</i> (%) = 95.0–99.0	(Zawadzki et al. 2018)
US/H ₂ O ₂	Aniline	Reaction time = 45.0 min H ₂ O ₂ concentration = 0.01 mol/L Optimal pH = 3.0 Initial aniline concentration = 20.0 mg/L Ultrasound frequency = 50.0 Hz Volume = 100.0 cm ³	<i>R</i> (%) ≈ 96.0%	(Rahdar et al. 2019)
TiO ₂ /activated carbon fibres	Methylene blue	Reaction time = 120.0 min Temperature = 30 ± 0.5 °C Initial dye concentration = 85.0 mg/L Catalyst dose = 1.0 g/L Volume = 350.0 cm ³	<i>R</i> (%) = 79.0	(Yuan et al. 2005)
US/ZnO/PDS	Ciprofloxacin (CIP)	Reaction time = 15.0 min Persulfate concentration ≈ 476.0 mg/L Optimal pH = 7.0 Initial CIP concentration = 25.0 mg/L Ultrasound frequency = 60.0 Hz Volume = 100.0 cm ³	<i>R</i> (%) = 99%	(Igwegbe et al. 2020)
Ozone	Methylene blue	Reaction time = 45.0 min Ozone flux = 1.92 mg/min Initial dye concentration = 100.0 mg/L Pressure = 0.06 MPa Volume = 1000.0 cm ³ Temperature = 30 ± 0.2 °C	<i>R</i> (%) = 95.0	(Liu et al. 2015)
MgO/NPs/US	Penicillin G (PG)	Reaction time = 60.0 min Nano-particle concentration = 1.5 g/L Optimal pH = 3.0 Initial PG concentration = 80.0 mg/L Ultrasound frequency = 60.0 Hz	<i>R</i> (%) ≈ 81.0	(Rahdar et al. 2018)

Table 6 (continued)

Process	Compound	Conditions	Effectiveness	Literature
Thermal activation of persulfates	Acid blue	Initial dye concentration = 200.0 mg/L Persulfate concentration = 0.5 mM pH = 5.0 Reaction time = 75.0 min Temperature = 333.0 K	R (%) = 86.0	(Ahmadi et al. 2019)
Electrochemical degradation in the presence of sulfate ions	Methylene blue	Initial dye concentration = 21.0 mg/L Room temperature Volume = 100.0 cm ³ Sulfate concentration = 0.1 mg/L	R (%) = 73.0	(Samide et al. 2014)

by the constant reaction rate k (Table 5). For example, to the PDS-6/100S/Vis system after adding hydroquinone, the reaction rate constant was $k = 0.0102 \text{ min}^{-1}$, while after adding methanol, it decreased to $k = 0.0043 \text{ min}^{-1}$.

The $\text{SO}_4^{\cdot-}$ and OH^{\cdot} radicals were removed from the system with methyl alcohol and t-butyl alcohol. As presented earlier, t-butanol reacts with sulfate radicals much slower compared with the reaction with hydroxide radicals ($k_{\text{OH}^{\cdot}} > k_{\text{SO}_4^{\cdot-}}$). Hence, based on the rate of degradation of methylene blue after the addition of methanol and t-butanol, it can be identified whether sulfate radicals are generated during the reaction. The effect of individual radical scavengers in Fig. 9 illustrates the reduction of MB degradation after the addition of t-butanol and methanol compared with the system without the addition of inhibitors (control), which indicates that sulfate and hydroxyl radicals are involved in the dye decomposition reaction. In the PDS-6/100G/Vis + methanol system, the degradation efficiency decreased to 27% (at 73% for pure PDS), while in the PDS-6/100G/Vis + t-butanol system, it decreased to 65%. It can therefore be concluded that at pH = 6.0, degradation of methylene blue under the influence of PDS activated visible light in the presence of sugars and sucrose is caused by sulfate anions SO_4^{2-} (which results from Eq. 12) and to a lesser extent by hydroxyl radicals. In turn, at pH = 12.0, hydroxyl radicals dominate.

3.4 Comparison with Other AOPs Processes Conducted Under the Exposure of Visible Light

Comparative results of organic pollutant decomposition in various advanced oxidation processes are presented in Table 6. The removal of organic pollutants in the examples presented was carried out using advanced oxidation processes such as ozonation, photocatalysis and sulfate radical decomposition. It can be stated that the proposed MB photodegradation process is an equally interesting method of dye decomposition compared with other advanced oxidation processes. The proposed method is promising and comparatively innovative to other studies presented in the literature regarding the decomposition of dyes (Ahmadi et al. 2019; Yuan et al. 2005; Liu et al. 2015; Samide et al. 2014) and other organic pollutants (Zawadzki et al. 2018; Rahdar et al. 2019; Igwegbe et al. 2020; Rahdar et al. 2018). It can be particularly useful where the dye concentrations are not high and it is possible to use, e.g. existing open

reservoirs to conduct a cleaning reaction under the influence of the visible light. This process is characterized by simplicity of the process, no need for energy-intensive UV lamps, low consumption of chemical reagents and a relatively short reaction time. In addition, chemical reagents used to activate PDS with visible light are cheap compared with other catalysts used and do not show a toxic effect (Watts et al. 2018). Activation of PDS in the presence of glucose was possible both at high pH and lower pH values; hence, it can also be stated that the presented method is suitable for the treatment of coloured wastewater characterized by a wide pH range, as the efficiency of dye decomposition in each of the tested pH ranges was not less than 50%.

4 Conclusions

The following conclusions can be drawn from the present study:

1. Activation of sodium persulfate is possible due to the use of Vis radiation in the presence of glucose and sucrose. This is an interesting alternative to in situ purification compared to other purification processes.
2. A positive effect of glucose and sucrose on increasing the efficiency of methylene blue degradation under the influence of visible light has been demonstrated.
3. The degree of methylene blue degradation increases with increasing pH of the solution.
4. Studies have shown the sensitivity of dye decolorisation to changes in the reaction environment.
5. The efficiency of dye decomposition in PDS/100G/Vis and PDS/100S/Vis systems regardless of the pH of the environment is still higher compared with the decomposition under the influence of PDS alone.
6. Dye decolorisation with PDS activated with Vis radiation in the presence of sugars is accompanied by the generation of sulfate, hydroxyl and superoxide radicals. At low pH, MB decomposes under the influence of sulfate radicals, while in high pH under the influence of hydroxyl radicals. The dominant radicals involved in the reaction are superoxide radicals.

Acknowledgements The presented study was performed in the framework of the research work in the Central Mining Institute in Poland, financially supported by the Polish Ministry of Science and Higher Education (No. 11158029-340).

References

- Ahmad, M., Teel, A. L., & Watts, R. J. (2013). Mechanism of persulfate activation by phenols. *Environmental Science & Technology*. <https://doi.org/10.1021/es400728c>.
- Ahmadi, S., Igwegbe, C. A., & Rahdar, S. (2019). The application of thermally activated persulfate for degradation of Acid Blue 92 in aqueous solution. *International Journal of Industrial Chemistry*. <https://doi.org/10.1007/s40090-019-0188-1>.
- Anipsitakis, G. P., & Dionysiou, D. D. (2004). Radical generation by the interaction of transition metals with common oxidants. *Environmental Science & Technology*. <https://doi.org/10.1021/es035121o>.
- Azarpira, H., Sadani, M., Abtahi, M., Vaezi, N., Rezaei, S., Atafar, Z., MoMohseni, S. M., Sarkhosh, M., Ghaderpoori, M., Keramati, H., Pouyaj, R. H., Akbari, A., & Fanai, V. (2019). Photo-catalytic degradation of triclosan with UV/iodide/ZnO process: performance, kinetic, degradation pathway, energy consumption and toxicology. *Journal of Photochemistry and Photobiology, A: Chemistry*. <https://doi.org/10.1016/j.jphotochem.2018.10.041>.
- Buxton, G. V., Greenstock, C. L., Helman, W. P., & Ross, A. B. (1988). Critical review of rate constants for reactions of hydrated electrons, hydrogen atoms and hydroxyl radicals ($^{\bullet}\text{OH}/^{\bullet}\text{O}$) in aqueous solution. *Journal of Physical and Chemical Reference Data*. <https://doi.org/10.1063/1.555805>.
- Cai, T., Liu, Y., Wang, L., Dong, W., Chen, H., Zeng, W., Xia, X., & Zeng, G. (2019). Activation of persulfate by photoexcited dye for antibiotic degradation: Radical and nonradical reactions. *Chemical Engineering Journal*. <https://doi.org/10.1016/j.cej.2019.122070>.
- Chen, W.S. & Su., Y.C. (2012). Removal of dinitrotoluenes in wastewater by sono-activated persulfate. *Ultrasonics Sonochemistry*, DOI: <https://doi.org/10.1016/j.ultsonch.2011.12.012>.
- Clayden, J., Greeves, N., & Warren, S. (2012). *Organic chemistry*. Oxford University Press.
- Criquet, J., Karpel, N., & Leitner, V. (2011). Electron beam irradiation of aqueous solution of persulfate ions. *Chemical Engineering Journal*. <https://doi.org/10.1016/j.cej.2011.02.025>.
- Deng, Y., & Zhao, R. (2015). Advanced oxidation processes (AOPs) in wastewater treatment. *Current Pollution Reports*. <https://doi.org/10.1007/s40726-015-0015-z>.
- DHI, Milieu Ltd. and Protection Through Knowledge (PKT) Ltd.(n.d.), 2008. Appendix 2. Review of Annex IV o regulation (EC) NO. 1907/2006 (REACH). Evaluation of existing entries in Annex IV [online: https://ec.europa.eu/environment/chemicals/reach/pdf/6b_appendix_2.pdf].
- Eberson, L. (1987). *Electron transfer reactions in organic chemistry*. Berlin: Springer.
- Furman, O., Teel, A. L., & Watts, R. J. (2010). Mechanism of base activation of persulfate. *Environmental Science & Technology*. <https://doi.org/10.1021/es1013714>.
- Furman, O., Teel, A. L., & Watts, R. J. (2011). Effect of basicity on persulfate reactivity. *Journal of Environmental Engineering*. [https://doi.org/10.1061/\(ASCE\)EE.1943-7870.0000323](https://doi.org/10.1061/(ASCE)EE.1943-7870.0000323).
- Hassaan, M.A. & Nemr, A.E. (2017). Health and environmental impacts of dyes: mini review. *American Journal of*

- Environmental Science and Engineering, <https://doi.org/10.11648/j.ajese.20170103.11>.
- Hayon, E., Treinin, A., & Wilf, J. (1972). Electronic spectra, photochemistry, and autoxidation mechanism of the sulfite-bisulfite-pyrosulfite systems: the SO_2^- , SO_3^- , SO_4^- and SO_5^- radicals. *Journal of the American Chemical Society*. <https://doi.org/10.1021/ja00756a009>.
- Herrmann, J. (2005). Heterogeneous photocatalysis: state of the art and present applications. *Topics in Catalysis*. <https://doi.org/10.1007/s11244-005-3788-2>.
- Herrmann, H. (2007). On the photolysis of simple anions and neutral molecules as sources of O-/OH, SOx- and Cl in aqueous solution. *Physical Chemistry Chemical Physics*. <https://doi.org/10.1039/B618565G>.
- Huang, K. C., Couttenye, R. A., & Hoag, G. E. (2002). Kinetics of heat-assisted persulfate oxidation of methyl tert-butyl ether (MTBE). *Chemosphere*. [https://doi.org/10.1016/S0045-6535\(02\)00330-2](https://doi.org/10.1016/S0045-6535(02)00330-2).
- Hung, C. M., Chen, C. W., Liu, Y. Y., & Dong, C. D. (2016). Decolorization of methylene blue by persulfate activated with FeO magnetic particles. *Water Environment Research*. <https://doi.org/10.2175/106143016X14609975746848>.
- Igwegbe, C.A., Ahmadi, S., Rahdar S., Ramazani A., Mollazehi, A.R. (2020). Environmental engineering research, <https://doi.org/10.4491/eer.2018.058>.
- Ji, Y., Xie, W., Fan, Y., Shi, Y., Kong, D., & Lu, J. (2016). Degradation of trimethoprim by thermo-activated persulfate oxidation: reaction kinetics and transformation mechanisms. *Chemical Engineering Journal*. <https://doi.org/10.1016/j.cej.2015.10.050>.
- Lei, Y., Chen, C. S., Tu, Y. J., Huang, Y. H., & Zhang, H. (2015). Heterogeneous degradation of organic pollutants by persulfate activated by $\text{CuO-Fe}_3\text{O}_4$: mechanism, stability, and effects of pH and bicarbonate ions. *Environmental Science & Technology*. <https://doi.org/10.1021/acs.est.5b00623>.
- Li, W., Orozco, R., Camargos, N., & Liu, H. (2017). Mechanisms on the impacts of alkalinity, pH, and chloride on persulfate-based groundwater remediation. *Environmental Science & Technology*. <https://doi.org/10.1021/acs.est.6b04849>.
- Lisiak, A., & Miklas, M. (2007). Problem of harmfulness of azo-dyes. *Przegląd włókienniczy – Włókno, Odzież, Skóra*, 3, 38–40.
- Liu, C. S., Higgins, C. P., Wang, F., & Shih, K. (2012). Effect of temperature on oxidative transformation of perfluorooctanoic acid (PFOA) by persulfate activation in water. *Separation and Purification Technology*. <https://doi.org/10.1016/j.seppur.2011.09.047>.
- Liu, X., Hou, Y., Guo, J., Wang, Y., Zuo, Q., & Wang, C. (2015). Catalytic ozone aqueous decomposition of methylene blue using composite metal oxides. *Materials Science and Engineering*. <https://doi.org/10.1088/1757-899X/87/1/012031>.
- Melgoza, D., Hernandez-Ramirez, A., & Peralta-Hernandez, J. M. (2009). Comparative efficiencies of the decolourisation of methylene blue using Fenton's and photo-Fenton's reactions. *Photochemical & Photobiological Sciences*. <https://doi.org/10.1039/b817287k>.
- Nakarada, D., & Petkovic, M. (2018). Mechanistic insights on how hydroquinone disarms OH and OOH radicals. *Quantum chemistry*. <https://doi.org/10.1002/qua.25496>.
- Norzaee, S., Bazrafshan, E., Djahed, B., Mostafapour, F. K., & Khaksefidi, R. (2017). UV activation of persulfate for removal of penicillin G antibiotics in aqueous solution. *Scientific World Journal*. <https://doi.org/10.1155/2017/3519487>.
- Nunez, L., Garcia-Hortal, J. A., & Torrades, F. (2007). Study of kinetic parameters related to decolorization and mineralization of reactive dyes from textile dyeing using Fenton and photo-Fenton processes. *Dyes and Pigments*. <https://doi.org/10.1016/j.dyepig.2006.07.014>.
- Ocampo, A.M. (2009). Persulfate activation by organic compounds, Washington State University.
- Rahdar, S., Igwegbe, C. A., Rahdar, A., & Ahmadi, S. (2018). Efficiency of sono-nano-catalytic process of magnesium oxide nano particle in removal of penicillin G from aqueous solution. *Desalination and Water Treatment*. <https://doi.org/10.5004/dwt.2018.22102>.
- Rahdar, S., Igwegbe, C. A., Ghasemi, M., & Ahmadi, S. (2019). Degradation of aniline by the combined process of ultrasound and hydrogen peroxide ($\text{US}/\text{H}_2\text{O}_2$). *MethodsX*. <https://doi.org/10.1016/j.mex.2019.02.033>.
- Rao, P. S., & Hayon, E. (1975). Redox potentials of free radicals. IV. Superoxide and hydroperoxy radicals O_2^- and HO_2 . *The Journal of Physical Chemistry: A*. <https://doi.org/10.1021/j100571a021>.
- Samide, A., Tutunaru, B., Tigae, C., Efreem, R., Moanta, A., & Dragoi, M. (2014). Removal of methylene blue and methyl blue from wastewater by electrochemical degradation. *Environment Protection Engineering*. <https://doi.org/10.5277/epe140408>.
- Waldemer, R. H., Tratnyek, P. G., Johnson, R. L., & Nurmi, J. T. (2007). Oxidation of chlorinated ethenes by heat-activated persulfate: kinetics and products. *Environmental Science & Technology*. <https://doi.org/10.1021/es062237m>.
- Wang, J., & Wang, S. (2018). Activation of persulfate (PS) and peroxymonosulfate (PMS) and application for the degradation of emerging contaminants. *Chemical Engineering Journal*. <https://doi.org/10.1016/j.cej.2017.11.059>.
- Wang, W., Wang, H., Li, G., An, T., Zhao, H., & Wong, P. K. (2019). Catalyst-free activation of persulfate by visible light for water disinfection: efficiency and mechanisms. *Water Research*. <https://doi.org/10.1016/j.watres.2019.03.071>.
- Watts, R. J., Ahmad, M., Hohner, A. K., & Teel, A. L. (2018). Persulfate activation by glucose for in situ chemical oxidation. *Water Research*. <https://doi.org/10.1016/j.watres.2018.01.050>.
- www1 <https://www.indiamart.com/>, access: 25.09.2019.
- www2 https://www.thorlabs.com/newgrouppage9.cfm?objectgroup_id=6361, access: 30.09.2019.
- www3 https://www.accessdata.fda.gov/drugsatfda_docs/label/2016/204630s000lbl.pdf, access: 28.09.2019.
- www4 <https://chem.nlm.nih.gov/chemidplus/rn/50-99-7>, access: 28.09.2019.
- www5 <https://chem.nlm.nih.gov/chemidplus/rn/57-50-1>, access: 28.09.2019.
- www6 <https://www.drugbank.ca/drugs/DB01914>, access: 28.09.2019.
- www7 <https://pubchem.ncbi.nlm.nih.gov/compound/Sucrose>, access: 28.09.2019.
- Yuan, R., Guan, R., Shen, W., & Zheng, J. (2005). Photocatalytic degradation of methylene blue by a combination of TiO_2 and

- activated carbon fibers. *Journal of Colloid and Interface Science*. <https://doi.org/10.1016/j.jcis.2004.08.143>.
- Zawadzki, P., Kudlek, E., & Dudziak, M. (2018). Kinetics of the photocatalytic decomposition of Bisphenol A on modified photocatalysts. *Journal of Ecological Engineering*. <https://doi.org/10.12911/22998993/89651>.
- Zhang, R., Sun, P., Boyer, T. H., Zhao, L., & Huang, C. H. (2015). Degradation of pharmaceuticals and metabolite in synthetic human urine by UV, UV/H₂O₂, and UV/PDS. *Environmental Science & Technology*. <https://doi.org/10.1021/es504799n>.
- Zhao, D., Liao, X., Yan, X., Huling, S. G., Chai, T., & Tao, H. (2013). Effect and mechanism of persulfate activated by different methods for PAHs removal in soil. *Journal of Hazardous Materials*. <https://doi.org/10.1016/j.jhazmat.2013.03.056>.

Publisher's Note Springer Nature remains neutral with regard to jurisdictional claims in published maps and institutional affiliations.

Article

TiO₂ Modified with Organic Acids for the Decomposition of Chlorfenvinphos under the Influence of Visible Light: Activity, Performance, Adsorption, and Kinetics

Piotr Zawadzki 

Department of Water Protection, Central mining Institute, Plac Gwarków 1, 40-166 Katowice, Poland; pzewadzki@gig.eu; Tel.: +48-32-259-2801

Received: 25 November 2019; Accepted: 5 January 2020; Published: 8 January 2020



Abstract: Photocatalytic decomposition of chlorfenvinphos (CFVP) in the presence of titanium dioxide (TiO₂) modified with organic acids: pyruvic (PA) and succinic (SA) under the visible light radiation has been studied. The following tests were examined: dose of photocatalysts, adsorption time, pH of the model solution, deactivation of catalysts, the role of oxygen, identification of free radicals for the CFVP decomposition, Langmuir-Hinshelwood kinetics. The synthesized materials were characterized by Scanning Electron Microscopy (SEM) and UV-Vis. At 10 wt.% of acid (90:10) decomposition of chlorfenvinphos was the most effective in the following conditions: dose of catalyst 50.0 mg/L, time of adsorption = 20 min, pH of model solution = 3.0. Under these conditions the order of photocatalyst efficiency has been proposed: TiO₂/PA/90:10 > TiO₂/SA/90:10 > TiO₂ with the removal degree of 85, 72 and 48%. The mathematically calculated half-life at this conditions was 27.0 min and 39.0 min for TiO₂/PA/90:10 and TiO₂/SA/90:10 respectively, compared to 98 min for pure TiO₂. It has been determined that the O₂^{•-} radicals and holes (h⁺) are the main reactive species involved in the photodegradation of chlorfenvinphos. The results of this study showed that method may be an interesting alternative for the treatment of chlorfenvinphos contaminated wastewater.

Keywords: TiO₂; pyruvic acid; succinic acid; chlorfenvinphos; adsorption; photocatalysis; radicals; scavenger test; modified photocatalysts; kinetics

1. Introduction

The progress of civilization and the increase in the world's population have made the use of plant protection products in recent years a necessary and comprehensive solution in the elimination of pests in regions poor in food. It is, therefore, an important element of modern agriculture, without which it would be impossible to fight insects, weeds, fungi and other harmful factors for plants. The use of pesticides has brought undoubted benefits to eliminate pests, but taking into account their impact and chronic toxicity, these compounds pose a threat to many living organisms, including humans. Interest in pesticides has focused for many years on four basic properties: selective toxicity, persistence in the environment, bioaccumulation and mobility. The persistence in the environment is probably the most decisive factor when considering the extent of their use. The persistence is often expressed in terms of half-life. The decomposition of pesticides may occur as a result of biological processes as well as chemical and photochemical reactions. The fact that a pesticide loses its characteristic activity does not necessarily mean that it has become a harmless substance. As a result of chemical reactions compounds that are more toxic than primary compounds are often produced [1–3].

One of the groups of pesticides belonging to very toxic environmental pollutants are organophosphate insecticides. The organophosphate insecticides are derivatives of phosphoric acid in which the hydroxyl

group (-OH) was replaced by the -OR groups derived from alcohol. The organophosphate pesticides inhibit the activity of acetylcholinesterase—one of the most important enzymes for the peripheral and central nervous systems. [(E)-2-Chloro-1-(2,4-dichlorophenyl)ethenyl]diethyl phosphate (IUPAC), commonly known as chlorfenvinphos (CFVP), is one of the most important representatives of the organophosphate insecticides family. The CFVP is sold under trade names such as Birlane, Dermatone, and Sapecron. This compound is widely used as a mammalian low toxicity insecticide against pests that destroy potato, rice, carrot, oil seed and maize crops.

The subject pesticide is identified in samples taken from waters around the world [4]. In the United Kingdom, studies focused on monitoring chemicals used for sheep baths were carried out. The study showed that the taken samples of surface water contained such organophosphate pesticides as diazinon, propetamphos, pyrethroids (e.g., cypermethrin, flumethrin) and chlorfenvinphos. The chlorfenvinphos was present at concentrations between 1.0–242.0 ng/L. This compound was also found in groundwater and seawater at around 20.0 ng/L [5,6]. The presence of chlorfenvinphos has also been documented in some surface waters in Poland. According to the results of surface water quality study conducted in 2016 [7], chlorfenvinphos was identified in 32 places at 137 control points in Silesia Region. The pesticide concentration ranged from 0.001–47.4 µg/L. The maximum concentration of the pesticide (47.4 µg/L) was identified in the Wąwolnica stream—intake into the Przemsza River. This state results from the fact that chemicals have been accumulated in the river valley for years as a remnant of the activity of a former chemical plant.

The problem of elimination of substances posing a health hazard for humans and animals has become the reason for the development of new purification technologies, such as the Advanced Oxidation Processes (AOPs) conducted in the presence of titanium (IV) oxide or another semiconductor (a process of photocatalysis). The AOPs methods, although carried out in different reaction variants, have one common chemical feature—the generation of hydroxyl radicals (OH•). In the photocatalytic process carried out in the presence of TiO₂, it is necessary to provide radiation of an appropriate wavelength, carrying energy higher than the bandwidth banned. Titanium dioxide can be activated by light energy with a wavelength $\lambda \leq 400$ nm, so it is necessary to provide expensive lamps emitting ultraviolet radiation in the range of $\lambda = 300\text{--}388$ nm. Despite the numerous advantages that TiO₂ has, the attention of engineers and scientists around the world is now directed towards modified photocatalysts. For the practical application of heterogeneous processes involving semiconductors, it is important to increase the efficiency of the visible photocatalysis process, eliminate the agglomeration of TiO₂ particles, reduce the phenomenon of blocking active sites by intermediate products, and increase the efficiency of separation of catalysts particles from the reaction mixture. Therefore, much attention is currently paid to TiO₂ modification [8–12]. The above effects can be achieved by using organic acids such as succinic acid or pyruvic acid. In this study, succinic and pyruvic acid were selected for modification of commercial TiO₂. Pyruvic and succinic acids are naturally available acids (Krebs Cycle Compounds). Pyruvic acid is the simplest of the alpha-keto acids and succinic acid is a dicarboxylic acid. They are characterized by low toxicity towards living organisms. For example, the EC₅₀ after 48 h relative to *Daphnia magna* is 374.2 mg/L (succinic acid), while the LD₅₀ relative to mice is 3.5 g/kg (pyruvic acid). The amounts used during the study were several hundred times smaller. Modification with these organic acids is a simple and fast technology of modification [13,14], because carboxyl groups (-COOH) from pyruvic acid and carboxyl and ketone (C=O) groups from succinic acid can form bonds with metal oxide nanoparticles and play a positive role in extending the wavelength response range [15,16]. The use of succinic and pyruvic acid ensures higher photocatalytic activity of the catalysts by forming new absorption bands (waves above 400 nm), i.e., in the visible light range. This is due to the transfer of electrons from PA/SA to the conduction band of TiO₂ and the appearance of a new C-O-Ti bond [17]. The role of acids is also to improve adsorption of pollutants by increasing the specific surface area, to reduce the phenomenon of the TiO₂ agglomerate formation and to inhibit the anatase-rutile transformation [18,19]. According to literature data [20], thermal treatment of semiconductors leads to the formation of materials with a lower specific surface area due

to agglomeration of nanoparticles of catalysts. The use of acids reduces this phenomenon, leads to an increase in crystallites and thus an increase in the active surface of the catalysts.

The literature review shows that the decomposition process conducted in the presence of titanium (IV) oxide is an efficient and effective method of pollutants degradation but poor reuse of TiO₂, energy-consuming UV lamps and long photooxidation time are required. The novelty of the presented study, in comparison to other methods described in the literature, is the possibility of TiO₂ activation with low energy-consuming Vis lamp due to the use of succinic and pyruvic acids as photocatalyst modifiers, greater adsorption of chlorfenvinphos, photooxidation over a wide pH range, possibility of reuse of catalyst.

In order to remove pollutants that show low biodegradability and high toxicity, it is economically justified to applied method as presented in this study. This method turns out to be an interesting alternative to other treatment techniques.

The aim of the study was to examine the possibility of decomposition of chlorfenvinphos in the presence of photocatalysts modified with organic acids (pyruvic and succinic) under visible light radiation.

2. Materials and Methods

2.1. Materials

The chlorfenvinphos PESTANAL[®] with a purity of >95% was purchased from Sigma-Aldrich (Poznań, Poland). Physico-chemical characteristics of the compound is presented in Table 1. Modified catalysts obtained on the basis of titanium (IV) oxide (Sigma-Aldrich, Poznań, Poland) were used as catalysts for the pesticide decomposition process. The physico-chemical characteristics of commercial TiO₂ are summarized in Table 2. All chemicals were of analytical grade and the highest purity available.

Table 1. Physico-chemical characteristics of chlorfenvinphos.

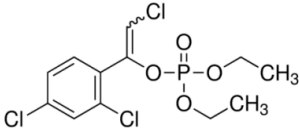
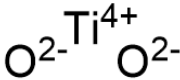
Chemical Structure	Physico-Chemical Properties	
	molecular formula	C ₁₂ H ₁₄ Cl ₃ O ₄ P
	molecular weight (g/mol)	359.57
	CAS number	470-90-6
	Water solubility at 20 °C (mg/L)	124.0
	Density (g/L)	1.36
	Vapor pressure (25 °C) (mmHg)	7.5 × 10 ⁻⁶
	logKOW (-)	3.81

Table 2. Physico-chemical characteristics of TiO₂.

Chemical Structure	Physico-Chemical Properties	
	Symbol, origin	P-25, Sigma-Aldrich (Poznań, Poland)
	Crystal structure	Anatase:rutile = 80:20
	Surface area (m ² /g)	35.0–65.0
	Particle size (nm)	21.0
	Density (g/cm ³)	4.26

2.2. Model Solution

Model solutions were prepared on the basis of deionized water with the addition of the analytical standard—chlorfenvinphos (CFVP) PESTANAL[®]. Solutions were prepared by diluting the chlorfenvinphos analytical standard in deionized water. The conductivity of model solutions was 0.196 mS/cm. To maintain a constant ionic strength, the model aqueous solutions contained 0.01 mol/L of NaNO₃. The solutions were stored at 4 °C in glass flasks, this ensured no adsorption of the pesticide particles on the walls of the vessel. In order to maintain satisfactory accuracy and repeatability of instrumental analysis, the initial concentration of the aqueous solution for all experiments was 1.0 mg/L.

The pH of the model solution before and after addition of the compound was 6.0. The pH of the solution was monitored using the Elmetron CPC-511 pH-meter (Zabrze, Poland).

2.3. Instrumental Analysis

The analytes contained in liquid samples before and after the advanced oxidation process were subjected to the HPLC chromatographic analysis with the UV detector model 1200 from Perlan Technologies (Warsaw, Poland) in accordance with PN-EN ISO 11369:2002 standard [21]. The analysis was preceded by the separation of the compound using the solid-phase extraction (SPE). Prior to the extraction, the particles of photocatalysts were separated from the samples using a filtration apparatus through a 0.45 μm filter made of cellulose acetate (Microlab Scientific Co., Ltd., USA). The filtration did not affect the retention of the tested compound on the filter. The extraction process was carried out on the CHROMABOND[®] C₁₈ ec columns. The extraction column was filled with a non-polar C18 sorbent (capacity of 6.0 mL, the adsorbent mass of 500.0 mg). The column bed was conditioned with methanol (5.0 mL) and deionized water (5.0 mL). Samples were dosed at flow rate of 5 mL/min. Then the columns were dried, in the first phase with air, then with inert gas (nitrogen). The compounds adsorbed on the bed were eluted with 1.0 mL of methanol with a 15 min retention time, then they were eluted with another 1.0 mL of methanol. The process was completed by concentrating the compound in vacuo with inert gas (nitrogen).

The extract was analysed using the HPLC liquid chromatograph (UV detector, $\lambda = 218 \text{ nm}$). The device was equipped with the Zorbax[®] SB-C18 packed column with dimensions of 15.0 cm \times 4.6 mm \times 5.0 μm .

2.4. Synthesis of Photocatalyst Samples

Modification of the photocatalysts is essentially aimed at obtaining active materials in visible light ($\lambda > 400 \text{ nm}$), and thus increasing the ability to absorb visible radiation. Another application of modifications (such as e.g., transition metals, ultrasound, activated carbon, polymers, elemental carbon, nitrogen, sulphur) is to increase adsorption of the pollutants, neutralization of intermediate decomposition products and better separation of TiO₂ suspension from the liquid phase after the process [22,23].

As part of the study, the commercial titanium (IV) oxide and two types of catalysts, consisting of titanium (IV) oxide and pyruvic or succinic acid, were evaluated. Each of the materials has been given an appropriate symbol (Table 3). The modified photocatalysts were obtained by the wet impregnation method, preparing a suspension of titanium dioxide in deionized water with the addition of an appropriate amount of acid. The mixture was shaken vigorously for 30 min in the dark, at room temperature, then dried at 100 °C for 16 h. Five pyruvic acid-modified photocatalysts and five succinic acid-modified photocatalysts were prepared. The photocatalysts contained various acid concentrations, i.e., 99:1; 90:10; 80:20; 50:50 and 20:80 (*w/w*). The dried catalysts were washed with distilled water to remove unbound acid and dried again at 100 °C for 16 h.

Table 3. Symbols of the photocatalysts.

Symbol	Explanation
TiO ₂	Pure Titanium(IV) Oxide
TiO ₂ /PA/99:1	TiO ₂ modified with pyruvic acid in a ratio of 99:1 (<i>w/w</i>)
TiO ₂ /PA/90:10	TiO ₂ modified with pyruvic acid in a ratio of 90:10 (<i>w/w</i>)
TiO ₂ /PA/80:20	TiO ₂ modified with pyruvic acid in a ratio of 80:20 (<i>w/w</i>)
TiO ₂ /PA/50:50	TiO ₂ modified with pyruvic acid in a ratio of 50:50 (<i>w/w</i>)
TiO ₂ /PA/20:80	TiO ₂ modified with pyruvic acid in a ratio of 20:80 (<i>w/w</i>)
TiO ₂ /SA/99:1	TiO ₂ modified with succinic acid in a ratio of 99:1 (<i>w/w</i>)
TiO ₂ /SA/90:10	TiO ₂ modified with succinic acid in a ratio of 90:10 (<i>w/w</i>)
TiO ₂ /SA/80:20	TiO ₂ modified with succinic acid in a ratio of 80:20 (<i>w/w</i>)
TiO ₂ /SA/50:50	TiO ₂ modified with succinic acid in a ratio of 50:50 (<i>w/w</i>)
TiO ₂ /SA/20:80	TiO ₂ modified with succinic acid in a ratio of 20:80 (<i>w/w</i>)

2.5. Experimental Procedures

2.5.1. Characterization of Photocatalysts Samples

The photocatalytic activity of each sample was determined by examining the degree of decomposition of chlorfenvinphos and conducting an analysis of the photocatalytic kinetics. The photocatalysts were examined by the diffuse reflection spectroscopy (UV-DRS) and the scanning electron microscopy (SEM). The UV-Vis photocatalysts absorption spectra were measured using the V-750 spectrophotometer (Cracow, Poland) made by Jasco. The morphology and structure of semiconductors were examined using the Hitachi SU-3500N electron microscope (SEM, Krefeld, Germany). The catalyst samples were applied to a graphite adhesive plaster and placed on a microscope (variable vacuum).

2.5.2. Effect of Different Dose of Catalysts

Studies on the selection of the optimal dose of the photocatalysts were carried out at room temperature and ambient pressure in a glass reactor of 500.0 mL volume. The ionic strength of the solution was maintained with 0.01 mol/L of NaNO_3 . The mixture containing pesticide at a concentration of 1.0 mg/L was placed on a magnetic stirrer and then mixed with the addition of selected catalysts in the dose range from 10.0 to 125.0 mg/L. The selected dose range is smaller than the optimal doses presented in the literature [24,25], while from the economic point of view, reduction of the amount of catalyst should be considered. For example, in the research of Garg et al. [26] the decomposition of bisphenol A was studied in the dose range from 20 to 175 mg/L. It should also be remembered that the intention of this study was to determine the basic operating parameters of the reaction system, so the tests were carried out under “ideal” conditions, e.g., without the influence of inorganic substances or other organic substances. Pure titanium (IV) oxide and two randomly selected modified semiconductors: $\text{TiO}_2/\text{PA}/99:1$ and $\text{TiO}_2/\text{SA}/80:20$ were used for the study. The source of Vis radiation was switched on immediately after the catalysts were introduced into the reaction mixture, therefore the results obtained in this step do not take into account the degree of the compound adsorption. The reaction mixture was irradiated with Vis continuously for 60 min. After that time, samples were taken for analysis. The 10 W tungsten lamp QTH10/M from Thorlabs Inc. (Newton, NJ, USA), located above the reaction vessel (Figure 1), was used for exposure. The lamp emits radiation with a wavelength $\lambda = 400\text{--}2200$ nm, but for the purpose of the study the FGS900M filter, mounted using a cage filter wheel (model LCFW5) system from Thorlabs Inc., was used to cut off the radiation spectrum bands above 710 nm. Thus the lamp emitted radiation in the visible light range ($\lambda = 400\text{--}710$ nm). The photodegradation process was carried out without adding an external oxygen source comes from an aeration pump. The only source of oxygen was water, in which the process was conducted. The impact of the presence of external oxygen source on the efficiency of the compound decomposition is discussed in Section 2.5.7.

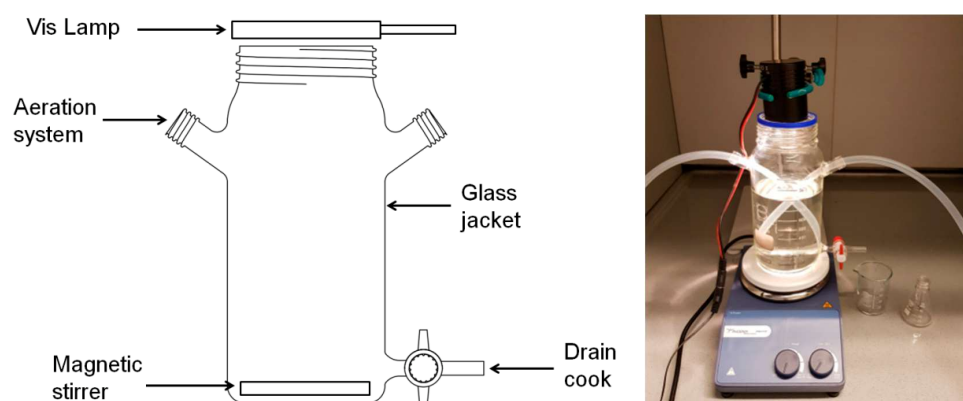


Figure 1. Scheme of conducting the chlorfenvinphos decomposition process under the influence of visible light.

2.5.3. Optimal Modification of the Catalysts

Based on the decomposition of chlorfenvinphos in the presence of pure TiO₂ and the photocatalysts modified with organic acids, as a result of irradiation of the model solutions with visible radiation, the catalysts were selected and further tested. The dose of photocatalysts was 50.0 mg/L. Tests were carried out under the same conditions as described in Section 2.5.2. The only change was the sampling times for testing. Irradiation was carried out continuously for 60 min, with samples for testing taken after 5, 10, 15, 30 and 60 min by means of a drain cook, which is an integral part of the reactor. The photodegradation process was carried out without oxygen present in the reaction system.

2.5.4. Optimal Adsorption Time

Determining the contact time of the adsorbate (CFVP) with the adsorbent (catalyst) is an important issue from the point of view of the process of pollutants removing. The initial volume under the study was 500.0 mL. An amount of pesticide was added to the model solution so that the final concentration of adsorbate was 1.0 mg/L. The dose of adsorbents was 50.0 mg/L. During the experiment, no aeration pump (oxygen source) was used. Sorption of pollutants proceeded in the dark. The test solution was placed on a magnetic stirrer for 30 min continuously, and samples were taken after 1, 3, 5, 8, 10, 15, 20, 25 and 30 min.

2.5.5. Effect of pH

As part of the experiments, the effect of the initial pH of the solution on the efficiency of decomposition of chlorfenvinphos was investigated. The following pH values were tested: pH = 3.0; pH = 6.0 and pH = 9.0. The pH was corrected with 0.1 mol/L of HCl or 0.2 mol/L of NaOH obtained from Sigma-Aldrich. The change in pH was monitored using the CPC-511 pH-meter from Elmetron (Zabrze, Poland). The model solution with a concentration of 1.0 mg/L was added before the pH was corrected. Then, after reaching the desired pH, appropriate amount of catalysts were added to the solution to the final dose of 50.0 mg/L. Before switching the radiation source, the 20-min contact time of the catalysts with the model solution has been provided (adsorption). Sorption of the pollutants proceeded in dark, then the Vis lamp was switched on. The study was carried out continuously for 60 min, with samples for chromatographic analysis taken after 5, 10, 15 and 30 and 60 min of the process duration. The photodegradation process did not take place with participation of oxygen supplied to the reaction system.

2.5.6. Deactivation Tests

Deactivation of the photocatalysts was carried out under similar conditions to those described in the previous sections. The pH of the model solution was 6.0. Studies on the determination of materials viability were carried out based on 5 cycles of the chlorfenvinphos decomposition at a constant catalyst concentration. The decomposition degree of the compound was determined after each cycle of the conducted decomposition. The duration of the photodegradation process was 60 min. After this time, samples were taken for analysis. Then another cycle of irradiation of the mixture was started, preceded by separation of the catalyst particles. The photocatalysts particles were recovered by filtering the reaction suspension through a filtration apparatus, equipped with a 0.45 µm membrane filter made of cellulose acetate (Microlab Scientific Co., Ltd.). The reaction vessel was flushed and the contents of the vessel were subjected to filtration. As part of preliminary tests, it was determined that the recovery rate of the catalyst particles was >99.9%. The photodegradation process did not take place in the presence of oxygen supplied to the reaction system.

2.5.7. Influence of Oxygen

In order to determine the effect of dissolved oxygen on the efficiency of the chlorfenvinphos photocatalytic oxidation, the tests were carried out comparatively, with and without the addition of

oxygen. The research procedure was similarly to the previous section. The photodegradation time was set to 60 min and after that time the samples were taken. An aeration pump (Miniboost 200, Aquael Company, Warsaw, Poland) with a capacity of 2×100 L/h was used as a source of oxygen.

2.5.8. Radical Scavenger Test

The radical scavenger test was used to determine the main radical species involved in the degradation of chlorfenvinphos. Scavengers inhibit the free radicals or deactivate them, thus preventing them from reaction with the compounds present in water. The testing procedure was carried out similarly to the previous studies. The ethylenediamine tetraacetate (EDTA-2Na) of 98.5% purity, hydroquinone of $\geq 99.5\%$ purity and methanol (MeOH) of 99.8% purity from Sigma-Aldrich were added to the test samples before adding the catalysts. The scavengers were always used in concentration of $D_{\text{scav.}} = 50.0 \mu\text{M}$.

All the experiments described in Sections 2.5.2–2.5.8 were carried out independently in triplicate. The data presented in the next sections include the average values.

2.6. Kinetics

Many studies suggest that the oxidation rate of organic substances fit with the Langmuir-Hinshelwood (L-H) kinetics model [27,28]. Under ideal conditions, the L-H model can be expressed by Equation (1). Based on this equation, the kinetics of the chlorfenvinphos decomposition was analysed and the following pseudo first-order reaction parameters were determined: reaction rate constant k , determination coefficient R^2 , and half-life $t/2$.

$$r = -\frac{dc}{dt} = \frac{k \times KC}{1 + KC} \quad (1)$$

where:

r —oxidation rate of pollutants, mg min/L

C —concentration of pollutants, mg/L

k —reaction rate constant, min^{-1}

K —constant balance

t —contact time, min

3. Results of Tests and Their Discussion

3.1. UV-DRS and SEM Test

The modification changed the optical properties of the commercial titanium (IV) oxide. The results are shown in Figure 2. The commercial TiO_2 shows an absorption edge at approx. 380 nm, while the modification of the photocatalysts shifted the absorption of light towards the visible light. Compared to the pure TiO_2 a shift was observed in the absorption maximum to a wavelength equal to $\lambda = 468$ nm for $\text{TiO}_2/\text{SA}/90:10$ and $\lambda = 528$ nm in the case of a semiconductor marked with a symbol $\text{TiO}_2/\text{PA}/90:10$. The band gap energy was calculated on the basis of [29]. Samples modified with organic acids did not show a sharp absorption edge as in the case of the pure TiO_2 and were characterized by having a “tail” reaching about 800 nm. The appearance of new absorption spectra may indicate changes in the structure of TiO_2 modified with organic acids, that were caused by reaction between the groups present on the surface of titanium dioxide and the products of acid decomposition [13].

Figure 3 shows micrographs obtained for the pure TiO_2 and titanium dioxide modified with pyruvic (90:10) and succinic (90:10) acid. The pure titanium (IV) oxide has a homogeneous, regular, spherical shape with a single particle size below 100 nm. Modified TiO_2 surface study showed that the modification of the photocatalyst does not significantly affect the shape of titanium (IV) oxide nanoparticles in comparison to the pure TiO_2 particles. However, after modification with

acid, the shape of the new semiconductor slightly lengthened, which could have contributed to the higher photocatalytic activity of the TiO₂/PA and TiO₂/SA particles in comparison to pure TiO₂ [30]. In addition, in the synthesized catalysts the TiO₂ particles were not found as complex of agglomerates as in the case of a commercial semiconductor. The dispersion of particles increases the specific surface area, which improves the photocatalytic properties of the catalysts labelled as TiO₂/PA/90:10 and TiO₂/SA/90:10 [31]. Studies shows that the increase in the specific surface area of the catalysts as a result of acid interaction may result from a change in the size of TiO₂ crystallites. Catalysts with smaller crystal sizes have a larger specific surface area, which increases the adsorption of pollutants and ensures higher photocatalytic activity. The study [32] showed that catalysts with smaller crystallite sizes have a larger surface area. Research conducted by Mair et al. [33] showed that a smaller size of crystallites affects a higher degree of adsorption and mineralization through a more of edges and corner sites for the formation of TiO³⁺ centers where O²⁻ radicals are formed. Apparently, the addition of acids increased the specific surface area by reducing particle agglomeration and reducing TiO₂ crystals. This in turn can affect the degree of interaction between the photocatalyst and organic pollutants.

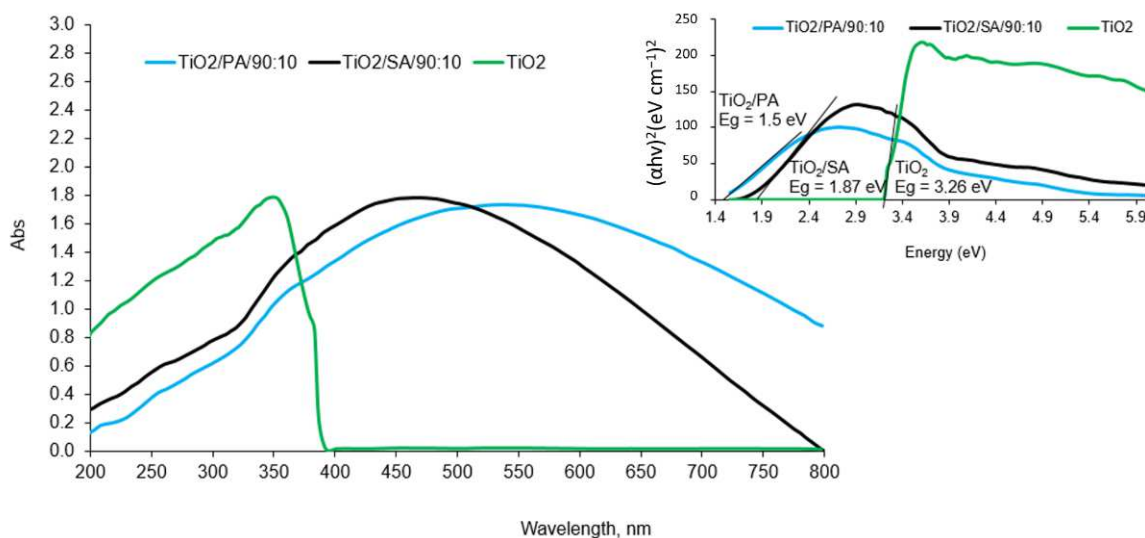
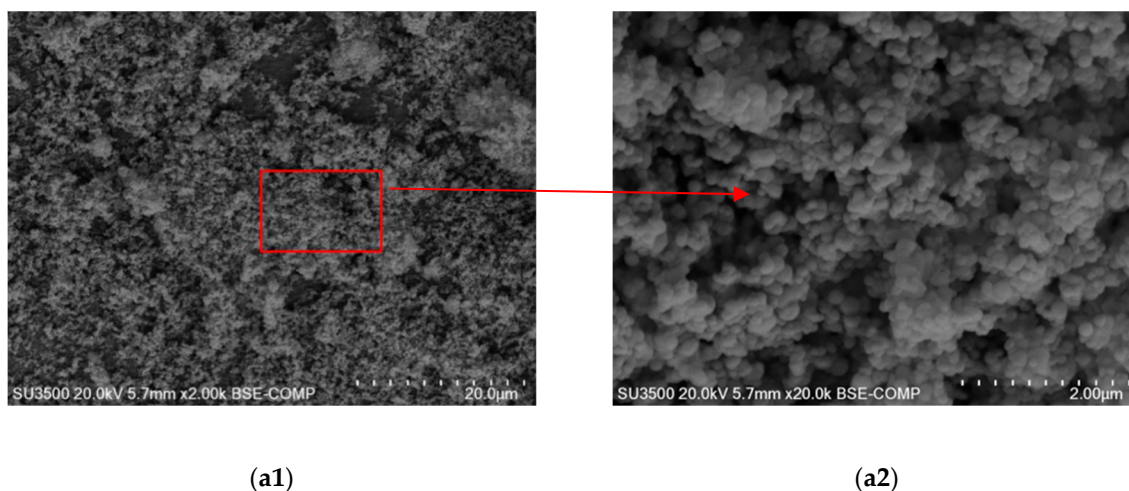


Figure 2. The UV-Vis spectra of the tested photocatalysts.



(a1)

(a2)

Figure 3. Cont.

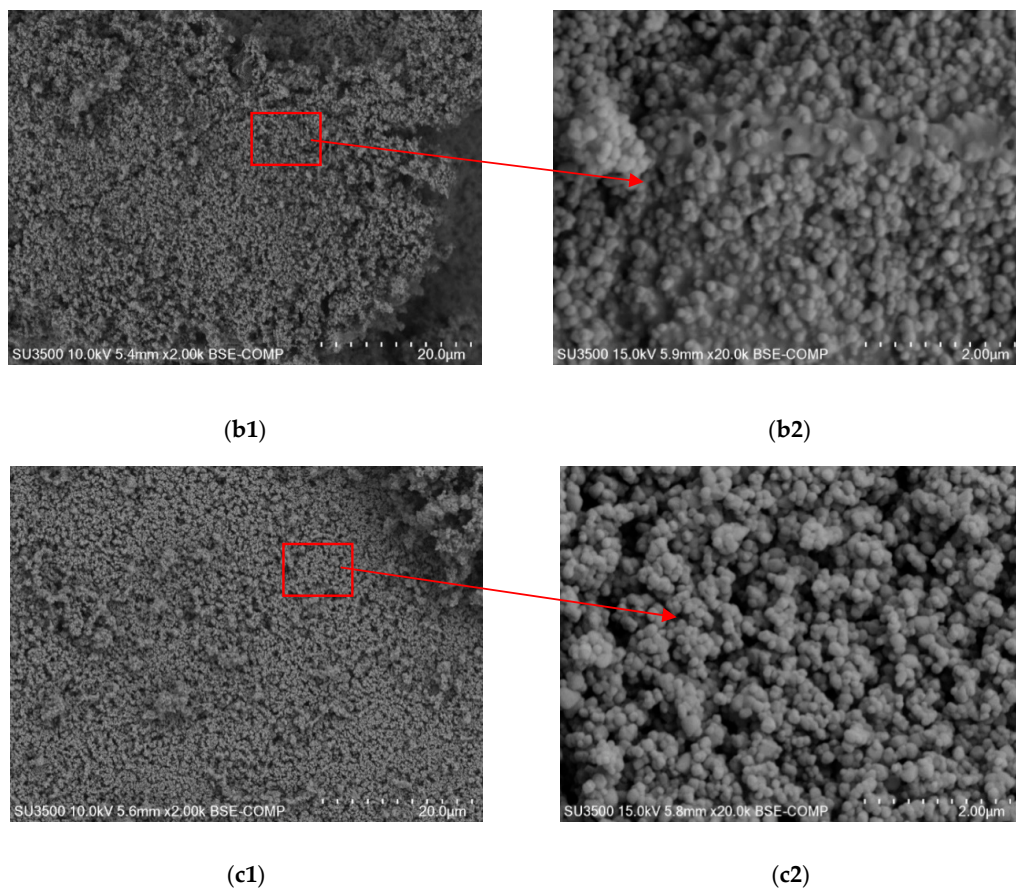


Figure 3. Comparison of SEM images for the pure TiO_2 (a1,a2) and the catalysts modified with pyruvic acid (b1,b2) and succinic acid (c1,c2) in proportions 90:10.

The values of the band gap energy and the location of valence and conduction bands are shown in Figure 4. The band gap energy was calculated according to [29]. The energy of the conduction band was calculated according to the formula $E_{\text{CB}} = E_{\text{VB}} - E_g$, while the energy of the valence band according to the formula $E_{\text{VB}} = 1.46 + 0.5E_g$ on the base of [34,35]. Due to the reduction of the band gap energy of the modified photocatalysts, the transfer of electrons from the valence band (VB) to the conductivity band (CB) is facilitated. This phenomenon has been commented in Section 3.8.

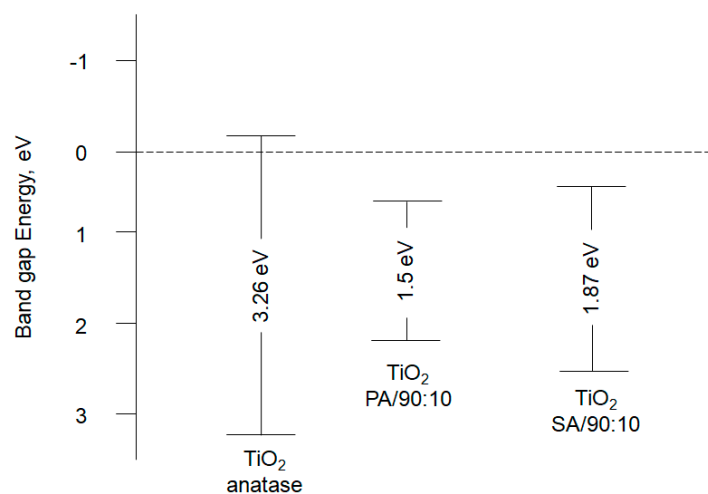


Figure 4. Valence and conduction bands of the tested photocatalysts.

3.2. Effect of Catalyst Dosage

Application of an optimal dose of a photocatalyst makes the decomposition process to be carried out in the most effective way. The photocatalyst dose limit value was determined based on the initial concentration of chlorfenvinphos removed from solution as well as the operating conditions and geometry of the reactor in which the decomposition was carried out.

The optimal dose of the catalysts used during the tests was determined experimentally. Therefore, the commercial titanium (IV) oxide and the selected photocatalysts doped with different amounts of acids ($\text{TiO}_2/\text{PA}/99:1$ and $\text{TiO}_2/\text{SA}/80:20$) and in the doses ranging from 10.0 to 125.0 mg/L were introduced into the model solution and irradiated with Vis. The presented results do not include adsorption of the compound. The phenomenon of the CFVP adsorption was investigated in Section 3.4. As shown in Figure 5, the dose of the catalyst had an impact on chlorfenvinphos degradation. In the low dose range of the tested materials (from 10.0 to 50.0 mg/L), an increase in the decomposition efficiency of the tested compound was observed. In turn, at higher doses (from 75.0 to 125.0 mg/L) the increase in decomposition compared to the dose of 50.0 mg/L was insignificant or lower. Therefore, it was determined that the decomposition of model compound occurs with the highest efficiency at the dose of 50.0 mg/L of the photocatalysts. Despite the fact that CFVP decomposition was higher in the presence of the dose of 75 mg/L than 50 mg/L, the difference between this efficiency was insignificant (~1%). In addition, economic aspects were also taken account. Slight differences in the CFVP removal and the risk of faster sedimentation of the catalysts determined the choice of the 50 mg/L dose. That dose was chosen as optimal for further study. The increase in efficiency of the chlorfenvinphos decomposition along with the increase in the catalysts doses can be attributed to the adsorption of the compound on the surface of the catalysts and inside its pores, as well as the generation of more free radicals, that leads to a higher degradation of the pollutant. Whereas the reduction in the photodegradation efficiency can be explained by faster sedimentation of the catalyst particles to the bottom of the reactor, the effect of radiation shielding, and the effect of screening of the excessive amount of particles. Particular importance is attached to the shielding effect, which results from the negative impact of pollutants present in the solution, and a high dose of the photocatalyst. In the study we probably deal with the second case, i.e., the increase in turbidity of the solution, caused by too high dose of catalysts, limits the possibility of radiation reaching the surface of the catalyst. These phenomena depend on the geometry of the reactor and the operating conditions of the system. The similar results were noted by the authors of the works [24,36–38]. However, as part of this research stage, it can be stated that the modification of commercial TiO_2 with organic acids brings satisfactory results. First of all, the addition of acids, in particular succinic acid, caused that the degree of the CFVP photodegradation was not only higher but was similar in almost whole range of the tested doses. This may indicate a positive effect of succinic acid on the elimination of radiation shielding phenomenon.

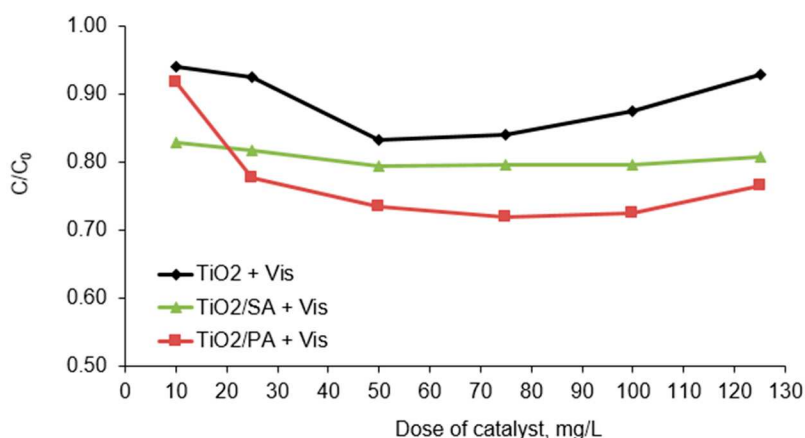


Figure 5. Decomposition degree of chlorfenvinphos in the presence of the selected catalysts. Conditions of experiment: $C_0 = 1.0$ mg/L; $V_r = 500.0$ mL; $t_{ir} = 60.0$ min; pH = 6.0.

3.3. Modification of the Catalyst

The results of the conducted study, on the basis of which the optimal modification of the photocatalysts was selected, are shown in Figure 6. The presented results do not take into account the adsorption process. The phenomenon of the CFVP adsorption was studied in Section 3.4. Among the tested pyruvic and succinic acid-modified catalysts, the highest efficiency was observed for the materials mixed in proportions 90:10. For the pyruvic acid-modified catalyst, the degree of the chlorfenvinphos decomposition was 51.0% after 60.0 min of the reaction. The use of larger amounts of acid reduced the efficiency of the compound decomposition. For example, for the catalyst labelled as 20:80, i.e., the highest of the tested acid content, the degree of decomposition decreased to 13.0% after 60 min of the photodegradation process. A similar phenomenon was observed for the succinic acid-modified catalyst. Increasing the share of acid in the total mass of the catalyst caused a reduction of the efficiency of the chlorfenvinphos degradation, from 33.0% for the catalyst with the symbol 90:10 to about 20.0% for materials with a higher participation of acid.

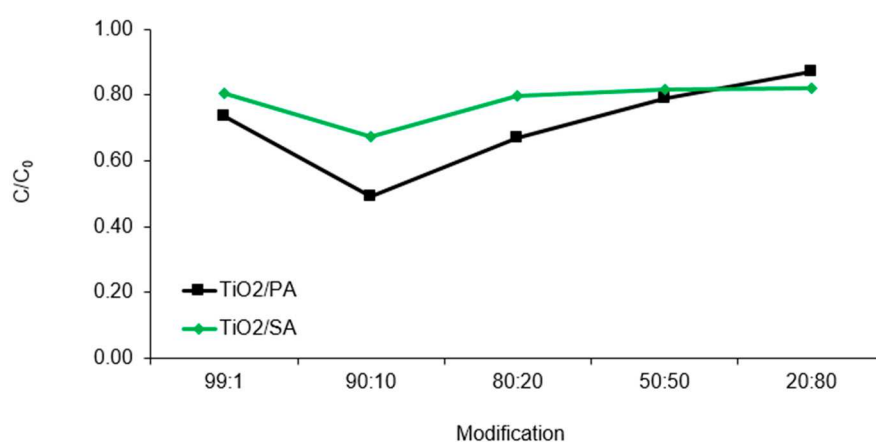


Figure 6. Chlorfenvinphos decomposition in the presence of various modifications of photocatalysts. Condition of experiment: $C_0 = 1.0$ mg/L; $D_c = 50.0$ mg/L; $V_r = 500.0$ mL; $t_{ir} = 60.0$ min; pH = 6.0.

The photodegradation processes catalysed by TiO₂/PA/90:10 and TiO₂/SA/90:10 proceeded more intensively compared to the other tested materials, as evidenced by the kinetic parameters presented in Table 4. The kinetics of the conducted processes indicated that the reaction rate constant k for the TiO₂/PA/90:10 catalyst is more than three times higher than the value of k determined for other pyruvic acid-modified catalysts. Also for the TiO₂/SA/90:10 catalyst the reaction rate constant was twice as high compared to other modifications carried out with succinic acid. The shortest half-life $t/2$ was observed for the material with the symbol TiO₂/PA/90:10 (63 min). It also turned out that the use of too much of the pyruvic acid in the TiO₂/PA/20:80 catalyst resulted in elongation of the decomposition half-life to 315.0 min, and it was longer time compared to the pure titanium (IV) oxide.

Table 4. Impact of the TiO₂ modification on the pseudo first-order parameters.

TiO ₂ /PA				TiO ₂ /SA			
Symbol	k , 1/min	R^2	$t/2$, min	Symbol	k , 1/min	R^2	$t/2$, min
TiO ₂	0.0027	0.86	257.0	TiO ₂	0.0027	0.86	257.0
99:1	0.0046	0.87	151.0	99:1	0.0034	0.94	204.0
90:10	0.0110	0.93	63.0	90:10	0.0064	0.93	108.0
80:20	0.0063	0.93	110.0	80:20	0.0039	0.91	178.0
50:50	0.0036	0.81	193.0	50:50	0.0031	0.86	224.0
20:80	0.0022	0.91	315.0	20:80	0.0031	0.80	224.0

Although it was found higher CFVP decomposition compared to the pure TiO_2 , the increase in the amount of acid contributed to the decrease in efficiency of the pollutant decomposition. The decrease in the photocatalytic activity of the catalysts could have been associated with the blocking of active sites on the photocatalyst surface, therefore the particles of CFVP could not attach to them and undergo decomposition. In addition, higher amounts of acids might cause a weaker shift of the absorption band in the visible light compared to the optimal dopant of acid. However, at the smallest proportion (99:1) there could also be no shift of the absorption band in the visible light, which for the pure TiO_2 is $\lambda < 400$ nm. It is also worth adding that during preparation procedure the pyruvic acid-modified catalysts changed colour from white to yellow, while those modified with succinic acid changed into dark orange. The sensibilization effect could also contribute to higher activity of the modified semiconductors. The color change of the photocatalysts may results from the structure of titanium (IV) oxide. It is characterized by nearly 40% of incompletely coordinated Ti atoms that can accept two lone electron pairs from electron donors (succinic or pyruvic acids). The color change of titanium dioxide can be attributed to the charge transfer from PA/SA to TiO_2 as a result of which the PA- TiO_2 or SA- TiO_2 complex is formed. The sensibilization of catalysts by means of other admixtures was shown in the studies [29,39,40].

3.4. Optimal Adsorption Time

In the next step the optimal sorption time was determined. It is important to consider the contact time from the point of view of the proper distribution of the catalyst in the whole volume of the solution and ensuring the highest degree of adsorption of the contaminant before starting the photodegradation process. It was observed that in the case of the tested photocatalysts the CFVP adsorption takes place in the first 20 min of the experiment (Figure 7). This time is needed to reach the adsorption-desorption balance. After 20 min of contact time, the achieved degree of removal was 16.0%, 33.0%, and 17.0% respectively for the TiO_2 , $\text{TiO}_2/\text{PA}/90:10$ and $\text{TiO}_2/\text{SA}/90:10$. In the following minutes, the CFVP adsorption was not significant. The degree of compound removal was the highest after 20 min of time, but already in the first minute about 2% removal of chlorfenvinphos was obtained, which is related to the physical properties of the tested materials, i.e., the effect of their specific surface area, which for the commercial TiO_2 is about 50 ± 15.0 m^2/g . For the pyruvic acid-modified TiO_2 , the degree of CFVP removal was twice as high as for the pure TiO_2 and succinic acid-modified TiO_2 . Chemical modification of inorganic titanium (IV) oxide particles using the organic particles, is of particular importance and causes stabilization of the TiO_2 nanoparticles, prevents agglomeration of the catalyst particles and improves the surface properties. The results suggest that the specific surface area of the catalyst may have been increased by pyruvic acid, resulting in an increase in the amount of chlorfenvinphos adsorbed by this material. The increase in the specific surface area is important in terms of the amount of active sites of TiO_2 on which its photocatalytic activity depends. As the surface increases, the amount of adsorbed pollutants and the amount of free radicals increases. Similar conclusions were drawn in studies [32,39,41].

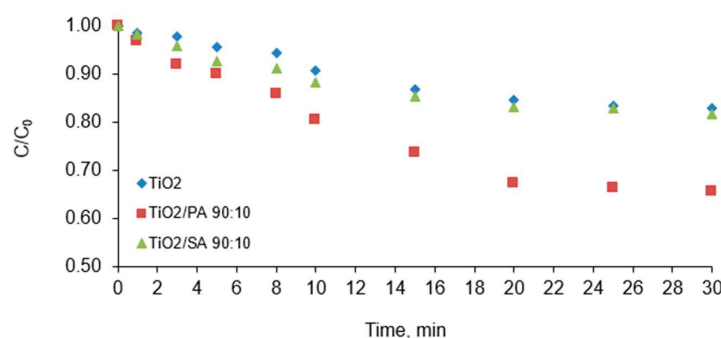


Figure 7. Effect of the contact time on the degree of chlorfenvinphos adsorption. Condition of experiment: $C_0 = 1.0$ mg/L; $D_c = 50.0$ mg/L; $V_r = 500.0$ mL; $t_{\text{sor}} = 30.0$ min; pH = 6.0.

3.5. Effect of pH on the Chlorfenvinphos Degradation

The decomposition of chlorfenvinphos catalysed by the selected semiconductors was tested in the pH range from 3.0 to 9.0 for 60 min. As shown in Figure 8, the change in the initial pH of the solution affected on the CFVP decomposition efficiency. After 60 min of irradiation at the pH = 6.0, the 30% decomposition degree of CFVP in the process catalysed by pure TiO₂ was found. This value was the highest compared to other pH tested and was associated with the value of semiconductor isoelectric point (pH_{pzc}). For the titanium dioxide particles, the value of pH_{pzc} is in the range from 6.0 to 6.5, on average about 6.25 [42,43]. This is due to the effect of pH on the surface charge of TiO₂. In an alkaline environment (pH > 6.0) the surface of a pure semiconductor is positively charged, while in an acidic (pH < 6.0) it is negatively charged. After 60 min of irradiation the concentration of CFVP was reduced by 24% at pH = 9.0, while the lowest degree of the CFVP decomposition was observed at the lowest of the tested pH, i.e., pH = 3.0 (28.0%). However, the change in the pH of the model solution had the greatest effect on the adsorption of the compound. The degree of the CFVP adsorption at pH = 3.0 was the highest in each of the tested catalysts. For example, adsorption of the compound by pyruvic acid-modified semiconductor at pH = 3.0 was 47% compared to 25% at pH = 9.0. In the presence of the catalyst labelled as TiO₂/SA/90:10 the change in pH of the model solution did not have a significant impact on the final chlorfenvinphos decomposition. After 60 min of the photocatalysis, the CFVP decomposition was about 50%. Process carried out in the presence of TiO₂/SA/90:10 remained active over a wide pH range, suggesting it has low sensitivity to pH changes. The analysis of photocatalytic oxidation kinetics also demonstrated similarity in this case (Table 5). The reaction rate constant was between $k = 0.0063$ and $k = 0.0082 \text{ min}^{-1}$, while the half-life was between 85 and 102 min. In turn, the highest degree of the CFVP decomposition was observed in the pH = 3.0, to which the pyruvic acid-modified catalyst was added. After 60 min of irradiation, the calculated decomposition degree was 72%, and it was a value of 12% and 22% higher for pH = 6.0 and pH = 9.0 respectively. The mathematically calculated half-life was determined at $t/2 = 67.0$ min. Due to the high adsorption potential of the TiO₂/PA/90:10 semiconductor, tested compound was more degraded as a results the generated free radicals. The change in pH of the model solution directly affects the photocatalyst surface charge, its hydrophobic properties and the amount of generated radicals [44]. The change in pH also affects the change in the micropollutants electric charge, thus resulting in a change in their susceptibility to adsorption on the catalyst surface. The CFVP dissociation constant pK_a has not been determined, but based on the analysis of dissociation constants of other organophosphorus pesticides it can be concluded that this pesticide is negatively charged at pH > 6, therefore it is better adsorbed at lower pH. For organic pollutants (e.g., azo dyes), similar conclusions were made by Alkaim et al. (2014) [45]. At pH <6, strong dye adsorption was observed on TiO₂ particles as a result of electrostatic attraction of positively charged TiO₂. At pH >6.8, negatively charged dye particles are repelled. Modification of the TiO₂ surface with pyruvic acid could cause change in the surface properties of titanium (IV) oxide, hence the high degree of chlorfenvinphos decomposition resulted from the generation of more oxidizing radicals. A similar explanation was proposed by Fernandez-Domene et al. (2019) [46].

Table 5. Effect of pH on the kinetics of the process.

pH	Catalyst	k , 1/min	R^2	$t/2$, min
3	TiO ₂	0.0019	0.85	365.0
	TiO ₂ /PA/90:10	0.0104	0.97	67.0
	TiO ₂ /SA/90:10	0.0063	0.95	110.0
6	TiO ₂	0.0031	0.94	224.0
	TiO ₂ /PA/90:10	0.0084	0.91	83.0
	TiO ₂ /SA/90:10	0.0082	0.98	85.0
9	TiO ₂	0.0027	0.82	257.0
	TiO ₂ /PA/90:10	0.0057	0.82	122.0
	TiO ₂ /SA/90:10	0.0078	0.86	89.0

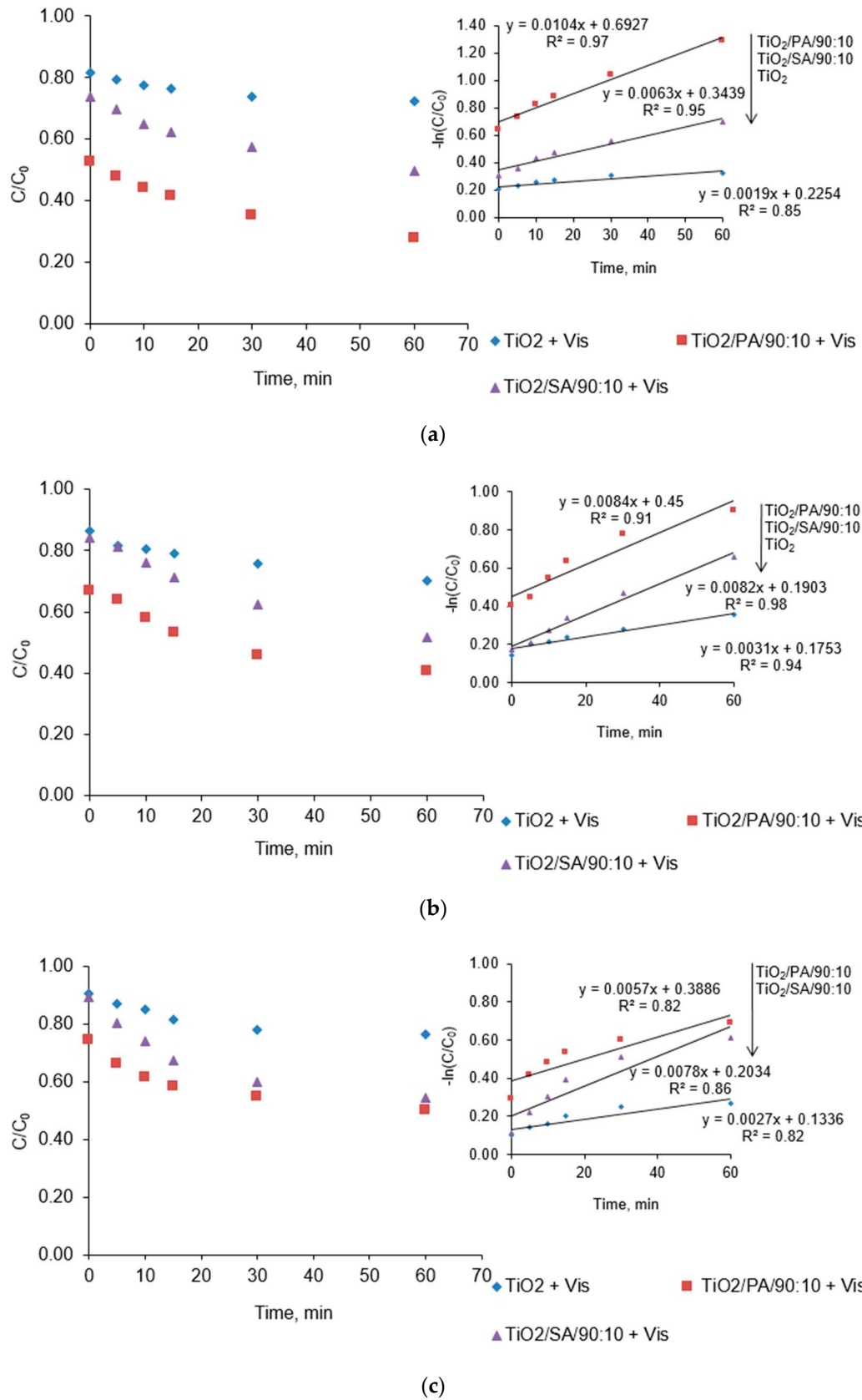


Figure 8. Reduction in the initial concentration of CFVP in the model solution at (a) pH = 3.0, (b) pH = 6.0, (c) pH = 9.0. Conditions of experiment: $C_0 = 1.0$ mg/L; $D_c = 50.0$ mg/L; $V_r = 500.0$ mL; $t_{\text{sor}} = 20.0$ min; $t_{\text{ir}} = 60.0$ min.

3.6. Lifetime of the Catalysts

Pure TiO_2 , $\text{TiO}_2/\text{PA}/90:10$ and $\text{TiO}_2/\text{SA}/90:10$ catalyst were used to determine the possibility of photocatalysts reuse. The experiment was carried out in five decomposition cycles of chlorfenvinphos. After the first cycle, the catalysts were separated from the solution and used for further cycles. Easier separation of the modified catalysts from the solution compared to pure TiO_2 has been found. For pure TiO_2 the process of filtering the reaction slurry required five times flushing, while for the modified TiO_2 the reactor was flushed three times. The particles of modified catalysts sedimented after about 10 min, while the commercial titanium (IV) oxide particles after about 30 min. The similar separation tests were conducted by Liu et al. (2007) [47] in which the TiO_2 modified with activated carbon sedimented after 5 min, while the pure titanium dioxide after 20 min. Despite faster sedimentation of modified photocatalysts, their performance was still higher than in commercial TiO_2 .

The results presented in Figure 9 show that activity of pure TiO_2 during 5 cycles decreased from 27% to 2% (reduction of efficiency by 25%). However, the decomposition of CFVP in the presence of $\text{TiO}_2/\text{PA}/90:10$ decreased after 5 cycles by 12%, while the decomposition efficiency was still high (50%) after the fifth cycle. The decomposition of chlorfenvinphos catalysed by $\text{TiO}_2/\text{SA}/90:10$ reached value of 36% after the fifth cycle, while the decomposition degree decreased by 10% in comparison to the first cycle. The results of this experiment are extremely important from the practical point of reuse of the materials for pollutants removing from water and wastewater, especially from the economic point of view. The phenomenon of reducing the efficiency of the CFVP decomposition on commercial TiO_2 is associated with the blocking of active sites on the catalyst surface by the intermediate decomposition products, formed during the process. It is a competitive process in relation to the decomposition of compound, resulting in a reduction of the activity of the catalysts. The modifications of the commercial TiO_2 probably reduced the phenomenon of formation of the TiO_2 agglomerates, so there was no active surface reduction effect, and thus it was possible to generate more free radicals. In addition, the organic acids used in the study are electron acceptors, which prevents recombination of electron-hole pairs [48]. The results indicate that the proposed method creates promising possibilities for the reuse and applied in practice for the degradation of chlorfenvinphos with great efficiency.

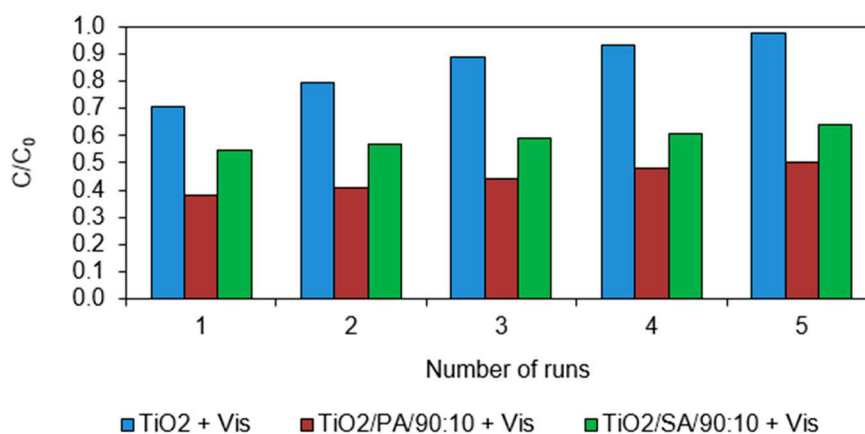


Figure 9. Effect of the number of cycles on the CFVP decomposition on the tested catalysts. Conditions of experiment: $C_0 = 1.0$ mg/L; $D_c = 50.0$ mg/L; $V_r = 500.0$ mL; $t_{\text{SOR}} = 20.0$ min; $t_{\text{ir}} = 60.0$ min.

3.7. Effect of Oxygen

A comparative assessment was carried out for the chlorfenvinphos photocatalysis process with and without oxygen. Based on the results presented in Figure 10 it can be concluded that the presence of dissolved oxygen in the reaction mixture plays a significant role in the process of removing chlorfenvinphos. It should be emphasized that the results presented in earlier sections concerned the processes without the oxygen in the reaction system. After 60 min of the process, the CFVP decomposition was about 27%, 63%, and 48% for pure TiO_2 , $\text{TiO}_2/\text{PA}/90:10$ and $\text{TiO}_2/\text{SA}/90:10$

respectively. Conducting the process of chlorfenvinphos decomposition with aeration resulted in an increase in the efficiency of the degradation process by about 20%. The increase in the efficiency of reactions carried out in the presence of oxygen was also confirmed on the base of reaction kinetics analysis (Table 6). Oxygen introduced into the reaction system contributes to a more effective decomposition of CFVP, reducing the half-life from 257 min to 98 min in the presence of the pure titanium (IV) oxide. The mathematically calculated half-life of CFVP has been reduced by about two times in the presence of the modified photocatalysts. The reason for this phenomenon is adsorption of oxygen on the catalysts surface. Oxygen is an electron acceptor and prevents the recombination of the electron-hole pairs. In addition, oxygen participates in the oxidation reaction of the chlorfenvinphos and intermediate products formed during the reaction [49,50].

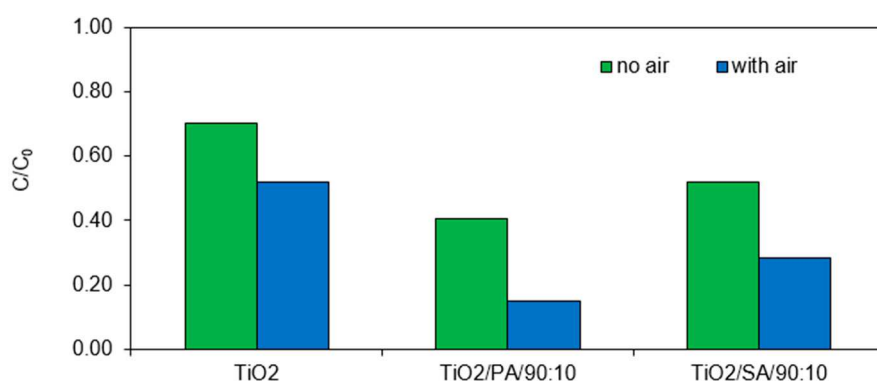


Figure 10. The efficiency of the chlorfenvinphos photodegradation in the presence of selected photocatalysts, with and without additional aeration. Conditions of experiment: $C_0 = 1.0$ mg/L; $D_c = 50.0$ mg/L; $V_r = 500.0$ mL; pH = 6.0; $t_{sor} = 20.0$ min; $t_{ir} = 60.0$ min.

Table 6. Effect of aeration of systems on the process kinetics.

Without Aeration				With Aeration			
Symbol	k , 1/min	R^2	$t/2$, min	Symbol	k , 1/min	R^2	$t/2$, min
TiO ₂	0.0031	0.94	224.0	TiO ₂	0.0071	0.92	98.0
TiO ₂ /PA/90:10	0.0084	0.91	83.0	TiO ₂ /PA/90:10	0.0255	0.97	27.0
TiO ₂ /SA/90:10	0.0082	0.98	85.0	TiO ₂ /SA/90:10	0.0178	0.93	39.0

3.8. Radical Scavengers Test

In order to identify the main active species involved in the CFVP photodegradation, tests were carried out. Methanol, hydroquinone and EDTA-2Na were used in the experiments as OH^\bullet scavengers, $\text{O}_2^{\bullet-}$ scavengers and h^+ holes scavengers respectively. These compounds are commonly used as radical scavengers by the authors of many papers [51–55]. The scavengers were always used in the concentration of 50.0 μM . The effect of individual scavengers is shown in Figure 11. In general, as a result of irradiating solutions with the Vis light, the degree of the CFVP degradation decreased after the addition of the $\text{O}_2^{\bullet-}$ scavenger (hydroquinone) and the hole scavenger (EDTA-2Na) (Figure 10a). On the other hand, the addition of the OH^\bullet radical scavenger did not reduce the effectiveness of pesticide degradation. In the presence of pure titanium (IV) oxide, the reduction of CFVP concentration (in the range from 15 to 19%) was mainly due to the adsorption of the pesticide by the adsorbent (TiO₂). In the TiO₂/Vis system, the inhibition of the chlorfenvinphos decomposition by the addition of methanol is due to the fact that it is partially activated by visible radiation, however, if solar radiation is used, only 3–5% of the energy can be used for the TiO₂ activation [56]. The addition of hydroquinone and EDTA-2Na to the TiO₂/VIS system did not cause significant inhibition of the process. As shown in Figure 10b,c, addition of $\text{O}_2^{\bullet-}$ and h^+ scavengers in the systems of TiO₂/PA and TiO₂/SA contributed to significant inhibition of the CFVP decomposition process. For example, in the system of TiO₂/PA/90:10

the pesticide degradation rate after adding hydroquinone has decreased from $k = 0.046 \text{ min}^{-1}$ (control) to $k = 0.0024 \text{ min}^{-1}$ (Table 7). The half-life of chlorfenvinphos under these conditions has lengthened from 151.0 min to 289.0 min and 231.0 min after adding hydroquinone and EDTA-2Na respectively. Similar effects were observed for the $\text{TiO}_2/\text{SA}/90:10$. The reaction rate constant of the control sample decreased from $k = 0.039 \text{ min}^{-1}$ ($t/2 = 462.0 \text{ min}$) to $k = 0.026 \text{ min}^{-1}$ ($t/2 = 267.0 \text{ min}$) after adding EDTA-2Na. The addition of methanol as an OH^\bullet inhibitor does not significantly reduce the rate of CFVP degradation. Therefore it can be concluded that in the photodegradation process of the tested pesticide, the most active radical is $\text{O}_2^{\bullet-}$, then h^+ and least OH^\bullet .

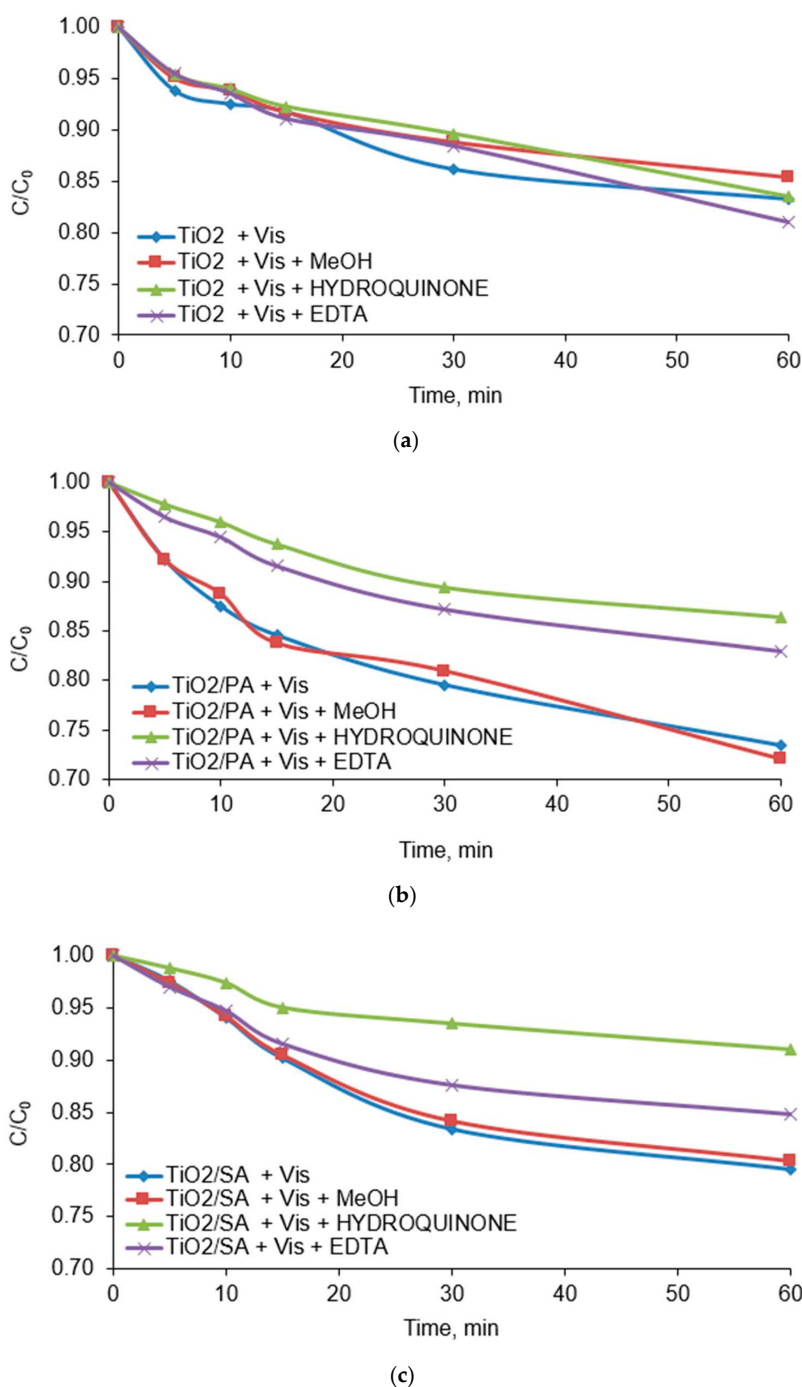


Figure 11. Photodegradation of the CFVP catalysed by (a) TiO_2 , (b) $\text{TiO}_2/\text{PA}/90:10$ and (c) $\text{TiO}_2/\text{SA}/90:10$ in the presence of radical scavengers. Conditions of experiment: $C_0 = 1.0 \text{ mg/L}$; $D_c = 50.0 \text{ mg/L}$; $V_r = 500.0 \text{ mL}$; $\text{pH} = 6.0$; min ; $t_{\text{ir}} = 60.0 \text{ min}$, $D_{\text{scav.}} = 50.0 \text{ }\mu\text{M}$.

Table 7. Effect of radical scavengers on photodegradation kinetics.

Catalyst	Scavenger	<i>k</i> , 1/min	<i>R</i> ²	<i>t</i> /2, min
TiO ₂	Control	0.0027 *	0.86	257.0
	MeOH	0.0023	0.87	301.0
	Hydroquinone	0.0027	0.94	257.0
	EDTA	0.0032	0.95	217.0
TiO ₂ /PA/90:10	Control	0.0046	0.87	151.0
	MeOH	0.0049	0.90	141.0
	Hydroquinone	0.0024	0.92	289.0
	EDTA	0.0030	0.92	231.0
TiO ₂ /SA/90:10	Control	0.0039	0.91	178.0
	MeOH	0.0037	0.91	187.0
	Hydroquinone	0.0015	0.90	462.0
	EDTA	0.0026	0.88	267.0

* The difference between values *k*, *R*², and *t*/2 presented in Sections 3.5 and 3.6 and the values in the Table above results from the fact that the CFVP adsorption is included in the mentioned sections.

The dominance of O₂^{•−} radicals may result from the reduction in the size of the band gap energy of the synthesized catalysts. The values of the band gap energy and the location of valence and conduction bands were shown in Section 3.1 (Figure 4). Due to the reduction of the band gap energy of the modified photocatalysts, the transfer of electrons from the valence band (VB) to the conductivity band (CB) is facilitated. Along with the transfer of electron, an electron hole (h⁺) is created, i.e., an unoccupied energy level that is involved in the photooxidation processes of pollutants adsorbed on the surface of the TiO₂/PA and TiO₂/SA photocatalysts. The more electrons (e[−]) go into the conductivity band, the more O₂^{•−} radicals are generated.

4. Summary

A TiO₂/PA and TiO₂/SA photocatalysts with visible-light photocatalytic activity in the chlorfenvinphos pesticide degradation was synthesized. It was found that the pyruvic and succinic acid can be used for modification of the commercial TiO₂ and improvement of its photocatalytic activity.

Modification of the commercial titanium (IV) oxide with organic acids allowed to decompose the pesticide under the influence of visible light. The effect of photocatalysts dose on the chlorfenvinphos decomposition efficiency was found. Too low dose contributed to the unsatisfactory parameters of the compound decomposition. The high dose caused too fast sedimentation of the catalysts and their photooxidizing potential was not used. The dose of 50 mg/L was chosen as the optimal dose of the photocatalysts.

The use of modification extended the life of the catalysts with high photodegradation efficiency. Moreover, in the presence of dissolved oxygen the degree of the compound degradation increased by approximately 20%. However, the oxidation processes of chlorfenvinphos, catalysed by the modified TiO₂, were more effective even without the introduction of an additional source of oxygen.

Due to the surface charge of the catalysts, the processes carried out in the presence of the commercial TiO₂ were most effective at pH close to the isoelectric point value (pH_{pzc}), i.e., at the pH = 6.0. In turn, the value of the pH_{pzc} point of the modified photocatalysts probably changed, because at low values (pH = 3.0) the chlorfenvinphos photodegradation was the most effective.

The dominant species involved in the CFVP photodegradation process were peroxide radicals and electron holes. The hydroxyl radicals were least involved in the CFVP decomposition process.

The photodegradation process conducted in the presence of the modified composites increases the rate of the chlorfenvinphos degradation, as indicated by the analysis of the pseudo first-order parameters. The half-life of the tested compound was on average three times lower than in the case of solutions containing the pure TiO₂.

According to the presented results, higher photocatalytic activity of the TiO₂/PA and TiO₂/SA can be attributed to: reducing the phenomenon of the TiO₂ agglomerate formation, which in turn led to the increase in size of the active surface, and thus TiO₂ activity (a); increase in specific surface area of the modified photocatalysts, thus increasing the adsorption capacity (b); inhibition of transformation of anatase into rutile by eliminating formation of the structural defects during modified catalysts preparation (c); slowing down the recombination process of electron-hole pairs through the separation of excited charges (d); reduction of the band gap energy relative to the pure titanium dioxide (e). The photooxidation of chlorfenvinphos under the influence of visible light could also be possible as a result of photosensibilization of the commercial TiO₂ due to the transfer of electrons from PA/SA to the TiO₂ conductivity band and appearing of a new C-O-Ti bond (shift of the absorption band towards longer waves $\lambda > 400$ nm), where the elemental carbon (C) comes from the pyruvic or succinic acid [18,19,57,58].

Funding: This research was funded by POLISH minISTRY OF SCIENCE AND HIGHER EDUCATION, grant number No. 11158029-340.

Conflicts of Interest: The authors declare no conflict of interest.

References

1. Ravoet, J.; Reybroeck, W.; de Graaf, D.C. Pesticides for apicultural and/or agricultural application found in belgian honey bee wax combs. *Bull. Env. Contam. Toxicol.* **2015**, *94*, 543–548. [CrossRef] [PubMed]
2. Laws, E.A. (Ed.) *Environmental Toxicology: Selected Entries from the Encyclopedia of Sustainability Science and Technology*; Springer-Verlag: New York, NY, USA, 2013. [CrossRef]
3. Mahdy, F.M.; El-Maghraby, S.I. Effect of processing on 14C-Chlorfenvinphos residues in maize oil and bioavailability of its cake residues on rats. *Bull. Environ. Contam. Toxicol.* **2010**, *84*, 582–586. [CrossRef] [PubMed]
4. Environment Agency. *Welsh Steep Dip Monitoring Programme 1999*; Environment Agency Wales: Cardiff, UK, 2000.
5. Boxall, A.B.A.; Fogg, L.A.; Blackwell, P.A.; Blackwell, P.; Kay, P.; Pemberton, E.J.; Croxford, A. Veterinary Medicines in the Environment. In *Reviews of Environmental Contamination and Toxicology*; Reviews of Environmental Contamination and Toxicology; Springer: New York, NY, USA, 2004; pp. 1–91. [CrossRef]
6. State Environmental Monitoring, Results of Surface Water Tests-Rivers. 2016. Available online: http://www.katowice.wios.gov.pl/monitoring/informacje/stan2016/wody_pow/rzeki.pdf (accessed on 5 November 2019).
7. Ismael, M. Highly effective ruthenium-doped TiO₂ nanoparticles photocatalyst for visible-light-driven photocatalytic hydrogen production. *New J. Chem.* **2019**, *43*, 9596–9605. [CrossRef]
8. Deng, Y.; Zhao, R. Advanced oxidation processes (AOPs) in wastewater treatment. *Curr. Pollut. Rep.* **2015**, *1*, 167–176. [CrossRef]
9. Seery, M.K.; George, R.; Floris, P.; Pillai, S.C. Silver doped titanium dioxide nanomaterials for enhanced visible light photocatalysis. *J. Photochem. Photobiol. A Chem.* **2007**, *189*, 258–263. [CrossRef]
10. Xing, B.; Shi, C.; Zhang, C.; Yi, G.; Chen, L.; Guo, H.; Huang, G.; Cao, J. Preparation of TiO₂/Activated Carbon Composites for Photocatalytic Degradation of RhB under UV Light Irradiation. Available online: <https://www.hindawi.com/journals/jnm/2016/8393648/> (accessed on 20 November 2019).
11. Reddy, P.A.L.; Reddy, P.V.L.; Kwon, E.; Kim, K.-H.; Akter, T.; Kalagara, S. Recent advances in photocatalytic treatment of pollutants in aqueous media. *Environ. Int.* **2016**, *91*, 94–103. [CrossRef]
12. Zawadzki, P.; Kudlek, E.; Dudziak, M. Influence of the photocatalyst type and pH of solution on photocatalytic decomposition efficiency of bisphenol A. *Proc. ECOPELE* **2017**, *11*, 661–669. [CrossRef]
13. Mert, E.H.; Yalçın, Y.; Kılıç, M.; San, N.; Çınar, Z. Surface modification of TiO₂ with ascorbic acid for heterogeneous photocatalysis: theory and experiment. *J. Adv. Oxid. Technol.* **2016**, *11*, 199–207. [CrossRef]
14. D'Amato, C.A.; Giovannetti, R.; Zannotti, M.; Rommozzi, E.; minicucci, M.; Gunnella, R.; Di Cicco, A. Band gap implications on Nano-TiO₂ surface modification with ascorbic acid for visible light-active polypropylene coated photocatalyst. *Nanomaterials* **2018**, *8*, 599. [CrossRef]
15. Li, H.; Liu, B.; Yin, S.; Sato, T.; Wang, Y. Visible light-driven photocatalytic activity of oleic acid-coated TiO₂ nanoparticles synthesized from absolute ethanol solution. *Nanoscale Res. Lett.* **2015**, *10*, 415. [CrossRef]

16. Maeda, K.; Kuriki, R.; Ishitani, O. Photocatalytic activity of carbon nitride modified with a Ruthenium(II) complex having carboxylic- or phosphonic acid anchoring groups for visible-light CO₂ reduction. *Chem. Lett.* **2016**, *45*, 182–184. [CrossRef]
17. Ma, S.; Gu, J.; Han, Y.; Gao, Y.; Zong, Y.; Ye, Z.; Xue, J. Facile fabrication of C-TiO₂ nanocomposites with enhanced photocatalytic activity for degradation of tetracycline. *ACS Omega* **2019**, *4*, 21063–21071. [CrossRef] [PubMed]
18. Huang, H.; Xiao, K.; He, Y.; Zhang, T.; Dong, F.; Du, X.; Zhang, Y. In situ assembly of BiOI@Bi₂O₃ P-n junction: Charge induced unique front-lateral surfaces coupling heterostructure with high exposure of BiOI {001} active facets for robust and nonselective photocatalysis. *Appl. Catal. B Environ.* **2016**, *199*, 75–86. [CrossRef]
19. Huang, H.; Li, X.; Wang, J.; Dong, F.; Chu, P.K.; Zhang, T.; Zhang, Y. Anionic group self-doping as a promising strategy: Band-gap engineering and multi-functional applications of high-performance CO₃²⁻-Doped Bi₂O₃. *ACS Catal.* **2015**, *5*, 4094–4103. [CrossRef]
20. Górska, P.; Zaleska, A.; Kowalska, E.; Klimczuk, T.; Sobczak, J.; Skwarek, E.; Janusz, W.; Hupka, J. TiO₂ photoactivity in Vis and UV light: The influence of calcination temperature and surface properties. *Appl. Catal. B* **2008**, *84*, 440–447. [CrossRef]
21. International Organization for Standardization. *Water Quality—Determination of Selected Plant Treatment Agents—Method Using High Performance Liquid Chromatography with UV Detection After Solid-Liquid Extraction*; ISO 11369; International Organization for Standardization: Geneva, Switzerland, 1997.
22. Lee, J.Y.; Jo, W.-K. Application of ultrasound-aided method for the synthesis of CdS-Incorporated three-dimensional TiO₂ photocatalysts with enhanced performance. *Ultrason. Sonochem.* **2017**, *35*, 440–448. [CrossRef]
23. Elhalil, A.; Elmoubarki, R.; Farnane, M.; Machrouhi, A.; Sadiq, M.; Mahjoubi, F.Z.; Qourzal, S.; Barka, N. Photocatalytic degradation of caffeine as a model pharmaceutical pollutant on mg doped ZnO-Al₂O₃ heterostructure. *Environ. Nanotechnol. Monit. Manag.* **2018**, *10*, 63–72. [CrossRef]
24. Herrmann, J.-M. Heterogeneous Photocatalysis: State of the art and present applications in honor of Pr. R.L. Burwell Jr. (1912–2003), Former Head of Ipatieff Laboratories, Northwestern University, Evanston (Ill). *Top. Catal.* **2005**, *34*, 49–65. [CrossRef]
25. Ibhaddon, A.O.; Fitzpatrick, P. Heterogeneous photocatalysis: Recent advances and applications. *Catalysts* **2013**, *3*, 189–218. [CrossRef]
26. Garg, A.; Singhanian, T.; Singh, A.; Sharma, S.; Rani, S.; Neogy, A.; Yadav, S.R.; Sangal, V.K.; Garg, N. Photocatalytic degradation of bisphenol-A using N, Co Codoped TiO₂ catalyst under solar light. *Sci. Rep.* **2019**, *9*, 1–13. [CrossRef]
27. Kumar, K.V.; Porkodi, K.; Rocha, F. Langmuir–hinshelwood kinetics—A theoretical study. *Catal. Commun.* **2008**, *9*, 82–84. [CrossRef]
28. Asenjo, N.G.; Santamaría, R.; Blanco, C.; Granda, M.; Álvarez, P.; Menéndez, R. Correct Use of the Langmuir–Hinshelwood equation for proving the absence of a synergy effect in the photocatalytic degradation of phenol on a suspended mixture of Titania and activated carbon. *Carbon* **2013**, *55*, 62–69. [CrossRef]
29. Kusiak-Nejman, E.K. Preparation and Study of TiO₂/C photocatalysts for Water and Wastewater Treatment. 2012. Available online: <https://zbc.ksiaznica.szczecin.pl/dlibra/publication/30931/edition/29344/content> (accessed on 5 November 2019).
30. Mashtalir, O.; Kurtoglu, M.; Pogulay, S.; Gogotsi, A.; Naguib, M.; Gogotsi, Y. Photocatalytic WO₃ and TiO₂ films on brass. *Int. J. Appl. Ceram. Technol.* **2013**, *10*, 26–32. [CrossRef]
31. Guo, H.; Lin, K.; Zheng, Z.; Xiao, F.; Li, S. Sulfanilic acid-modified P25 TiO₂ nanoparticles with improved photocatalytic degradation on congo red under visible light. *Dye. Pigment.* **2012**, *92*, 1278–1284. [CrossRef]
32. Ao, C.H.; Lee, S.C.; Yu, J.C. Photocatalyst TiO₂ supported on glass fiber for indoor air purification: Effect of NO on the photodegradation of CO and NO₂. *J. Photochem. Photobiol. A Chem.* **2003**, *156*, 171–177. [CrossRef]
33. Maira, A.J.; Yeung, K.L.; Soria, J.; Coronado, J.M.; Belever, C.; Lee, C.Y.; Augugkario, V. Gas-phase photo-oxidation of toluene using nanometer-size TiO₂ catalysts. *Appl. Catal. B Environ.* **2001**, *29*, 327–336. [CrossRef]
34. Hsieh, M.-S.; Su, H.-J.; Hsieh, P.-L.; Chiang, Y.-W.; Huang, M.H. Synthesis of Ag₃PO₄ crystals with tunable shapes for facet-dependent optical property, photocatalytic activity, and electrical conductivity examinations. *ACS Appl. Mater. Interfaces* **2017**, *9*, 39086–39093. [CrossRef]

35. Lin, H.; Ye, H.; Xu, B.; Cao, J.; Chen, S. Ag₃PO₄ quantum dot sensitized BiPO₄: A novel p–n junction Ag₃PO₄/BiPO₄ with enhanced visible-light photocatalytic activity. *Catal. Commun.* **2013**, *37*, 55–59. [CrossRef]
36. Inamdar, J.; Singh, S.K. Photocatalytic detoxification method for zero effluent discharge in dairy industry: Effect of operational parameters. *World Acad. Sci. Eng. Technol. J. Civ. Environ. Eng.* **2008**, *2*, 10–14. [CrossRef]
37. Kudlek, E. The Sequential System Photocatalysis—Membrane Pressure Process in Depth Treatment of Effluents Containing Pharmaceutical Active Compounds from Municipal Wastewater Treatment Plants. 2016. Available online: <http://delibra.bg.polsl.pl/dlibra/doccontent?id=37846> (accessed on 5 November 2019).
38. Rauf, M.A.; Ashraf, S.S. Fundamental principles and application of heterogeneous photocatalytic degradation of dyes in solution. *Chem. Eng. J.* **2009**, *151*, 10–18. [CrossRef]
39. Nsib, M.F.; Maayoufi, A.; Moussa, N.; Tarhouni, N.; Massouri, A.; Houas, A.; Chevalier, Y. TiO₂ modified by salicylic acid as a photocatalyst for the degradation of monochlorobenzene via pickering emulsion way. *J. Photochem. Photobiol. A Chem.* **2013**, *251*, 10–17. [CrossRef]
40. Ni, W.; Wu, S.; Ren, Q. Preparation and Characterization of silanized TiO₂ nanoparticles and their application in toner. *Ind. Eng. Chem. Res.* **2012**, *51*, 13157–13163. [CrossRef]
41. Afrin, U.; Mian, M.R.; Breedlove, B.K.; Hossain, M.M. Enhanced photocatalytic activity of an acid-modified TiO₂ surface for degradation of the azo dye remazol red. *ChemistrySelect* **2017**, *2*, 10371–10374. [CrossRef]
42. Kosmulski, M. The PH-dependent surface charging and points of zero charge: V. update. *J. Colloid Interface Sci.* **2011**, *353*, 1–15. [CrossRef] [PubMed]
43. Yang, H.; An, T.; Li, G.; Song, W.; Cooper, W.J.; Luo, H.; Guo, X. Photocatalytic degradation kinetics and mechanism of environmental pharmaceuticals in aqueous suspension of TiO₂: A Case of β-blockers. *J. Hazard. Mater.* **2010**, *179*, 834–839. [CrossRef]
44. Udom, I.; Myers, P.D.; Ram, M.K.; Hepp, A.F.; Archibong, E.; Stefanakos, E.K.; Goswami, D.Y. Optimization of photocatalytic degradation of phenol using simple photocatalytic reactor. *Am. J. Anal. Chem.* **2014**, *5*, 743–750. [CrossRef]
45. Alkaim, A.F.; Aljeboree, A.M.; Alrazaq, N.A.; Baqir, S.J.; Hussein, F.H.; Lilo, A.J. Effect of pH on adsorption and photocatalytic degradation efficiency of different catalysts on removal of methylene blue. *Asian J. Chem.* **2014**, *26*, 8445–8448. [CrossRef]
46. Fernández-Domene, R.M.; Roselló-Márquez, G.; Sánchez-Tovar, R.; Lucas-Granados, B.; García-Antón, J. Photoelectrochemical removal of chlorfenvinphos by using WO₃ nanorods: Influence of annealing temperature and operation PH. *Sep. Purif. Technol.* **2019**, *212*, 458–464. [CrossRef]
47. Liu, S.X.; Chen, X.Y.; Chen, X. A TiO₂/AC Composite photocatalyst with high activity and easy separation prepared by a hydrothermal method. *J. Hazard. Mater.* **2007**, *143*, 257–263. [CrossRef]
48. Li Puma, G.; Bono, A.; Krishnaiah, D.; Collin, J.G. Preparation of titanium dioxide photocatalyst loaded onto activated carbon support using chemical vapor deposition: A review paper. *J. Hazard. Mater.* **2008**, *157*, 209–219. [CrossRef]
49. Nadia, E.M.; Moustapha, B.; Yahia, A.I. UV/TiO₂ photocatalytic oxidation of commercial pesticide in aqueous solution. *Am. J. Innov. Res. Appl. Sci.* **2018**, *5*, 36–43.
50. Fujishima, A.; Zhang, X.; Tryk, D.A. TiO₂ Photocatalysis and related surface phenomena. *Surf. Sci. Rep.* **2008**, *63*, 515–582. [CrossRef]
51. Tseng, C.-S.; Wu, T.; Lin, Y.-W. Facile synthesis and characterization of Ag₃PO₄ microparticles for degradation of organic dyestuffs under white-light light-emitting-diode irradiation. *Materials* **2018**, *11*, 708. [CrossRef] [PubMed]
52. Cheng, X.; Zu, L.; Jiang, Y.; Shi, D.; Cai, X.; Ni, Y.; Lin, S.; Qin, Y. A titanium-based photo-fenton bifunctional catalyst of Mp-MXene/TiO_{2-x} nanodots for dramatic enhancement of catalytic efficiency in advanced oxidation processes. *Chem. Commun.* **2018**, *54*, 11622–11625. [CrossRef] [PubMed]
53. Nakarada, Đ.; Petković, M. Mechanistic insights on how hydroquinone disarms OH and OOH radicals. *Int. J. Quantum Chem.* **2018**, *118*, e25496. [CrossRef]
54. Azarpira, H.; Sadani, M.; Abtahi, M.; Vaezi, N.; Rezaei, S.; Atafar, Z.; Mohseni, S.M.; Sarkhosh, M.; Ghaderpoori, M.; Keramati, H.; et al. Photo-catalytic degradation of triclosan with UV/Iodide/ZnO process: Performance, kinetic, degradation pathway, energy consumption and toxicology. *J. Photochem. Photobiol. A Chem.* **2019**, *371*, 423–432. [CrossRef]

55. Pelaez, M.; Falaras, P.; Likodimos, V.; O'Shea, K.; de la Cruz, A.A.; Dunlop, P.S.M.; Byrne, J.A.; Dionysiou, D.D. Use of selected scavengers for the determination of NF-TiO₂ reactive oxygen species during the degradation of microcystin-Lr under visible light irradiation. *J. mol. Catal. A Chem.* **2016**, *425*, 183–189. [[CrossRef](#)]
56. Abdullah, H.; Khan, M.R.; Pudukudy, M.; Yaakob, Z.; Ismail, N.A. CeO₂-TiO₂ as a visible light active catalyst for the photoreduction of CO₂ to methanol. *J. Rare Earths* **2015**, *33*, 1155–1161. [[CrossRef](#)]
57. Huang, H.; Tu, S.; Zeng, C.; Zhang, T.; Reshak, A.H.; Zhang, Y. Macroscopic polarization enhancement promoting photo- and piezoelectric-induced charge separation and molecular oxygen activation. *Angew. Chem.* **2017**, *56*, 11860–11864. [[CrossRef](#)]
58. Chen, F.; Huang, H.; Guo, L.; Zhang, Y.; Ma, T. The role of polarization in photocatalysis. *Angew. Chem.* **2019**, *58*, 10061–10073. [[CrossRef](#)]



© 2020 by the author. Licensee MDPI, Basel, Switzerland. This article is an open access article distributed under the terms and conditions of the Creative Commons Attribution (CC BY) license (<http://creativecommons.org/licenses/by/4.0/>).

Comparative studies of Rhodamine B decolorization in the combined process $\text{Na}_2\text{S}_2\text{O}_8$ /visible light/ultrasound

Piotr Zawadzki

Laboratory of Water and Sewage Technologies, Department of Water Protection, Central Mining Institute, Plac Gwarków 1, 40-166 Katowice, Poland, Tel. 0048 32 259-28-01; email: pzawadzki@gig.eu

Received 25 May 2020; Accepted 30 September 2020

ABSTRACT

In this study, the possibility of rhodamine B (RhB) decomposition in the presence of ultrasound (US) and sodium persulfate ($\text{Na}_2\text{S}_2\text{O}_8$) activated by visible light (Vis) was investigated. A combination of these processes ($\text{Na}_2\text{S}_2\text{O}_8$ /Vis/US) were examined. As a part of this study, the optimal dose of $\text{Na}_2\text{S}_2\text{O}_8$, glucose dose, reaction time, and RhB concentration were selected. In addition, radical scavenger test was conducted. Under optimal conditions (RhB concentration = 10.0 mg dm^{-3} ; pH = 6.0; reaction time: 60.0 min; $\text{Na}_2\text{S}_2\text{O}_8$ dose = 20.0 mM; glucose dose = 200.0 mM; US power: 60 W; US frequency: 40 kHz; temperature: 295 K), RhB decomposition in the $\text{Na}_2\text{S}_2\text{O}_8$ /Vis/US process was set to 85%. Under the same conditions, the RhB decomposition in the US, $\text{Na}_2\text{S}_2\text{O}_8$, $\text{Na}_2\text{S}_2\text{O}_8$ /Vis and $\text{Na}_2\text{S}_2\text{O}_8$ /US processes was 17%, 29%, 49% and 67%, respectively. The determined parameters of the pseudo-first-order reaction showed the advantage of the dynamics of the $\text{Na}_2\text{S}_2\text{O}_8$ /Vis/US process over the US, $\text{Na}_2\text{S}_2\text{O}_8$, $\text{Na}_2\text{S}_2\text{O}_8$ /Vis and $\text{Na}_2\text{S}_2\text{O}_8$ /US processes. The mathematically calculated half-life ($t/2$) for the combined process was 2.1 min, while half-life values for the US, $\text{Na}_2\text{S}_2\text{O}_8$, $\text{Na}_2\text{S}_2\text{O}_8$ /Vis and $\text{Na}_2\text{S}_2\text{O}_8$ /US processes are 25.5, 15.9, 7.8 and 4.6 min, respectively. Hydroxyl radicals were mainly responsible for the decolorization of rhodamine B. The conducted studies showed that the activation of sodium persulfate in the combined process of sodium persulfate-visible light-ultrasound is an interesting alternative for the purification of solutions containing rhodamine B with variable dye concentrations (up to 20 mg dm^{-3}).

Keywords: Rhodamine B; Advanced oxidation process; Sodium persulfate; Visible light; Ultrasound

1. Introduction

In the presence of the deepening global water crisis, the world may experience a 40% reduction in water availability by 2030. It is predicted that half of the world's population will be at risk of water scarcity by 2050 [1]. The presence of organic and inorganic compounds disturbing the functioning of living organisms in water ecosystems is of great concern these days. These substances are classified as micropollutants, and their presence in aquatic ecosystems

is documented. Micropollutants are usually defined as compounds occurring in concentrations of ng/dm^3 or mg/dm^3 . Micropollutants are characterized by two toxic effects namely: (1) effects that appear after a short time of exposure and (2) effects that appear after a long time (long-term health effects). Micropollutants can generally be divided into organic and inorganic substances. The organic group of micropollutants is very extensive and may include endocrine active compounds, disinfection by-products, polychlorinated biphenyls, pesticides, dyes, surfactants and

polycyclic aromatic hydrocarbons [2–5]. Among the compounds belonging to the group of micropollutants, there are rhodamines – organic chemical compounds from the group of triphenylmethyl xanthene dyes. Rhodamine B (RhB) is a compound which belongs to this group.

Rhodamine B is used as a dye in numerous industries, such as chemical, textile, paper or dyeing. It is a fluorescent dye, which is also used in biological research on animals due to its easy accumulation, for example, in animal hair and teeth. RhB is toxic to humans and animals. Symptoms of the negative influence of this chemical compound are skin, eyes and respiratory system irritation. It also displays mutagenic and carcinogenic potential. This dye has a high affinity for proteins involved in basic cell metabolism [6,7].

The development of industry leads to the fact that rhodamine B is one of the main components identified in the industrial wastewater of dyeing and textile. The use of conventional purification processes such as activated carbon, coagulation, filtration, activated sludge does not bring satisfactory results due to high concentration of dyes, low biodegradability and higher stability of newly synthesized dyes [8]. For this reason, it is justified to search for new solutions in the field of water and wastewater treatment.

Advanced oxidation processes (AOPs) have gained great interest in the recent years. AOPs are listed as one of the best available techniques for colored wastewater treatment [9]. A common feature of AOPs is the oxidation of organic compounds by generating hydroxyl radicals OH^\bullet ($E^0 = 2.80 \text{ V}$). Scientific data show that a lot of work is devoted to the use of sulfate radicals $\text{SO}_4^{\bullet-}$ ($E^0 = 2.50\text{--}3.10 \text{ V}$) for the decomposition of organic pollutants [10,11]. The generation of sulfate radicals occurs through the activation of persulfate ions ($\text{S}_2\text{O}_8^{2-}$) by means of UV radiation, heat, ionizing radiation, high pH and transition metal ions [12–16]. Activation with transition metal ions at low oxidation levels such as Fe^{2+} , Ni^{2+} , Co^{2+} and Ag^+ is most commonly used. Persulfates react with the transition metal electron donor to form a single sulfate radical (Eq. (1)) [17].



The high cost of conventional activation methods indicates that new methods for the generation of sulfate radicals are gaining interest. New methods of activation, for example, ultrasound, ozone or carbon nanotubes are studied [18,19]. However, there are few studies on the activation of

persulfates with visible light [20,21]. This is due to the very poor quantum efficiency of sulfate radicals at the wavelength of $\lambda > 400 \text{ nm}$ [22].

Unconventional methods of activation should be equally efficient and cost-effective compared with conventional methods. Materials that allow the activation of persulfates (PDS) under the influence of visible light may be, for example, acids and sugars [23]. Sugar prices may be even twice lower compared with $\text{FeSO}_4 \cdot 7\text{H}_2\text{O}$, a compound commonly used to activate persulfates. Moreover, sugars are ingredients present in wastewater. Thus, a fully-recognized wastewater composition will minimize the amount of this reagent. In addition, the dose of sugars used to activate PDS is too low to be toxic to living organisms.

The use of ultrasound is a hybrid method of activation. During the ultrasound process, the cavitation bubbles break down, which locally causes the formation of high temperatures and pressure. The combination of these factors generates hydroxyl (OH^\bullet), superoxide ($\text{O}_2^{\bullet-}$) and H_2O_2 [24,25] radicals. Ultrasonic technology is a safe and efficient method for potential use in water and wastewater treatment. Activation of PDS with ultrasound is characterized by higher efficiency compared with, for example, the $\text{H}_2\text{O}_2/\text{US}$ system [26,27].

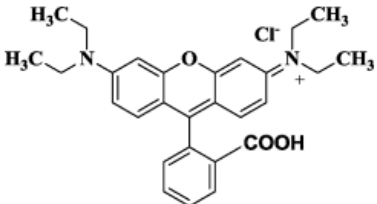
The aim of this study is to assess the efficiency of rhodamine B degradation in the AOP carried out in the presence of sodium persulfate activated by visible light and ultrasound. The optimum doses of PDS and glucose have been carried out. The effect of initial RhB concentration on the final degree of dye decolorization was investigated.

2. Materials and methods

2.1. Model solution

Model solutions were prepared on the basis of deionized water with the addition of rhodamine B (RhB) standard. The physical and chemical characteristics of RhB are presented in Table 1. Dye with a purity of $\geq 95.0\%$ was obtained from Sigma-Aldrich (Poznań, Poland). The pH of the model solution before and after the addition of the dye solution was $\text{pH} = 6.0$. Any deviations from this value were corrected with $0.1 \text{ mol dm}^{-3} \text{ HCl}$ or $0.1 \text{ mol dm}^{-3} \text{ NaOH}$ from Sigma-Aldrich. The pH of the model solution was monitored using a CPC-511 pH meter from Elmetron (Zabrze, Poland). Other analytical grade reagents used

Table 1
Physicochemical characteristics of rhodamine B [28]

Chemical structure	Physicochemical properties	
	Chemical formula	$\text{C}_{28}\text{H}_{31}\text{ClN}_2\text{O}_3$
	Molecular weight (g mol^{-1})	479.01
	Nr CAS	81–88–9
	Water solubility at 20°C (g dm^{-3})	15.0
	Dissociation constant (pK_a)	3.7
	$\log K_{\text{OW}}$	1.9–2.0
	λ_{max} in water (nm)	554.0

during the study came from Avantor Performance Materials Poland S.A. (Gliwice, Poland).

2.2. Analysis of RhB

The absorbance of rhodamine B was tested using the Jasco V-750 spectrophotometer (Kraków, Poland). Fig. 1 shows the obtained RhB absorption spectrum. The absorption spectrum of the compound shows a peak at the wavelength $\lambda_{\max} = 554.0$ nm. Model solutions and resulting solutions were tested at this wavelength ($\lambda = 554.0$ nm).

2.3. Determination of advanced oxidation parameters

In the first stage of research, the optimal glucose dose was determined. The optimal dose of glucose enables to activate sodium persulfate with visible light. The process was carried out in reaction vessels containing 500.0 cm^3 of dye with a concentration of 10.0 mg dm^{-3} . The reaction vessels were placed on a magnetic stirrer for mixing and after stirring the vessels were irradiated with visible light for 60.0 min. The following sugar doses were tested: 100.00; 150.0; 200.0; 300.0 and 500.0 mM. The sodium persulfate dose was 10.0 mM. All experiments were conducted under these conditions: temperature of 295 K, atmospheric pressure equal to 1,013.0 hPa and $\text{pH} = 6.0$.

In order to select the optimal dose of sodium persulfate, the influence of various PDS concentrations was studied. The following doses were tested: 2.0; 5.0; 10.0; 20.0; 50.0 and 100.0 mM. Reaction vessels containing 10.0 mg dm^{-3} dye were placed on a magnetic stirrer.

Optimal process time is a significant parameter from an economic point of view and in terms of total pollutants removal. The study was conducted for 180 min. Samples were collected after 5, 10, 15, 20, 30, 45, 60, 120 and 180 min. Reaction vessels containing the model solution with the addition of a RhB standard at a concentration of 10.0 mg dm^{-3} were placed on a magnetic stirrer to be adequately mixed. The glucose dose was 200.00 mM and the $\text{Na}_2\text{S}_2\text{O}_8$ dose was 20.0 mM.

The effect of the initial RhB concentration was investigated. Four dye concentrations were used: 1.0, 5.0, 10.0 and 20.0 mg dm^{-3} . Samples were collected after 60.0 min. Reaction

vessels containing the model solution with the addition of tested concentrations were placed on a magnetic stirrer. The glucose dose was 200.00 mM, while the $\text{Na}_2\text{S}_2\text{O}_8$ dose was 20.0 mM.

All the experiments were carried out independently in triplicate. The data presented in the next section include average values.

2.4. Visible light activated persulfate tests

A 10 W Tungsten QTH10/M lamp from Thorlabs Inc. (New Jersey, United States) was used as the visible radiation source. The lamp emits radiation with a wavelength (λ) from 400 to 2,200 nm. For the purpose of the research, the FGS900M filter (Thorlabs Inc., United States) was used to cut off the spectrum bands above 710 nm. The filter was mounted using a Thorlabs Inc. circular cage system (Thorlabs Inc., United States; Fig. 2). The lamp emitted radiation from the visible light range. The experiments were conducted in an isolated chamber, without the possibility of exposure to another light source.

2.5. Ultrasound activated persulfate tests

Sonication was carried out using a Proclean 0.7 WH ultrasonic generator (Ulsonix Cleaning Instruments, Germany) with a capacity of 0.7 dm^3 . Persulfates activation was carried out under the following conditions: output power 60 W, ultrasound frequency 40 kHz, reactor dimensions $150 \times 86 \times 65 \text{ mm}$.

2.6. Reaction kinetics

According to the scientific literature data [29,30], to describe the decolorization kinetics of most rhodamine dyes, the pseudo-first-order reaction equation can be used (Eq. (2)).

$$-\ln\left(\frac{C}{C_0}\right) = kt \quad (2)$$

where C_0 – concentration of RhB before the purification process (mg dm^{-3}); C – concentration of RhB after the

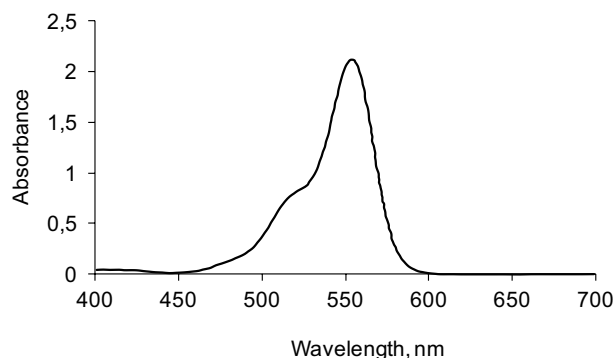


Fig. 1. Absorption spectrum of rhodamine B standard (10.0 mg dm^{-3}).

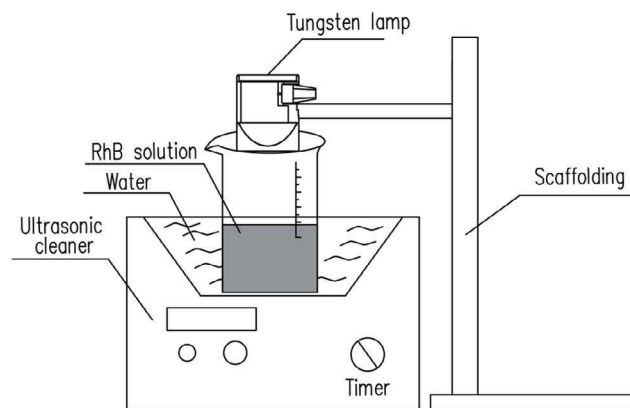


Fig. 2. Illustration of the experimental set-up.

purification process (mg dm^{-3}); k – reaction rate constant; t – reaction time (min).

The half-life of RhB ($t/2$) was calculated mathematically based on the reaction rate constant k as follows:

$$t/2 = \ln(2)/k \quad (3)$$

2.7. Radical scavenger test

A radical scavenger test was used to determine the major radical types involved in dye degradation. In the study, tert-butyl alcohol (BuOH) was used as an OH^\bullet radical scavenger, methanol (MeOH) as a $\text{SO}_4^{\bullet-}$ and OH^\bullet radical scavenger and hydroquinone as an $\text{O}_2^{\bullet-}$ radical scavenger. The applied compounds are most commonly used as radical scavengers by many researchers [31–33]. Radical scavengers at a dose of $50.0 \mu\text{M}$ were added before the AOP.

3. Results and discussion

3.1. Optimal glucose dose

At this stage, the optimal concentration of glucose was determined. The following sugar concentrations were tested: 100.00, 150.0, 200.0, 300.0 and 500.0 mM (Fig. 3). The process was carried out in the presence of visible light for 60 min. The dose of sodium persulfate was 10 mM. In the preliminary tests [20], the decolorization process was carried out in the presence of glucose only, without $\text{Na}_2\text{S}_2\text{O}_8$ and visible light addition. The results of the study did not confirm the dye degradation in the presence of glucose alone. A concentration of 200.0 mM was selected as the optimal glucose dose for further testing. The decomposition of rhodamine B under these conditions was about 42%. For the other concentrations analysed, the RhB decomposition was unsatisfactory. In addition, a high content of sugar resulted in the reduced effect of decolorization. This is due to the inhibition of radicals by higher glucose levels ($k_{\text{OH}^\bullet} = 1.5 \times 10^9$) [34].

Rhodamine B decomposition with addition of glucose may be due to the optical properties of sugar. Glucose is an optically active substance, that is, it tends to rotate the light plane, which may explain the higher dye decomposition in the presence of sugar compared with a solution purified only with persulfate. PDS activation by visible

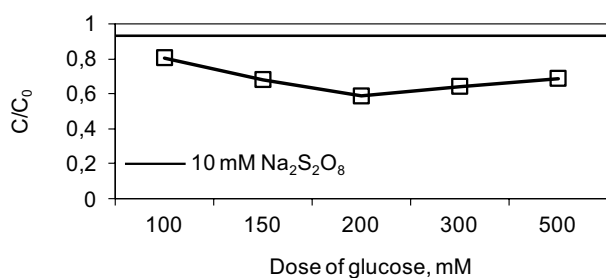
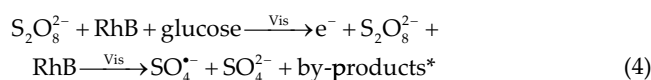


Fig. 3. Influence of glucose dose on the rhodamine B decolorization. Conditions: $C_{0[\text{RhB}]} = 10.0 \text{ mg dm}^{-3}$; pH = 6.0; reaction time = 60.0 min; $\text{Na}_2\text{S}_2\text{O}_8$ dose = 10.0 mM.

radiation in the presence of glucose may also result from the probable electron transfer from sugar towards PDS and its activation. Moreover glucose oxidation products may be able to activate PDS (Eq. (4)). It is related to the organic PDS activation with an external carbon source [35]. Ahmad et al. [36] performed a research on the activation of persulfates with two organic compounds: phenoxides and phenols. Phenoxides have been proved to be an effective persulfate activator. Literature data show that the mechanism of PDS activation by glucose is similar to the mechanism of activation by phenoxides [23]. Glucose oxidation causes the sugar decomposition, whereby compounds containing a functional group are generated. An example of such functional group is, for example, carbonyl group, which accepts the negative charge activating persulfates.



where * indicates that identification of rhodamine B degradation products was beyond the scope of this study.

3.2. Optimal $\text{Na}_2\text{S}_2\text{O}_8$ dose

The dependence of rhodamine B decolorization on the $\text{Na}_2\text{S}_2\text{O}_8$ dose is presented in Fig. 4. The process was carried out in the presence of visible light. The following doses of sodium persulfate were tested: 2.0, 5.0, 10.0, 20.0, 50.0 and 100.0 mM. The glucose concentration was 200.0 mM. The process was carried out for 60 min. The RhB decomposition depended on the initial persulfate dose, that is, it increased with increasing PDS dose. The increase in the degree of decolorization results from the increase in the density of generated active species. The addition of 20.0 mM persulfate after 60.0 min caused the dye to be removed in approximately 47%. Higher doses of PDS (50.0 and 100.0 mM) did not cause a significant increase in purification efficiency. Taking into account economic aspects, 20.0 mM was chosen as the optimal dose of $\text{Na}_2\text{S}_2\text{O}_8$. Degradation of pollutants in the PDS system without the use of catalysts is possible, whereas the degree of removal of organic pollutants without the use of catalysts is lower. Without activation, the persulfate anion will react only with some organic chemicals. The removal degree is smaller than in activated persulfate system, because persulfate

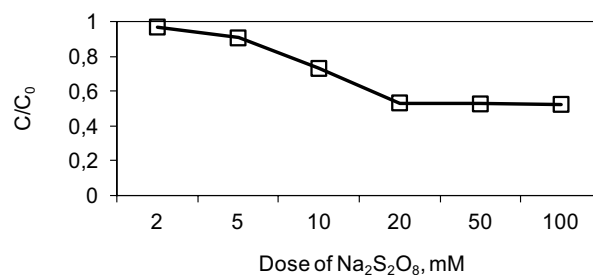


Fig. 4. Influence of the $\text{Na}_2\text{S}_2\text{O}_8$ dose on the rhodamine B decolorization. Conditions: $C_{0[\text{RhB}]} = 10.0 \text{ mg dm}^{-3}$; pH = 6.0; reaction time = 60.0 min; glucose concentration = 200.0 mM.

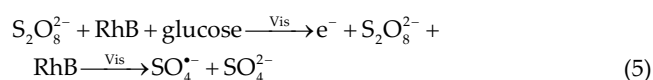
ion ($E^0 = 2.01$ V) has lower oxidation potential compared with sulfate ion ($E^0 = 2.50$ – 3.10 V) [37].

3.3. Optimal RhB decomposition time

Fig. 5a depicts the influence of process time on the degree of RhB decolorization in $\text{Na}_2\text{S}_2\text{O}_8$, US, $\text{Na}_2\text{S}_2\text{O}_8/\text{Vis}$ and $\text{Na}_2\text{S}_2\text{O}_8/\text{US}$ systems. Process was carried out for 180.0 min. It was found that the dye decolorization effect increased with the duration time. After 30 min of the process, the efficiency of the $\text{Na}_2\text{S}_2\text{O}_8/\text{Vis}$ system was 32%, while in the $\text{Na}_2\text{S}_2\text{O}_8/\text{US}$ system it was 49%. A satisfying decolorization effect was achieved after 60.0 min of reaction. In that time, the dye decomposition was 49% and 67% for visible and ultrasound activated persulfate, respectively. As shown in Fig. 5, continuation of the process caused a slight increase in efficiency by about 1%–2%. Ultrasound (US) cleaning had the least effect on the decomposition of rhodamine B. The decomposition of this compound did not exceed 25% after 180.0 min. The highest degree of dye removal was obtained in the combined visible–ultrasound system ($\text{Na}_2\text{S}_2\text{O}_8/\text{Vis}/\text{US}$). About 85% RhB was removed within 60.0 min in this system, whereas after 180.0 min the degradation efficiency slightly increased to 95.0%. Due to the need to limit reactor volume during plant design and a slight difference in the decomposition degree after 120.0 and 180.0 min of the purification process, 60.0 min time of reaction was selected as the optimal contact time.

Persulfate activation in the $\text{Na}_2\text{S}_2\text{O}_8/\text{Vis}$ system is the result of a synergistic relationship between visible light and the enhanced effect of glucose electron transfer from this

sugar towards persulfate (Eq. (5)). The study by Zawadzki [20] showed that the addition of only sugar without visible light irradiation does not contribute to the activation of persulfate. Scientific literature data indicates that in an alkaline reaction (pH = 6.0), in which the present experiments were carried out, the addition of glucose promotes persulfate activation since its functional groups (e.g., carbonyl group) accept partially negative charge.



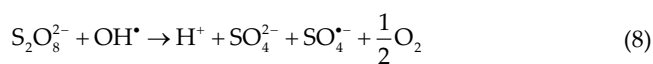
As shown in Fig. 5a, it was established that the decolorization effect in the $\text{Na}_2\text{S}_2\text{O}_8/\text{US}$ system was higher compared with the $\text{Na}_2\text{S}_2\text{O}_8/\text{Vis}$ system. First of all, this is because of the applied persulfate activation method.

In the ultrasound activated persulfates, the role of ultrasound occurs in two possible ways [38,39]. In the first mechanism, persulfate is activated by heat from ultrasonic cavitation (Eq. (6)), which generates cavitation bubbles. During the ultrasound process, the cavitation bubbles break down, which locally causes the formation of high temperatures ($T \approx 5,000$ K) and pressure ($P \approx 1,000$ atm). As reported by Fedorov et al. [40], equally to conventional persulfate activation methods, the energy released during the collapse of the cavitation bubbles catalyse the activation of persulfate to produce $\text{SO}_4^{\cdot-}$ radicals. Ultrasound cleaning can induce a cavitation phenomenon, which is an essential agent in the activation of persulfates. A study by Ghanbari and Moradi [41] showed that this process is found to consist of numerous reverse and side reactions generating $\text{SO}_4^{\cdot-}$ and OH^{\cdot} radicals.

In the second mechanism, cavitation bubbles initiate the dissociation of water molecules to generate hydroxyl radical (Eq. (7)). Dissociation of water molecules takes place inside the bubbles as well as in the interface between the gas phase and surrounding liquid [42]. Generated hydroxyl radical attacks persulfate ions forming sulfate radical anion ($\text{SO}_4^{\cdot-}$), bisulfate ion and oxygen (Eqs. (8) and (9)).



where the symbol “US” indicates ultrasound.



Conducted studies confirm that the Langmuir–Hinshelwood (L-H) model can be used to describe the kinetics of rhodamine B degradation. This result can be justified by considering Fig. 5b. The analysis of the correlation coefficient R^2 showed very good fit of experimental data (95%–99%). Half-life $t/2$ and reaction rate constants k were determined using the L-H model. The results are summarized in Table 2. Taking into account the relationship

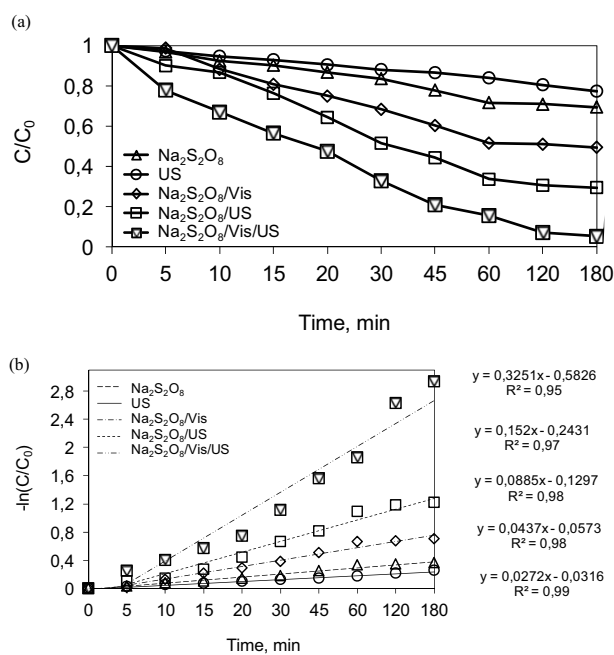


Fig. 5. Influence of reaction time on the rhodamine B decomposition in various systems (a) and reaction kinetics (b). Conditions: $C_{0[\text{RhB}]}$ = 10 mg dm^{-3} ; glucose dose = 200.0 mM ; $\text{Na}_2\text{S}_2\text{O}_8$ dose = 20.0 mM ; pH = 6.0; US frequency = 40.0 kHz ; temperature = 295 K ; US power = 60 W .

Table 2
Parameters of pseudo-first-order reaction

Process	k (min ⁻¹)	R^2	$t/2$ (min)
Na ₂ S ₂ O ₈	0.044	0.98	15.9
US	0.027	0.99	25.5
Na ₂ S ₂ O ₈ /Vis	0.089	0.98	7.8
Na ₂ S ₂ O ₈ /US	0.152	0.97	4.6
Na ₂ S ₂ O ₈ /Vis/US	0.325	0.95	2.1

between $-\ln(C/C_0)$ and reaction time, the two-stage oxidation process, which is a characteristic phenomenon, for example, for heterogeneous oxidation processes [43,44] was not found. The two-stage oxidation process is mainly attributed to the indirect reaction of oxygenating species with by-products or decreasing amount of radicals during the reaction. However, the identification of intermediates was beyond the scope of this study.

The results indicate that the activation of persulfate affects the kinetic parameters of rhodamine B degradation. Reaction rate constant k was the lowest in the case of the ultrasonic cleaning process. As reported in the study by Hou et al. [45], this is due to the small amount of radicals generated during the fragmentation of water molecules. The highest value of the reaction rate constant was observed in the combined system (Na₂S₂O₈/Vis/US). The mathematically calculated half-life ($t/2$) of RhB in this system was 2.1 min.

Table 3 presents the classification of the chemical reaction rate based on the mathematically calculated half-life $t/2$. The dynamics of ultrasonic cleaning was the lowest among the processes tested. The reaction was classified as slow. Four out of five treatment systems tested were found to be at a moderate rate ($<10^3$ s).

3.4. Effects of different RhB concentrations

The efficiency of rhodamine B decolorization has been studied depending on different dye concentrations (1, 5, 10 and 20 mg dm⁻³). The process was carried out for 60 min. Abatement curves are shown in Fig. 6. It was found that the final dye concentration depends on its initial concentration. This is common for both AOPs [47] and activated persulfates [48]. Because the conditions for each of the experiments were the same (Na₂S₂O₈ dose, glucose dose, pH, temperature), the amount of sulfate radicals generated was constant and decreased with increasing RhB concentration. As shown in the study by Cai et al. [49], the collision probability of oxygenating radicals decreases with increasing concentration of dye molecules. High concentration of dye molecules causes greater consumption of radicals resulting in an insufficient amount of radicals to decompose the excess of RhB. This results in a reduced efficiency of dye removal. Moreover, intermediates may consume active species, which results in a poor dye decolorization (competitiveness effect). Despite the unfavorable conditions for RhB degradation (high dye concentration), the combination of visible light and ultrasound persulfate activation

Table 3
Classification of reaction rate based on half-life [46]

Half-life, s	Time span for near-completion	Rate classification
10 ⁻¹⁵ –10 ⁻¹²	ps or less	Ultra fast rate
10 ⁻¹² –10 ⁻⁶	μs or less	Very fast rate
10 ⁻⁶ –1	Seconds	Fast rate
1–10 ³	minutes or hours	Moderate rate
10 ⁶ –10 ³	Weeks	Slow rate
>10 ⁶	weeks or years	Very slow rate

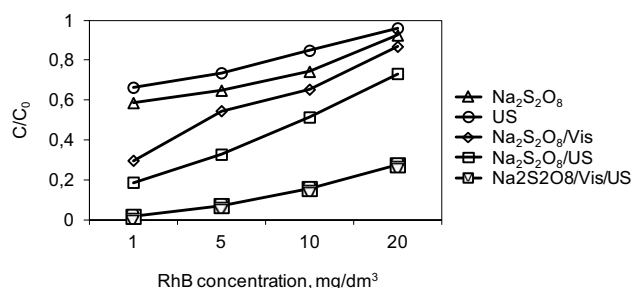


Fig. 6. Efficiency of rhodamine B decolorization depending on the initial dye concentration in various systems. Conditions: reaction time = 60.0 min; pH = 6.0; US frequency = 40.0 kHz; US power = 60 W; temperature = 295 K; Na₂S₂O₈ dose = 20.0 mM; glucose dose = 200.0 mM.

processes (Na₂S₂O₈/Vis/US) allowed to achieve a high RhB degradation at the level of 80% at the highest dye concentration (20.0 mg dm⁻³). In comparison, similar efficiency was obtained in the Na₂S₂O₈/US system, but at the lowest concentration (1.0 mg dm⁻³).

When only ultrasound is used, a similar situation can be observed. With an increasing RhB concentration, a decrease in the efficiency of rhodamine B decomposition was noticed. Similar to the Na₂S₂O₈, Na₂S₂O₈/Vis and Na₂S₂O₈/US systems, this is due to the amount of radicals generated. The amount of radicals generated in high dye concentrations is insufficient to break down excess of RhB particles. As the literature data shows, the other reason is the changing viscosity of the solution at high dye concentrations. It creates a barrier to the enucleation process, thus insufficient amount of radicals is formed [50].

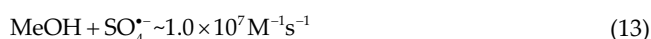
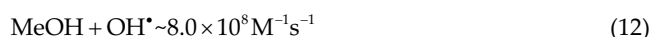
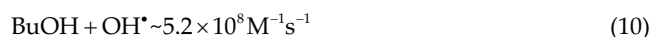
3.5. Radical scavenger tests

Identification of the main active species was carried out for the combined Na₂S₂O₈/Vis/US process. It was the most effective of all the tested systems; therefore it was selected for further studies. Radical scavengers were used at a concentration of 50.0 mM. The process was carried out for 60 min. Radical scavenger test has been carried out with and without SO₄^{-•}, OH[•] and O₂^{-•} scavengers to evaluate their influence on RhB degradation. The resulting solution without the addition of scavengers was marked as “control”. RhB degradation is essentially inhibited by all scavengers

presented in the solution. This indicates that sulfate $\text{SO}_4^{\cdot-}$, hydroxyl OH^{\cdot} and superoxide $\text{O}_2^{\cdot-}$ radicals are generated. As shown in Fig. 8a, the addition of BuOH and MeOH most inhibited the decomposition of rhodamine B. This indicates the significant role of sulfate and hydroxyl radicals in the dye degradation reaction carried out in the presence of persulfate activated with visible light and ultrasound. The addition of hydroquinone ($k_{\text{O}_2^{\cdot-}} = 1.7 \times 10^7 \text{ M}^{-1} \text{ s}^{-1}$) [51] did not significantly affect the degradation process in its initial phases. Within 5–20 min, the inhibition of RhB degradation efficiency is insignificant. Inhibition becomes visible after 20 min, which may indicate delayed formation of $\text{O}_2^{\cdot-}$ radicals.

The obtained results were similar to those obtained by Nasser et al. [11], who applied a radical scavenger test on peroxydisulfate activated by ultrasound irradiation. It was concluded that OH^{\cdot} radical was found to be predominant for the degradation by US/PDS process.

The results showed that under following conditions: RhB concentration = 10.0 mg dm^{-3} ; $\text{Na}_2\text{S}_2\text{O}_8$ dose = 20.0 mM ; pH = 6.0; $T = 295 \text{ K}$; glucose dose = 200.0 mM ; US frequency = 40.0 kHz ; US power = 60 W , RhB degradation was inhibited by nearly 80% by methanol addition. Methanol is a strong scavenger for hydroxyl and weaker for sulfate radicals, while tert-butyl alcohol inhibits only sulfate radicals (Eqs. (10)–(13)) [52].



The $\text{Na}_2\text{S}_2\text{O}_8/\text{Vis}/\text{US}$ process has shown promising efficiency in the degradation of rhodamine B. The degradation degree was significantly inhibited by the addition of methanol (MeOH) and tert-butyl alcohol (BuOH). The results indicate that the RhB degradation was primarily due to hydroxyl radicals, and second due to sulfate radicals. Therefore, the degradation of RhB is attributed to OH^{\cdot} radical. Literature data reported that the hydroxyl radical is formed in the reaction of $\text{SO}_4^{\cdot-}$ with water at the whole range of pH values [53]. Hence, degradation of RhB can be explained by the radical mechanism. Those results are corresponding with the data reported by Lu et al. [54].

To study in detail the mechanism of RhB degradation, not only the absorbance value at the wavelength $\lambda_{\text{max}} = 554.0 \text{ nm}$ was considered but also a full UV-Vis spectrum ($\lambda = 200\text{--}800 \text{ nm}$) of the rhodamine B resulting solutions treated in the $\text{Na}_2\text{S}_2\text{O}_8/\text{Vis}/\text{US}$ process was taken into account, as presented in Fig. 7. Two phenomena were observed during the $\text{Na}_2\text{S}_2\text{O}_8/\text{Vis}/\text{US}$ experiment. First, which was also reported by Wang et al. [55], the absorbance intensity decreased with the process time, as observed in section 3.3. Then, maximum absorbance shift (around 3 nm) was found after 45 min of decolorization ($\lambda_{\text{max}} = 551 \text{ nm}$).

After 60 min of the process, the shift of the absorption peak was set to approximately 6 nm ($\lambda_{\text{max}} = 548 \text{ nm}$). In literature, this phenomenon is found as a hypsochromic shift. In the first case, the reduction of RhB concentration is attributed to chromophore cleavage. Bleaching through the cleavage of conjugated chromophore structure is one of the possible mechanisms of RhB degradation in the AOPs such as photocatalysis and persulfate oxidation [56]. Literature [57,58] revealed that for photodegradation process under visible light irradiation, for some of N-alkylamine-containing dyes (e.g., crystal violet or rhodamine B), the absorption shift is related to the N-demethylation. However, since the absorption shift is insignificant, the major mechanism of rhodamine B degradation in the $\text{Na}_2\text{S}_2\text{O}_8/\text{Vis}/\text{US}$ process is the process of N-deethylation.

The study of reaction kinetics confirmed the above observations. The values of pseudo-first-order reaction and their regression coefficients R^2 are presented in Table 4. Based on experimental results, kinetics of RhB decolorization showed a significant difference in the rate of dye degradation after the addition of radical scavengers. A logarithmic trendline has been shown in Fig. 8b. As a result of the inhibition of hydroxyl and sulfate radicals, the mathematically calculated half-life increased from 2.7 to 10.6 min and then to 24.7 min after the addition of BuOH and MeOH, respectively. The reaction between hydroquinone and $\text{O}_2^{\cdot-}$ radicals resulted in a 46% increase in half-life comparing with the control sample. The reaction rate constant was the lowest after the addition of methanol. These findings are similar to previous studies in the persulfate oxidation system [59].

4. Comparison with other AOPs systems

As presented in Table 5, the proposed method is an interesting alternative to eliminate RhB in comparison with prior studies conducted by the researchers. As is shown, the $\text{Na}_2\text{S}_2\text{O}_8/\text{Vis}/\text{US}$ process has great potential for the degradation of rhodamine B, particularly where the dye concentrations are not high (up to 20 mg dm^{-3}). Energy-saving equipment, relatively short reaction time (60.0 min) and low consumption of reagents are benefits of using this method.

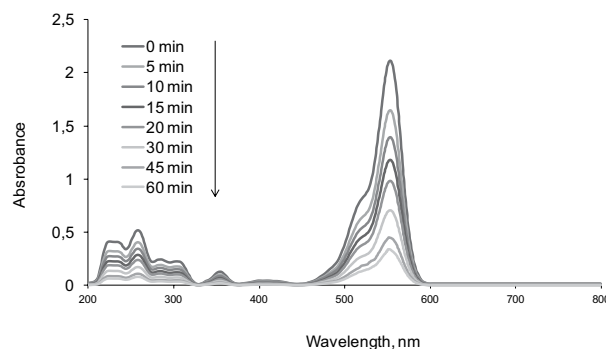


Fig. 7. UV-vis absorption spectra of RhB model solution. Conditions: $C_{0[\text{RhB}]} = 10.0 \text{ mg dm}^{-3}$; $\text{Na}_2\text{S}_2\text{O}_8$ dose = 20.0 mM ; pH = 6.0; $T = 295 \text{ K}$; glucose dose = 200.0 mM ; US frequency = 40.0 kHz ; US power = 60 W .

Table 4
Parameters of pseudo-first-order reaction

Process	k (1/min)	R^2	$t/2$ (min)
$\text{Na}_2\text{S}_2\text{O}_8/\text{Vis}/\text{US}$ (control)	0.2601	0.96	2.7
$\text{Na}_2\text{S}_2\text{O}_8/\text{Vis}/\text{US} + \text{MeOH}$	0.0281	0.83	24.7
$\text{Na}_2\text{S}_2\text{O}_8/\text{Vis}/\text{US} + \text{BuOH}$	0.0655	0.93	10.6
$\text{Na}_2\text{S}_2\text{O}_8/\text{Vis}/\text{US} + \text{hydroquinone}$	0.1396	0.98	5.0

The proposed method is characterized by a low-power radiation source (10 W compared with e.g., 300 W in the study by Wang et al. [60]). The reaction time needed to achieve 85% decolorization is over five times shorter compared with the research performed by Zhang et al. [61]. To limit residual reagents and harmful by-products in the AOP effluent, process optimization should be carried out for specific wastewater.

5. Conclusions

This study showed that the activation of sodium persulfate in the combined visible light–ultrasound system significantly affects the degree of rhodamine B decolorization. Sodium persulfate activated by visible light and ultrasound proved to be highly efficient in the decomposition of rhodamine B. In this system, the degree of rhodamine B decolorization after 60.0 min of reaction was 85%. After 60.0 min of the reaction, mathematically calculated half-life in the $\text{Na}_2\text{S}_2\text{O}_8/\text{Vis}/\text{US}$ system was only 2.1 min under the following conditions: $\text{Na}_2\text{S}_2\text{O}_8$ dose of 20.0 mM; glucose dose of 200.0 mM; US power = 60 W; US frequency = 40 kHz; RhB concentration of 10.0 mg dm^{-3} and initial pH at 6.0. For this system, half-life was over seven times higher compared with the purification process carried out in the presence of $\text{Na}_2\text{S}_2\text{O}_8$ only. Activation of sodium persulfate in the combined system showed high resistance to high RhB concentrations. An 80% of the dye was decomposed after 60.0 min reaction at a concentration of 20.0 mg dm^{-3} in contrast to 40% in a system purified only with persulfate at a concentration of 1.0 mg dm^{-3} . It was determined

Table 5
Efficiency of Rhodamine B degradation in different AOPs

Process	Conditions	Efficiency (%)	Literature
$\text{Na}_2\text{S}_2\text{O}_8/\text{Vis}/\text{US}$	Reaction time = 60.0 min; $C_{0[\text{RhB}]}$ = 10.0 mg dm^{-3} ; $\text{Na}_2\text{S}_2\text{O}_8$ dose = 20.0 mM; pH = 6.0; T = 295 K; glucose dose = 200.0 mM; lamp = 10 W; US frequency = 40.0 kHz; US power = 60 W	85.0	This study
Feather keratin/ CdS/Vis	Reaction time = 70.0 min; $C_{0[\text{RhB}]}$ = 20.0 mg dm^{-3} ; FK/CdS dose = 10 g dm^{-3} ; lamp = 300 W	96.6	[60]
Au-ZnO/Vis	Reaction time = 330.0 min; $C_{0[\text{RhB}]}$ = 1.0 mg dm^{-3} ; Au-ZnO dose = 500 mg dm^{-3} ; pH = 4.76; lamp = 300 W	92.0	[61]
Electro-Fenton	Reaction time = 180.0 min; $C_{0[\text{RhB}]}$ = 10 mg dm^{-3} ; electrode dose = 15 mg dm^{-3} ; pH = 2.0; voltage = 8 V	97.7	[62]
Carbon aerogel/ persulfate	Reaction time = 60.0 min; $C_{0[\text{RhB}]}$ = 10 mg dm^{-3} ; persulfate dose = 1.0 mM; pH = 7.0; T = 298 K; carbon aerogel dose = 100 mg dm^{-3}	80.0	[63]

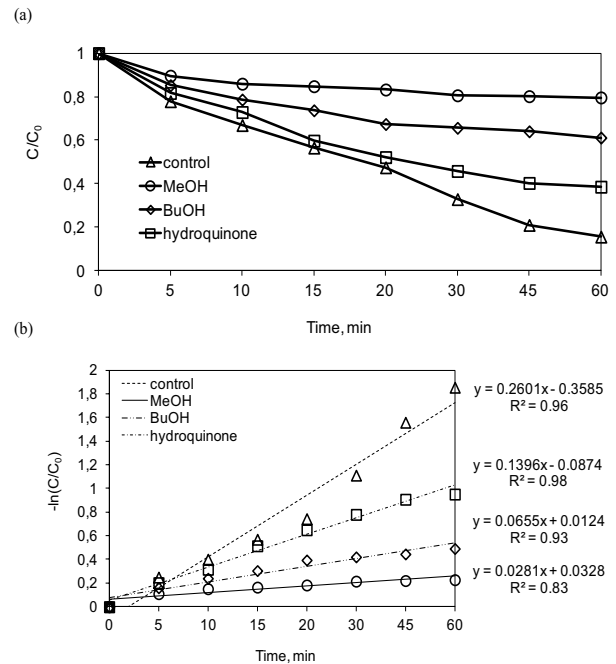


Fig. 8. Decomposition of rhodamine B in the presence of various radical scavengers (a) and reaction kinetics (b). Conditions: $C_{0[\text{RhB}]} = 10.0 \text{ mg dm}^{-3}$; $\text{Na}_2\text{S}_2\text{O}_8$ dose = 20.0 mM; pH = 6.0; $T = 295 \text{ K}$; glucose dose = 200.0 mM; US frequency = 40.0 kHz; US power = 60 W.

that sulfate and hydroxyl radicals were mainly responsible for the decolorization of rhodamine B. Hydroxyl radicals were the dominant radicals enabling RhB degradation.

Funding

The presented study was performed in the framework of the research work in the Central Mining Institute in Poland, financially supported by the Polish Ministry of Science and Higher Education (No. 11158020–340).

References

- [1] Global Water Crisis, The Facts, 2020. Available at: <https://inweh.unu.edu/wp-content/uploads/2017/11/Global-Water-Crisis-The-Facts.pdf> (Accessed on: 10 May 2020).
- [2] R. Tröger, P. Klöckner, L. Ahrens, K. Wiberg, Micropollutants in drinking water from source to tap - method development and application of a multiresidue screening method, *Sci. Total Environ.*, 627 (2018) 1404–1432.
- [3] C.C. Montagner, F.F. Sodr e, R.D. Acayaba, C. Vidal, I. Campestrini, M.A. Locatelli, I.C. Pescara, A.F. Albuquerque, G.A.  umbuzeiro, W.F. Jardim, Ten years-snapshot of the occurrence of emerging contaminants in drinking, surface and ground waters and wastewaters from S ao Paulo State, Brazil, *J. Braz. Chem. Soc.*, 30 (2019) 614–632.
- [4] J. Kozak, M. Włodarczyk-Makula, Comparison of the PAHs degradation effectiveness using CaO₂ or H₂O₂ under the photo-Fenton reaction, *Desal. Water Treat.*, 134 (2018) 57–64.
- [5] J. Kozak, M. Włodarczyk-Makula, The use of sodium percarbonate in the Fenton reaction for the PAHs oxidation, *Civil Environ. Eng. Rep.*, 28 (2018) 124–139.
- [6] K. Shakir, A.F. Elkafrawy, H.F. Ghoneimy, S.G. Elrab Beheir, M. Refaat, Removal of rhodamine B (a basic dye) and thoron (an acidic dye) from dilute aqueous solutions and wastewater simulants by ion flotation, *Water Res.*, 44 (2010) 1449–1461.
- [7] L. Yu, Y. Mao, L. Qu, Simple voltammetric determination of Rhodamine B by using the glassy carbon electrode in fruit juice and preserved fruit, *Food Anal. Methods*, 6 (2013) 1665–1670.
- [8] S.S. Imam, H.F. Babamale, A short review on the removal of rhodamine B dye Rusing agricultural waste-based adsorbents, *Asian J. Chem. Sci.*, 7 (2020) 25–37.
- [9] B. Dogan, M. Kerestecioglu, U. Ulku Yetis, Assessment of the best available wastewater management techniques for a textile mill: cost and benefit analysis, *Water Sci. Technol.*, 61 (2010) 963–970.
- [10] R. Zhang, P. Sun, T.H. Boyer, L. Zhao, C.H. Huang, Degradation of pharmaceuticals and metabolite in synthetic human urine by UV, UV/H₂O₂, and UV/PDS, *Environ. Sci. Technol.*, 49 (2015) 3056–3066.
- [11] S. Nasser, A.H. Mahvi, M. Seyedsalehi, K. Yaghmaeian, R. Nabizadeh, M. Aliomohammadi, G.H. Safari, Degradation kinetics of tetracycline in aqueous solutions using peroxydisulfate activated by ultrasound irradiation: effect of radical scavenger and water matrix, *J. Mol. Liq.*, 241 (2017) 704–714.
- [12] S.A. Hakim, S. Jaber, N.Z. Eddine, A. Baalbaki, A. Ghauch, Data for persulfate activation by UV light to degrade theophylline in a water effluent, *Data Brief*, 27 (2019) 104614.
- [13] Y. Ji, W. Xie, Y. Fan, Y. Shi, D. Kong, J. Lu, Degradation of trimethoprim by thermo-activated persulfate oxidation: reaction kinetics and transformation mechanisms, *Chem. Eng. J.*, 286 (2016) 16–24.
- [14] J. Criquet, N.K. Vel Leitner, Electron beam irradiation of aqueous solution of persulfate ions, *Chem. Eng. J.*, 169 (2011) 258–262.
- [15] O. Furman, A.L. Teel, R.J. Watts, Mechanism of base activation of persulfate, *Environ. Sci. Technol.*, 44 (2010) 6423–6428.
- [16] M. Nie, C. Yan, M. Li, X. Wang, W. Bi, W. Dong, Degradation of chloramphenicol by persulfate activated by Fe²⁺ and zerovalent iron, *Chem. Eng. J.*, 279 (2015) 507–515.
- [17] G.P. Anipsitakis, D.D. Dionysiou, Radical generation by the interaction of transition metals with common oxidants, *Environ. Sci. Technol.*, 38 (2004) 3705–3712.
- [18] W.S. Chen, Y.C. Su, Removal of dinitrotoluenes in wastewater by sono-activated persulfate, *Ultrason. Sonochem.*, 19 (2012) 921–927.
- [19] X. Cheng, H. Guo, Y. Zhang, G. Korshin, B. Yang, Insights into the mechanism of nonradical reactions of persulfate activated by carbon nanotubes: activation performance and structure-function relationship, *Water Res.*, 157 (2019) 406–414.
- [20] P. Zawadzki, Decolorisation of Methylene Blue with sodium persulfate activated with visible light in the presence of glucose and sucrose, *Water Air Soil Pollut.*, 230 (2019) 1–18.
- [21] W. Wang, H. Wang, G. Li, T. An, H. Zhao, P.K. Wong, Catalyst-free activation of persulfate by visible light for water disinfection: efficiency and mechanisms, *Water Res.*, 157 (2019) 106–118.
- [22] H. Herrmann, On the photolysis of simple anions and neutral molecules as sources of O[•]/OH, SO_x[•] and Cl in aqueous solution, *Phys. Chem. Chem. Phys.*, 9 (2007) 3935–3964.
- [23] R.J. Watts, M. Ahmad, A.K. Hohner, A.L. Teel, Persulfate activation by glucose for in situ chemical oxidation, *Water Res.*, 133 (2018) 247–254.
- [24] P. Gayathri, R.P.J. Dorathi, K. Palanivelu, Sonochemical degradation of textile dyes in aqueous solution using sulphate radicals activated by immobilized cobalt ions, *Ultrason. Sonochem.*, 17 (2010) 566–571.
- [25] G.J. Price, A.A. Clifton, Sonochemical acceleration of persulfate decomposition, *Polymer*, 37 (1996) 3971–3973.
- [26] K.H. Chu, Y.A.J. Al-Hamadani, C.M. Park, G. Lee, M. Jang, A. Jang, N. Her, A. Son, Y. Yoon, Ultrasonic treatment of endocrine disrupting compounds, pharmaceuticals, and personal care products in water: a review, *Chem. Eng. J.*, 327 (2017) 629–647.
- [27] A.B. Kurukutla, P.S.S. Kumar, S. Anandan, T. Sivasankar, Sonochemical degradation of Rhodamine B using oxidants, hydrogen peroxide/peroxydisulfate/peroxymonosulfate, with Fe²⁺ ion: proposed pathway and kinetics, *Environ. Eng. Sci.*, 32 (2015) 129–140.
- [28] Rhodamine B. Available at: <https://pubchem.ncbi.nlm.nih.gov/compound/Rhodamine-B>, 2020 (Accessed on: 10 May 2020).
- [29] K.P. Wai, Y.L. Pang, S. Lim, C.H. Koo, W.C. Chong, Hydrothermal modification of zinc oxide and titanium dioxide for photocatalytic degradation of Rhodamine B, *AIP Conf. Proc.*, 2157 (2019) 020006.
- [30] D. Melgoza, A. Hernandez-Ramirez, J.M. Peralta-Hernandez, Comparative efficiencies of the decolourisation of methylene blue Rusing Fenton’s and photo-Fenton’s reactions, *Photochem. Photobiol. Sci.*, 8 (2009) 596–599.
- [31] D. Nakarada, M. Petkovic, Mechanistic insights on how hydroquinone disarms OH and OOH radicals, *Quantum Chem.*, 118 (2018) 1–14.
- [32] J. Wang, S. Wang, Activation of persulfate (PS) and peroxymonosulfate (PMS) and application for the degradation of emerging contaminants, *Chem. Eng. J.*, 334 (2018) 1502–1517.
- [33] H. Azarpira, M. Sadani, M. Abtahi, N. Vaezi, S. Rezaei, Z. Atafar, S.M. Mohseni, M. Sarkhosh, M. Ghaderpoori, H. Keramati, R.H. Pouyaj, A. Akbari, V. Fanai, Photo-catalytic degradation of triclosan with UV/iodide/ZnO process: performance, kinetic, degradation pathway, energy consumption and toxicology, *J. Photochem. Photobiol. A*, 371 (2019) 423–432.
- [34] G.V. Buxton, C.L. Greenstock, W.P. Helman, A.B. Ross, Critical review of rate constants for reactions of hydrated electrons, hydrogen atoms and hydroxyl radicals (•OH/•O) in aqueous solution, *J. Phys. Chem. Ref. Data*, 17 (1988) 513–886.
- [35] T. Cai, Y. Liu, L. Wang, W. Dong, H. Chen, W. Zeng, X. Xia, G. Zeng, Activation of persulfate by photoexcited dye for antibiotic degradation: radical and nonradical reactions, *Chem. Eng. J.*, 375 (2019) 122070.
- [36] M. Ahmad, A.L. Teel, R.J. Watts, Mechanism of persulfate activation by phenols, *Environ. Sci. Technol.*, 47 (2013) 5864–5871.
- [37] S. Ahmadi, Ch.A. Igwegbe, S. Rahdar, The application of the thermally activated persulfate for degradation of Acid Blue 92 in aqueous solution, *Int. J. Ind. Chem.*, 10 (2019) 1–12.
- [38] Z. Wei, F.A. Villamena, L.K. Weavers, Kinetics and mechanism of ultrasonic activation of persulfate: an in-situ EPR spin trapping study, *Environ. Sci. Technol.*, 51 (2017) 3410–3417.
- [39] J.M. Monteagudo, A. Duran, R. Gonzalez, A.J. Exposito, In situ chemical oxidation of carbamazepine solutions using persulfate simultaneously activated by heat energy, UV light, Fe²⁺ ions, and H₂O₂, *Appl. Catal., B*, 176–177 (2015) 120–129.
- [40] K. Fedorov, M. Plata-Gryl, J.A. Khan, G. Boczkaj, Ultrasound-assisted heterogeneous activation of persulfate and peroxymonosulfate by asphaltene for the degradation of BTEX in water, *J. Hazard. Mater.*, 397 (2020) 122804.

- [41] F. Ghanbari, M. Moradi, Application of peroxymonosulfate and its activation methods for degradation of environmental organic pollutants: review, *Chem. Eng. J.*, 310 (2017) 41–62.
- [42] C.H. Weng, K.L. Tsai, Ultrasound and heat enhanced persulfate oxidation activated with Fe⁰ aggregate for the decolorization of C.I. Direct Red 23, *Ultrason. Sonochem.*, 29 (2016) 11–18.
- [43] P. Zawadzki, E. Kudlek, M. Dudziak, Kinetics of the photocatalytic decomposition of bisphenol A on modified photocatalysts, *J. Ecol. Eng.*, 19 (2018) 260–268.
- [44] E. Kudlek, M. Dudziak, G. Kamińska, J. Bohdziewicz, Kinetics of the photocatalytic degradation of selected organic micropollutants in the water environment, *J. Ecol. Eng.*, 18 (2017) 75–82.
- [45] L.W. Hou, H. Zhang, L.G. Wang, L. Chen, Y.D. Xiong, X.F. Xue, Removal of sulfamethoxazole from aqueous solution by sono-ozonation in the presence of a magnetic catalyst, *Sep. Purif. Technol.*, 117 (2013) 46–52.
- [46] M.R. Wright, *An Introduction to Chemical Kinetics*, John Wiley and Sons, England, 2004.
- [47] J.P. Zotesso, E.S. Cossich, V. Janeiro, C.R.G. Tavares, Treatment of hospital laundry wastewater by UV/H₂O₂ process, *Environ. Sci. Pollut. Res.*, 24 (2017) 6278–6287.
- [48] F. Liu, P. Yi, X. Wang, H. Gao, H. Zhang, Degradation of Acid Orange 7 by an ultrasound/ZnO-GAC/persulfate process, *Sep. Purif. Technol.*, 194 (2018) 181–187.
- [49] C. Cai, H. Zhang, X. Zhong, L.W. Hou, Ultrasound enhanced heterogeneous activation of peroxymonosulfate by a bimetallic Fe-Co/SBA-15 catalyst for the degradation of Orange II in water, *J. Hazard. Mater.*, 283 (2015) 70–79.
- [50] K. Thangavadivel, M. Megharaj, A. Mudhoo, R. Naidu, Degradation of Organic Pollutants Using Ultrasound, S.K. Sharma, A. Mudhoo, Eds., *Handbook on Application of Ultrasound: Sonochemistry for Sustainability*, CRC Press, Taylor & Francis Group, 2011, pp. 447–474.
- [51] P.S. Rao, E. Hayon, Redox potentials of free radicals. IV. Superoxide and hydroperoxy radicals •O₂⁻ and •HO₂, *J. Phys. Chem.*, 79 (1975) 397–402.
- [52] A.M. Ocampo, *Persulfate Activation by Organic Compounds*, Washington State University, Washington, 2009, pp. 1–77.
- [53] J.Y. Zhao, Y. Zhang, X. Quan, S. Chen, Enhanced oxidation of 4-chlorophenol using sulfate radicals generated from zero-valent iron and peroxydisulfate at ambient temperature, *Sep. Purif. Technol.*, 71 (2010) 302–307.
- [54] Y. Lu, X. Yang, L. Xu, Z. Wang, Y. X., G. Qian, Sulfate radicals from Fe³⁺/persulfate system for Rhodamine B degradation, *Desal. Water Treat.*, 57 (2016) 1–10.
- [55] S. Wang, Y. Jia, L. Song, H. Zhang, Decolorization and mineralization of Rhodamine B in aqueous solution with a triple system of Cerium(IV)/H₂O₂/hydroxylamine, *ACS Omega*, 3 (2018) 18456–18465.
- [56] Y. Fan, G. Chen, D. Li, Y. Luo, N. Lock, A.P. Jensen, A. Mamakhel, J. Mi, S.B. Iversen, Q. Meng, B.B. Iversen, Highly selective Deethylation of Rhodamine B on TiO₂ prepared in supercritical fluids, *Int. J. Photoenergy*, 173865 (2012) 1–7.
- [57] X. Hu, T. Moohamood, W. Ma, C. Chen, J. Zhao, Oxidative decomposition of Rhodamine B dye in the presence of VO₂⁺ and/or Pt(IV) under Visible Light Irradiation: N-Deethylation, chromophore cleavage, and mineralization, *J. Phys. Chem. B*, 110 (2006) 26012–26018.
- [58] C. Lops, A. Ancona, K. Di Cesare, B. Dumontel, N. Garino, G. Canavese, S. Hernandez, V. Cauda, Sonophotocatalytic degradation mechanisms of Rhodamine B dye via radicals generation by micro- and nano-particles of ZnO, *Appl. Catal. B Environ.*, 243 (2019) 629–640.
- [59] H. Wang, W. Guo, R. Yin, J. Du, Q. Wu, H. Luo, B. Liu, F. Sseguya, N. Ren, Biochar-induced Fe(III) reduction for persulfate activation in sulfamethoxazole degradation: insight into the electron transfer, radical oxidation and degradation pathways, *Chem. Eng. J.*, 362 (2019) 561–569.
- [60] Q. Wang, J. Lian, Q. Ma, Y. Bai, J. Tong, J. Zhong, R. Wang, H. Huang, B. Su, Photodegradation of Rhodamine B over a novel photocatalyst of feather keratin decorated CdS under visible light irradiation, *New J. Chem.*, 9 (2015) 7112–7119.
- [61] Y. Zhang, J. Zhou, Z. Li, Q. Feng, Photodegradation pathway of rhodamine B with novel Au nanorods @ ZnO microspheres driven by visible light irradiation, *J. Mater. Sci.*, 53 (2018) 3149–3162.
- [62] R. Jinisha, R. Gandhimathi, S.T. Ramesh, P.V. Nidheesh, S. Velmathi, Removal of rhodamine B dye from aqueous solution by electro-Fenton process using iron-doped mesoporous silica as a heterogeneous catalyst, *Chemosphere*, 200 (2018) 446–454.
- [63] L. Jiang, Y. Zhang, M. Zhou, L. Liang, K. Li, Oxidation of Rhodamine B by persulfate activated with porous carbon aerogel through a non-radical mechanism, *J. Hazard. Mater.*, 358 (2018) 53–61.

Elimination of chlorfenvinphos from treated municipal wastewater in advanced oxidation processes

Eliminacja chlorfenwinfosu z oczyszczonych ścieków komunalnych w procesach zaawansowanego utleniania

DOI: 10.15199/62.2021.3.11

Chlorfenvinphos (CFVP) was added to samples of treated municipal wastewater and oxidized in the presence of TiO_2 and UV, O_3 and UV radiation or sulfate radicals generated in the presence of $Na_2S_2O_8$, glucose and visible light (PDS + Vis) for 10 and 20 min. The CFVP content in the tested samples was detd. by HPLC method. The highest degree of CFVP degrdn. (82%) was obtained using the PDS + Vis method.

Przedstawiono wyniki badań procesów zaawansowanego utleniania chlorfenwinfosu z rzeczywistego strumienia ścieków komunalnych. Stopień eliminacji chlorfenwinfosu wyniósł 26–82% w zależności od zastosowanego procesu doczyszczania. Stwierdzono, że zaawansowane procesy utleniania stanowią interesującą alternatywę dla klasycznych procesów oczyszczania, w szczególności jako IV lub V etap doczyszczania ścieków.

Zapisy dyrektywy¹⁾ wskazują, że istnieje konieczność opracowania nowych technologii eliminacji substancji priorytetowych i priorytetowych substancji niebezpiecznych. Spośród związków lub

grupy związków zaliczanych do substancji priorytetowych wyróżnić można (Z)-2-chloro-1-(2,4-dichlorofenyl)winylo dietylofosforan, znany jako chlorfenwinfos (CFVP). Chlorfenwinfos jest jednym z najważniejszych przedstawicieli insektycydów fosforoorganicznych (pochodnych kwasu fosforowego). CFVP jest stosowany jako insektycyd o małej toksyczności względem ssaków. Jego działanie polega na hamowaniu aktywności acetylocholinoesterazy, jednego z ważniejszych enzymów dla obwodowego i ośrodkowego układu nerwowego²⁾.

CFVP jest identyfikowany w próbkach pobranych z mediów ciekłych (woda, ścieki) i stałych (osady dennie, osady ściekowe) na całym świecie^{3, 4)}. Badania wykazały, że występuje on w próbkach wód powierzchniowych w ilości od 1 ng/L do blisko 48 µg/L. Związek ten wykryto również w wodach gruntowych i wodach morskich na poziomie ok. 20 ng/L⁵⁾. Dane te dowodzą, że konwencjonalne technologie oczyszczania ścieków, takie jak sedymentacja i rozkład biologiczny, są niewystarczające. Co więcej, toksyczność CFVP negatywnie wpływa na aktywność mikroorganizmów osadu czynnego. Z tego względu konieczne jest poszukiwanie nowych, skutecznych i ekonomicznie opłacalnych metod eliminacji tego typu zanieczyszczeń.

Jedną z interesujących metod eliminacji substancji priorytetowych są procesy zaawansowanego utleniania (AOPs). Ze względu na koszty inwestycyjne i eksploatacyjne oraz ryzyko generowania ubocznych produktów utleniania, rekomendowane jest stosowanie AOPs jako ostatniego etapu oczyszczania ścieków (IV lub V stopień oczyszczania ścieków). Cechą wspólną AOPs jest wykorzystanie potencjału utleniającego rodników hydroksylowych OH[•]. Reakcje prowadzone w obecności tych rodników są nieselektywne, a potencjał utleniający E^0 wynosi ok. 2,80 V. Znanych jest wiele procesów, w których generowane są rodniki hydroksylowe, takich jak fotokataliza (TiO_2 +UV) lub ozonowanie wspomagane promieniowaniem ultrafioletowym (O_3 +UV). Według najnowszych doniesień literaturowych duże zainteresowanie wzbudza również utlenianie rodnikami siarczanowymi (np. za pomocą nadsiarczanu sodu)⁶⁾. Rodniki siarczanowe ($SO_4^{\cdot-}$) charakteryzują się podobnym potencjałem utleniającym ($E^0 = 2,70$ V). Rodniki siarczanowe powstają w wyniku oddziaływania różnych źródeł energii (np. ciepło, promieniowanie UV) na prekursor, taki jak nadsiarczan sodu ($Na_2S_2O_8$), lub w wyniku reakcji jonów metali przejściowych (np. Fe^{2+} , Co^{2+}).



Mgr inż. Piotr ZAWADZKI w roku 2018 ukończył studia na Wydziale Inżynierii Środowiska i Energetyki Politechniki Śląskiej w Gliwicach. W 2017 r. uzyskał tytuł finalisty konkursu Studencki Nobel 2017 w kategorii „Nauki przyrodnicze i energetyka”. W Głównym Instytucie Górniczo-Katowice pracuje od 2018 r. Specjalność – technologia wody i ścieków.

* Adres do korespondencji:

Zakład Ochrony Wód, Główny Instytut Górniczo-Katowice, Plac Gwarków 1, 40-166 Katowice, tel.: (32) 259-28-01, fax: (32) 259-21-54, e-mail: pzawadzki@gig.eu

Część doświadczalna

Materiały

Przedmiotem badań były próbki oczyszczonych ścieków komunalnych z dodatkiem wzorca CFVP o stężeniu 1 mg/L. Wzorec CFVP (PestanaL[®]) o czystości > 95% zakupiono w firmie Sigma-Aldrich (Poznań).

Oczyszczone ścieki, pobrane bezpośrednio z koryta odpływowego, pochodziły z komunalnej oczyszczalni ścieków zlokalizowanej w jednym z miast aglomeracji śląskiej. Obecnie oczyszczalnia pracuje w dwustopniowym systemie mechaniczno-biologicznym. W odpływie ścieków oczyszczonych z tej oczyszczalni nie zidentyfikowano chlorfenwinfosu.

Wykonane analizy wskazały, że oczyszczalnia spełnia wymagania dotyczące jakości ścieków odprowadzanych do środowiska zgodnie z obowiązującym pozwoleniem wodnoprawnym. Ze względu na niską barwę, mętność oraz niewielki udział zawieszin, próbki przed procesami doczyszczania nie były poddawane wstępnej filtracji.

Do rozkładu CFVP wykorzystywano różne źródła rodników utleniających (katalizatory, prekursorzy), takie jak tlenek tytanu(IV), nadsiarczan sodu oraz ozon. Wszystkie odczynniki chemiczne pochodziły z firmy Sigma-Aldrich (Poznań).

Aparatura

Procesy AOPs prowadzono w szklanym reaktorze laboratoryjnym o pojemności 0,5 L (rys. 1). Mieszaniny reakcyjne zawierające CFVP umieszczano na podstawie mieszadła magnetycznego, a następnie, w zależności od układu utleniającego, wprowadzano tlenek tytanu(IV) lub nadsiarczan sodu ($\text{Na}_2\text{S}_2\text{O}_8$). Procesy wspomagano poprzez umieszczenie w reaktorze lampy ultrafioletowej o mocy 10 W (Grech model CUV-510) lub lampy tungstenowej o mocy 10 W emitującej promieniowanie widzialne (model QTH10/M firmy Thorlabs Inc., New Jersey, Stany Zjednoczone) lub ozonatora o mocy 20 W (ZY-H103, Eltom, Warszawa).

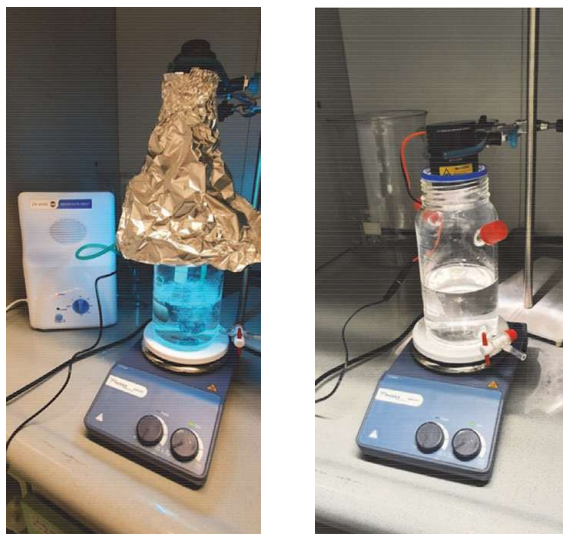


Fig. 1. Apparatus for CFVP degradation

Rys. 1. Aparatura do rozkładu CFVP

Metodyka badań

Proces fotokatalitycznego utleniania CFVP prowadzono w obecności ditlenku tytanu (układ TiO_2 +UV). Dawka TiO_2 wynosiła 50 oraz 100 mg/L. Przed włączeniem źródła promieniowania zapewniono 15-minutowy czas kontaktu katalizatora z mieszaniną reakcyjną (sorpacja). Zaawansowane utlenianie pod wpływem rodników hydroksylo- wych prowadzono także w obecności ozonu (układ O_3 +UV). Dawka

ozonu wynosiła 100 mg/L oraz 200 mg/L. Generowanie rodników siarczanowych prowadzono w obecności nadsiarczanu sodu (układ PDS +Vis), glukozy oraz światła widzialnego (innowacyjna metoda aktywacji). Dawki nadsiarczanu sodu wynosiły 10 i 20 mM, a dawka glukozy 100 mM. Wszystkie procesy AOPs prowadzono przez 10 i 20 min.

Metody analityczne

Anality znajdujące się w próbkach ciekłych przed i po procesach AOPs poddano analizie chromatograficznej HPLC z detektorem UV, zgodnie z normą⁷. Analizę poprzedzono wydzieleniem związku metodą ekstrakcyjną do fazy stałej (SPE) z wcześniejszym odseparowaniem ewentualnych pozostałości katalizatorów lub większych cząstek na filtrze 0,45 μm . Ekstrakcję prowadzono w kolumnkach Chromabond[®] C18 ec. Ekstrakt analizowano za pomocą chromatografu cieczonego HPLC model 1200 firmy Perlan Technologies (Warszawa).

Omówienie wyników

Na rys. 2 przedstawiono wyniki badań rozkładu CFVP w różnych konfiguracjach AOPs. Na podstawie uzyskanych wyników stwierdzono, że czas prowadzenia procesu ma wpływ na obniżenie początkowego stężenia CFVP. Wydłużenie czasu reakcji z 10 do 20 min spowodowało wzrost efektywności procesu średnio o 5–35%, niezależnie od zastosowanej dawki utleniaczy. Było to związane z procesem generowania rodników utleniających wraz z biegiem reakcji utleniającej⁸.

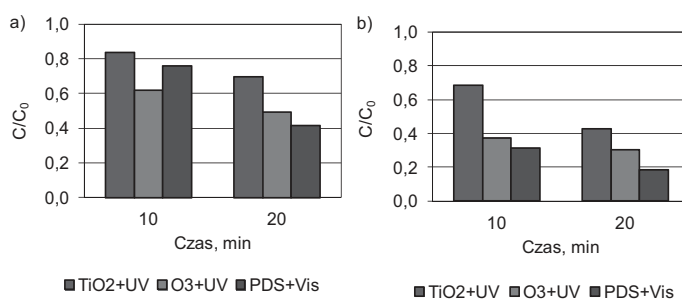


Fig. 2. Degradation of CFVP in different advanced oxidation processes: a) $\text{TiO}_2 = 50 \text{ mg/L}, \text{O}_3 = 100 \text{ mg/L}, \text{PDS} = 10 \text{ mM}$; b) $\text{TiO}_2 = 100 \text{ mg/L}, \text{O}_3 = 200 \text{ mg/L}, \text{PDS} = 20 \text{ mM}$

Rys. 2. Rozkład CFVP w różnych procesach zaawansowanego utleniania: a) dawki: $\text{TiO}_2 = 50 \text{ mg/L}, \text{O}_3 = 100 \text{ mg/L}, \text{PDS} = 10 \text{ mM}$; b) dawki: $\text{TiO}_2 = 100 \text{ mg/L}, \text{O}_3 = 200 \text{ mg/L}, \text{PDS} = 20 \text{ mM}$

Działanie promieniowania UV na fotokatalizator (układ TiO_2 +UV) powodowało jego aktywację, a w efekcie wielu reakcji powstawały dziury elektronowe reagujące z cząsteczkami wody, w wyniku czego tworzyły się rodniki hydroksylowe. Przy dawce TiO_2 50 mg/L po 10 min reakcji stopień eliminacji CFVP wyniósł 26%. Wydłużenie czasu reakcji do 20 min spowodowało wzrost efektywności do ok. 31%. Ponieważ zastosowana dawka fotokatalizatora była mniejsza od tych przedstawionych w danych literaturowych⁹, zastosowano dawkę dwa razy większą (100 mg/L). Przy tej dawce już po 20 min reakcji stopień rozkładu CFVP wyniósł ok. 57%.

Jak pokazują dane literaturowe¹⁰, skuteczny rozkład zanieczyszczeń można uzyskać, stosując kombinację działania ozonu i promieniowania ultrafioletowego (układ O_3 +UV). Ozonowanie ścieków przy jednoczesnym naświetlaniu badanych mieszanin promieniowaniem UV pozwoliło na uzyskanie ok. 50-proc. i 70-proc. stopnia rozkładu CFVP po 20 min reakcji, dla dawki odpowiednio 100 mg/L i 200 mg/L. Rozkład CFVP wynika z wielu reakcji, przy czym najczęściej przytaczany jest model dwuetapowy¹¹. Polega on w pierwszej kolejności na procesie fotoindukowanej homolizy cząsteczek ozonu, a następnie na generowaniu rodników hydroksylo- wych w wyniku reakcji wody z tlenem atomowym.

Rozkład CFVP prowadzono również za pomocą rodników siarczanowych (SO_4^-). Ich prekursorem był nadsiarczan sodu aktywowany światłem widzialnym w obecności glukozy (układ PDS+Vis). Szczegółowy mechanizm aktywacji PDS omówiono w pracy^[2]. Najwyższy stopień rozkładu CFVP uzyskano w układzie PDS+Vis (rys. 2). W wyniku oczyszczania ścieków komunalnych w układzie PDS+Vis stopień rozkładu CFVP przy dawce 10 mM PDS po 20 min reakcji wynosił ok. 60%. Dwukrotne zwiększenie dawki PDS pozwoliło na wzrost stopnia eliminacji CFVP do ok. 82% po 20 min utleniania, co było związane ze wzrostem gęstości generowanych rodników utleniających. Aktywacja nadsiarczanu sodu wynikała z synergistycznego współdziałania światła widzialnego i glukozy. Naświetlanie roztworów światłem widzialnym powodowało rozpad glukozy (substancja optycznie aktywna), transfer elektronu z cukru w kierunku PDS (aktywacja PDS) oraz utlenianie glukozy do produktów aktywujących $\text{Na}_2\text{S}_2\text{O}_8$ ^[3].

Niepełny rozkład CFVP mógł wynikać m.in. z negatywnego wpływu substancji przeszkadzających w procesach AOPs, takich jak jony CO_3^{2-} lub HCO_3^- . Przyczyną obniżonej efektywności mogły być także cząstki stałe zawieszone w oczyszczanych ściekach.

Podsumowanie

Identyfikacja pestycydów fosforoorganicznych, takich jak CFVP, w odpływach z różnych obiektów komunalnych na świecie pokazuje, że uzasadnione jest poszukiwanie nowych metod ich eliminacji. Przedstawione wyniki badań wskazują, że procesy AOPs stanowią interesujące rozwiązanie problemu odpływu zanieczyszczeń antropogenicznych wraz z odpływem oczyszczonych ścieków. Potencjalne wdrożenie takich układów oczyszczania, jak fotokataliza (TiO_2+UV), ozonowanie wspomaganie promieniowaniem ultrafioletowym (O_3+UV) lub utlenianie rodnikami siarczanowymi (PDS+Vis) wymaga jednak uwzględnienia negatywnych zjawisk wynikających ze zmiennej

w czasie jakości ścieków. Zbadane w ramach pracy procesy, przy odpowiednio dobranych parametrach dostosowanych do zmieniających się warunków pracy oczyszczalni, mogą być z powodzeniem stosowane jako IV lub V stopień doczyszczania ścieków.

Publikacja wykonana w ramach pracy statutowej (nr 11158020-340) obejmującej badania naukowe i/lub prace rozwojowe, finansowanej przez Ministerstwo Nauki i Szkolnictwa Wyższego, realizowanej w Głównym Instytucie Górnictwa w Katowicach.

Otrzymano: 11-01-2021

LITERATURA

- [1] Dyrektywa 2013/39/UE Parlamentu Europejskiego i Rady z dnia 12 sierpnia 2013 r. zmieniająca dyrektywy 2000/60/WE i 2008/105/WE w zakresie substancji priorytetowych w dziedzinie polityki wodnej, *Dz. Urz. UE* L 226, 1.
- [2] M. Sigurnjak, S. Ukic, M. Cvetnic, M. Markic, M.N. Stankov, B. Rasulev, H. Kusic, A.L. Bozic, M. Rogosic, T. Bolanca, *Chemosphere* 2020, **240**, 124973.
- [3] H. Pan, B. Xi, H. Lei, X. He, Y. Han, Q. Xu, *J. Residuals Sci. Technol.* 2017, **14**, nr 2, 239.
- [4] G. Perez-Lucas, N. Vela, A.E. Aatik, S. Navarro, *Pesticides. Use and misuse and their impact in the environment*, IntechOpen, London 2018.
- [5] M.S. Shaw, D.S. Silburn, M. Lenahan, M. Harris, *Pesticides in groundwater of the lower Burdekin floodplain*, Gov. Queensland, Australia, 2012.
- [6] W. Wang, H. Wang, G. Li, T. An, H. Zhao, P. Wong, *Water Res.* 2019, **157**, 106.
- [7] PN 11369:1997, *Jakość wody. Oznaczanie wybranych środków ochrony roślin. Metoda z zastosowaniem wysokosprawnej chromatografii cieczowej z detekcją UV po ekstrakcji ciała stałe-ciecz.*
- [8] G. Sujatha, S. Shanthakumar, F. Chiampo, *Environments* 2020, **7**, nr 6, 47.
- [9] P. Zawadzki, *Materials* 2020, **13**, nr 2, 289.
- [10] F. Jabbari, A. Eslami, J. Mahmoudian, *Health Scope* 2020, **9**, 2.
- [11] G.R. Peyton, W.H. Glaze, *Environ. Sci. Technol.* 1988, **22**, nr 7, 761.
- [12] P. Zawadzki, *Water Air Soil Pollut.* 2019, **230**, 313.
- [13] T. Cai, Y. Liu, L. Wang, W. Dong, H. Chen, W. Zeng, X. Xia, G. Zeng, *Chem. Eng. J.* 2019, **375**, 122070.

korozja kosztuje! *

***) straty korozyjne szacuje się na 3-6% PKB**



na życzenie wysyłamy bezpłatny egzemplarz okazowy:
redakcja@ochronapredkorozja.pl

Czasopismo
„Ochrona przed Korozją”
– forum wymiany wiedzy i doświadczeń na temat ochrony materiałów przed skutkami korozji

www.ochronapredkorozja.pl
www.sigma-not.pl



Evaluation of TiO_2/UV ; O_3/UV , and PDS/Vis for improving chlorfenvinphos removal from real municipal treated wastewater effluent

P. Zawadzki¹

Received: 17 September 2021 / Revised: 1 December 2021 / Accepted: 23 June 2022

© The Author(s) under exclusive licence to Iranian Society of Environmentalists (IRSEN) and Science and Research Branch, Islamic Azad University 2022

Abstract

This article investigates the advanced oxidation processes (TiO_2/UV ; O_3/UV , and PDS/Vis) for final treatment of real municipal treated wastewater containing chlorfenvinphos at a concentration of 1 mg/l. During the advanced oxidation processes, the mineralization tests and kinetics described by pseudo-first-order model were performed. An approach using specific energy consumption and electric energy per order indicators was used to estimate the minimum energy requirement to degrade the chlorfenvinphos. MICROTOX[®] was used for the assessment of toxicity. Within 20 min, chlorfenvinphos concentration in the three studied advanced oxidation processes was reduced by between 51 and 81%, but the most effective process was PDS/Vis. The Total Organic Carbon mineralization index indicated that chlorfenvinphos is not fully degraded. The maximum Total Organic Carbon removal percentage of 81% was obtained for the PDS/Vis process, as well as the reduction in toxicity was the highest for this process. The solutions subjected to the TiO_2/UV and PDS/Vis showed less toxicity than the chlorfenvinphos contaminated wastewater. The conducted study showed that the visible-light-driven activation of sodium persulfate is the most effective for: (1) lowering the final concentration of chlorfenvinphos, (2) the mineralization degree and (3) toxicity of the solution. PDS/Vis was also the most effective process from the economic point of view. Experimental research showed that the PDS/Vis process can be a valuable alternative to TiO_2/UV and O_3/UV processes.

Keywords Chlorfenvinphos · Municipal wastewater · Advanced oxidation process · Energy consumption · Microtox · Kinetics

Introduction

Among the compounds or a group of compounds classified as priority substances (Directive 2013/39/EU, 2013), chlorfenvinphos (CFVP), a pesticide belonging to the family of organophosphorus insecticides can be found. CFVP inhibits the activity of acetylcholinesterase, one of the essential enzymes for the peripheral and central nervous systems. It disturbs the hormonal balance and can be bioconcentrated (Sigurnjak et al. 2020).

CFVP was identified mainly in the surface and ground waters, raw and treated wastewater. CFVP was identified at

concentrations between 1 ng/l and 48 µg/l, although the contaminated sites may have even higher concentrations (Pan et al. 2017; Shaws et al. 2012).

CFVP was identified also in the effluents from wastewater treatment plants in Spain at the level of about 50–140 ng/l (Campo et al. 2013). As can be seen, the conventional wastewater treatment process does not always reduce the concentration of micropollutants, i.e., the CFVP. Toxicity of CFVP also limits the use of biological methods due to the sensitivity of microorganisms. Thus, it is necessary to search for new methods that are more effective and economically available than conventional wastewater treatment processes.

Advanced oxidation processes (AOPs) are an interesting alternative to conventional wastewater treatment processes (Krishnan et al. 2017). The difference between conventional chemical oxidation and AOPs is the oxidizing potential (E_0). The oxidation potential of conventional oxidants decreases in the following order: ozone ($E_0 = 2.08 \text{ V}$) > hydrogen peroxide ($E_0 = 1.76 \text{ V}$) > chlorine

Editorial responsibility: Maryam Shabani.

✉ P. Zawadzki
pzawadzki@gig.eu

¹ Department of Water Protection, Central Mining Institute, Plac Gwarków 1, 40-166 Katowice, Poland



dioxide ($E_0 = 1.71$ V) > permanganate ($E_0 = 1.51$ V) > chlorine ($E_0 = 1.36$ V) > oxygen ($E_0 = 1.23$ V) (Cuerda-Correa et al. 2020). The common feature of the AOPs is the use of the hydroxyl radicals (\bullet OH). The reactions carried out in the presence of hydroxyl radicals are non-selective. The oxidation potential is about $E_0 = 2.80$ V. Currently, there are number of AOPs in which hydroxyl radicals are generated, such as, e.g., O_3/UV , TiO_2/UV (photocatalysis), ultrasonication or H_2O_2/Fe^{2+} (Fenton's reagent). Literature data indicate that AOPs find application to remove pharmaceutical substances (Verma and Haritash 2020), dyes (Ding et al. 2020) and pesticides (Jiang et al. 2020).

Photocatalysis is a chemical reaction that involves the absorption of light and catalyst. Ultraviolet light is widely used for activation of photocatalyst. Due to low cost and non-toxic properties, TiO_2 is one of the most attractive semiconductor. Irradiated surface of the catalyst generates electrons produced at the conduction band, whereas positive holes are formed in the valence band. The holes may react either with electron donors or with hydroxide ion to produce hydroxyl radicals, which oxidize organic compounds (Vaya and Suroliya 2020). "Green catalysts" are also of great interest, because after modification (e.g., with carbon, nitrogen) they can absorb visible light (Cao and Yi 2020). It was shown that TiO_2 can degrade monocrotophos (organophosphate insecticide) at 94% after 120 min (Agarwal and Das 2014). However, the technological disadvantage of using TiO_2 may be the residues of nanoparticles after the treatment or energy-consuming UV lamps (e.g., 500 W as presented by Chen et al. 2007).

The combined O_3/UV process enhances the generation of hydroxyl radicals and accelerates the reaction compared to classical ozonation. During the O_3/UV process, a combination of reaction mechanisms, such as direct ozonation, direct photolysis, and indirect radical oxidation may be noticed. It was observed that around 95% of imidacloprid (insecticide belonging to the neonicotinoids) was degraded in the O_3/UV process (Baghirzade et al. 2021). Therefore, the main application of O_3/UV treatment is limited due to investment and operating cost (ozone generator, UV lamps, energy consumption) (Brienza and Katasoyiannis 2017).

Oxidation with sulfate radicals (e.g., sodium persulfate) is also of great interest (Wang et al. 2019a, b; Zawadzki, 2019). Sulfate radicals ($SO_4^{\bullet-}$) have a higher oxidizing potential ($E^0 = 2.5-3.1$ V) than hydroxyl radicals. The sulfate radical is formed as a result of the interaction of various energy sources (e.g., heat, UV radiation) with the radical precursor,

e.g., sodium persulfate ($Na_2S_2O_8$) or as a result of the reaction of transition of metal ions (e.g., Fe^{2+} , Co^{2+}).

AOPs represent a promising method for eliminating a wide range of pollutants identified in wastewater. However, due to the investment and operating costs and the risk of generating oxidation by-products, it is recommended to use advanced oxidation as the last stage of wastewater treatment. Municipal facilities around the world (e.g., Wastewater Treatment Plant in Waldwick, New Jersey, USA (NBCUA, 2021); Lyuberetskiye Wastewater Treatment Plant, Moscow, Russia (WATER WORLD, 2021); Neugut Wastewater Treatment Plant, Dübendorf, Switzerland (McArdell CS, 2015)) are examples of employing such wastewater treatment processes as AOPs. The examples show the enormous application potential of additional processes of wastewater treatment. However, not many WWTPs are using TiO_2/UV , O_3/UV . Persulfates are not used in full-scale. High energy consumption (the use of UV-light) may be one of the reasons. This article shows that the PDS/Vis process (persulfates activated by visible light), compared to the UV-assisted TiO_2 or O_3 processes, can be carried out under the influence of visible light. The use of renewable source of energy is a significant advantage compared to other AOPs.

Therefore, this study aimed to investigate the possibility of removing chlorfenvinphos from treated municipal wastewater with selected advanced oxidation processes. The following processes have been investigated: TiO_2/UV , O_3/UV and PDS/Vis. The above selection is motivated by a comparison of two quite well-researched technologies (TiO_2/UV and O_3/UV), and one that is of great interest in the recent years (PDS/Vis). Due to the documented risk of forming oxidation by-products, the mineralization degree (removal of Total Organic Carbon) and toxicity of resulting solutions were analyzed with the MICROTOX® biotest.

The PDS/Vis method is based on the activation of PDS (sodium persulfate) with use of non-toxic, pro-environmental reagents (in this study: glucose) and low-cost solar energy (Vis-visible light). The benefit of PDS/Vis process is the possibility of using naturally available source of energy (visible light) to activate the persulfates. However, exposing PDS to visible light only may not bring the expected results due to poor quantum efficiency of sulfate radicals at wavelength $\lambda > 400.0$ nm. As Herrmann (Herrmann, 2007) reported, that quantum efficiency of sulfate radicals decreases with the increase in wavelength in the range from 248.0 to 351.0 nm. Sugars (e.g., glucose) can



be utilized to activate PDS under the influence of visible light. The price of glucose may be even twice lower than $\text{FeSO}_4 \cdot 7\text{H}_2\text{O}$, a compound commonly used to activate persulfates. Furthermore, the price of PDS is drastically lower than TiO_2 (0.74 USD/kg for PDS vs. 16.0 USD/kg for TiO_2) (Krawczyk et al. 2020; Ragadhita et al. 2019). Recent data concerning the use of visible-light-driven persulfates showed that the efficiency of pollutants removal is similar or even higher than other AOPs methods, for example, activation of Au–ZnO catalyst with visible light (Zhang et al. 2018). The PDS/Vis process can be carried out in a wide range of pH, so this method is also promising for treatment of contaminated solutions characterized by varied pH.

The treated wastewater effluent was taken in 2021 from a municipal wastewater treatment plant (WWTP) located in one of the cities of the Silesian agglomeration (Silesia, Poland). The study was performed in certified laboratories of the Central Mining Institute in 2021.

Materials and methods

Materials

The study on real treated municipal wastewater can be considered a significant feature of this experiment. Artificially contaminated with 1 mg/l of CFVP samples of treated municipal wastewater were tested. The use of real treated wastewater in the experiment helped to bring the expected results closer to real practical situations. Investigation of the effects of interfering ions (e.g., NO_2^- , NO_3^- , HCO_3^- , Cl^- or CO_3^{2-}) was beyond the scope of this study. Noteworthy, as shown by Ahmed et al. (2021), ions can inhibit degradation process as a result of scavenging free radicals. Farner Budarz et al. (2017) determined the

following impact of inorganic anions on the reactivity of TiO_2 nanoparticles: carbonate>chloride>phosphate>nitrate>sulfate. The photoreactivity of TiO_2 is decreased as a result of specific reactions on the catalyst surface (e.g., ion adsorption competes with other compounds for TiO_2 active sites). Interfering compounds can affect the absorption of UV radiation, thus reducing the efficiency of the system. Ions can react with $\bullet\text{OH}$ or $\text{SO}_4^{\bullet-}$ to form the less reactive radicals. For example, carbonate and bicarbonate ions may react with $\bullet\text{OH}$ or $\text{SO}_4^{\bullet-}$ to form $\text{CO}_3^{\bullet-}$ ($E_0 = 1.63$ V, pH 8.4) (Liu et al. 2016).

AOPs experiments were used to verify whether TiO_2/UV , O_3/UV , and in particular PDS/Vis, could be used as wastewater treatment method contaminated with chlorfenvinphos. From an economic point of view, it was assumed that under real operating conditions, the wastewater samples will not be heated or cooled, and therefore the study of temperature influence was beyond the scope of the research. However, raising the reaction temperature should increase the reaction rate, and therefore, increase the removal efficiency (Xia et al. 2020; Buthiyappan et al. 2015).

The high concentration of the pesticide (greater than typical environmental concentrations) was used to obtain accurate and precise data of the analytical measurements. Chlorfenvinphos standard of > 95% purity was purchased from Sigma-Aldrich (Poznań, Poland). The pesticide characteristics are presented in Table 1.

Commercial titanium dioxide (TiO_2 P–25; anatase/rutile = 80/20) with the purity of 99.5% was used in the tests. The specific surface area of TiO_2 ranged from 35 to 65 m^2/g . The purity of the sodium persulfate ($\text{Na}_2\text{S}_2\text{O}_8$) was $\geq 99\%$. All the used chemical reagents were produced by Sigma-Aldrich (Poznań, Poland).

Table 1 Physico-chemical characteristics of chlorfenvinphos (PUBCHEM, 2021)

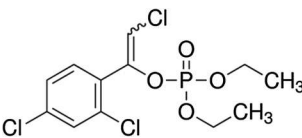
Chemical Structure	Physico-chemical properties	
	Molecular Formula	$\text{C}_{12}\text{H}_{14}\text{Cl}_3\text{O}_4\text{P}$
	Molecular Weight [g/mol]	359.57
	CAS Number	470–90–6
	Water solubility at 20 °C [mg/l]	124.0
	Density [g/l]	1.36
	Vapor pressure (at 25 °C) [mmHg]	7.5×10^{-6}
	$\log K_{\text{OW}}$ [-]	3.81



Table 2 Characteristic parameters of the tested wastewater

Parameter	Unit	Treated municipal wastewater
pH	–	7.08
Temperature	°C	19.30
Conductivity	µs/cm	701.30
Turbidity	NTU	10.0
Absorbance ($\lambda = 254$ nm)	nm	0.187
COD	mg O ₂ /l	38.0
TOC	mg C/l	13.0
Chlorfenvinphos concentration	mg/l	< LOD*

* < 0.05 ng/l

Wastewater samples

The treated wastewater effluent was taken from a municipal wastewater treatment plant (WWTP) located in one of the cities of the Silesian agglomeration (Silesia, Poland). In recent years, it has been improved to adjust the quality of wastewater effluent to the strict legal standards. Currently, the WWTP works in a mechanical and biological system. The mechanical part consists of grates, sand traps and preliminary settling tanks; the biological part consists of biological reactors.

Characteristic parameters of the treated municipal wastewater are presented in Table 2. No chlorfenvinphos was identified in the wastewater outflow. The WWTP meets the requirements according to the water permit. Due to the low color and turbidity, the sample was not pre-filtered before the AOPs. To inhibit any biological activity in the sample and eliminate adsorption of compounds on the glass vessel walls, the samples were stored at 4 °C until analyses (maximum for 48 h) in compliance with ISO 5667–3:2018 (ISO 5667–3:2018, 2018). Analyses were based on composite samples (three samples mixed together, from which the average value has been obtained) in compliance with ISO 5667–10:2020 (ISO 5667–10, 2020).

Instruments and analytical methods

In compliance with ISO 11369:1997 (ISO 11369:1997, 1997), the samples were determined by high-performance liquid chromatography coupled with a UV detector (HPLC–UV). Briefly, CFVP extraction before chromatographic analysis was performed by solid-phase extraction (SPE) on

CHROMABOND® C18 ec columns. HPLC analysis was performed using a HPLC model 1200 (Perlan Technologies, Warsaw, Poland).

Total organic carbon was determined by high-temperature combustion method with IR detection in compliance with PN–EN 1484:1999 (PN-EN 1484:1999, 1999).

Advanced oxidation experiments

Degradation of chlorfenvinphos in three advanced oxidation processes was investigated: ozonation catalyzed with UV radiation (O₃/UV), photocatalysis in the presence of titanium(IV) oxide and UV radiation (TiO₂/UV) and visible-light-driven activation of sodium persulfate (PDS/Vis).

Reaction mixtures with the addition of a catalyst–titanium(IV) oxide, were placed on a magnetic stirrer and then irradiated with a 10 W ultraviolet lamp (SunSun, model CUV–510). The lamp emitted primarily 254 nm ultraviolet radiation (UV). Before switching on the radiation source, the contact time between the photocatalyst (TiO₂) and the wastewater mixtures was 15 min. This step was carried out in a dark chamber. The dose of TiO₂ was set to 100 mg/l.

The ozone generator model 20 W ZY–H103 (Eltom, Warsaw, Poland) at flow 5.0 dm³ min^{–1} was used as the ozone source. Ozonation was catalyzed by irradiating the reaction solutions with a UV lamp (described earlier). The ozone dose was set to 100 mg/l. The process was carried out in a dark chamber.

Sodium persulfate (PDS) was used as the sulfate radical precursor. The dose of PDS was 20.0 mM. Visible radiation (Vis) of > 400.0 nm wavelength and glucose (dose = 100 mM) were used to activate PDS. Activation with sodium persulfate with visible radiation is possible, which is confirmed by literature data (Watts et al. 2018). A 10 W tungsten lamp model QTH10/M (Thorlabs Inc., New Jersey, United States), was used as the source of visible radiation. The lamp emitted $\lambda = 400–2200$ nm wavelength radiation. The FGS900M filter was used to cut off radiation spectrum bands above 710 nm. The process was carried out in the dark to eliminate additional light sources. All oxidation processes were carried out at 20 min. All the experiments were carried out independently in triplicate and the averaged values with statistical deviation were used for the data analysis. Statistical analysis in this study was conducted using Microsoft Excel program.

Kinetics studies

The oxidation of chlorfenvinphos follows the pseudo-first-order kinetic model (Zawadzki, 2020). The pseudo-first-order model can be expressed by Eq. (1).

$$-\frac{d[\text{CFVP}]}{dt} = k_{\text{obs}}[\text{CFVP}] \quad (1)$$

where [CFVP] is the concentration of chlorfenvinphos at reaction time t ; $[k_{\text{obs}}]$ is the pseudo-first-order rate constant.

Toxicity measurements

The toxic potential of the CFVP in wastewater samples before and after the AOPs was assessed with the commercial MICROTOX® biotest. The MICROTOX® biotest uses the *Aliivibrio fischeri* which has bioluminescent properties. The analysis was performed with the Microtox Model 500 analyzer (Tigret Sp. z o.o., Warsaw, Poland).

Bioluminescence inhibition (%) was measured after 5 min of exposure and compared with the control sample (2% NaCl). The toxicity of aqueous solutions was determined based on the toxicity classification system according to guidelines given by Santana et al. (2009).

Energy consumption

Electricity consumption is one of the essential criteria in the wastewater treatment process. In each AOPs studied, electricity consumption was estimated based on two indicators: specific energy consumption indicator E_s and electric energy per order indicator E_{EO} .

Specific energy consumption rate E_s is expressed as kWh/kg of removed TOC, based on the time required to remove 50% of the TOC. The assumed TOC value resulted from the maximum TOC removal in TiO_2/UV process. The specific energy consumption E_s was calculated with the following equation (Eq. 2) (Badawy et al. 2006):

$$E_s = \frac{P \cdot t}{[\Delta\text{TOC}] \cdot V} \quad (2)$$

where E_s (kWh/kg)-specific energy consumption rate, P (kW)-electrical power consumed by the UV or Vis lamp; equal to 0.01 kW, t (h)-the time at which 50% TOC is removed; equals 0.28; 0.30 and 0.17 h for the TiO_2/UV ; O_3/UV ;

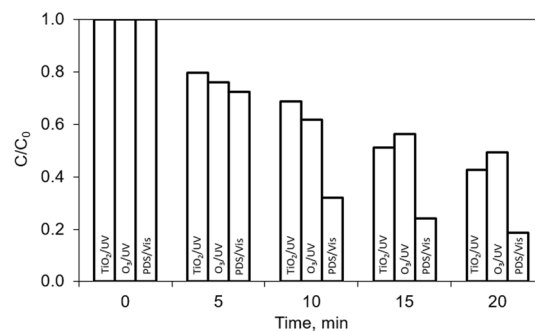


Fig. 1 Comparison of different AOPs (TiO_2/UV , O_3/UV , and PDS/Vis) during CFVP treatment

UV and PDS/Vis, respectively, $[\Delta\text{TOC}]$ (kg)-the change in TOC concentration; equal to 60.5×10^{-6} kg which represents 50% TOC removal of CFVP, V (L)-the irradiated reaction volume; equal to 0.4 L.

The E_{EO} electric energy per order indicator is expressed as kWh/m^3 of treated wastewater. The electric energy per order E_{EO} was calculated with the following equation (Eq. 3) (Poulopoulos et al. 2019):

$$E_{\text{EO}} = \frac{P \cdot t \cdot 1000}{\log\left[\frac{C_0}{C_f}\right] \cdot V \cdot 60} \quad (3)$$

where E_{EO} (kWh/m^3)-electric energy per order, P (kW)-electrical power consumed by the UV or Vis lamp; equal to 0.01 kW, t (h)-irradiation time; equal to 20 min, C_0 (mg/L)-the initial concentration of CFVP; equal to 1.0 mg/L, C_f (mg/L)-the final concentration of CFVP; equal to 0.43; 0.49 and 0.19 mg/L for the TiO_2/UV ; O_3/UV and PDS/Vis, respectively, V (L)-the irradiated reaction volume; equal to 0.4 L.

Results and Discussion

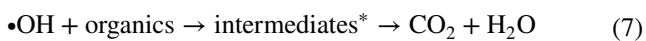
Advanced oxidation of chlorfenvinphos

The wastewater samples were submitted to advanced oxidation treatment by three types of AOPs: TiO_2/UV , O_3/UV and PDS/Vis. Figure 1 shows the efficiency of studied AOPs versus time. The use of studied AOPs results in 51–81% reduction of initial CFVP concentration within 20 min of the reaction time



(Fig. 1). The process time has a decisive impact on the effect of chlorfenvinphos removal. When the reaction time extended to 20 min, the efficiency of the CFVP removal increased from 13 to 26%, which results from the generation of free radicals (hydroxyl or sulfate), as confirmed by (Wang and Wang 2020).

In the TiO₂/UV system, hydroxyl radicals are generated as a result of the following reactions (Eqs.4, 5, 6 and 7) (Sujatha et al. 2020):



*identification of CFVP intermediates was beyond the scope of this study

Ultraviolet (UV) radiation is used to activate the TiO₂ photocatalyst (Etacheri et al. 2015). Activation of TiO₂ causes the transfer of electrons from the valence band to the conduction band. The electron-hole pair is generated which corresponds to the formation of the redox potential on the surface of the photocatalyst molecule. The reaction of electron holes with water molecules results in the formation of hydroxyl radicals.

Hydroxyl radicals are also generated during the ozonation process. However, the effectiveness of ozonation is determined by the parameters of the reactions, e.g., pH. Ozonation in an acidic environment (pH < 4) causes direct oxidation of pollutants with ozone. If the pH is close to neutral, the direct route is also observed. Ozone directly attacks double bonds –C=C– or –N=N– (Beltran and Rey 2018). As the research (Jabbari et al. 2020; Sgroi et al. 2021) shows, the use of the O₃/UV combination generates more hydroxyl radicals. Additionally, the generation of hydroxyl radicals in the combined process is effective over a wide pH range (Conti-Lampert et al. 2020), with the optimal value at pH=6.7, as reported by Buffle et al. (2007). An increase in pH to 7.9 did not significantly affect the production of •OH radicals.

As shown in Fig. 1, the O₃/UV process reduced the initial concentration of CFVP by 51% after 20 min of reaction. Oxidation of pollutants in the O₃/UV system may result from several reactions, with the two-stage model being

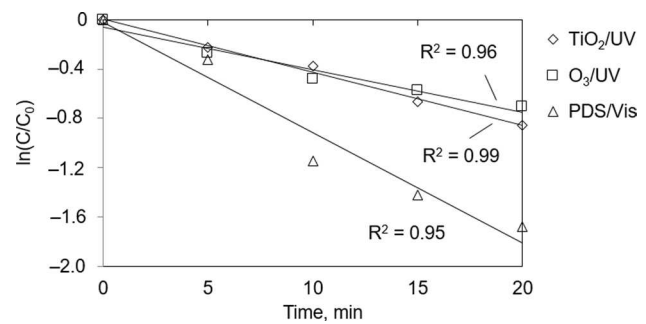
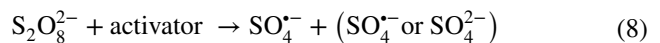


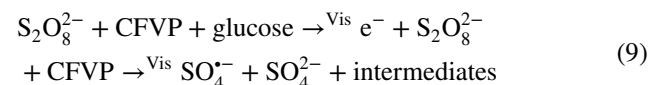
Fig. 2 Degradation kinetics of CFVP in different AOPs

the most frequently quoted (Cuerda-Correa et al. 2020). It involves the photo-induced homolysis of ozone molecules and then the generation of hydroxyl radicals as water reacts with atomic oxygen. Of course, there are also possible direct photolysis reactions with UV radiation, reactions of ozone with HO⁻ or HOO⁻ ions, and hydrogen peroxide photolysis.

Conventional activation methods of (Lee et al. 2020; Gao et al. 2019) inorganic peracid salts (e.g., sodium persulfate-PDS) focus on the use of heat, transition metal ions with a low oxidation state (e.g., Fe²⁺, Ni²⁺, Co²⁺), UV radiation or ionizing radiation, and high pH (Eq. 8). Sulfate radicals react with organic molecules by detaching a hydrogen atom, forming a double bond and transferring electrons.



As presented in (Zawadzki 2019), the oxidation of pollutants is possible both in the presence of visible radiation and without it. Without a catalyst, the efficiency is much lower. Figure 1 shows that in the visible-light-driven activation of sodium persulfate (PDS/Vis) results in 81% degradation degree of after 20 min of the reaction. More intensive decomposition of CFVP in the PDS/Vis system results from the synergistic interaction of visible light and glucose (Eq. 9). Glucose is an optically active substance. Under visible light, the breakdown of glucose, then the transfer of an electron from this sugar towards PDS and the oxidation of glucose to PDS activating products is observed (PDS activation) (Watts et al. 2018; Cai et al. 2019; Ahmad et al. 2013).

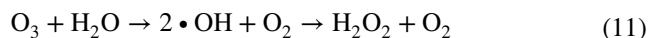


The kinetic characteristics of the studied AOPs showed a very good fit of experimental data ($R^2 = 95\text{--}99\%$). As can be seen in Fig. 2, the slope is maximized for PDS/Vis. Therefore, the acceleration of reaction corresponds to a high efficiency of CFVP removal. According to guidelines given by Wright (2004), based on the mathematically calculated half-life reactions were classified as slow rate for O_3/UV ($10^3\text{--}10^6$ s) and moderate rate for TiO_2/UV and PDS/UV ($1\text{--}10^3$ s).

The negative influence of interfering substances (e.g., CO_3^{2-} , HCO_3^- , etc.) can explain low chlorfenvinphos removal in the TiO_2/UV process (compared to the PDS/Vis system). Therefore, during the potential implementation of the TiO_2/UV system, pre-treatment processes such as coagulation, filtration, sedimentation should be taken into account to eliminate compounds that inhibit free radical reactions. Also, the recombination of the electron-hole pairs produced during the TiO_2 irradiation has impact on the photocatalytic process. Recombination of electron-hole pairs is a drawback of photocatalytic process, as both electrons and holes initiate reactions characteristic for photocatalysis. The phenomenon causes a decrease in photocatalytic activity due to a decrease in the concentration of charge carriers in the semiconductor material (Yadav et al. 2017; Sharma et al. 2021).

The low degree of CFVP removal could be caused by several limitations characteristic of the applied oxidant (O_3). The lowest efficiency of CFVP removal was observed during the O_3/UV (51% after 20 min of reaction). Low solubility of O_3 in water was indicated as a disadvantage of oxidation (Huling and Pivetz 2007). In another related works (Summerfelt 2003; Yao et al. 2018) authors postulated that the ozone mass transfer is the stage limiting the process effectiveness. The O_3/UV mechanism shows that the hydroxyl radicals generated during irradiation (Eq. 10) recombine

to H_2O_2 (Eq. 11). Then, H_2O_2 undergoes the reactions presented in Eqs. (12)–(17) (Litter and Quici 2010), which may interfere the final effect of pollutant removal.



Moreover, in contrary to many literature data on O_3/UV efficiency (Rekhate and Srivastava 2020; Srithep and Phattaratattamawong 2017; Wang et al. 2019a, b; Giri et al. 2010), authors noticed that the removal degree in the O_3/UV system was drastically reduced compared to ozonation alone, due to the negative influence of UV.

The above data show there is still a need for a detailed investigation of AOPs for micropollutants elimination, in particular concerning their potential use as the last stage of municipal wastewater treatment.

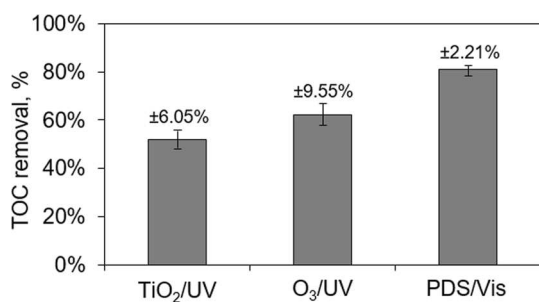


Fig. 3 TOC removal by AOPs after 20 min

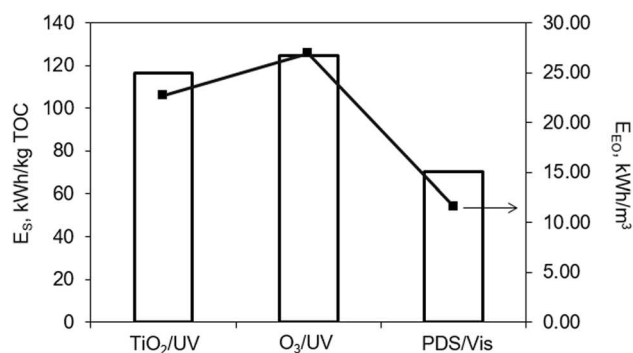


Fig. 4 Specific energy required for the degradation of chlorfenvinphos



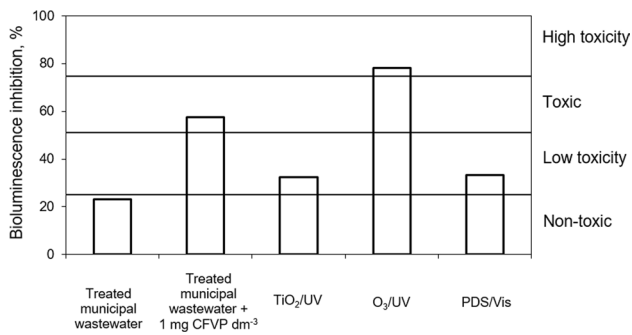


Fig. 5 *Aliivibrio fischeri* bioluminescence inhibition after 15 min contact time with resulting solution

TOC removal in AOPs

The TOC analysis aimed to facilitate the decision of potential further optimization of the processes and selecting the most favorable and safest wastewater treatment process. Therefore, the TOC was determined in samples of solutions before and after AOPs.

Figure 3 shows the degree of TOC reduction after a 20 min of the process. PDS/Vis has a higher degree of TOC removal than TiO₂/UV and O₃/UV. Within 20 min, 81% of TOC was removed with PDS/Vis, and 52% and 62% of TOC for TiO₂/UV and O₃/UV, respectively.

It can be assumed that the higher degree of TOC removal in O₃/UV than in TiO₂/UV resulted from the hydroxyl radicals generated during the process. In the TiO₂/UV process, only one molecule of •OH radical is produced (Eqs. 18, 19 and 20), while during O₃/UV, two molecules are produced (Eq. 11).



The principle of the PDS/Vis process is the generation of sulfate radicals. The potential of sulfate radicals SO₄^{-•} is higher ($E_0 = 2.5\text{--}3.1$ V vs. NHE) than of hydroxyl •OH radicals ($E_0 = 1.8\text{--}2.7$ V vs NHE), hence, a higher degree of mineralization. Wordofa (2014) showed that the radical SO₄^{-•} is more effective in degrading some refractory organic contaminants for its selective oxidation capacity. Higher CFVP mineralization in the PDS/Vis system could also result from a higher oxidation rate with sulfate radicals

(106–109 M/s) and longer lifetime ($t_{1/2} = 30\text{--}40$ μs compared to •OH radicals, $t_{1/2} = 10^{-3}$ μs) (Zawadzki 2021; Xia et al. 2020).

Figure 4 shows the mathematically calculated value of the electricity needed to remove 1 kg of TOC (E_s) and treat 1 m³ of solution (E_{EO}). It can be seen, the PDS/Vis process is more economical than TiO₂/UV and O₃/UV. However, it should be noted that the calculated values refer only to the conversion of UV radiation. For detailed calculations, other parameters such as electricity consumption of ozone generator, mixing and other factors should be considered.

Evaluation of toxicity

The relationship between the change in bioluminescence inhibition and examined AOP is presented in Fig. 5. It can be observed that TiO₂/UV and PDS/Vis processes enable a reduction in the toxicity of the artificially contaminated sample. On the other hand, probably due to the toxicity of the ozone, in the O₃/UV system the toxicity of the sample was about 20% higher than the sample of artificial contaminated wastewater not subjected to treatment process. This process is classified as very toxic. Ozone (O₃) is an active form of oxygen (O₂) and a powerful oxidizing agent. Ozone is one of the most powerful oxidants and is used for water disinfection. Hence, probably, the negative biological effect of the sample treated in the process. Regardless of the treatment system, none of the tested AOPs enabled to reduce the toxicity to a value below 25% (non-toxic sample). The higher toxicity probably results from incomplete removal of CFVP and from advanced oxidation by-products generated during AOP processes.

Despite the high efficiency of AOPs for the degradation of many pollutants, attention should be paid to the oxidation by-products. Oxidation by-products are compounds that are often more toxic than the original compound and more hazardous than raw wastewater. An effective method to eliminate contaminants should take such aspects as the dose of the oxidant and its type or the oxidation time into account. Even under optimal conditions, the toxicity measurements of resulting solutions should be tested.

However, in technical conditions, it is sometimes impossible (e.g., due to the costs) to control the process to avoid forming oxidation by-products (Alderete et al. 2021; Ike et al. 2019). Therefore, not only the efficiency of pollutant degradation, but also the risk of generating toxic by-products determines the effectiveness of AOPs.



As reported by Farré et al. (2005), for chlorfenvinphos detoxification is attained when the TOC remaining in solution becomes lower than 10 mg/l. Otherwise, an increased toxicity may result from generated by-products. Depending on the process (e.g., Photo-Fenton, photoelectrocatalysis using WO_3 , radiolytic decomposition), the oxidation by-products are different. It is reported in the literature that CFVP degradation by-products are, for example: 2-hydroxy-1-(2,4-dichlorophenyl) vinyl diethyl phosphate; 2,4-dichlorobenzoic acid; dicarboxylic acid; 2,4-dichlorophenol; triethyl phosphate; 4-hydroxybenzoic acid (Klamerth et al. 2009; Roselló-Márquez et al. 2021; Bojanowska et al. 2010). As can be seen, the by-products are aromatic acids or esters as well as toxic 2,4-dichlorobenzoic acid or triethyl phosphate.

Although PDS/Vis did not reduce the toxicity compared to the treated wastewater (uncontaminated), the advantages of using the PDS/Vis process cannot be neglected. The toxicity was lower than O_3/UV process, and nearly two times lower than that artificially contaminated wastewater. Therefore, it can be assumed that the environmental damage caused by the discharge of wastewater contaminated with CFVP without additional treatment or subjected to the O_3/UV process would be more serious than the potential environmental damage caused by the discharge of wastewater treated in the PDS/Vis process. On the other hand, an additional benefit of using PDS/Vis instead of TiO_2/UV is the possibility of using solar radiation (visible light) as a renewable energy source and lower operating costs (lower PDS price comparing to TiO_2).

Conclusion

The advanced oxidation processes were used to provide additional treatment of real municipal wastewater containing chlorfenvinphos (CFVP). The photocatalysis (TiO_2/UV), UV-catalyzed ozonation (O_3/UV), and visible-light-driven activation of sodium persulfate (PDS/Vis) were investigated. The main results are:

- In the following conditions: C_0 [CFVP] = 1.0 mg/l; $t = 20$ min; $\text{pH} = 7.0$; $T = 295.0$ K; $P = 1013.0$ hPa; $[\text{TiO}_2]_0 = 0.1$ g/l; $[\text{O}_3]_{\text{flow}} = 5.0$ dm^3/min ; $[\text{PDS}]_0 = 20.0$ mM, $[\text{glucose}]_0 = 100.0$ mM, the removal

efficiency of CFVP was set to 57, 51 and 81% for TiO_2/UV , O_3/UV and PDS/Vis, respectively;

- CFVP was not fully mineralized due to the generation of advanced oxidation by-products. The degree of mineralization ranged from 52 to 81%. The highest degree of mineralization was observed during the PDS/Vis process. It can be assumed that the high mineralization effect in the PDS/Vis system resulted from the high oxidizing potential of sulfate radicals ($E_0 = 2.5\text{--}3.1$ V) and their longer lifetime ($t_{1/2} = 30\text{--}40$ μs) than the hydroxyl radicals ($t_{1/2} = 10^{-3}$ μs);
- Energy consumption was the lowest in the PDS/Vis process. Specific energy consumption E_s was set to 70.25 kWh per kg of TOC removed; in turn, the electric energy per order E_{EO} was set to 11.55 kWh/m^3 ;
- Before and after the treatment processes, the samples showed different toxicity resulting from the by-products of advanced oxidation or the toxicity of the applied oxidants (mainly O_3). The O_3/UV process showed a very toxic effect, while the TiO_2/UV and PDS/Vis processes were characterized by lower toxicity than the artificially contaminated sample.

Acknowledgements The presented study was performed in the framework of the research work in the Central Mining Institute in Poland and financially supported by the Polish Ministry of Science and Higher Education (No. 11131041-340).

Author contribution PZ was responsible for the entire manuscript.

Funding Ministerstwo Nauki i Szkolnictwa Wyższego, 11131041-340, Piotr Zawadzki.

Data availability The datasets used and/or analyzed during the current study are available from the corresponding author on reasonable request.

Declarations

Conflict of interest The author declares that he has no conflict of interest.

Ethics approval This article does not contain any studies with human participants or animals performed by any of the authors.



References

- Agarwal V, Das S (2014) Degradation of monocrotophos pesticides using the advanced oxidation method. *J Environ Waste Manag* 1(1):2–10
- Ahmad M, Teel AL, Watts RJ (2013) Mechanism of persulfate activation by phenols. *Environ Sci Technol* 47:5864–5871. <https://doi.org/10.1021/es400728c>
- Ahmed N, Vione D, Rivoira L, Carena L, Castiglioni M, Bruzoniti MC (2021) A review on the degradation of pollutants by fenton-like systems based on zero-valent iron and persulfate: effects of reduction potentials, pH, and anions occurring in waste waters. *Molecules* 26:4584. <https://doi.org/10.3390/molecules26154584>
- Alderete BL, Silva JD, Godoi R, Silva FR, Taffarel SR, Silva LP, Garcia AL, Júnior HM, Amorim HL, Picada J (2021) Evaluation of toxicity and mutagenicity of a synthetic effluent containing azo dye after advanced oxidation process treatment. *Chemosphere* 263:128291. <https://doi.org/10.1016/j.chemosphere.2020.128291>
- Badawy MI, Ghaly MY, Gad-Allah TA (2006) Advanced oxidation processes for the removal of organophosphorus pesticides from wastewater. *Desalination* 194(1–3):166–176. <https://doi.org/10.1016/j.desal.2005.09.027>
- Baghirzade BS, Yetis U, Dilek FB (2021) Imidacloprid elimination by O₃ and O₃/UV: kinetics study, matrix effect, and mechanism insight. *Waste Biomass Manag Valoriz* 28:24535–24551. <https://doi.org/10.1007/s11356-020-09355-2>
- Beltran FJ, Rey A (2018) Free radical and direct ozone reaction competition to remove priority and pharmaceutical water contaminants with single and hydrogen peroxide ozonation systems. *Ozone Sci Eng* 40(4):251–265. <https://doi.org/10.1080/01919512.2018.1431521>
- Bojanowska-Czajka A, Gałęzowska A, Marty JL, Trojanowicz M (2010) Decomposition of pesticide chlorfenvinphos in aqueous solutions by gamma-irradiation. *J Radioanal Nucl Chem* 285:215–221. <https://doi.org/10.1007/s10967-010-0567-8>
- Brienza M, Katasoyiannis IA (2017) Sulfate radical technologies as tertiary treatment for the removal of emerging contaminants from wastewater. *Sustainability* 9:1604. <https://doi.org/10.3390/su9091604>
- Buffle MO, Schumacher J, Meylan S, Jekel M, von Gunten U (2007) Ozonation and advanced oxidation of wastewater: effect of o₃ dose, pH, DOM and HO•-scavengers on ozone decomposition and HO• generation. *Ozone Sci Eng* 28(4):247–259. <https://doi.org/10.1080/01919510600718825>
- Buthiyappan A, Aziz ARA, Daud WMAW (2015) Degradation performance and cost implication of UV-integrated advanced oxidation processes for wastewater treatments. *Rev Chem Eng* 31(3):263–302. <https://doi.org/10.1515/revce-2014-0039>
- Cai T, Liu Y, Wang L, Dong W, Chen H, Zeng W, Xia X, Zeng G (2019) Activation of persulfate by photoexcited dye for antibiotic degradation: radical and nonradical reactions. *Chem Eng J* 375:122070. <https://doi.org/10.1016/j.cej.2019.122070>
- Campo J, Masiá A, Blasco C, Picó Y (2013) Occurrence and removal efficiency of pesticides in sewage treatment plants of four Mediterranean River Basins. *J Hazard Mater* 263:146–157. <https://doi.org/10.1016/j.jhazmat.2013.09.061>
- Cao G, Yi N (2020) Nitrogen modified titanium dioxide (N-TiO₂) promotes carbon monoxide oxidation over copper catalysts. *New J Chem* 44(35):14781–14785. <https://doi.org/10.1039/d0nj03353g>
- Chen J, Wang D, Zhu M, Gao C (2007) Photocatalytic degradation of dimethoate using nanosized TiO₂ powder. *Desalination* 207:87–94. <https://doi.org/10.1016/j.desal.2006.06.012>
- Conti-Lampert AD, Mater L, Radetski-Silva R, Somendi CA, Poyer-Radetski L, Schmitz F, Dalpiaz FL, Radetski CM (2020) Influence of desorption process and pH adjustment on the efficiency of O₃, O₃/H₂O₂ and O₃/UV treatment of water and soil samples contaminated by crude petroleum. *J Environ Sci Health Part A* 55(5):563–572. <https://doi.org/10.1080/10934529.2020.1711669>
- Cuerda-Correa EM, Alexandre-Franco MF, Fernandez-Gonzalez C (2020) Advanced Oxidation Processes for the removal of antibiotics from water. *An Overview Water* 12:102. <https://doi.org/10.3390/w12010102>
- Ding X, Gutierrez L, Croue JP, Li M, Wang L, Wang Y (2020) Hydroxyl and sulfate radical-based oxidation of RhB dye in UV/H₂O₂ and UV/persulfate systems: Kinetics, mechanisms, and comparison. *Chemosphere* 253:126655. <https://doi.org/10.1016/j.chemosphere.2020.126655>
- Directive 2013/39/EU of the European Parliament and of the Council of 12 August 2013 amending Directives 2000/60/EC and 2008/105/EC as regards priority substances in the field of water policy
- Etacheri V, Di Valentin C, Schneider J, Bahnemann D, Pillai SC (2015) Visible-light activation of TiO₂ photocatalysts: advances in theory and experiments. *J Photochem Photobiol, C* 25:1–29. <https://doi.org/10.1016/j.jphotochemrev.2015.08.003>
- Farner BJ, Turolla A, Piasecki AF, Bottero JY, Antonelli M, Wiesner MR (2017) Influence of aqueous inorganic anions on the reactivity of nanoparticles in TiO₂ photocatalysis. *Langmuir* 33(11):2770–2779. <https://doi.org/10.1021/acs.langmuir.6b04116>
- Farré MJ, Franch MI, Malato S, Ayllón JA, Peral J, Doménech X (2005) Degradation of some biorecalcitrant pesticides by homogeneous and heterogeneous photocatalytic ozonation. *Chemosphere* 58(8):1127–1133. <https://doi.org/10.1016/j.chemosphere.2004.09.064>
- Gao Y, Gao N, Chu W, Zhang Y, Zhang J, Tin D (2019) UV-activated persulfate oxidation of sulfamethoxypyridazine: kinetics, degradation pathways and impact on DBP formation during subsequent chlorination. *Chem Eng J* 370:706–715. <https://doi.org/10.1016/j.cej.2019.03.237>
- Giri RR, Ozaki H, Ota S, Takanami R, Taniguchi S (2010) Degradation of common pharmaceuticals and personal care products in mixed solutions by advanced oxidation techniques. *Int J Environ Sci Technol* 7:251–260. <https://doi.org/10.1007/BF03326135>
- Herrmann H (2007) On the photolysis of simple anions and neutral molecules as sources of O⁻/OH, SO_x⁻ and Cl in aqueous solution. *Phys Chem Chem Phys* 30(9):3935–3964. <https://doi.org/10.1039/B618565G>
- Huling SG, Pivetz BE (2006) In-situ chemical oxidation. Environmental Protection Agency Washington DC Office Of Water, Ada, USA



- Ike IA, Karanfil T, Cho J, Hur J (2019) Oxidation byproducts from the degradation of dissolved organic matter by advanced oxidation processes—a critical review. *Water Res* 164:114929. <https://doi.org/10.1016/j.watres.2019.114929>
- ISO 11369:1997 Water quality—Determination of selected plant treatment agents—Method using high performance liquid chromatography with UV detection after solid-liquid extraction
- ISO 5667–3:2018 Water quality—Sampling—Part 3: Preservation and handling of water samples
- ISO 5667–10:2020 Water quality—Sampling—Part 10: Guidance on sampling of waste water
- Jabbari F, Eslami A, Mahmoudian J (2020) Degradation of Diclofenac in Water Using the O₃/UV/S₂O₈ Advanced Oxidation Process. *Health Scope* 9(2):1–9. <https://doi.org/10.5812/jhealthscope.99436>
- Jiang Z, Li J, Jiang D, Gao Y, Chen Y, Wang W, Cao B, Ta Y, Wang L, Zhang Y (2020) Removal of atrazine by biocharsupported zero-valent iron catalyzed persulfate oxidation: reactivity, radical production and transformation pathway. *Environ Res* 184:109260. <https://doi.org/10.1016/j.envres.2020.109260>
- Klamerth N, Gernjak W, Malato S, Agüera A, Lendl B (2009) Photo-Fenton decomposition of chlorfenvinphos: determination of reaction pathway. *Water Res* 43(2):441–449. <https://doi.org/10.1016/j.watres.2008.10.013>
- Krawczyk K, Waclawek S, Kudlek E, Silvestri D, Kukulski T, Grübel K, Padil VVT, Černík M (2020) UV-catalyzed persulfate oxidation of an anthraquinone based dye. *Catalysts* 2020(10):456. <https://doi.org/10.3390/catal10040456>
- Krishnan S, Rawindran H, Sinnathambi CM, Lim JW (2017) Comparison of various advanced oxidation processes used in remediation of industrial wastewater laden with recalcitrant pollutants. In: IOP Conference Series: Materials Science and Engineering, 206, 012089. <https://doi.org/10.1088/1757-899x/206/1/012089>
- Lee J, von Gunten U, Kim JH (2020) Persulfate-based advanced oxidation: critical assessment of opportunities and roadblocks. *Environ Sci Technol* 54(6):3064–3081. <https://doi.org/10.1021/acs.est.9b07082>
- Litter MI, Quici N (2010) Photochemical advanced oxidation processes for water and wastewater treatment. *Recent Pat Eng* 4:217–241. <https://doi.org/10.2174/187221210794578574>
- Liu N, Ding F, Weng CH, Hwang CC, Lin YT (2016) Minimizing the interference of carbonate ions on degradation of SRF3B dye by Fe⁰-aggregate-activated persulfate process. *Sep Purif Technol* 169:230–240. <https://doi.org/10.1016/j.seppur.2016.05.039>
- McArdell CS (2015) [WWW Document]. URL: https://www.dora.lib4ri.ch/eawag/islandora/object/eawag%3A9226/datastream/PDF/McArdell-2015-The_first_full-scale_advanced_ozonation-%28published_version%29.pdf (Accessed 15.08.2021)
- NBCUA (2021) Northwest Bergen County Utilities Authority [WWW Document]. URL: <http://nbcua.com/Sections-read-4.html> (Accessed 15.08.2021)
- Pan H, Xi B, Lei H, He X, Han Y, Xu Q (2017) Investigating organochlorine and organophosphorus pesticides in paddy field soil, groundwater and surface water in Eastern China. *J Residuals Sci Technol*, 14
- PN-EN 1484:1999-Guidelines for the determination of Total Organic Carbon (TOC) and Dissolved Organic Carbon (DOC). Polish Committee for Standardization
- Poulopoulos SG, Yerkinova A, Ulykbanova G, Inglezakis VJ (2019) Photocatalytic treatment of organic pollutants in a synthetic wastewater using UV light and combinations of TiO₂, H₂O₂ and Fe(III). *PLoS ONE* 14(5):e0216745. <https://doi.org/10.1371/journal.pone.0216745>
- PUBCHEM (2021) [WWW Document]. URL: <https://pubchem.ncbi.nlm.nih.gov/compound/Chlorfenvinphos> (Accessed 15.08.2021)
- Ragadhita R, Nandiyanto ABD, Maulana AC, Oktiani R, Sukmafitri A, Machmud A, Surachman E (2019) Techo-economic analysis for the production of titanium dioxide nanoparticles produced by liquid-phase synthesis method. *J Eng Sci Technol* 14(3):1639–1652
- Rekhate C, Srivastava JK (2020) Recent advances in ozone-based advanced oxidation processes for treatment of wastewater—a review. *Chem Eng J Adv* 3:1000031. <https://doi.org/10.1016/j.cej.2020.100031>
- Roselló-Márquez G, Fernández-Domene RM, García-Antón J (2021) Organophosphorus pesticides (chlorfenvinphos, phosmet and fenamiphos) photoelectrodegradation by using WO₃ nanostructures as photoanode. *J Electroanal Chem* 894:115366. <https://doi.org/10.1016/j.jelechem.2021.115366>
- Santana CM, Sosa FZ, Torres Padron ME, Santana Rodríguez JJ (2009) Methodologies for the extraction of phenolic compounds from environmental samples: new Approaches. *Molecules* 14:298–320. <https://doi.org/10.3390/molecules14010298>
- Sgroi M, Anumol T, Vagliasindi FGA, Snyder SA, Roccaro P (2021) Comparison of the new Cl₂/O₃/UV process with different ozone- and UV-based AOPs for wastewater treatment at pilot scale: removal of pharmaceuticals and changes in fluorescing organic matter. *Sci Total Environ* 765:142720. <https://doi.org/10.1016/j.scitotenv.2020.142720>
- Sharma HK, Sharma SK, Vemula K, Koirala AR, Yadav HM, Singh BP (2021) CNT facilitated interfacial charge transfer of TiO₂ nanocomposite for controlling the electron-hole recombination. *Solid State Sci* 112:106492. <https://doi.org/10.1016/j.solidstateciences.2020.106492>
- Shaw MS, Silburn DS, Lenahan M, Harris M (2012) Pesticides in groundwater in the Lower Burdekin floodplain. Department of Environment and Resource Management, Queensland Government, Brisbane
- Sigurnjak M, Ukic S, Cvetnic M, Markic M, Novak SM, Rasulev B, Kusic H, Loncaric BA, Rogosic M, Bolanca T (2020) Combined toxicities of binary mixtures of alachlor, chlorfenvinphos, diuron and isoproturon. *Chemosphere* 240:124973. <https://doi.org/10.1016/j.chemosphere.2019.124973>
- Srithep S, Phattarapattamawong S (2017) Kinetic removal of haloacetonitrile precursors by photo-based advanced oxidation processes (UV/H₂O₂, UV/O₃, and UV/H₂O₂/O₃). *Chemosphere* 176:25–31. <https://doi.org/10.1016/j.chemosphere.2017.02.107>
- Sujatha G, Shanthakumar S, Chiampo F (2020) UV light-irradiated photocatalytic degradation of coffee processing wastewater using TiO₂ as a catalyst. *Environments* 7(6):47. <https://doi.org/10.3390/environments7060047>
- Summerfelt ST (2003) Ozonation and UV irradiation—an introduction and examples of current applications. *Aquacult Eng* 28(1–2):21–36. [https://doi.org/10.1016/S0144-8609\(02\)00069-9](https://doi.org/10.1016/S0144-8609(02)00069-9)
- Vaya D, Suroliia PK (2020) Semiconductor based photocatalytic degradation of pesticides: an overview. *Environ Technol Innov* 20:101128. <https://doi.org/10.1016/j.eti.2020.101128>



- Verma M, Haritash AK (2020) Review of advanced oxidation processes (AOPs) for treatment of pharmaceutical wastewater. *Adv Environ Res* 9(1):1–17. <https://doi.org/10.12989/aer.2020.9.1.001>
- Wang J, Wang S (2020) Reactive species in advanced oxidation processes: Formation, identification and reaction mechanism. *Chem Eng J* 401:126158. <https://doi.org/10.1016/j.cej.2020.126158>
- Wang Y, Li H, Yi P, Zhang H (2019a) Degradation of clofibric acid by UV, O₃ and UV/O₃ processes: Performance comparison and degradation pathways. *J Hazard Mater* 379:120771. <https://doi.org/10.1016/j.jhazmat.2019.120771>
- Wang W, Wang H, Li G, An T, Zhao H, Wong PK (2019b) Catalyst-free activation of persulfate by visible light for water disinfection: efficiency and mechanisms. *Water Res* 157:106–118. <https://doi.org/10.1016/j.watres.2019.03.071>
- WATER WORLD (2021) Made in Moscow: World's Largest UV Plant [WWW Document]. URL: <https://www.waterworld.com/international/desalination/article/16200914/made-in-moscow-worlds-largest-uv-plant> (Accessed 15.08.2021)
- Watts RJ, Ahmad M, Hohner AK, Teel AL (2018) Persulfate activation by glucose for in situ chemical oxidation. *Water Res* 133:247–254. <https://doi.org/10.1016/j.watres.2018.01.050>
- Wordofa DN (2014) Application of Iron Activated Persulfate for Disinfection in Water Treatment. In: PhD Thesis, University Of California, Riverside
- Wright MR (2004) *An Introduction to Chemical Kinetics*; John Wiley and Sons: Hoboken, NJ, USA
- Xia X, Zhu F, Li J, Yang H, Wei L, Li Q, Jiang J, Zhang G, Zhao Q (2020) A review study on sulfate-radical-based advanced oxidation processes for domestic/industrial wastewater treatment: degradation, efficiency, and mechanism. *Front Chem* 8:1092
- Yadav M, Yadav A, Fernandes R, Popat Y, Orlandi M, Dashora A, Kothari DC, Miotello A, Ahuja BL, Patel N (2017) Tungsten-doped TiO₂/reduced Graphene Oxide nano-composite photocatalyst for degradation of phenol: A system to reduce surface and bulk electron-hole recombination. *J Environ Manag*, 203, 1, 364–374. <https://doi.org/10.1016/j.jenvman.2017.08.010>
- Yao W, Rehman SWR, Wang H, Yang H, Yu G, Wang Y (2018) Pilot-scale evaluation of micropollutant abatements by conventional ozonation, UV/O₃, and an electro-peroxone process. *Water Res* 138:106–117
- Zawadzki P (2019) Decolorisation of methylene blue with sodium persulfate activated with visible light in the presence of glucose and sucrose. *Water Air Soil Pollut* 230(313):1–18. <https://doi.org/10.1007/s11270-019-4372-x>
- Zawadzki P (2020) TiO₂ modified with organic acids for the decomposition of chlorfenvinphos under the influence of visible light: activity, performance, adsorption, and kinetics. *Materials* 13(2):289. <https://doi.org/10.3390/ma13020289>
- Zawadzki P (2021) Comparative studies of Rhodamine B decolorization in the combined process Na₂S₂O₈/visible light/ultrasound. *Desalin Water Treat* 213:296–278. <https://doi.org/10.5004/dwt.2021.26694>
- Zhang Y, Zhou J, Li Z, Feng Q (2018) Photodegradation pathway of rhodamine B with novel Au nanorods @ ZnO microspheres driven by visible light irradiation. *J Mater Sci* 53:3149–3162. <https://doi.org/10.1007/s10853-017-1779-x>





Persulfate activation by organic compounds: advancements and challenges

Piotr Zawadzki*

In the context of contaminants of emerging concern occurring in the environment, the urgent need to develop technologies for their effective removal is justified. The use of highly reactive sulfate radicals ($\text{SO}_4^{\cdot-}$) appears to be a valuable alternative to conventional oxidants used in water and wastewater technologies. Transition metal ions, thermal, photolytic, sonolytic, and radiolytic methods are conventional methods of persulfate (PS) activation to generate $\text{SO}_4^{\cdot-}$ radicals. In recent years, research has moved to alternative technologies of PS activation, that is, organic compounds (e.g. ascorbic acid, glucose, or quinones), to improve the degradation efficiency of contaminants. This paper discusses the organic compounds used to activate PS, critically reviewing their effectiveness in removing organic contaminants from water or wastewater.

Address

Central Mining Institute, Department of Water Protection, Plac Gwarków 1, 40-166 Katowice, Poland

Corresponding author: Piotr Zawadzki (pzawadzki@gig.eu)
*ORCID ID: 0000-0003-1020-5926

Abbreviations: POPs, Persistent Organic Pollutants; AOPs, Advanced Oxidation Processes; PS, Persulfate; $\text{SO}_4^{\cdot-}$, Sulfate radical; $\bullet\text{OH}$, Hydroxyl radical; US, Ultrasound; UV, Ultraviolet; PCP, Pentachlorophenol; AA, Ascorbic acid; RhB, Rhodamine B; MB, Methylene Blue; TC-H, Tetracycline hydrochloride; TCE, Trichloroethylene; EY, Eosin; DCF, Diclofenac; CECs, Contaminants of Emerging Concern

Current Opinion in Chemical Engineering 2022, 37:100837

This review comes from a themed issue on **Sulfate radical based advanced oxidation processes for environmental decontamination**

Edited by **PV Nidheesh** and **Parag R Gogate**

For complete overview of the section, please refer to the article collection, "[Sulfate radical based advanced oxidation processes for environmental decontamination](#)"

Available online 2th June 2022

<https://doi.org/10.1016/j.coche.2022.100837>

2211-3398/© 2022 The Author(s). Published by Elsevier Ltd. This is an open access article under the CC BY-NC-ND 4.0 license (<http://creativecommons.org/licenses/by/4.0/>).

Introduction

The analysis of literature data shows that, for years, advanced oxidation processes (AOPs) have been an interesting alternative to conventional treatment processes.

The common feature of AOPs is the chemical reaction between the generated hydroxyl ($\bullet\text{OH}$) or sulfate radicals ($\text{SO}_4^{\cdot-}$) and organic contaminants present in the treated medium (e.g. water, wastewater, sludge, and contaminated soils). These radicals are highly reactive and capable to mineralize the hazardous substances into nontoxic, environmentally inert simple chemical compounds [1].

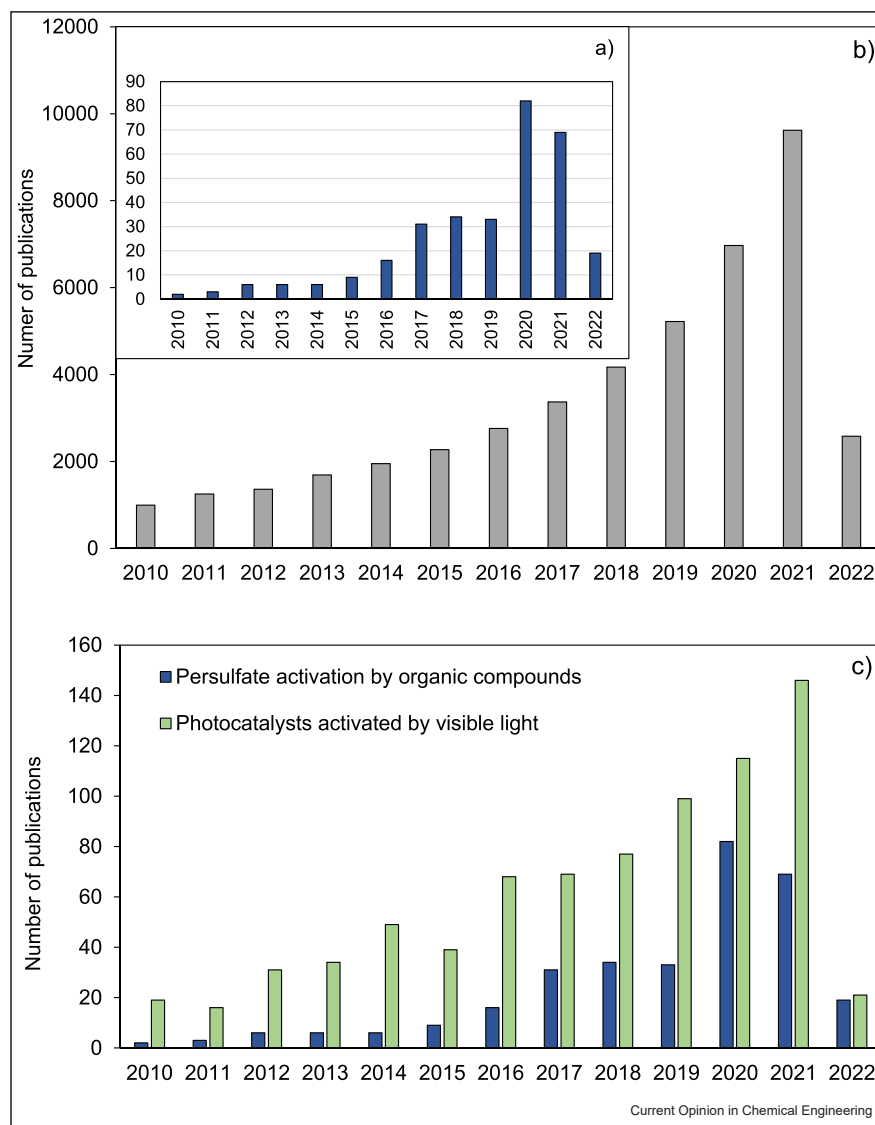
Among the AOPs, oxidation by persulfate (PS) using $\text{SO}_4^{\cdot-}$ radicals is a method of significant interest [31–33]. A radical precursor (e.g. sodium persulfate ($\text{Na}_2\text{S}_2\text{O}_8$)) requires activation to generate $\text{SO}_4^{\cdot-}$ radicals. PS has the chemical structure $[\text{O}_3\text{S-O-O-SO}_3]^{2-}$. The essence of the mechanism of PS activation is to excite PS, break the $-\text{O}-\text{O}-$ bond and generate $\text{SO}_4^{\cdot-}$ radicals [2]. The removal of organic pollutants without PS activation is possible, however, the oxidative potential of the generated PS anion is about 1/3 lower than the $\text{SO}_4^{\cdot-}$ radical [3]. Activation of the PS results in the generation of the $\text{SO}_4^{\cdot-}$ radical and accelerates the contaminant degradation reactions. Sonolytic (ultrasonic (US)), photolytic (ultraviolet radiation (UV)), and thermal (high temperature), as well as activation with low-oxidation transition metal ions are used for PS activation [34,35]. Activation by UV, US, or heat results in the formation of two $\text{SO}_4^{\cdot-}$ radicals (Eq. (1)) [36]. The PS and the transition metal electron donor reaction form a single $\text{SO}_4^{\cdot-}$ radical (Eq. (2)) [37].



One of the niches in AOPs in the presence of PS is its activation with organic compounds. Organic compounds allow to increase the degree of pollutants removal, simplify the ways of conventional PS activation methods, and carry out treatment of water and/or wastewater of fluctuating quality [4].

The results from the Web of Science database show that the number of publications on the application of organic compounds for PS activation has increased in recent years (Figure 1a); however, the number of publications is much lower than when searching for the phrase "Photocatalysts activated by visible light (Vis)" (Figure 1c). The total number of results (2010–2022) for the search phrase "PS activation by organic compounds" is 44 203 (including the

Figure 1



Trend of the number of publications per year search by words in (a) Web of Science (inset figure); (b) SCHOLAR database: "PS activation by organic compounds" and (c) Web of Science: "PS activation by organic compounds" and "Photocatalysts activated by Vis" from the years 2010 to 2022.

number of citations) (Figure 1b) compared to 138 140 results for the words "Photocatalysts activated by Vis."

Organic compounds that are used to activate PS must be as effective as conventional activation methods. This method can be considerably cheaper than those commonly used, providing that the process parameters are appropriately selected. The advantage of organic compounds is, for example, the lack of sediment generation (compared to, for example, Fe^{2+} transition metal ions), lower electricity consumption (compared to, for example, thermal activation methods), or the use of low energy-consuming lamps (compared to, for example, UV radiation). The review of

scientific data showed that organic acids (e.g. ascorbic acid (AA)), ketoacids, alcohols, sugars (e.g. glucose and sucrose), humic acids, and aldehydes, are organic compounds that can be used to activate PS [5,17,24,25].

The high pressure of pollutants on the environment, combined with the scarcity of water resources in the world, justifies the need to optimize the already applied methods, and search for new advanced and effective technologies to remove pollutants present in water and wastewater. Based on the latest literature review, the purpose of this paper is to present a review of the current knowledge on the use of organic compounds for PS

Table 1

OPs utilized for PS activation and its mechanics.

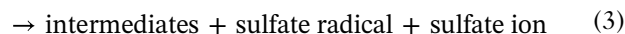
Organic compound	A brief description of the activation mechanism	References
Glucose (G) Sucrose (S)	Degradation mechanism caused by $\text{SO}_4^{\cdot-}$ and $\cdot\text{OH}$ radicals. Glucose and sucrose are optically active substances, that is, they tend to rotate the light plane and are active in Vis. The activation mechanism of PS may be due to the generation of Krebs cycle compounds during sucrose hydrolysis. When glucose is used, PS activation may result from the probable electron transfer from sugar towards PS. Higher degradation efficiency is observed while sucrose is used because sucrose is hydrolyzed into glucose.	[7,8]
AA	Degradation mechanism caused by $\text{SO}_4^{\cdot-}$ and $\cdot\text{OH}$ radicals. AA is a reducing agent, releases two protons, and can promote PS activation (electron transfer from AA to PS). AA undergoes two-step oxidation by PS to generate $\text{SO}_4^{\cdot-}$ radicals. Depending on the pH, the following dominate: $\text{SO}_4^{\cdot-}$ radicals at low pH, at higher pH, the generated $\text{SO}_4^{\cdot-}$ radicals are converted into $\cdot\text{OH}$ radicals.	[5•,9]
RhB, EY, MB	The main mechanism is the radical reaction caused by the reduction of PS by photogenerated electrons of the dye; the second mechanism is a nonradical reaction involving the transfer of electrons via the dye from the pollutant to the oxidized dye.	[10]
BQ	Degradation mechanism caused mainly by $\text{SO}_4^{\cdot-}$ radicals. $\text{SO}_4^{\cdot-}$ reacts by: abstraction of hydrogen atoms, addition of $\text{SO}_4^{\cdot-}$ on unsaturated bonds, and electron transfer, among which electron transfer is the most important. Excess quinone acts as an inhibitor and reduces the degradation of pollutants.	[11•]
Ferrocene-based metal-organic framework microspheres (Co-Fe-MOFs)	Degradation mechanism caused mainly by $\text{SO}_4^{\cdot-}$, then by $\cdot\text{OH}$ radicals. $\text{SO}_4^{\cdot-}$ radicals were mainly responsible for pollutant degradation. The Co-Fe-MOF composite promoted PS activation due to the rapid Fe/Co valence transfer. Co ion promotes oxidation-reduction reactions.	[12••]
Ferrous MOFs with strong electron-donating properties	Degradation mechanism caused by $\text{SO}_4^{\cdot-}$, $\cdot\text{OH}$ and $\text{O}_2^{\cdot-}$ ions. Activation of PS by binding PS to the Fe (II) surface. Fe (II) acts as an active site from where electrons are transferred to PS or dissolved O_2 .	[13•]
Surfactants	Degradation mechanism caused both by $\text{SO}_4^{\cdot-}$ and $\cdot\text{OH}$, but $\cdot\text{OH}$ plays a key role. Nonionic surfactants facilitate the treatment process, cause a decrease in surface tension, and are easier to agglomerate by salting out. The degradation is caused by breaking the C–C bond and shortening the carbon chain to simpler compounds, including for example, CO_2 and water.	[14••]

activation. The reaction mechanism is briefly summarized, and a summary of the most critical parameters affecting PS activation by organic promoters (OPs) is discussed.

Types of organic promoters utilized for persulfate activation

Organic compounds that can be used to activate PS contain an oxidation-sensitive functional group that allows the transfer of electrons from the organic substance towards the PS. The PS activation mechanism can generally be described by Eq. (3) [6]. Intermediates can inhibit the degradation process by scavenging free radicals, affecting radiation absorption, or may consume active species, which results in poor pollutant degradation. Meanwhile, the sulfate ion may both scavenge free radicals, leading to the generation of less reactive species (e.g. Cl^- , HO_2^-), and lead to the generation of $\text{SO}_4^{\cdot-}$ radicals [38]. New methods of PS activation and the effect of free radicals generated are important for future research. Therefore, further studies should also focus on investigating the effect of OPs on sulfate ion generation.

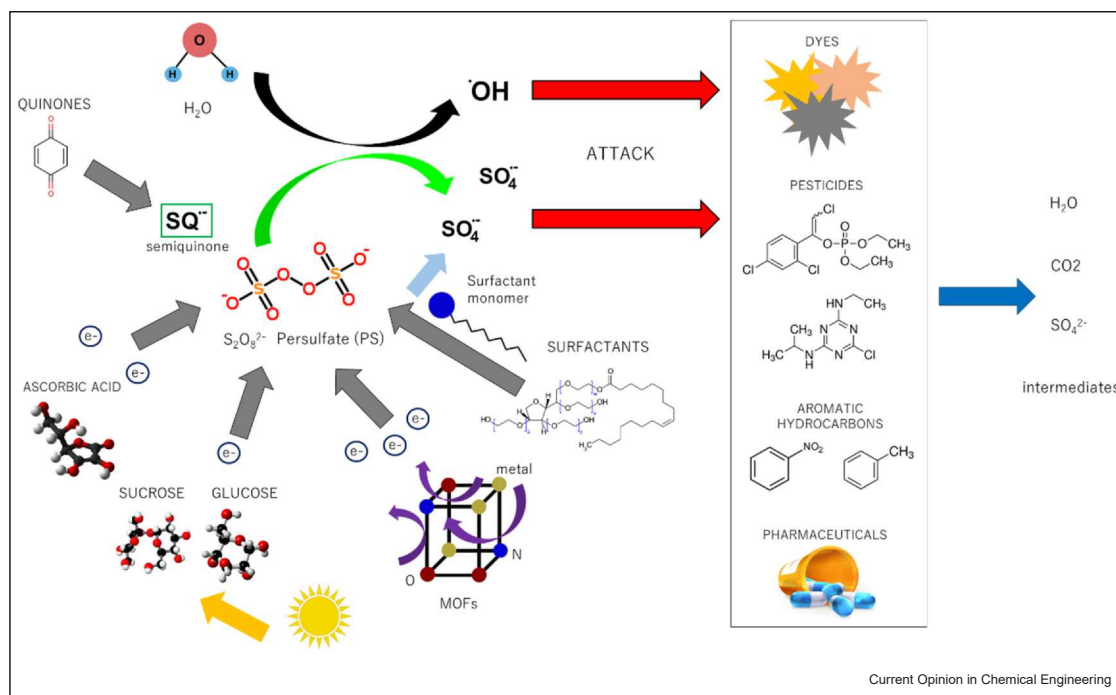
organic + PS



The forms in which organic compounds are used for PS activation are single molecules, organic chelates, and metal-organic frameworks (MOFs). MOFs are based on the characteristics of organic compounds that promote chemical oxidation reactions. MOFs are used to improve the generation of $\text{SO}_4^{\cdot-}$ radicals. An overview of OPs that are used for PS activation and their activation mechanism is presented in Table 1.

OPs reduce the operating costs of conventional activation methods, shorten reaction times, and increase degradation efficiency. The decision to choose OPs should be preceded by the selection of optimal process parameters, such as dose, pH, type of contaminant and its form, and the preferred quality of the water or wastewater. Electricity consumption also determines operating costs. Several activation methods are based on UV

Figure 2



Summary of PS activation method.

radiation to eliminate the need for catalysts. Nevertheless, the use of energy-consuming ultraviolet lamps is a drawback of this activation method. Sugars (e.g. glucose and sucrose) are an interesting OPs used to activate PS under Vis, especially considering that Vis is a renewable energy source. The summarized PS activation methods are presented in Figure 2.

Ascorbic acid

Cao et al. investigated AA as one of the OPs to activate PS [9]. Pentachlorophenol (PCP) was studied as the target contaminant. The authors determined that the degradation of PCP is carried out by $\text{SO}_4^{\bullet-}$ and $\bullet\text{OH}$ radicals, resulting in a final production of CO_2 and H_2O , preceded by the following reactions: dechlorination, hydroxylation, destruction of benzene and quinone rings, and formation of small-molecule acids. An approximately 71.3% removal of PCP was obtained after 180 min of reaction with 40 mM of PS and 1 mM of AA. The 1 mM of AA dose showed the highest degree of activity against PCP removal. Above this value, the removal efficiency decreased. For example, at 2 mM of AA, the degree of PCP degradation was about 50%. The degradation of PCP was strongly dependent on the pH value since AA is a binary acid and dissociates into ascorbate anion ($\text{pK}_{\text{a}1} = 4.25$) or dianionic AA ($\text{pK}_{\text{a}2} = 11.79$). Hence, the pH of the solution may indirectly influence the activation of PS. At lower pH, when the $\text{SO}_4^{\bullet-}$ radical dominates (no or minimal contribution of

e.g. OH^- , HO_2^-), decomposition of pollutants is facilitated. The distribution of AA in the form of $\text{C}_6\text{H}_8\text{O}_6$ was the highest at pH 2.5 (degradation rate constant of PCP was set to approx. 0.025 min^{-1}). When pH increased to 8 (reactions between OH^- , $\bullet\text{OH}$, and $\text{SO}_4^{\bullet-}$), the transition of AA to the $\text{C}_6\text{H}_7\text{O}_6^-$ form, and a reduction in the degradation rate constant to about 0.008 min^{-1} was observed. At $\text{pH} > 12.5$, the base activation mechanism dominates, and the contribution of AA decreases ($\text{C}_6\text{H}_6\text{O}_6^{2-}$ form dominates). Hou et al. confirmed by Electron Spin Resonance and Density Functional Theory calculations that AA-mediated activation of PS occurs by electron transfer from the AA towards the PS [5•].

Glucose

Zawadzki used Vis and glucose as an organic PS activator and Rhodamine B (RhB) as a target contaminant [4]. Glucose was used to enhance PS activity in Vis. The effects of glucose and PS on the removal degree of RhB were analyzed. It was shown that the optimal dose of glucose at an initial concentration of $C_{0[\text{RhB}]} = 10 \text{ mg L}^{-1}$ was 200 mM. At lower doses, a reduction in the efficiency of RhB decolorization was observed. On the other hand, higher doses of glucose also caused a reduction in the degree of decolorization, as glucose may be responsible for the inhibition of free radical reactions. The activation mechanism by glucose is similar to that of activation by phenoxides. An electron from glucose is

transferred to PS, causing its activation, while glucose is oxidized to products that can activate PS. This involves the activation of PS with an external carbon source [7].

Sucrose

PS activation by sucrose is similar to the activation mechanism by glucose [8]. PS activation by sucrose is probably due to the Krebs cycle compounds (e.g. citric acid, succinic acid, malic acid, levulinic acid, pyruvic acid, and oxalic acid). Compounds from the ketoacid group (Krebs cycle compounds) containing both a carboxyl group ($-\text{COOH}$) and a ketone group ($\text{C}=\text{O}$ bonded to two carbon atoms) are most likely to activate the PS.

Photoexcited dyes

In the last five years, few publications have examined the simultaneous elimination of organic pollutants and PS activation by organic contaminants themselves. Cai et al. performed a study using RhB, Eosin Y (EY), and Methylene Blue (MB) using these dyes simultaneously to remove tetracycline hydrochloride (TC-H) (an antibacterial antibiotic) and to activate PS [10]. The authors proved that RhB, EY, and MB, as photo-excited dyes, can activate PS in the presence of Vis. The addition of RhB increased the degradation of TC-H from about 32% (without RhB addition) to about 55% (with RhB addition) after 40 min of the reaction. Noteworthy is the use of Vis as an additional PS activating agent. When solar radiation is used, only 3–5% of this energy can be utilized, so the use of UV lamps, as energy-intensive devices, is a severe limiting factor for AOPs [29]. Vis is a curious alternative to UV radiation, and this type of PS activation method should be further developed.

Quinones

Quinones and organic substances containing quinone-containing groups are interesting materials for promoting PS activation. However, special attention needs to be paid to the fact that quinone-containing compounds are radical scavengers [30]. For example, hydroquinone is used as an $\text{O}_2^{\bullet-}$ scavenger ($k_{\text{O}_2^{\bullet-}} = 1.7 \times 10^7 \text{ M}^{-1} \text{ s}^{-1}$) [15].

Quinone groups as OPs include, for example, tetrafluoro-1,4-benzoquinone, 2,6-dichloro-1,4-benzoquinone and 2,6-dimethyl-1,4-benzoquinone (DMBQ) [16]. Shi et al. investigated the effect of 1,4-benzoquinone (BQ); 2-methyl-1,4-benzoquinone (MBQ); and 2,5-dimethyl-1,4-benzoquinone (DMBQ) for PS activation to eliminate, for example, benzene, p-xylene, chlorobenzene, and p-chlorotoluene (P-CT) [11•]. This study revealed that BQ ($\text{C}_{0[\text{BQ}]} = 0.5 \text{ mM}$) showed the highest performance of the quinones used, and, in its presence, an approximately 90–95% removal rate was achieved after 240 min of reaction (PS dose for all experiments was set to 5 mM). In general, an increase in BQ dose increased the

contaminants removal rates, while a decrease in efficiency was observed at excessive concentrations.

Surfactants

Zhang, Jiang and Bai performed a very meaningful study on removing oily sludge by a combined process using surfactants (anionic: sodium dodecylbenzene sulfonate and sodium dodecyl sulfonate; nonionic: Tween-80 and TX-100) and PS [14••]. Most researchers perform studies using only one of the selected substances as a model contaminant. What should be emphasized is that the authors of this paper have researched oil removal rate of the oily sludge. Oily sludge are characterized by their complex composition, thus it causes great difficulty in purification procedures. Oily sludge may contain, for example, saturated hydrocarbons, gum, or aromatic hydrocarbons. Taking into account some approximations, it can be claimed that this investigation was performed under conditions very close to real conditions, or at least simulated the real composition of sludge. Therefore, the real effect of the sludge composition on the treatment method was identified. The authors achieved about 95% removal of oily sludge with a residual oily sludge content of 0.57%. This value met the acceptable standard for discharge. Similar results were obtained by García-Cervilla et al. [26].

Factors affecting the performance of the persulfate oxidation process

A literature review showed that in PS activation processes with organic compounds, the degradation of pollutants by $\text{SO}_4^{\bullet-}$ radical oxidation is determined by parameters including initial pollutant concentration, process time, dose, pH, lamp type, and lamp power.

A summary of the identified process parameters that affect the degradation of organic pollutants is presented in Table 2.

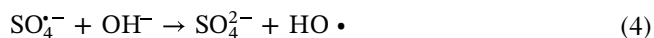
Effect of pH

One of the most critical parameters affecting both PS activation and removal rate is pH. The pH value influences the effectiveness of OPs, the direction of radical generation, and, as a result, the degradation of contaminants. For example, the pH value influenced the kinetics of the diclofenac (DCF) removal rate during PS activation with an organic $\text{Co}_3\text{O}_4\text{-g-C}_3\text{N}_4$ composite [17]. In an alkaline environment ($\text{pH} = 11$), 75% removal of DCF was achieved, but in an acidic environment ($\text{pH} = 3$), nearly 100% removal of DCF was achieved. Literature data show that $\text{SO}_4^{\bullet-}$ radicals dominate at $\text{pH} < 7$, hence an increase in pH values results in the formation of $\bullet\text{OH}$ radicals [18]. When the pH value is greater than 7, hydroxyl ion (OH^-) dominates (concentration of $\text{OH}^- > 10^{-7}$). At $\text{pH} > 7$, the reaction of $\text{SO}_4^{\bullet-}$ free radicals with hydroxyl ions resulted in the

Table 2**The experimental conditions and removal efficiency of the PS activated by OPs.**

Organic compound	Target pollutant	Conditions	Removal efficiency [%]	References
Glucose	Nitrobenzene (NB)	Concentration $C_{0[NB]} = 1 \text{ mM}$; Glucose dosage = 5 mM; Sodium hydroxide:PS molar ratio = 2:1; PS dosage = 0.5 M; Process time = 480 min	99.9	[7]
Glucose	Chlorfenvinphos (CFVP)	Concentration $C_{0[CFVP]} = 1 \text{ mg L}^{-1}$; Glucose dosage = 100 mM; PS dosage = 20 mM; Process time = 20 min; pH = 6; Type of lamp = Tungsten; Lamp power = 10 W	81	[23]
Glucose	MB	Concentration $C_{0[MB]} = 2 \text{ mg L}^{-1}$; Process time = 90 min; Glucose dosage = 100 mM; PS dosage = 0.065 mM; pH = 12; Temp. = room temperature; Type of lamp = Tungsten; Lamp power = 10 W	84	[8]
Sucrose	MB	Concentration $C_{0[MB]} = 2 \text{ mg L}^{-1}$; Process time = 90 min; Sucrose dosage = 100 mM; PS dosage = 0.065 mM; pH = 12; Temp. = room temperature; Type of lamp = Tungsten; Lamp power = 10 W	83	
AA	PCP	Concentration $C_{0[PCP]} = 10 \text{ mg L}^{-1}$; PS dosage = 40 mM; AA dosage = 1 mM; Process time = 180 min; pH = neutral; Temp. = room temperature	71.3	[9]
AA	ATR	Concentration $C_{0[ATR]} = 10 \text{ mg L}^{-1}$; PS dosage = 4 mM; AA dosage = 0.1 mM; Process time = 360 min; pH = 3.8; Temp. = $25 \pm 2^\circ\text{C}$	99.9	[5•]
BQ	Trichloroethylene (TCE)	Concentration $C_{0[PCP]} = 0.1 \text{ mg L}^{-1}$; PS dosage = 5 mM; BQ dosage = 0.1 mM; Process time = 240 min; pH = 3.0	40	[11•]
	P-CT	Concentration $C_{0[PCP]} = 0.1 \text{ mg L}^{-1}$; PS dosage = 5 mM; BQ dosage = 0.1 mM; Process time = 240 min; pH = 10.0	95	
RhB	TC-H	Concentration $C_{0[RhB]} = 10 \text{ mg L}^{-1}$; Concentration $C_{0[TC-H]} = 10 \text{ mg/l}$; PS dosage = 0.65 mM; Process time = 40 min; Temp. = room temperature; Lamp = 300 W Xe (Vis)	55	[10]
Ferrocene-based metal-organic framework microspheres (Co-Fe-MOFs)	OA7	Concentration $C_{0[PCP]} = 20 \text{ mg L}^{-1}$; PS dosage = 4 mM; Co-Fe-MOFs dosage = 0.25 g L ⁻¹ ; Process time = 90 min; pH = 7.01	84	[12••]
Ferrous MOFs with strong electron-donating properties (Fe(PyBDC))	Sulfamethoxazole (SMX)	Concentration $C_{0[SMX]} = 0.04 \text{ mM}$; PS dosage = 2 mM; Fe(PyBDC) dosage = 0.5 g L ⁻¹ ; Process time = 120 min; pH = ambient; Temp. = 30°C	97	[13•]

formation of sulfate ions and $\bullet\text{OH}$ free radicals (Eq. (4)). Therefore, the removal efficiency is decreased due to the scavenging of the $\text{SO}_4^{\bullet-}$ by $\bullet\text{OH}$ (Eq. (5)). Similar results have been reported by Oliveros et al. [27].



Effect of initial pollutant concentration

Medkour, Bechiri and Lachter studied the effect of different concentrations of MB on the MB removal percentage from an aqueous solution [19]. The study confirmed that a higher concentration of MB interferes with the reactions between free radicals and the dye molecules. Moreover, the high concentration of the dye may lead to a competition effect between the dye molecules, the by-products, and the generated radicals. Han et al. and Rizal et al. also investigated the effect of MB concentration on the final decolorization degree [20,21]. Both studies confirmed that higher dye concentrations inhibit radical reactions with dye molecules. Furthermore, high particle concentrations can lead to competitive effects between dye molecules, reaction by-products, and generated radicals.

Effect of persulfate concentration

The PS concentration is an important process parameter for at least two reasons. First, it affects operating costs. Second, it reduces the processing time, simultaneously improving pollutant removal. The effect of PS concentration activated with organic compounds has been studied by Lv et al. [12••]. Generally, an increase in PS concentration increases the removal rate of organic pollutants. The authors observed that increasing the PS concentration from 2 mM to 8 mM increased the degradation of Orange Acid 7 (OA7) from 73% to 89%. Interestingly, higher PS concentration causes a drastic decrease in the removal rate. This phenomenon characterizes not only PS oxidation but also occurs in photocatalytic processes [28]. It is mainly related to possible particle aggregation or oxidation of $\text{SO}_4^{\bullet-}$ radicals by other oxidizing forms, for example, $\text{S}_2\text{O}_8^{2-}$. Excessive adsorption on the surfaces of MOFs may also occur, thus the degradation efficiency is reduced.

Effect of process time

The reaction time is an essential parameter from an economic point of view. This parameter influences, for example, the retention time (e.g. for batch reactors), but also affects the flow reactors, and therefore the volume of the reactor. It is also significant in terms of costs for electricity, automation, and electronics, etc. In general, the removal degree of the contaminant increases with the processing time. The time required for contaminant decomposition ranges from a few minutes to a few hours. For example, Hou et al. using AA-activated PS, needed

about 360 min to degrade nearly 100% of atrazine (ATR) [5•]. In contrast, Sabri et al. required 90 min to remove almost 100% of MB [22]. However, the reaction time does not always depict the actual efficiency of a method, since oxidants and contaminants in different forms, concentrations, and susceptibility to removal are used in the tests. Therefore, further research on the effect of different initial concentrations of contaminants should be conducted.

Effect of organic promoter dose

Zawadzki described the influence of an OPs (glucose) on the degree of MB decolorization in the oxidation process with $\text{Na}_2\text{S}_2\text{O}_8$ in the presence of Vis [8]. In general, an increase in the glucose dose increases the efficiency of the process. However, the higher the concentration of glucose, the higher the inhibition of the process. This is due to the scavenging properties of glucose ($k_{\text{OH}\bullet} = 1.5 \times 10^9$), which was also confirmed by Watts et al. [7]. In turn, Cai et al. showed that the dose and the type of organic compounds (photoexcited dyes) also increase the degradation efficiency [10]. Among the three dyes (RhB, EY, and MB), RhB showed the highest potential for PS activation under the following operating conditions: PS dose = 0.65 mM, $C_{0[\text{dye}]}$ = 10 mg L⁻¹, process time = 60 min, under Vis.

Challenges, conclusion, and future research directions

This short review considers publications from the last five years, emphasizing the last two years, in the scope of PS activation with organic compounds. The use of OPs has been discussed, the mechanism of PS activation by OPs has been presented, and the factors affecting the degradation of the pollutants have been analyzed. PS activation by OPs shows great application potential for removing contaminants of emerging concern. With sufficiently selected operating conditions, nearly 100% degradation of contaminants is possible.

Considering publications from the last five years, more attention should be focused on the practical aspects in the field of PS activated by organic compounds. It is known that the economic aspect is one of the principal factors that influencing the treatment method decision. Investment and operational costs determine the economic viability of a treatment process; thus at least the dose rate and energy consumption, for example, per 1 kg of TOC, should be determined. Afterward, decision-makers concentrate on operational simplicity, crew safety, and operational results. Another key aspect is the complex composition of water or wastewater. Water and wastewater treatment is difficult due to the complex mixture of substances. The key problem for selecting proper treatment technology is the large number of chemicals used in industrial, communal and rural areas.

Therefore, research on the removal of contaminants in complex solutions should be more widely studied. Oxidation by-products are another phenomenon that is not commonly considered. It has been proven that the use of oxidants may produce intermediates. This aspect is often overlooked, although much literature data show higher toxicity of intermediates than their parent compounds. Therefore, toxicity tests should be used as one part of chemical monitoring during PS oxidation. Notwithstanding, using only one test organism may be insufficient to identify all toxicity. For this reason, various organisms with different sensitivities (e.g. bacteria, higher plants, invertebrates, and arthropods) should be tested.

Funding sources

This research did not receive any specific grant from funding agencies in the public, commercial, or not-for-profit sectors.

Author contributions

Piotr Zawadzki was responsible for the entire manuscript.

Declaration of Competing Interest

The authors declare that they have no known competing financial interests or personal relationships that could have appeared to influence the work reported in this paper.

References and recommended reading

Papers of particular interest, published within the period of review, have been highlighted as:

- of special interest
- of outstanding interest

1. Xiong Z, Jiang Y, Wu Z, Yao G, Lai B: **Synthesis strategies and emerging mechanisms of metal-organic frameworks for sulfate radical-based advanced oxidation process: a review.** *Chem Eng Sci* 2021, **421**:127863, <https://doi.org/10.1016/j.ces.2020.127863>
 2. Li X, Jie B, Lin H, Deng Z, Qian J, Yang Y, Zhang X: **Application of sulfate radicals-based advanced oxidation technology in degradation of trace organic contaminants (TrOCs): recent advances and prospects.** *J Environ Manag* 2022, **308**:114664, <https://doi.org/10.1016/j.jenvman.2022.114664>
 3. Karim AV, Jiao Y, Zhou M, Nidheesh PV: **Iron-based persulfate activation process for environmental decontamination in water and soil.** *Chemosphere* 2021, **265**:129057, <https://doi.org/10.1016/j.chemosphere.2020.129057>
 4. Zawadzki P: **Comparative studies of Rhodamine B decolorization in the combined process Na₂S₂O₈/visible light/ultrasound.** *Desalin Water Treat* 2021, **213**:269-278, <https://doi.org/10.5004/dwt.2021.26694>
 5. Hou X, Zhan G, Huang X, Wang N, Ai Z, Zhang L: **Persulfate activation induced by ascorbic acid for efficient organic pollutants oxidation.** *Chem Eng J* 2020, **382**:122355, <https://doi.org/10.1016/j.ces.2019.122355>
- The study addresses the application of PS activated by AA for organic pollutants degradation (e.g. ATR, PCP, alachlor, tetracycline, and chloramphenicol). Authors also perform a comprehensive study on the effects of process parameters (e.g. pH, temperature, air influence, background common ions and natural organic matters) on PS activation by AA.
6. Song W, Li J, Wang Z, Zhang X: **A mini review of activated methods to persulfate-based advanced oxidation process.** *Water Sci Technol* 2019, **79**:573-579, <https://doi.org/10.2166/wcc.2018.168>
 7. Watts RJ, Ahmad M, Hohner AK, Teel AL: **Persulfate activation by glucose for in situ chemical oxidation.** *Water Res* 2018, **133**:247-254, <https://doi.org/10.1016/j.watres.2018.01.050>
 8. Zawadzki P: **Decolorisation of methylene blue with sodium persulfate activated with visible light in the presence of glucose and sucrose.** *Water Air Soil Pollut* 2019, **230**:313, <https://doi.org/10.1007/s11270-019-4372-x>
 9. Cao M, Hou Y, Zhang E, Tu S, Xiong S: **Ascorbic acid induced activation of persulfate for pentachlorophenol degradation.** *Chemosphere* 2019, **229**:200-205, <https://doi.org/10.1016/j.chemosphere.2019.04.135>
 10. Cai T, Liu Y, Wang L, Dong W, Chen H, Zeng W, Xia X, Zeng G: **Activation of persulfate by photoexcited dye for antibiotic degradation: radical and nonradical reactions.** *Chem Eng Sci* 2019, **375**:122070, <https://doi.org/10.1016/j.ces.2019.122070>
 11. Shi J, Long T, Zhou Y, Wang L, Jiang C, Pan D, Zhu X: **Efficiency and quantitative structure-activity relationship of monoaromatics oxidation by quinone-activated persulfate.** *Front Chem* 2021, **9**:580643.
- The study describes the application of quinones for PS activation over a variety of volatile organic compounds. Shi et al. validated their experiments using QSAR model to investigate the oxidation mechanism in the presence of PSs activated by quinones.
12. Lv X, Leng Y, Wang R, Wei Y, Ren X, Guo W: **Persulfate activation by ferrocene-based metal-organic framework microspheres for efficient oxidation of orange acid 7.** *Environ Sci Pollut Res* 2022, **29**:34464-34474, <https://doi.org/10.1007/s11356-022-18669-2>.
- The work describes process parameters (dosage, PS concentration, and pH) on the degradation of acid orange 7 under the influence of three ferrocenes MOFs. Lv et al. highlight the potential of Co-Fc-MOFs as high-efficiency heterogeneous catalysts due to their high degradation efficiency and stability.
13. Pu M, Niu J, Brusseau ML, Sun Y, Zhou C, Deng S, Wan J: **Ferrous metal-organic frameworks with strong electron-donating properties for persulfate activation to effectively degrade aqueous sulfamethoxazole.** *Chem Eng Sci* 2020, **394**:125044, <https://doi.org/10.1016/j.ces.2020.125044>.
- The review elaborately describes the application of strong electron-donating ferrous MOF for PS activation to degrade SMX. Particularly noteworthy is the study of the reaction mechanism of SMX degradation and the degradation pathways of SMX.
14. Zhang Q, Jiang Q, Bai Y, Li H, Xue J, Gao Y, Cheng D: **Optimization and mechanism of oily sludge treatment by a novel combined surfactants with activated-persulfate method.** *Sci Total Environ* 2021, **800**:149525, <https://doi.org/10.1016/j.scitotenv.2021.149525>.
- A high-resolution study that shows application of the PS activated by surfactants for real oily sludge in a quasi-experimental design. An understanding of the degradation mechanism in real wastewater is crucial for future research in this field.
15. Nakarada Đ, Petković M: **Mechanistic insights on how hydroquinone disarms OH and OOH radicals.** *Int J Quantum Chem* 2018, **118**:e25496, <https://doi.org/10.1002/qua.25496>
 16. Zhang H, Qiao L, He J, Li N, Zhang D, Yu K, You H, Jiang J: **Activating peroxydisulfate by halogenated and methylated quinones: performance and mechanism.** *RSC Adv* 2019, **9**:27224-27230, <https://doi.org/10.1039/C9RA04789A>
 17. Shao H, Zhao X, Wang Y, Mao R, Wang Y, Qiao M, Zhao S, Zhu Y: **Synergistic activation of peroxydisulfate by Co₃O₄ modified g-C₃N₄ for enhanced degradation of diclofenac sodium under visible light irradiation.** *Appl Catal B: Environ* 2017, **218**:810-818, <https://doi.org/10.1016/j.apcatb.2017.07.016>
 18. Urán-Duque L, Saldarriaga-Molina JC, Rubio-Clemente A: **Advanced oxidation processes based on sulfate radicals for**

- wastewater treatment: research trends. *Water* 2021, **13**:2445, <https://doi.org/10.3390/w13172445>
19. Medkour A, Bechiri O, Lachter S: **Activation of persulfate by transition substituted Wells-Dawson-type heteropolitungstomolybdates to degrade a toxic dye in aqueous solution.** *Arab J Sci Eng* 2021, **46**:6519-6530, <https://doi.org/10.1007/s13369-020-05186-y>
 20. Rizal MY, Saleh R, Taufik A, Yin S: **Photocatalytic decomposition of methylene blue by persulfate-assisted Ag/Mn₃O₄ and Ag/Mn₃O₄/graphene composites and the inhibition effect of inorganic ions.** *Environ Nanotechnol Monit Manag* 2021, **15**:100408, <https://doi.org/10.1016/j.enmm.2020.100408>
 21. Han F, Ye X, Chen Q, Long H, Rao Y: **The oxidative degradation of diclofenac using the activation of peroxymonosulfate by BiFeO₃ microspheres — kinetics, role of visible light and decay pathways.** *Sep Purif Technol* 2020, **232**:115967, <https://doi.org/10.1016/j.seppur.2019.115967>
 22. Sabri M, Habibi-Yangjeh A, Chand H, Krishnan V: **Activation of persulfate by novel TiO₂/FeOCl photocatalyst under visible light: facile synthesis and high photocatalytic performance.** *Sep Purif Technol* 2020, **250**:117268, <https://doi.org/10.1016/j.seppur.2020.117268>
 23. Zawadzki P: **Elimination of chlorfenvinphos from treated municipal wastewater in advanced oxidation processes.** *Chem Rev* 2021, **1**:89-91, <https://doi.org/10.15199/62.2021.3.11>
 24. Kim C, Chin Y-P, Son H, Hwang I: **Activation of persulfate by humic substances: stoichiometry and changes in the optical properties of the humic substances.** *Water Res* 2022, **212**:118107, <https://doi.org/10.1016/j.watres.2022.118107>
 25. Yang W, Jiang Z, Hu X, Li X, Wang H, Xiao R: **Enhanced activation of persulfate by nitric acid/annealing modified multi-walled carbon nanotubes via non-radical process.** *Chemosphere* 2019, **220**:514-522, <https://doi.org/10.1016/j.chemosphere.2018.12.136>
 26. García-Cervilla R, Santos A, Romero A, Lorenzo D: **Compatibility of nonionic and anionic surfactants with persulfate activated by alkali in the abatement of chlorinated organic compounds in aqueous phase.** *Sci Total Environ* 2021, **751**:141782, <https://doi.org/10.1016/j.scitotenv.2020.141782>
 27. Oliveros AN, Pimentel JAI, de Luna MDG, Garcia-Segura S, Abarca RRM, Doong R-A: **Visible-light photocatalytic diclofenac removal by tunable vanadium pentoxide/boron-doped graphitic carbon nitride composite.** *Chem Eng J* 2021, **403**:126213, <https://doi.org/10.1016/j.cej.2020.126213>
 28. Mahanthappa M, Kottam N, Yellappa S: **Enhanced photocatalytic degradation of methylene blue dye using CuSCdS nanocomposite under visible light irradiation.** *Appl Surf Sci* 2019, **475**:828-838, <https://doi.org/10.1016/j.apsusc.2018.12.178>
 29. Ghernaout D, Elboughdiri N: **Water reuse: emerging contaminants elimination — progress and trends.** *OALib J* 2019, **6**:1-9, <https://doi.org/10.4236/oalib.1105981>
 30. Sadatsharif M, Purgel M: **Radical scavenger competition of alizarin and curcumin: a mechanistic DFT study on antioxidant activity.** *J Mol Model* 2021, **27**:166, <https://doi.org/10.1007/s00894-021-04778-1>
 31. Khan JA, He X, Khan HM, Shah NS, Dionysiou DD: **Oxidative degradation of atrazine in aqueous solution by UV/H₂O₂/Fe²⁺, UV/S₂O₈²⁻/Fe²⁺ and UV/HSO₅⁻/Fe²⁺ processes: a comparative study.** *Chem Eng J* 2013, **218**:376-383, <https://doi.org/10.1016/j.cej.2012.12.055>
 32. Khan JA, He X, Shah NS, Khan HM, Hapeshi E, Fatta-Kassinos D, Dionysiou DD: **Kinetic and mechanism investigation on the photochemical degradation of atrazine with activated H₂O₂, S₂O₈²⁻ and HSO₅⁻.** *Chem Eng J* 2014, **252**:393-403, <https://doi.org/10.1016/j.cej.2014.04.104>
 33. Shah NS, He X, Khan HM, Khan JA, O'Shea KE, Boccelli DL, Dionysiou DD: **Efficient removal of endosulfan from aqueous solution by UV-C/peroxides: a comparative study.** *J Hazard Mater* 2013, **263**:584-592, <https://doi.org/10.1016/j.jhazmat.2013.10.019>
 34. Fernandes A, Makos P, Khan JA, Boczkaj G: **Pilot scale degradation study of 16 selected volatile organic compounds by hydroxyl and sulfate radical based advanced oxidation processes.** *J Clean Prod* 2019, **208**:54-64, <https://doi.org/10.1016/j.jclepro.2018.10.081>
 35. Fedorov K, Plata-Gryl M, Khan JA, Boczkaj G: **Ultrasound-assisted heterogeneous activation of persulfate and peroxymonosulfate by asphaltenes for the degradation of BTEX in water.** *J Hazard Mater* 2020, **397**:122804, <https://doi.org/10.1016/j.jhazmat.2020.122804>
 36. Khan JA, He X, Shah NS, Sayed M, Khan HM, Dionysiou DD: **Degradation kinetics and mechanism of desethyl-atrazine and desisopropyl-atrazine in water with OH and SO₄⁻ based-AOPs.** *Chem Eng J* 2017, **325**:485-494, <https://doi.org/10.1016/j.cej.2017.05.011>
 37. Shah NS, He X, Khan JA, Khan HM, Boccelli DL, Dionysiou DD: **Comparative studies of various iron-mediated oxidative systems for the photochemical degradation of endosulfan in aqueous solution.** *J Photochem Photobiol A: Chem* 2015, **306**:80-86, <https://doi.org/10.1016/j.jphotochem.2015.03.014>
 38. Devi LG, Munikrishnappa C, Nagaraj B, Rajashekhar KE: **Effect of chloride and sulfate ions on the advanced photo Fenton and modified photo Fenton degradation process of Alizarin Red S.** *J Mol Catal A Chem* 2013, **374-375**:125-131, <https://doi.org/10.1016/j.molcata.2013.03.023>



Visible Light–Driven Advanced Oxidation Processes to Remove Emerging Contaminants from Water and Wastewater: a Review

Piotr Zawadzki

Received: 19 February 2022 / Accepted: 15 August 2022 / Published online: 3 September 2022
© The Author(s) 2022

Abstract The scientific data review shows that advanced oxidation processes based on the hydroxyl or sulfate radicals are of great interest among the currently conventional water and wastewater treatment methods. Different advanced treatment processes such as photocatalysis, Fenton’s reagent, ozonation, and persulfate-based processes were investigated to degrade contaminants of emerging concern (CECs) such as pesticides, personal care products, pharmaceuticals, disinfectants, dyes, and estrogenic substances. This article presents a general overview of visible light–driven advanced oxidation processes for the removal of chlorfenvinphos (organophosphorus insecticide), methylene blue (azo dye), and diclofenac (non-steroidal anti-inflammatory drug). The following visible light–driven treatment methods were reviewed: photocatalysis, sulfate radical oxidation, and photoelectrocatalysis. Visible light, among other sources of energy, is a renewable energy source and an excellent substitute for ultraviolet radiation used in advanced oxidation processes. It creates a high application potential for solar-assisted advanced oxidation processes in water and wastewater technology. Despite numerous publications of advanced oxidation processes (AOPs), more extensive research is needed to investigate the mechanisms of contaminant

degradation in the presence of visible light. Therefore, this paper provides an important source of information on the degradation mechanism of emerging contaminants. An important aspect in the work is the analysis of process parameters affecting the degradation process. The initial concentration of CECs, pH, reaction time, and catalyst dosage are discussed and analyzed. Based on a comprehensive survey of previous studies, opportunities for applications of AOPs are presented, highlighting the need for further efforts to address dominant barriers to knowledge acquisition.

Keywords Contaminants of emerging concern · Advanced oxidation process · Photocatalysis · Persulfate radical · Photoelectrocatalysis · Visible light

Abbreviations

AOPs	Advanced oxidation processes
BCF	Bioconcentration factor
$C_{0[CFVP]}$	Initial concentration of chlorfenvinphos
$C_{0[DCF]}$	Initial concentration of diclofenac
$C_{0[MB]}$	Initial concentration of methylene blue
CECs	Contaminants of emerging concern
CFVP	Chlorfenvinphos
DCF	Diclofenac
E^0	Oxidation potential
EC_{50}	Median effective concentration
E_g	Activation energy
HSO_5^-	Peroxymonosulfate

P. Zawadzki (✉)
Department of Water Protection, Central Mining Institute,
Plac Gwarków 1, 40-166 Katowice, Poland
e-mail: pzawadzki@gig.eu

K_{OC}	Organic carbon–water partition coefficient
K_{OW}	<i>n</i> -Octanol/water partition coefficient
LC ₅₀	Median lethal concentration
LED	Light-emitting diode
MB	Methylene blue
MPs	Microplastics
MSAs	Methanesulfonic acids
Na ₂ S ₂ O ₈	Sodium persulfate
NSAID	Non-steroidal anti-inflammatory drug
•OH	Hydroxyl radical
PDS	Peroxydisulfate
PEC	Photoelectrocatalysis
pH _{pzc}	PH of the point of zero charge
PMS	Peroxymonosulfate
PS	Persulfate
S ₂ O ₈ ²⁻	Peroxydisulfate/persulfate ion
SO ₄ ^{•-}	Sulfate radical
TBBPA	Tetrabromobisphenol A
UV	Ultraviolet
Vis	Visible

1 Introduction

The problem of contaminants of emerging concern (CECs) is an issue that is constantly being developed. CECs have been identified in groundwater and surface water, in treated municipal and industrial wastewaters, and even in drinking water (Bolong et al., 2009; Coadou et al., 2017; Montagner et al., 2019; Tröger et al., 2018). New groups of compounds have also been reported as potential substances classified as emerging contaminants: halogenated methanesulfonic acids (MSAs) such as chloro-, bromo-, or iodo-methanesulfonic acids (Zahn et al., 2016); microplastics (MPs) (Wright & Kelly, 2017); flame retardants including tetrabromobisphenol A (TBBPA) (Ballesteros-Gómez et al., 2017); compounds used in ultraviolet (UV) filters and sun creams such as ethylhexyl dimethylaminobenzoate and benzocaine (Li et al., 2017; Tsui et al., 2017); contrast agents used in computed tomography such as those containing gadolinium (Rogowska et al., 2018); pharmaceutical substances such as lidocaine (Jakab et al., 2020); and even drugs such as cocaine and its metabolites identified in pool waters (Fantuzzi et al., 2018).

The presence of contaminants of emerging concern in the environment is not normally related to their negative impact on living organisms at high

doses (acute toxicity). Their low concentrations in water and wastewater (c.a. few ng/dm³) and long-term effects on humans and animals (chronic toxicity) should be of potential concern. The toxic effects of these substances have been confirmed by, e.g., Leusch et al. (2017) and Lempart et al. (2020).

Since these compounds are often identified in the environment and because of their negative impact on living organisms, it is justified to develop new technologies of water treatment and municipal and industrial wastewater treatments. The scientific data reviews show that one of the interesting alternatives to the conventional processes used in environmental engineering is advanced oxidation processes (AOPs). The common feature of AOPs is the physicochemical reaction between the generated hydroxyl radical (•OH) or sulfate radical (SO₄^{•-}) and organic contaminants. AOPs are non-selective and allow the complete or partial decomposition of hazardous substances by mineralization into environmentally neutral, simple chemical compounds (Mazivila et al., 2019; Waclawek et al., 2017).

The differences between the various AOPs are the radical generation method, efficiency, and complexity. Most of them are photochemical processes, i.e., conducted in the presence of ultraviolet radiation ($\lambda < 400$ nm). A significant drawback is a catalytic activity, which requires using an expensive catalyst activation method with artificial light sources. The most frequently used radiation source is a lamp emitting radiation below 400 nm (UV light). This is essential for activating catalysts such as titanium(IV) oxide. Lasers, solar radiation, xenon, and sodium lamps are rarely used. When solar radiation is used, only 3–5% of this energy can be utilized, so the use of UV lamps, as energy-intensive devices, is a severe limiting factor for using these methods in the elimination of micropollutants (Gheraout & Elboughdiri, 2019; Palit, 2014).

The scientific data also show that many works are devoted to using sulfate radicals SO₄^{•-} ($E^0 = 2.5\text{--}3.1$ V) for the degradation of organic contaminants (Hu et al., 2020b; Zhou et al., 2020). The generation of sulfate radicals is carried out by activation of persulfate ions (S₂O₈²⁻) by UV radiation, heat, ionizing radiation, high pH > 11.0, and transition metal ions (Criquet and Karpel Vel Leitner, 2012; Peng et al., 2017; Manz et al., 2018; Al Hakim et al., 2019). Activation with transition metal ions at low oxidation levels such

as Fe^{2+} , Ni^{2+} , Co^{2+} , and Ag^+ is used most frequently. As a result of the reaction, the ion $\text{S}_2\text{O}_8^{2-}$ reacts with the electron donor from the transition metal to form a single sulfate radical (Nasseri et al., 2017).

A review of results in the Scholar database (Google Scholar Database, 2022) showed that, in recent years, there have been an increasing number of studies on the application of modifications of advanced oxidation processes, including the visible light-driven AOPs (Fig. 1). In recent years, researchers have focused on modifications of advanced oxidation processes (Cheng et al., 2019; Zawadzki et al., 2020; Zawadzki, 2020; Nguyen et al., 2020). Modifications simplify the way catalysts are activated, and increase the degree of pollutant removal efficiency with variable wastewater quality.

One example of modifications used in heterogeneous oxidation processes (in the presence of solid catalysts, e.g., titanium dioxide (TiO_2)) is carbonaceous materials (e.g., activated carbon), acids (e.g., succinic acid, ascorbic acid), or metal and non-metal species (e.g., carbon, nitrogen, sulfur, ferrum). Activation processes of persulfates (precursors of sulfate radicals) under visible light have also attracted widespread interest (Du et al., 2020; Wang et al., 2019; Zawadzki, 2019; Zhang et al., 2020), and it is described as effective as conventional activation methods. Appropriately chosen treatment parameters and optimal modification methods can lower costs compared to classical methods.

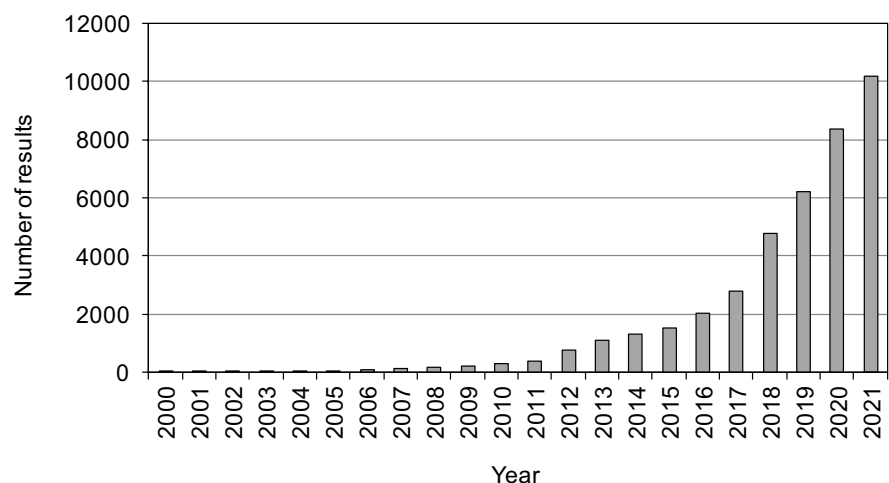
The increasing pressure of contaminants on the environment, combined with the scarcity of water

resources in the world, justifies the need to develop new and optimize already applied methods for the efficient removal of contaminants from water and wastewater. This work presents examples of methods for the advanced oxidation of micropollutants such as chlorfenvinphos, methylene blue, and diclofenac carried out in the presence of visible light.

Micropollutants have a high susceptibility to migrate in the environment and thus bioaccumulate and migrate in the environment (Fig. 2). Micropollutants are also relatively resistant to decomposition. The emission of micropollutants to the environment is mainly due to industrial activities. It is primarily connected with thermal and chemical processes. Coking plants, power plants, waste incineration plants, and chemical plants are direct sources of micropollutants. Excessive amounts of pesticides, pharmaceuticals, and antibacterial substances are of great importance. Micropollutants are primarily identified in surface water, but their concentration is also increasing in groundwater. They are mainly transported to aquatic ecosystems with treated or poorly treated industrial and domestic wastewaters, atmospheric precipitation, and through surface runoff from agricultural land and poorly protected landfills (Dubey et al., 2021; Menger et al., 2021; Ngweme et al., 2021).

The following representatives from a group of CECs were selected as model contaminants: chlorfenvinphos, methylene blue, and diclofenac. These contaminants differ from each other in their physicochemical properties, degree of impact on

Fig. 1 Trend of the number of publications per year search by words in the Scholar database: “visible-light driven advanced oxidation processes” from the years 2000–2021



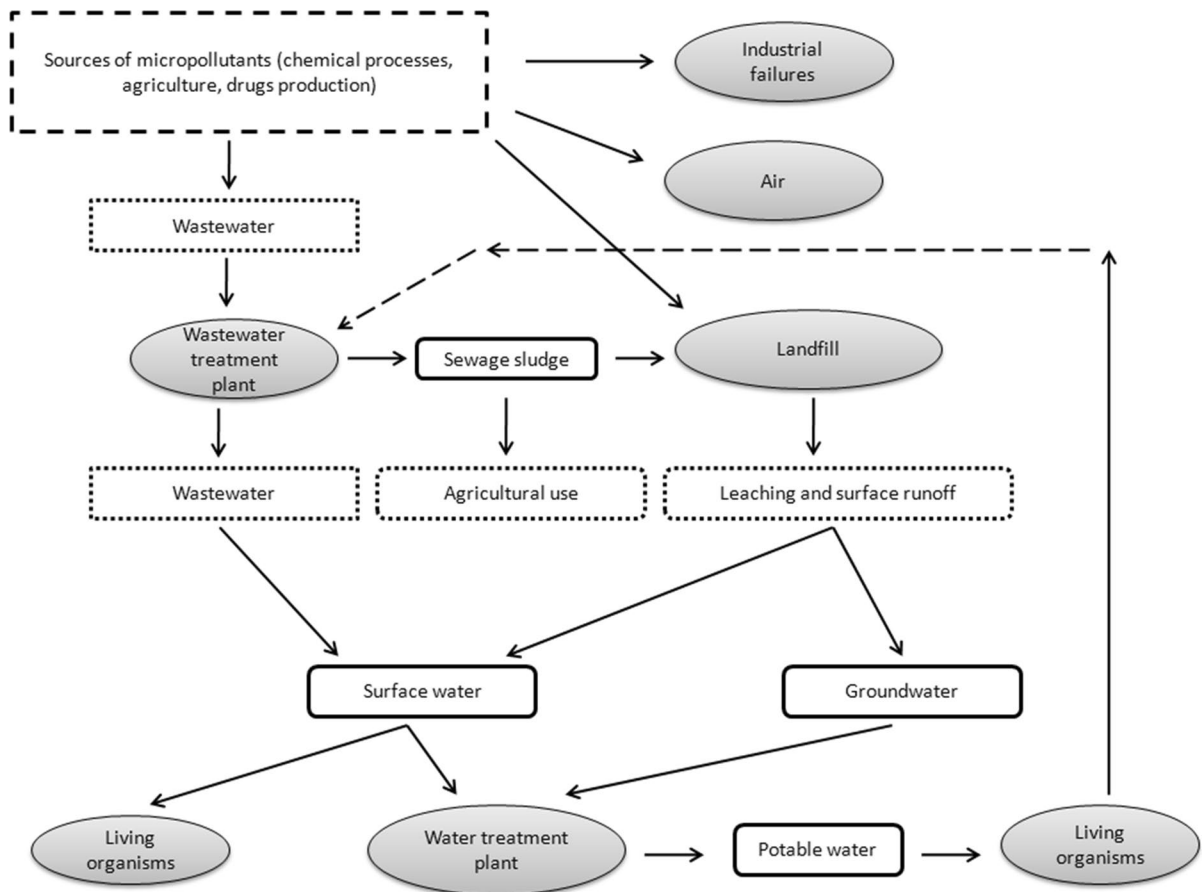


Fig. 2 Migration of micropollutants in the environment

living organisms, and persistence in the environment (Table 1).

In recent years, the number of publications on the applications of AOPs based on hydroxyl or sulfate radicals has been widely studied for water, wastewater, and soil treatment (Gheraout & Elboughdiri, 2021; Lee et al., 2020; Ma et al., 2021; Miklos et al., 2018; Zhou et al., 2019). Despite numerous publications and reviews on AOPs, there is a lack of collected and systematized information regarding visible light–driven advanced oxidation processes for the removal of emerging contaminants. Very few studies reviewed this treatment technology (Serpone et al., 2017; Tian et al., 2022; Yang et al., 2021); therefore, there is a paucity of a broad overview of its application and discussion of influencing parameters. Although the large number of publications on conventional AOPs (e.g., using UV)

shows great success, due to the energy crisis and the continuously increasing electricity prices, it is important to present the potential, possibilities, and influencing parameters affecting AOPs using solar radiation as a renewable energy source. Thus, solar radiation can be applied as a free source of energy, reducing operating costs on an industrial scale. Therefore, this review article summarizes various methods of removing contaminants of emerging concern from water and wastewater by visible light–driven AOPs. An important aspect in the work is the analysis of process parameters affecting the degradation process to enhance the efficiency of the visible light–driven AOP system. Specifically, the main mechanisms involved in visible light activation are also discussed. Concluding perspectives and guidelines for future research are proposed at the end of this paper.

Table 1 Toxicological and physicochemical profile of CFVP, MB, and DCF

Compound	CFVP	MB	DCF
Chemical formula	C ₁₂ H ₁₄ Cl ₃ O ₄ P	C ₁₆ H ₁₈ ClN ₃ S	C ₁₄ H ₁₁ Cl ₂ NO ₂
Molecular weight (g/mol)	359.6	319.85	296.1
CAS number	470–90-6	61–73-4	15,307–86-5
Form	Amber liquid	Dark green crystals or powder	Solid; crystals from ether–petroleum ether
Toxicity	<i>Daphnia magna</i> : LC ₅₀ (24 h) = 28.00 µg/l <i>Daphnia magna</i> : EC ₅₀ (24 h) = 1.2 µg/l <i>Gammarus fasciatus</i> : LC ₅₀ (24 h) = 27 µg/l <i>Gammarus fasciatus</i> : LC ₅₀ (96 h) = 9.6 µg/l	<i>Daphnia</i> : EC ₅₀ (48 h) = 2.26 mg/l Fish: LC ₅₀ (96 h) = 18.0 mg/l	<i>Dunaliella tertiolecta</i> (phytoplankton): EC ₅₀ (96 h) = 185.69 mg/l <i>Daphnia magna</i> : EC ₅₀ (48 h) = 123.30 mg/l
log K _{OW} (–)	3.81	5.85	4.51
log K _{OC} (–)	2.44	ND	3.81–4.30 ^a
Bioconcentration factor (BCF) (–)	36.6–661.0	< 100	10
Solubility in water (at 25 °C) (mg/l)	124.0 (at 20 °C)	43,600.0	2.37
Vapor pressure at 25 °C (mmHg)	7.5 × 10 ⁻⁶	7.0 × 10 ⁻⁷	6.14 × 10 ⁻⁸
Environmental concentration (µg/l)	Surface water: 0.001–47.4 Seawater and groundwater: 0.02 Rainwater: 0.05–0.12 Wastewater (effluent): 0.05–0.14	10 × 10 ³ –10 × 10 ⁵ ^b	Surface water: 4.62 × 10 ⁻³ –0.057 Groundwater: 2.5 × 10 ⁻³ –13.48 Drinking water: 2.5 × 10 ⁻³ –56 ng/l Wastewater effluent: 4.5 × 10 ⁻³ –19.0
References	Chlorfenvinphos (Safety Data Sheet 2022Zgheib et al., 2012; Campo et al., 2013; Ccancapa et al., 2016Pérez-Lucas et al., 2018) Chlorfenvinfos (Compound Summary 2022)	Methylene blue (Material Safety Data Sheet 2022Rahman et al., 2012; Almaamary et al., 2017) Methylene blue (Compound Summary 2022)	Scheytt et al. (2005) DeLorenzo and Fleming (2008) Memmert et al. (2013) De Oliveira et al. (2016) Sathishkumar et al. (2020) Diclofenac (Compound Summary 2022)

CFVP chlorfenvinphos, MB methylene blue, DCF diclofenac, ND no data.

^alog K_{OC} values based on equations by Karickhoff et al. (1979): log K_{OC} = 1.0 log K – 0.21.

^bNo data about MB concentrations in wastewater was found: the presented data refer to initial concentrations removed during laboratory experiments.

1.1 Methylene Blue

Industrial wastewater contains chemical compounds (e.g., dyes, phenols, pesticides, heavy metals), which are by-products of the technological processes, e.g., in the textile, chemical, food, and tanning industries. These industries generate the most significant industrial wastewater containing synthetic dyes (Khamparia & Jaspal, 2018). The composition of colored industrial effluents is chemically diverse. The synthetic dyes commonly found in this type of

wastewater can be divided into azo dyes, reactive dyes, triphenylmethane dyes, heterocyclic dyes, and polymeric dyes (Guadie et al., 2017).

One example of a compound belonging to the group of azo dyes is methylene blue (MB). Azo dyes contain the azo functional group R–N=N–R', in which R and R' can be substituted with alkyl or aryl groups. Azo dyes are one of the leading organic compounds identified in colored industrial effluents and can account for up to 70% of total dye production (Oveisi et al., 2019). Azo dyes trigger histamine, which

can cause, for example, urticaria and can aggravate asthma symptoms and cause uterine contractions in pregnant women, causing miscarriage. MB is a cationic thiazine dye containing a six-membered heterocyclic ring with sulfur and a nitrogen atom (phenothiazine ring). Methylene blue is widely used in the textile, paper, cosmetics, plastics, and food industries (Zawadzki, 2019). Recent literature also indicates the potential use of MB in treating COVID-19, a disease caused by the SARS-CoV-2 virus (Gendrot et al., 2020; Scigliano & Scigliano, 2021).

For organic substances with a $\log K_{OW}$ value less than 4.5, the affinity for the lipids of the organism is assumed to be insufficient to exceed the bioaccumulation criterion (bioconcentration factor (BCF)=2000). The BCF is the ratio of the concentration of a substance in an organism and water, depending on the organism and the conditions. Methylene blue exceeds this factor ($\log K_{OW}=5.85$). Chemicals with high $\log K_{OW}$ values (>4.5) are of more significant concern as they have the potential to bioconcentrate in living organisms. However, MB is not expected to bioaccumulate significantly as the estimated BCF is below 100.

Due to the potential danger to humans and the high resistance to biodegradation, there is a need to develop technologies to eliminate methylene blue from water and wastewater. Removal of dyes by conventional processes, including activated sludge, does not bring the expected results. Due to their low biodegradability, almost 90% of the dyes present in wastewater is not removed by conventional treatment processes. Therefore, the degradation of dyes from wastewater has attracted considerable interest from researchers worldwide (Deng and Zhao, 2015). In recent years, interesting, advanced oxidation processes driven by visible light have been developed to remove methylene blue from colored wastewater.

1.2 Chlorfenvinphos

For many years, interest in pesticides has focused on four basic properties: selective toxicity, persistence in the environment, bioaccumulation, and mobility. Persistence in the environment is probably the most decisive factor when considering the extent of their use. Persistence is often expressed in terms of half-life. Pesticide degradation can occur through biological processes and chemical and photochemical reactions.

A pesticide losing its characteristic activity does not necessarily mean that it has become a harmless substance. Chemical reactions often result in more toxic compounds than the original compounds (Mahdy & El-Maghraby, 2010; Laws 2013; Ravoet et al., 2015).

Chlorfenvinphos (CFVP) is one of the most important members of the organophosphorus insecticide family. Technical chlorfenvinphos, consisting of E and Z isomers, contains about 80–90% of this compound. CFVP is a low-mammalian toxicity insecticide. It is used against pests destroying crops of potatoes, rice, carrots, oilseeds, and maize. Organophosphate insecticides are phosphoric acid derivatives in which the hydroxyl group (–OH) has been replaced by –OR groups derived from alcohols. Organophosphate pesticides inhibit the activity of acetylcholinesterase, one of the essential enzymes for the peripheral and central nervous systems. Chlorfenvinphos can cause structural and functional changes in the liver (Lutz et al., 2006; Sismeiro-Vivas et al., 2007; Sosnowska et al., 2013).

Chlorfenvinphos has a moderate bioconcentration potential as indicated by a $\log K_{OW}$ value of 3.81. The degree of bioconcentration of CFVP ranges from BCF=36.6 to 661.0. The organic carbon/soil partition coefficient ($\log K_{OC}$) value is approximately 2.44. The $\log K_{OC}$ value shows a moderate susceptibility to adsorb in bottom sediments and suspended matter, and therefore, the transport of the compound to the solid phase is to be expected. CFVP hydrolyzes slowly in slightly alkaline, acidic, and neutral conditions. The half-life ($t_{1/2}$) at pH 3 to 6 is between 170 and 200 days ($T=20\text{--}30\text{ }^{\circ}\text{C}$). Chlorfenvinphos is more resistant to decomposition in biologically active waters, with half-lives ranging from 1 to 25 days. It only decomposes thermally at high temperatures ($T>150\text{ }^{\circ}\text{C}$). Despite its ban in Europe, it is identified in water samples worldwide (Serrano et al., 1997; Wu et al., 2011; Sire and Amouroux, 2016; Ccancapa et al., 2016; Koranteng et al., 2018; Pérez-Lucas et al., 2018).

The number of publications on the application of advanced processes to eliminate chlorfenvinphos is not significant. The number of results in the Scholar database in 2000–2021 containing the phrase “advanced oxidation process for chlorfenvinphos removal” is 1050, while that containing the words “visible-light-driven advanced oxidation process for chlorfenvinphos removal” is 154. Compared

to atrazine, an herbicide from the triazine group (17,500 in 2000–2021 for the phrase “advanced oxidation process for atrazine removal” and 5170 for the phrase “visible-light-driven advanced oxidation process for atrazine removal”), diuron, a phytotoxic herbicide from the group of total herbicides (12,400 for “advanced oxidation process for diuron removal” and 1220 for “visible-light-driven advanced oxidation process for diuron removal”), has a relatively low number. Therefore, there is a gap between the removal processes for individual organophosphorus pesticides investigated so far. This is important because atrazine, diuron, and chlorfenvinphos are on the list of priority substances for water policy (Directive, 2013).

1.3 Diclofenac

Among the analyzed CECs, there is a group of pharmaceutical substances. The largest pharmaceutical substances come from hospitals, households, veterinary centers, and livestock farms. Municipal wastewater discharge is considered the dominant source of pharmaceuticals, while discharges from manufacturing plants, hospitals, and farms are locally significant (Wöhler et al., 2020). Pharmaceuticals are designed to perform a precise function in the human body. Significant fractions of pharmaceutical substances are generally excreted, mainly through urine (Barreto et al., 2021). Pharmaceutical products for use in both humans and animals are developing together with the global population increase and healthcare. The number of pharmaceuticals discharged into the environment is an increasingly severe problem. More than 3500 pharmaceutical substances have been identified in surface water and treated wastewater, excluding metabolites and other transformation products (Aissaoui et al., 2017).

Diclofenac (DCF) is a non-steroidal anti-inflammatory drug (NSAID) (Sathishkumar et al., 2020). Anti-inflammatory painkillers are among the most popular drugs available, mostly over-the-counter. The most commonly purchased painkillers include ibuprofen, paracetamol, naproxen, diclofenac, carbamazepine, and salicylic acid. Diclofenac is used in both humans and livestock. Worldwide annual consumption of diclofenac is estimated to be around 1000 mg (Moreira et al., 2018; Tomul et al., 2019).

The widespread use of pharmaceuticals results in the almost continuous emission of these compounds and their metabolites into the environment. The increased importance of pharmaceutical substances has prompted several actions to limit or monitor these compounds. For example, by Commission Implementing Decision (EU) No. 2015/495 of 20 March 2015 establishing a watch list of substances for monitoring purposes, diclofenac was included in the first watch list. According to the current Commission Implementing Decision (EU) No. 2020/1161 of 4 August 2020 establishing a watch list of substances for monitoring purposes, as many as four compounds from the group of pharmaceuticals have been included: amoxicillin (a semi-synthetic β -lactam antibiotic with bactericidal activity), ciprofloxacin (a second-generation quinolone chemotherapeutic with bactericidal activity), sulfamethoxazole (a bacteriostatic antibiotic), trimethoprim (a chemotherapeutic agent), venlafaxine, and *O*-desmethylvenlafaxine (a multifunctional organic chemical compound used as an antidepressant) (Commission Implementing Decision (EU) 2015/495; Commission Implementing Decision (EU) 2020/1161). Furthermore, Font et al. (2019) developed a model to predict the current and future dilution of pharmaceuticals in freshwater ecosystems such as rivers and lakes. Their model was applied to diclofenac, a commonly used anti-inflammatory drug to reduce pain.

Approximately 65% of the diclofenac dose is excreted in urine and 35% in bile as conjugates of unchanged diclofenac and its metabolites (Voltaren—Prescribing Information 2022). Diclofenac tends to adsorb to the organic matter in soil or sediments due to their low affinity for water ($\log K_{OW}=4.51$ and $\log K_{OC}=3.81-4.30$). The bioconcentration degree of DCF is 10 (diclofenac is not expected to bioaccumulate significantly).

Conventional treatment processes have DCF removal efficiencies ranging from a few % to 93% (Lonappan et al., 2016; Verlicchi et al., 2012). Zhang et al. (2008) reported diclofenac removal efficiencies by wastewater treatment plants ranging from 0 to 80%, mainly in the 21–40% range. Zorita et al. (2009) showed that the DCF reduction factor could also be harmful, which is attributed to de-conjugation or hydrolysis of pharmaceutical metabolites, reformation of the parent molecule, or pharmaceutical desorption from colloids and suspension (sewage

sludge). Therefore, DCF persists in the aquatic environment and is detected in raw wastewater, treated wastewater, surface water, and even drinking water (Loos et al., 2017; Sharma et al., 2019).

2 Visible Light–Driven Advanced Oxidation Processes

There are currently many technologies for the removal of emerging contaminants. These include chemical precipitation, flotation, adsorption on activated carbon, wet air oxidation, supercritical water oxidation, Fenton's reagent, hydrogen peroxide treatment, ultrasonic oxidation, ozonation, membrane processes (microfiltration, ultrafiltration, reverse osmosis, electrodialysis), and biological processes, as well as combined processes such as membrane bioreactors (biological processes and membrane processes) or biological activated carbons (Dhaka et al., 2019; Gogoi et al., 2018; Rodriguez-Narvaez et al., 2017). However, the above methods have some disadvantages. For example, coagulation generates large amounts of sludge formation and additional equipment for sedimentation and filtration of the resulting sludge is required. Sorption processes require optimal adsorbents with a high affinity for the contaminants. On the other hand, membrane processes require pre-treatment of the wastewater to eliminate substances that limit the life of the membranes. Wet air oxidation uses air as an oxidant mixed with the contaminated medium and then passed through a catalyst with increased temperature and pressure (high-temperature process and high electricity consumption are limitations of this process). In contrast, microorganisms in biological methods are sensitive to toxic substances, and pre-treatment before biological treatment is required. Most of the mentioned methods do not degrade the contaminants but only transfer them to another phase, so CECs are still present in the environment (Tungler et al., 2015; De Gisi et al., 2016; Obotey Ezugbe & Rathilal, 2020).

In recent years, the interest of researchers has focused on the development of AOPs that, under appropriately chosen conditions (e.g., reaction time, oxidant dose, reactor volume), allow the degradation of almost 100% of the contaminants and minimize the risk of generating oxidation by-products. The use of energy-consuming UV lamps (Zou et al., 2020), the

recombination of hole–electron pairs (photocatalysts) (Sharma et al., 2021), the influence of interfering ions (Ahmed et al., 2021), the result of suspended matter (slurry), the formation of post-process residues (nanoparticles of photocatalysts, negatively affecting ecosystems and human health by entering, for example drinking water sources) (Zhang et al., 2017), and the use of energy- and cost-intensive activation methods (high temperature, high pH, chemical reactants, e.g., Fe^{2+} for radical generation processes $\text{SO}_4^{\bullet-}$) (Hu et al., 2020a, 2020b; Zawadzki, 2019; Zrinyi & Pham, 2017) are significant limitations of AOPs. Therefore, new and efficient, technologically and economically effective processes are sought in environmental engineering to achieve simultaneously high removal results of CECs. The analysis of literature data has shown that three basic types of visible light–driven AOPs are used for CFVP, DCF, and MB elimination processes: photocatalysis, radical sulfate oxidation, and electrochemical processes. A summary of the identified visible light–driven processes is presented in Table 2.

2.1 Visible Light–Driven Photocatalysis

IUPAC defines photocatalysis as the initiation of a reaction or a change in its rate under the influence of solar (Vis), UV, and infrared (IR) radiation in the presence of a photocatalyst (semiconductor), which, by absorbing the radiation, participates in the transformation of the reaction substrates (Braslavsky, 2007). Photocatalysis is carried out in the presence of metal oxides, including TiO_2 , zinc oxide (ZnO), WO_2 , CeO_2 , and Fe_2O_3 , or sulfides CdS and ZnS . Photochemical processes are most often carried out in TiO_2 . The advantage of TiO_2 is its chemical and biological stability. Titanium(IV) oxide is non-toxic and practically insoluble. From the economic point of view, it is relatively cheap and easy to produce. In a photocatalytic process carried out in the presence of TiO_2 , it is necessary to provide radiation of an appropriate wavelength, at an energy amount higher than that of bandgap energy. The minimum energy required for its activation is equal to the energy of the excited band and is $E_g = 3.02$ V for rutile form and $E_g = 3.2$ V for anatase form. The excitation of a semiconductor causes the transfer of an electron from the valence band (VB) to the conduction band (CB). A so-called electron–hole is produced, which

Table 2 The experimental conditions and removal efficiency of visible light-driven AOPs for CFVP, MB, and DCF degradation

CEC	Process	Removal efficiency (%)	Details	References
Chlorfenvinphos	Visible light-driven photoelectrochemical degradation in the presence of WO ₃ nanosheets/nanorods	95	Thermal treatment (annealing) of nanostructured electrodes = 600 °C; concentration C _{0[CFVP]} = 20 mg/l; process time = 360 min; pH = 1; Temp. = 20 °C; the bias potential (vs. SCE) = +1 V; type of lamp = Xe lamp; lamp power = 1000 W	Fernández-Domene et al. (2019)
Chlorfenvinphos	Photocatalysis in the presence of pyruvic acid (PA)-doped TiO ₂ (TiO ₂ /PA)	85	Concentration C _{0[CFVP]} = 1.0 mg/l; adsorption time = 20 min; process time = 60 min; catalyst dosage = 50 mg/l; pH = 3; type of lamp = tungsten; lamp power = 10 W	Zawadzki (2020)
Chlorfenvinphos	Photodegradation by using WO ₃ nanostructures	95	Thermal treatment (annealing) of nanostructured electrodes = 600 °C; anodization in electrolyte: 1.5 M CH ₄ O ₃ S; 0.05 M H ₂ O ₂ ; concentration C _{0[CFVP]} = ND; process time = 1440 min; the bias potential (vs. SCE) = +1 V; Temp. = room temperature; type of lamp = Xe lamp; lamp power = 500 W	Roselló-Márquez et al. (2021)
Chlorfenvinphos	Visible (Vis) light activation of persulfate (PS) by glucose (PS/Vis/Glu)	81	Concentration C _{0[CFVP]} = 1 mg/l; glucose dosage = 100 mM; PS dosage = 20 mM; process time = 20 min; pH = 6; type of lamp = tungsten; lamp power = 10 W	Zawadzki (2021b)
Methylene blue	Photocatalysis in the presence of copper phthalocyanine-sensitized TiO ₂ nanopowders (CuPc/TiO ₂)	70	Concentration C _{0[MB]} ≈ 192 mg/l; catalyst dosage ≈ 333.33 mg/l; concentration of Cu = 4.7 wt%; adsorption time = 30 min; process time = 150 min; Temp. = room temperature; type of lamp = xenon; lamp power = 150 W	Cabir et al. (2017)
Methylene blue	Photocatalysis in the presence of nanostructured Fe/FeS powder	96	Concentration C _{0[MB]} = 5 mg/l; catalyst dosage = 1000 mg/l; adsorption time = 30 min; process time = 200 min; pH = 11; type of lamp = ND; lamp power = 400 W	Esmaili et al. (2018)
Methylene blue	Photocatalysis in the presence of CuS-CdS nanocomposite	99.97	Concentration C _{0[MB]} = 10 mg/l; catalyst dosage = 200 mg/l; adsorption time = ND; process time = 10 min; type of lamp = tungsten; lamp power = 250 W	Mahanthappa et al. (2019)

Table 2 (continued)

CEC	Process	Removal efficiency (%)	Details	References
Methylene blue	Photocatalysis in the presence of ZnO-supported Au/Pd bimetallic nanocomposites	97	Concentration of Au = 10 wt%; concentration of Pd = 5 wt%; concentration $C_{0[MB]}$ = 16 mg/l; catalyst dosage = 5 mg/l; adsorption time = 30 min; process time = 180 min; Temp. = room temperature; type of lamp = xenon; lamp power = 200 W	Lee et al. (2019)
Methylene blue	Photocatalysis in the presence of Fe ₂ O ₃ /graphene/CuO (FGC) nanocomposite	94	Concentration $C_{0[MB]}$ = 20 mg/l; catalyst dosage = 500 mg/l; adsorption time = 120 min; process time = 40 min; Temp. = 25 °C; type of lamp = ND; lamp power = 100 W	Nuengmatcha et al. (2019)
Methylene blue	Photocatalysis in the presence of Gd-doped ZnO nanoparticles	93	Concentration of Gd = 3%; concentration $C_{0[MB]}$ = 10 mg/l; catalyst dosage ≈ 360 mg/l; adsorption time = 30 min; process time = 90 min; type of lamp = LED; lamp power = 40 W	Selvaraj et al. (2019)
Methylene blue	Photocatalysis in the presence of magnetic TiO ₂ /NiFe ₂ O ₄ /reduced graphene oxide nanocomposite	71	Concentration of graphene = 120 mg; concentration $C_{0[MB]}$ = 10 mg/l; catalyst dosage = 100 mg/l; H ₂ O ₂ dosage = 725 mg/l; adsorption time = 60 min; process time = 90 min; pH = 11; type of lamp = halogen; lamp power = 500 W	Ziarati Saravani et al. (2019)
Methylene blue	Photocatalysis in the presence of CdS/SnO ₂ nanoparticles	80	Concentration of CdS = 5 wt%; concentration $C_{0[MB]}$ = 6.4 mg/l; catalyst dosage = 1000 mg/l; adsorption time = 30 min; process time = 180 min; Temp. = 30–35 °C; type of lamp = mercury; lamp power = 16 W	El-Katori et al. (2020)
Methylene blue	Photocatalysis in the presence of molybdenum disulfide composed by LDH composite (MoS ₂ /LDH)	95	Ratio of molybdate to thiourea = 1:5; concentration $C_{0[MB]}$ = 20 mg/l; catalyst dosage = 200 mg/l; adsorption time = 30 min; process time = 180 min; pH = 4; type of lamp = xenon; lamp power = 300 W	Chen et al. (2020)
Methylene blue	Photocatalysis in the presence of CdS-NiFe ₂ O ₄ /reduced graphene oxide photocatalyst	92	Concentration $C_{0[MB]}$ = 10 mg/l; catalyst dosage = 400 mg/l; adsorption time = 60 min; process time = 120 min; pH = 7; Temp. = 25 °C ± 2 °C; type of lamp = mercury; lamp power = 250 W	Bagherzadeh et al. (2018)
Methylene blue	Degradation by sodium persulfate activated by glucose (PS/G/Vis)	84	Concentration $C_{0[MB]}$ = 2 mg/l; process time = 90 min; glucose dosage = 100 mM; PS dosage = 0.065 mM; pH = 12; Temp. = room temperature; type of lamp = tungsten; lamp power = 10 W	Zawadzki (2019)

Table 2 (continued)

CEC	Process	Removal efficiency (%)	Details	References
Methylene blue	Degradation by peroxymonosulfate (PMS) and BiVO ₄	99	Concentration C _{0[MB]} = 5 mg/l; BiVO ₄ dosage = 200 mg/l; PMS dosage = 1 mM; adsorption time = 10 min; process time = 90 min; pH = 6; type of lamp = LED; lamp power = 30 W	Tang (2020)
Methylene blue	PS activated by TiO ₂ /FeOCl	100	Concentration of FeOCl = 20 wt%; concentration C _{0[MB]} = 3.2 mg/l; catalyst dosage = 400 mg/l; PS dosage = 1.48 mM; adsorption time = 60 min; process time = 90 min; Temp. = 25 °C; type of lamp = LED; lamp power = 50 W	Sabri et al. (2020)
Methylene blue	PS activated by Ag/Mn ₃ O ₄ (Ag/Mn ₃ O ₄ -0.5)	82	Ag:Mn ₃ O ₄ ratio = 1:0.5; concentration C _{0[MB]} = 40 mg/l; catalyst dosage = 500 mg/l; process time = 90 min; PS dosage = 12 mM; pH = 7; Temp. = room temperature; type of lamp = xenon; lamp power = 40 W	Rizal et al. (2021)
Methylene blue	PS activated by Ag/Mn ₃ O ₄ /graphene composites (Ag/Mn ₃ O ₄ -5G)	100	Ag:Mn ₃ O ₄ ratio = 1:0.5; graphene composites concentration = 5 wt%; concentration C _{0[MB]} = 40 mg/l; catalyst dosage = 500 mg/l; process time = 60 min; PS dosage = 12 mM; pH = 7; Temp. = room temperature; type of lamp = xenon; lamp power = 40 W	
Methylene blue	PMS activated by surface-tailored carbon quantum dots (CQDs)	90.1	Concentration C _{0[MB]} = 20 mg/l; PMS dosage = 246 mg/l; catalyst dosage = 4000 mg/l; adsorption time = 30 min; process time = 60 min; Temp. = 25 °C; type of lamp = LED; lamp power = 40 W	Han et al. (2020a)
Methylene blue	Photoelectrocatalysis in the presence of cadmium sulfide-sensitized titanium dioxide film	88	Number of CdS layer = 6; concentration C _{0[MB]} = 5 mg/l; adsorption time = 60 min; effective area of photoelectrode = 2 cm ² ; the bias potential (vs. SCE) = + 4 V; process time = 180 min; type of lamp = xenon; lamp power = 300 W	Wu et al. (2019)
Methylene blue	Photoelectrocatalysis in the presence of F-doped TiO ₂ photoelectrode	92	Concentration of F = 15 wt%; concentration C _{0[MB]} = 10 mg/l; adsorption time = 30 min; effective area of photoelectrode = 50 cm ² ; the bias potential (vs. SCE) = + 1.4 V; pH = 6.89; process time = 240 min; type of lamp = metal halide; lamp power = 450 W	Liu et al. (2017a)

Table 2 (continued)

CEC	Process	Removal efficiency (%)	Details	References
Methylene blue	Photoelectrocatalysis in the presence of ZnO-coated nanoporous silicon by atomic layer deposition	88	Concentration $C_{0[MB]}$ = 20 mg/l; adsorption time = 120 min; effective area of photoelectrode = 16 cm ² ; the bias potential (vs. SCE) = +6 V; process time = 105 min; type of lamp = xenon; lamp power = 300 W	Sampath et al. (2016)
Methylene blue	Photoelectrocatalysis in the presence of TiO ₂ -decorated CuCr ₂ O ₄ (CCO) nanocomposite	97.28	Concentration $C_{0[MB]}$ = 10 mg/l; CCO dosage = 400 mg; adsorption time = 30 min; effective area of photoelectrode = 0.12 cm ² ; catalyst dosage ≈ 833 mg/l; H ₂ O ₂ dosage = 4 mM; the bias potential (vs. SCE) = +0.71 V; process time = 15 min; T = room temperature; type of lamp = LED; lamp power = 50 W	Ghorai et al. (2021)
Methylene blue	Photoelectrocatalysis in the presence of Cu ₂ O photocathode in conjunction with a WO ₃ /BiVO ₄	97	Concentration $C_{0[MB]}$ = 5 mg/l; the bias potential (vs. SCE) = +0.4 V; process time = 180 min; type of lamp = tungsten; lamp power = 60 W	Thongthep et al. (2021)
Methylene blue	Photoelectrocatalysis in the presence of CdMoO ₄ /g-C ₃ N ₄ nanocomposite (CMO/CN)	95	CMO:CN ratio = 10 wt%; concentration $C_{0[MB]}$ = 10 mg/l; adsorption time = 30 min; effective area of photoelectrode = 0.071 cm ² ; process time = 150 min; type of lamp = xenon; lamp power = 35 W	Gandamalla et al. (2021)
Methylene blue	Photoelectrocatalysis in the presence of FTO/WO ₃ /BiVO ₄	94	Concentration $C_{0[MB]}$ = 5 mg/l; the bias potential (vs. SCE) = +2 V; process time = 180 min; type of lamp = ND; lamp power = 20 W	Nareejun and Ponchio (2020)
Methylene blue	Photoelectrocatalysis in the presence of In ₂ O ₃ -ZnO nanocomposites	95	In:Zn ratio = 0.05:1 (5%); concentration $C_{0[MB]}$ = 20 mg/l; adsorption time = 60 min; effective area of photoelectrode = 4 cm ² ; the bias potential (vs. SCE) = +0.2 V; process time = 60 min; type of lamp = xenon; lamp power = ND	Zhao et al. (2019)
Diclofenac	Photocatalysis in the presence of tungsten trioxide-doped TiO ₂ (TiO ₂ -WO ₃)	91	Concentration $C_{0[DCF]}$ = 25 mg/l; pH = 5; catalyst dosage = 600 mg/l; adsorption time = 30 min; process time = 240 min; type of lamp = metal halide; lamp power = 400 W	Mugunthan et al. (2018)
Diclofenac	Photocatalysis in the presence of vanadium oxide/boron-co-doped graphitic carbon nitride (V ₂ O ₅ -BCN)	80–100	Concentration $C_{0[DCF]}$ = 5–50 mg/l; pH = 5–9; catalyst dosage = 500–2000 mg/l; process time = 120 min; type of lamp = monochromatic blue; lamp power = 8 W	Oliveros et al. (2021)

Table 2 (continued)

CEC	Process	Removal efficiency (%)	Details	References
Diclofenac	Photocatalysis in the presence of bismuth oxychloride/graphene oxide (BiOCl-GO) composite	95	Concentration $C_{0[DCF]}$ = 5 mg/l; pH = 6; catalyst dosage = 1000 mg/l; process time = 120 min; type of lamp = mercury; lamp power = 96 W (12 × 8 W)	Rashid et al. (2020)
Diclofenac	Photocatalysis in the presence of tungsten trioxide-doped ZnO (ZnO-WO ₃)	90	Concentration $C_{0[DCF]}$ = 15 mg/l; pH = 6; catalyst dosage = 800 mg/l; adsorption time = 30 min; process time = 270 min; type of lamp = metal halide; lamp power = 400 W	Mugunthan et al. (2019)
Diclofenac	Photocatalysis in the presence of Ti-doped BiOI microspheres (TB450)	99.2	Concentration $C_{0[DCF]}$ = 10 mg/l; pH = 5; catalyst dosage = 250 mg/l; process time = 90 min; type of lamp = ND; lamp power = ND	Liu et al. (2019)
Diclofenac	Photocatalysis in the presence of cobalt(II) and cobalt(III) oxide and tungsten(VI) oxide composites (Co ₃ O ₄ /WO ₃)	98.7	Concentration $C_{0[DCF]}$ = 10 mg/l; pH = 6.8; catalyst dosage = 30 mg/l; adsorption time = 30 min; process time = 180 min; type of lamp = mercury; lamp power = 80 W	Malefane, Feleni, & Kuvarega (2019)
Diclofenac	Photocatalysis in the presence of CQD-modified BiOOH photocatalysts (CQDs/BiOOH)	100	Concentration $C_{0[DCF]}$ = 4 mg/l; pH = 7; catalyst dosage = 600 mg/l; process time = 60 min; type of lamp = xenon; lamp power = 350 W	Chen et al. (2018)
Diclofenac	Photoelectrocatalysis in the presence of persulfate activated by Cu cathode	86.3	Concentration $C_{0[DCF]}$ = 10 mg/l; pH = 5.62; catalyst dosage = 10 mM; the bias potential (vs. SCE) = +1.5 V; process time = 120 min; type of lamp = xenon; lamp power = 300 W	Liu et al. (2017b)
Diclofenac	Degradation by peroxydisulfate activated by Co ₃ O ₄ -modified g-C ₃ N ₄ (Co ₃ O ₄ -g-C ₃ N ₄)	100	Concentration $C_{0[DCF]}$ = 10 mg/l; pH = 6.7; catalyst dosage = 500 mg/l; process time = 30 min; type of lamp = xenon; lamp power = 50 W	Shao et al. (2017)
Diclofenac	Degradation by PMS activated by BiFeO ₃ microspheres (BFO)	82	Concentration $C_{0[DCF]}$ = 0.025 mM; pH = 7; PMS dosage = 0.5 mM; BFO dosage = 500 mg/l; adsorption time = 60 min; process time = 60 min; type of lamp = LED; lamp power = ND	Han et al. (2020b)
Diclofenac	Visible light-driven photoelectrocatalytic degradation by N, S-TiO ₂ /TiO ₂ NT photoelectrode	73.3	Concentration $C_{0[DCF]}$ = 5 mg/l; adsorption time = 120 min; effective area of photoelectrode = 4 cm ² ; the bias potential (vs. SCE) = +0.4 V; process time = 720 min; type of lamp = xenon; lamp power = 35 W	Cheng et al. (2015)

Table 2 (continued)

CEC	Process	Removal efficiency (%)	Details	References
Diclofenac	Photoelectrocatalytic degradation at g-C ₃ N ₄ /BiVO ₄ composite	32	Concentration C _{0(DCF)} = 10 mg/l; effective area of photoelectrode = 6 cm ² ; the bias potential (vs. SCE) = + 1 V; pH = 6.52; process time = 180 min; type of lamp = xenon; lamp power = 300 W	Sun et al. (2018)
	H ₂ O ₂ -assisted photoelectrocatalytic degradation at g-C ₃ N ₄ /BiVO ₄ composite	93.4	Concentration C _{0(DCF)} = 10 mg/l; effective area of photoelectrode = 6 cm ² ; the bias potential (vs. SCE) = + 1 V; pH = 3.17; process time = 180 min; type of lamp = xenon; lamp power = 300 W; H ₂ O ₂ dosage = 10 mM	

corresponds to the formation of redox potential on the surface of the photocatalyst molecule. Titanium dioxide can be activated with light energy with a wavelength of $\lambda < 400$ nm. This is only a fraction of sunlight (<5%), so it is necessary to provide expensive lamps that emit ultraviolet radiation in the range $\lambda = 300\text{--}388$ nm. Among the main disadvantages of the process of photocatalytic oxidation of contaminants, the following can be mentioned: the decomposition time of contaminants, the use of energy-consuming UV lamps, the presence of substances (salts) that reduce the efficiency of contaminant removal, the nanoparticle nature of TiO₂, and therefore, the problematic isolation from aqueous solutions, as well as the pH dependence of photodegradation process (Ameta et al., 2018; Xing et al., 2016; Zhang et al., 2018).

For the practical application of heterogeneous processes involving semiconductors, it is vital to increase the efficiency of the photocatalysis process in visible light and to immobilize titanium dioxide nanoparticles on larger surfaces. Therefore, many works are devoted to TiO₂ modification. Currently, green photocatalysts capable of absorbing radiation in the visible light range ($\lambda > 400$ nm) are of great interest. Over the last years, authors of many works have attempted to produce photocatalysts active in visible light or develop methods and/or materials for semiconductor modification. This issue has been extensively discussed in the works of Parnicka et al. (2017), Liao et al. (2018), D'Amato et al. (2018), Farhadian et al. (2019), Qi et al. (2019), and Zawadzki (2020). In brief, various types of metal or non-metal dopants (e.g., carbon, silver, gold, neodymium), activated carbon (granular or powdered), graphene oxide or carbon nanotubes or biopolymers (e.g., chitosan), and organic acids (e.g., ascorbic acid, succinic acid, pyruvic acid) are used to modify semiconductors.

The modifications are changing the structure of photocatalysts, which increases the photostability of semiconductors, and thus, their activity in visible light and better adsorption properties are observed. The adsorption of the micropollutants on the catalyst surface is the key to successful photocatalysis. Due to the nanoparticle nature of titanium dioxide and its difficult isolation from water, it has been found beneficial to modify the TiO₂ by high porous carbon. The dopants make it possible to broaden the absorption of visible light by introducing additional energy states,

inhibiting the transformation of anatase to rutile, and intensifying the conductivity of the catalysts (Fig. 3).

CFVP removal processes during visible light-driven photocatalysis have not been carried out by many studies. The use of modified titanium(IV) oxide to degrade CFVP has been studied by Zawadzki (2020). Approximately 85% degradation of CFVP (initial concentration $C_{0[\text{CFVP}]} = 1 \text{ mg/l}$) in the presence of TiO_2 modified with pyruvic acid in a 90:10 ratio (TiO_2 :pyruvic acid (PA), 90:10) was achieved. The decomposition of chlorfenvinphos was most effective under the following conditions: catalyst dose = 50 mg/l, adsorption time = 20 min, photocatalysis time = 60 min, and pH of standard solution = 3. The visible light source was a 10-W tungsten lamp. The modified titanium(IV) oxide showed activity in visible light with activation energy (E_g) = 1.5 eV. The study showed that the visible light-activated TiO_2 :PA (90:10) can be used several times in the photocatalytic process. After 5 cycles, the decomposition of CFVP decreased by 12% in the presence of modified TiO_2 . Based on the study, it can be concluded that modification of TiO_2 with organic acids can reduce the recombination of hole-electron pairs (acids are electron acceptors), similarly stated by Li Puma et al. (2008).

Residual organic pollutants may be adsorbed on the catalyst surface, successively reducing the number of active sites of the catalysts, resulting in lower catalyst performance. Modification of TiO_2 with tungsten(VI) oxide (WO_3) maintained a high degradation efficiency (c.a. 80%) of diclofenac in 4 reaction cycles (Mugunthan et al., 2018). The TiO_2 - WO_3

catalyst activated under visible light allowed to obtain 91% degradation of DCF within 4 h. Some phenomena such as the recombination of hole-electron pairs, blocking of TiO_2 active sites, or generation of reaction by-products can be reduced or eliminated due to the catalyst modifications.

Ahmed et al. (2021) reported that the advanced oxidation process can be affected by interfering ions. Such ions include, for example, Cl^- , NO_2^- , NO_3^- , PO_4^{3-} , HCO_3^- , or CO_3^{2-} . Ions can inhibit the degradation process by scavenging free radicals, affecting radiation absorption, or reacting with oxidative radicals to form less reactive forms (Farner Budarz et al., 2017). The influence of interfering ions is important in AOP, also during DCF degradation, so Oliveros et al. (2021) investigated the effect of chlorides, nitrates, sulfates, and phosphates on the photocatalytic degradation of diclofenac in the presence of vanadium pentoxide (V_2O_5)-boron-doped graphitic carbon nitride (BCN) catalyst. The V_2O_5 -BCN catalyst was prepared by combining V_2O_5 with BCN. High concentrations of anionic compounds decrease the reaction kinetics. When the concentration of negatively charged electrolytes is increased, the efficiency of DCF degradation decreases. This phenomenon is related to the competition of anionic compounds for catalytic sites and/or their reaction with oxidative radicals. A similar phenomenon was observed by Rehman et al. (2021).

In general, DCF removal efficiency depends on the following parameters: initial DCF concentration, pH of the solution, temperature, catalyst dosage, and catalyst type.

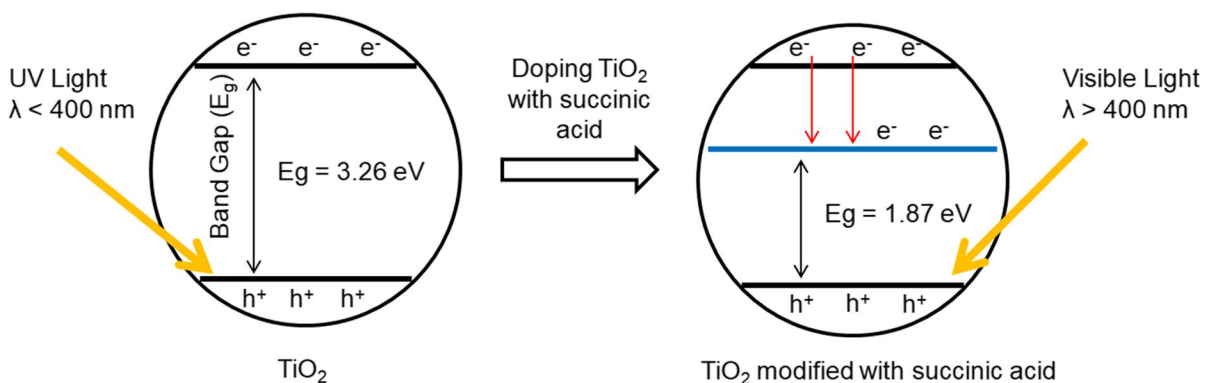


Fig. 3 Charge transfer process in TiO_2 modified with succinic acid under the irradiation of ultraviolet (UV) light and visible (Vis) light

Mainly xenon, mercury, halogen, or monochromatic blue lamps ranging from a few W to 400 W are used for DCF degradation (Chen et al., 2018; Mugunthan et al., 2019; Oliveros et al., 2021; Shao et al., 2017). The time required to reach adsorption equilibrium is usually provided before photocatalysis. This time ranges from 20 to 30 min. To obtain a DCF removal above 90%, typically 30 to 270 min is needed, depending on the photocatalysis configuration.

In the process studied by Oliveros et al. (2021), the removal efficiency of diclofenac ranged from about 80% to almost 100% after 120 min of reaction. The removal rate of DCF increased with increasing catalyst dose and pH, while it decreased with increasing initial pharmaceutical concentration. Similar results were obtained by Rashid et al. (2020).

An important parameter determining the oxidation reactions occurring on the surface of photocatalysts is the pH of the solution. This parameter is related to the value of the semiconductor isoelectric point (pH_{pzc}), corresponding to the pH value for which the total charge of the photocatalyst particle is zero. For TiO_2 particles, the pH_{pzc} ranges from 6.0 to 6.5 (Kosmulski, 2011). With the change in pH, the solubility of the substance also changes. The dissociation constant of diclofenac ($\text{p}K_{\text{a}} \approx 4$) determines its solubility: below $\text{p}K_{\text{a}}$, diclofenac is insoluble, and above $\text{p}K_{\text{a}}$, the DCF is negatively charged. Changing the pH also alters the electrical charge of the substances removed, resulting in a change in their ability to adsorb on the catalyst surface and the efficiency of photodegradation. Modifications of TiO_2 can positively influence the decomposition of contaminants. For example, the amphoteric properties of titanium(IV) oxide can be changed, which can increase the potential to catalyze the degradation of negatively charged contaminants. In the work of Oliveros et al. (2021), the DCF degradation efficiency decreased with decreasing pH. Complete removal of DCF was achieved within 100 min at $\text{pH} > 7$, while at pH 6 and 5, the removal rates were 96.4% and 84.2%, respectively. This is slightly different for other AOPs, where, for example, an increase in pH causes a decrease in reaction efficiency, e.g., the UV/peroxymonosulfate (PMS)/ Fe^{2+} process (Rehman et al., 2021). This can be explained mainly by the effect of the catalyst used and, at the same time, justifies the need to select the optimum catalyst depending on the reaction conditions for DCF removal.

Mugunthan et al. (2019) investigated the effect of different pH values on the DCF degradation efficiency in a process catalyzed by ZnO-WO_3 composite (zinc oxide doped with tungsten precursor). The visible radiation source was a 400-W halogen lamp. With an initial concentration of $C_{0[\text{DCF}]} = 20 \text{ mg/l}$ and a ZnO-WO_3 dose = 800 mg/l, the highest removal of DCF (about 75%) was achieved at neutral $\text{pH} = 6$. This was due to the surface charge properties of ZnO-WO_3 ($\text{pH}_{\text{pzc}} = 7.35 \pm 0.2$), so the catalyst surface was positively charged, and diclofenac should be negatively charged.

The methylene blue removal in the advanced oxidation processes continues to attract considerable interest. In the Scholar database (Google Scholar Database, 2022), between 2019 and 2021, the total number of articles containing the phrase “advanced oxidation of methylene blue” was 67,700 (in 2019, 19,000; in 2020, 20,700; in 2021, 28,000).

In general, the efficiency of MB removal in photocatalytic processes is determined by the following parameters: initial concentration, pH of the solution, temperature, dose, and type of catalyst.

Before irradiation, the contaminants should be adsorbed on the surface of the photocatalyst to achieve adsorption–desorption equilibrium. Greater adsorption on the catalyst reaction site leads to increased MB degradation. Before MB photodegradation, the adsorption time (conducted in the dark) is usually from 30 min (El-Katori et al., 2020; Lee et al., 2019), but depending on the catalyst used, this time can be 60 min (Ziarati Saravani et al., 2019) or even 120 min (Nuengmatcha et al., 2019). In the photocatalytic process involving $\text{TiO}_2/\text{NiFe}_2/\text{reduced}$ graphene oxide, approximately 55% MB adsorption was achieved after 60 min (Ziarati Saravani et al., 2019). In comparison, for pure TiO_2 , the adsorption efficiency was set to 38%. In contrast, by using a nanostructured Fe/FeS catalyst, Cabir et al. (2017) obtained about 18% adsorption of methylene blue after 30 min.

Most MB degradation work uses xenon, LED, halogen, mercury, and tungsten lamps ranging from a few W to 500 W. However, high-power lamps dominate ($> 100 \text{ W}$) (Esmaili et al. 2018; Mahanthappa et al., 2019). Higher lamp power results in higher MB removal rates. For example, Nuengmatcha et al. (2019) studied the effect of visible light irradiation at different intensities (0–130 W). With an initial

MB concentration $C_{0[\text{MB}]}=20$ mg/l and a catalyst dose = 100 mg/l, a 25% removal rate was obtained for 40 W, 40% for 60 W, and 60% for 100 W. Increasing the irradiation intensity above 100 W had no significant effect on increasing the removal rate of DCF (62%). The increase in the removal rate of DCFs with increasing radiation intensity was due to an increase in the intensity of oxidative radical production, which was also confirmed by Liu et al. (2019).

The initial pH of the solution has a significant influence on the efficiency of MB photodegradation in visible light-driven processes, as it affects the interaction between the adsorbent (catalyst) and the adsorbate (MB). In a conventional process using pure titanium(IV) oxide, the value of pH_{pzc} is approx. 6.0–6.5. Kaur et al. (2018) achieved the highest degree of adsorption of MB on TiO_2 at $\text{pH}=11$ (from about 41% to about 82% depending on the sample), while at $\text{pH}\leq 6$, the amount of adsorption was the lowest, ranging from about 1% to about 6%. The MB molecule is positively charged, so high pH ($>\text{pH}_{\text{pzc}}$) favors adsorption on the catalyst surface as it is then negatively charged. Similar observations were noted by Esmaili et al. (2018). The authors investigated the effect of pH on the removal rate of MB using Fe/FeS nanopowder as the catalyst. The highest removal rate (96%) was obtained at $\text{pH}=11$. Lowering the pH resulted in a severe efficiency drop to 78% at $\text{pH}=9$ and 25% at $\text{pH}=4$.

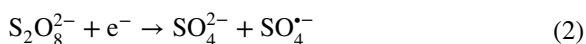
Typically, achieving a minimum removal rate of 90% required photocatalytic time ranging from 10 to 200 min, with an average time of 120–180 min. For example, Lee et al. (2019) needed 180 min to achieve a 97% removal rate of MB using a bimetallic Au/Pd nanocomposite catalyst supported by ZnO. In contrast, Selvaraj et al. (2019) required 90 min to achieve 93% dye removal. The shorter process time was probably due to the lower initial MB concentration (10 mg/l) and higher catalyst dose (360 mg/l). Increasing the photocatalyst dose may improve the MB removal efficiency (Mahanthappa et al., 2019). An increase in photodegradation efficiency was observed in the process using a CuS-CdS catalyst at concentrations ranging from 40 to 240 mg/l. The removal rate of MB ranged from 40% to nearly 100%, while the highest removal rate was found at a dose of 200 mg/l (nearly 100%). Higher catalyst doses probably cause aggregation of nanoparticles and their faster sedimentation. The so-called radiation shielding effect of excessive particles may also occur

(Rauf & Ashraf, 2009). The photodegradation efficiency also decreases with increasing dye concentration. Bagherzadeh et al. (2018) investigated the effect of MB concentration on its photocatalytic degradation efficiency. An increase in DCF concentration from 10 to 20 mg/l resulted in decreased process efficiency from 92 to 73%. This phenomenon is characteristic of AOPs (Liu et al., 2018; Zotesso et al., 2017). With increasing concentration, the consumption of oxidative radicals is higher, and the probability of collision of oxidative radicals with dye molecules decreases (Zawadzki, 2021a).

2.2 Visible Light Activation of Persulfate

In a sulfate radical oxidation process, a radical precursor (e.g., sodium persulfate $\text{Na}_2\text{S}_2\text{O}_8$) requires activation. Persulfate without activation can only react with some organic compounds, and the efficiency of the process is significantly lower compared to that of activated persulfates. Without activation, the persulfate anion has an oxidizing potential about 33% lower than that of the sulfate radical (Karim et al., 2021; Zhu et al., 2019). While activation can be achieved by thermal, photolytic, sonolytic, and radiolytic actions (Criquet, Karpel & Leitner 2011; Chen & Su, 2012; Zhang et al., 2015; Ji et al., 2016; Ahmadi et al., 2019), the most used activation method is the application of low-oxidation transition metal ions such as Fe^{2+} , Ni^{2+} , Co^{2+} , and Ag^+ . Current publications also include laboratory experiments on developing new activation methods for persulfate. These techniques include activation at high pH (>11), electrolysis, the use of carbon nanotubes or polymers (polyimides), and ozone (Ding et al., 2020; Fernandes et al., 2021; Ren et al., 2019; Zou et al., 2021). Some of the selected persulfate activation methods are graphically shown in Fig. 4.

In persulfate (PS) activation processes, the energy transferred to the persulfate anion by UV light, ultrasound, or heat results in the cleavage of the peroxide bond and the formation of two sulfate radicals (Eq. (1)). The persulfate can also react with an electron donor from the transition metal to form a single sulfate radical (Eq. (2)) (Karim et al. 2020).



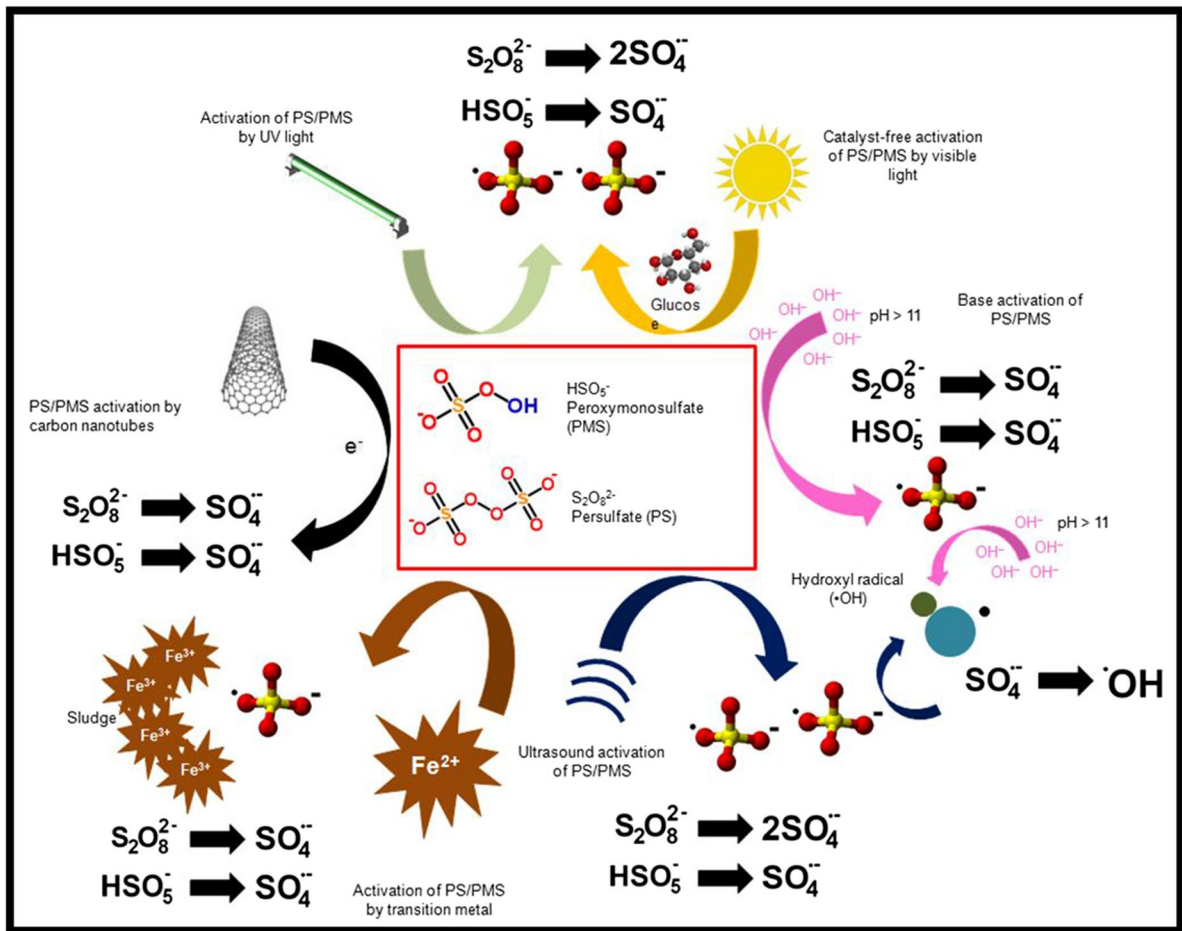


Fig. 4 Selected methods of persulfate activation

An alternative method for visible light activation of persulfates has also received increasing attention in recent years. Alternative activation methods should be as effective and cost-efficient as conventional methods. Materials for visible light activation of persulfates can be acids (e.g., ascorbic acid) and sugars (e.g., glucose, sucrose) (Hou et al., 2020b; Watts et al., 2018; Zawadzki, 2019). Degradation of micropollutants in the presence of persulfate and visible light is also achieved in processes involving catalysts, e.g., TiO₂ (Du et al., 2020), or combined methods, e.g., ultrasound and visible light-activated sodium persulfate (Zawadzki, 2021a). Recently, a promising approach to activate persulfates is the innovative material perylene diimide (PDI). PDI has excellent charge separation efficiency. Electron injection from PDI into PS can more efficiently

produce active forms of oxidative radicals (Ji et al., 2021).

The generation of sulfate radicals was carried out in the presence of sodium persulfate (Na₂S₂O₈), glucose, and visible light (an innovative activation method) in the research by Zawadzki (2021a). Glucose was essential to activate Na₂S₂O₈ in visible light. Literature data indicate that the activation mechanism by glucose is similar to that by phenoxides (Ahmad et al., 2013; Watts et al., 2018). Glucose is an optically active substance (Ashenhurst 2022). An electron from glucose is transferred to persulfate and activates it; in turn, glucose is oxidized to products that can activate persulfate. Some functional groups, such as the carbonyl group, accept a negative charge, activating persulfate at near-neutral pH. Zawadzki (2021b) performed a study on the advanced oxidation of

chlorfenvinphos from real treated municipal wastewater as stage IV of municipal wastewater treatment. Under optimal conditions (pH=6; room temperature; $\text{Na}_2\text{S}_2\text{O}_8$ dose = 20 mM; glucose dose = 100 mM; process time = 20 min), an 81% removal rate of CFVP was achieved. Irradiation of the solutions with visible light caused the glucose decomposition, electron transfer from sugar towards $\text{Na}_2\text{S}_2\text{O}_8$ (activation), and oxidation of glucose to sodium persulfate activation products.

Besides the CFVP removal, studies show that diclofenac can be effectively removed during reactions in the presence of sulfate radicals generated in the presence of visible light. In AOPs, an important parameter is the pH of the solution, which affects the performance of oxidants and catalysts and the degradation degree of pollutants. Shao et al. (2017) investigated the effect of initial solution pH on DCF degradation during peroxymonosulfate activation by g- C_3N_4 -modified Co_3O_4 nanoparticles (Co_3O_4 -g- C_3N_4). It was observed that the first-order kinetic constant (k) decreases with increasing pH, which also affected the final removal rate of DCF. For example, in a strongly alkaline medium (pH = 11), a 75% removal rate of DCF was achieved. In contrast, in a strongly acidic environment (pH = 3), nearly 100% removal rate of DCF was achieved. As explained by Ao et al. (2018) and Xia et al. (2020), under pH < 7, the predominant radicals are $\text{SO}_4^{\bullet-}$, whereas above pH > 7, sulfate radicals are converted to $^{\bullet}\text{OH}$ radicals by reacting with O_2^- . At pH = 11, Urán-Duque et al. (2021) observed a significant inhibition of the degradation process. Han et al. (2020a) also used BiFeO₃ microsphere-activated (BFO) PMS to degrade diclofenac. Bismuth ferrite (BiFeO₃, BFO) is a heterogeneous catalyst used in the work of Hussain et al. (2018) and Ouyang et al. (2020), among others, due to its multiferroic properties and high chemical stability, i.e., resistance to strong acids and bases. The authors of this study achieved an approximately 82% removal rate of DCF using a BFO dose of 500 mg/l, a PMS dose of 0.5 mM, and a processing time of 60 min. The source of Vis radiation was a led lamp. The operational parameters for the removal of diclofenac in the BFO/PMS process such as process time, pH, BFO dose, and PMS dose were also determined. Firstly, the efficiency of DCF elimination is affected by the reaction time,

i.e., the longer the reaction time, the higher the removal degree (about 60% after 20 min of reaction and 80% after 60 min of reaction under the following conditions: DCF concentration = 0.025 mM, BiFeO₃ dose = 300 mg/l, and PMS dose = 0.5 mM). The highest degree of DCF removal was obtained after 60 min. Afterwards, the pH value of which was indicated as optimal at pH = 3. However, iron leaching was observed at pH = 3, which did not occur at higher pH. At pH = 3, the highest degree of pharmaceutical removal was obtained (approx. 80%) under the following conditions: DCF concentration = 0.025 mM, BiFeO₃ dose = 300 mg/l, and PMS dose = 0.5 mM. The reduction in sulfate radical generation may also have been due to an increase in the mutual repulsion between BFO and PMS. The authors observed a significant increase in efficiency between the BFO dose of 400 mg/l and 500 mg/l (from about 65% to about 82%), whereas an increase in dose to 600 mg/l resulted in virtually no increase in removal efficiency. Also for the PMS, generally an increase in dose resulted in an increase in DCF removal with the optimum value at 0.5 mM PMS.

Many studies on MB degradation by PS or PMS in the presence of visible light primarily focus on the activation of PS or PMS with solid catalysts (e.g., TiO₂, ZnO, carbon nanotubes, or other modified photocatalysts) and then the role of visible light. However, there are few studies on the oxidation of MB by sulfate radicals without the introduction of solid catalysts (e.g., sugars, acids, and other electron sources). As presented in the literature (El-Sheshtawy et al., 2020; Habib et al., 2021; Sun et al., 2020), the degradation of methylene blue is determined by the following operational parameters; among others are as follows: initial MB concentration, process time, catalyst dose (PMS/PS), pH, lamp type, and power.

Zawadzki (2019) determined the operational parameters for MB removal in the visible light oxidation process with sodium persulfate ($\text{Na}_2\text{S}_2\text{O}_8$) activated by glucose and sucrose, such as reaction time, pH, glucose/sucrose dose, and $\text{Na}_2\text{S}_2\text{O}_8$ dose. The highest degree of MB degradation (84%) was observed in the presence of sodium persulfate (6.5 mM) after 90 min of visible light irradiation for the process carried out in the presence of glucose (100 mM) at pH = 12. It was determined that the radicals responsible for the decolorization

of methylene blue were $\text{SO}_4^{\bullet-}$, $\bullet\text{OH}$, and $\text{O}_2^{\bullet-}$. At $\text{pH}=12$, hydroxyl radicals were mainly responsible for the degradation of methylene blue. The results were similar to those obtained by Watts et al. (2018).

For reactions carried out in the presence of sulfate radicals, xenon, LED and tungsten lamps are used, similar to photocatalytic processes. However, a significant difference in the lamp power used has been observed. Namely, lower-wattage lamps (up to 50 W) are used for MB removal processes in the presence of persulfates/peroxymonosulfates and catalysts, which may probably be due to the applied synergistic effect in these processes between catalysts and PMS/PS. The combination of photocatalysis and PMS activation promotes charge separation in the photocatalytic system as an electron capturing agent and improves light utilization in the photocatalyst (Hu et al., 2019).

The combination of photocatalysis and PMS activation also extends the pH range in which the process can still be carried out efficiently. For example, Tang (2020) obtained a BiVO_4 catalyst to activate PMS. First, a 99% removal rate of MB was achieved after 90 min of reaction (conditions as in Table 2). Then, increasing the pH from 4 to 10, a similar degree of BM removal determined as 95–99% was obtained. At $\text{pH}=2$, the reaction efficiency decreased slightly to about 78%. The presented method may therefore be suitable for the treatment of colored effluents characterized by a wide pH range, as the efficiency of dye decomposition in each of the pH ranges examined was higher than 75%.

In general, the removal rate in all analyzed processes depended on the reaction time. The optimal process time is also an important parameter from an economic point of view (reactor volume, electricity costs, automation, electronics). Typically, a period of 60–90 min is needed to remove MB concentrations from 2 to 40 mg/l. To remove 100% MB with a concentration of 3.2 mg/l, Sabri et al. (2020) needed 90 min (for the conditions set in Table 2). The time required for the complete removal of MB can be reduced by increasing the dose of PS or PMS. For example, in the study by Rizal et al. (2021), nearly 100% MB degradation was achieved after 70 min (PS concentration = 2 mM; $\text{Ag}/\text{Mn}_3\text{O}_4/\text{graphene}$ catalyst = 500 mg/l). However, by increasing the dose to 4 mM, this time was reduced to 40 min, and at a dose of 12 mM to 30 min.

Han et al. (2020b) and Rizal et al. (2021) also investigated the effect of initial MB concentration on the dye removal rate. Both studies confirm that higher dye concentrations inhibit the radical reactions with dye molecules. Furthermore, a high concentration of molecules can lead to competition effects between dye molecules, reaction by-products, and generated radicals (Zawadzki, 2021a).

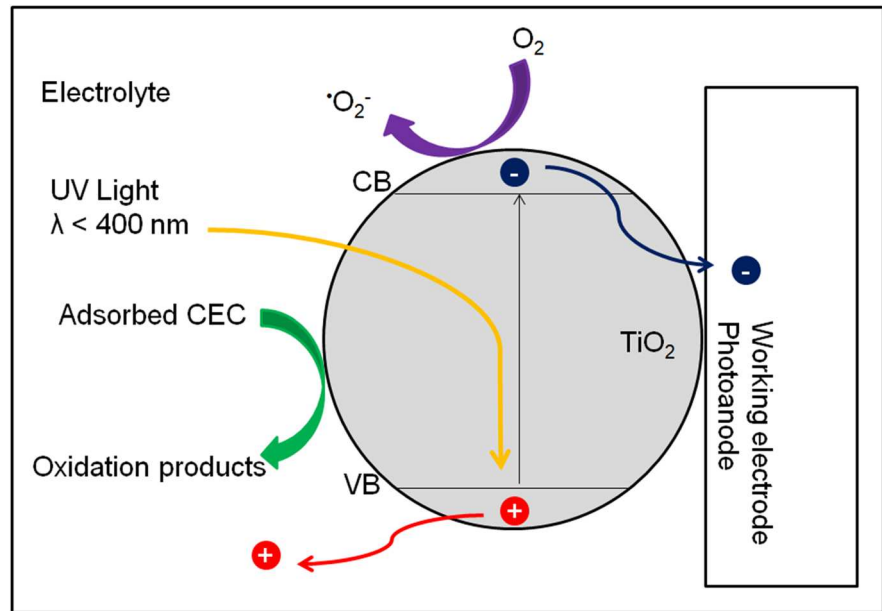
2.3 Visible Light–Driven Photoelectrocatalysis

Photoelectrocatalysis (PEC) is a combined process of photocatalysis and electrochemistry (Hou et al., 2020a; Xu et al., 2019). PEC primarily aims to suppress the negative recombination phenomenon of hole–electron pairs generated by photocatalysis.

In this method, a semiconductor is attached to the surface of a conductive substrate and used as a photoelectrode. Photogenerated holes on the surface of the semiconductor trigger oxidation reactions and electrons flow through the counter electrode where reduction reactions take place. Thus, charge recombination is minimized, and the quantum efficiency of the photocatalytic process is improved. Irradiation of an *n*-type semiconductor (e.g., TiO_2) with radiation of an energy higher than the activation energy results in the generation of charge carriers. Most of the research on photocatalysis is devoted to the removal of contaminants from a liquid medium in which the semiconductor is held in suspension. This way of using catalytic nanoparticles introduces the need to separate them from the liquid phase after the photodegradation process. This can be avoided by coating the conductive substrate with film-forming particles (immobilization). In the PEC process, the dissolved organic substances in the electrolyte are oxidized through the holes formed, and the electrons are transported to the conductive substrate (Fig. 5) (Bessegato et al., 2015).

PEC shows an advantage over photocatalysis because it applies a potential to the photoanode on which the catalyst is deposited. This configuration allows for more efficient separation of the charges (e^-/h^+) formed in the process, thereby increasing the lifetime of electron–hole pairs (Hou et al., 2020a, 2020b; Li et al., 2018; Su et al., 2016). Photoelectrocatalysis has been shown to efficiently degrade chlorfenvinphos (Fernández-Domene et al., 2019; Roselló-Márquez et al., 2021), diclofenac (Cheng et al., 2015; Liu et al., 2017b), and methylene blue (Rosa et al.,

Fig. 5 Mechanism of photoelectrocatalysis in the presence of *n*-type semiconductor (TiO_2). Own study based on the literature (Bessegato, Guaraldo & Zanoni 2014; Bessegato et al., 2015; Ge et al., 2016)



2020; Wu et al., 2019). Advances in electrochemistry and materials science (new materials active in visible light) have led to increased interest in using photoelectrochemical processes to eliminate CECs. Photoelectrocatalysis and visible light-driven photocatalysis have emerged as promising strategies for clean, low-cost, and environmentally friendly renewable energy production and removal of contaminants (Pan et al., 2020; Zhong et al., 2020).

In the work of Fernández-Domene et al. (2019) and Roselló-Márquez et al. (2021), the photoelectrochemical decomposition of chlorfenvinphos with tungsten trioxide (WO_3) nanotubes was investigated. Chlorfenvinphos solutions with an initial concentration of 20 ppm were treated with visible radiation, the source of which was a 1000-W xenon lamp. Innovative nanostructured electrodes produced by anodizing tungsten and annealed at 400 °C and 600 °C were added to the treated solutions. The process studied achieved a 95% removal rate of CFVP under the operating parameters shown in Table 2. A more than 65% reduction in total organic carbon was also achieved.

In a similar study, Roselló-Márquez et al. (2021) used a 500-W xenon lamp (visible light source). Under the room temperature and after 24 h of treatment, a 95% removal degree of CFVP was obtained. The analysis of reaction intermediates during photoelectrochemical oxidation of CFVP also showed interesting results. As reported by

Farré et al. (2005), detoxification of chlorfenvinphos is achieved when the TOC remaining in solution is below 10 mg/l. Otherwise, increased toxicity may be due to generated by-products. Depending on the process (e.g., photo-Fenton, radiolytic decomposition), the oxidation by-products may differ. In the literature, CFVP degradation by-products are reported to be, for example, 2-hydroxy-1-(2,4-dichlorophenyl)vinyl diethyl phosphate, 2,4-dichlorobenzoic acid, dicarboxylic acid, 2,4-dichlorophenol, triethyl phosphate, and 4-hydroxybenzoic acid (Klamerth et al., 2009; Bojanowska-Czajka et al., 2010; Roselló-Márquez et al., 2021). The by-products are therefore aromatic acids or esters, but also toxic products, e.g., 2,4-dichlorobenzoic acid or triethyl phosphate. Photoelectrocatalysis in the presence of WO_3 resulted in the generation of, among others, 2,4-dichlorobenzoic acid, triethyl phosphate, and ethyl dimethyl phosphate (Roselló-Márquez et al., 2021).

Similar efficiency was obtained during the removal of diclofenac in PEC. Liu et al. (2017b) used a photoelectrocatalytic purification system in the presence of PS. The photoelectrocatalytic system consisted of a *c*- Bi_2MoO_6 photoanode and a copper foil cathode. At an applied voltage of +1.5 V and an initial solution pH value of 5.62, the removal efficiency of DCF with an initial concentration of 10 mg/l was 86.3% with the addition of 10 mM PS.

In visible light photoelectrocatalysis, voltages between +0.4 and +2.0 V are generally used for CFVP degradation. In general, the degradation degree increases with increasing voltage, whereas the increase is not relatively high. For example, a study by Sun et al. (2018) found that the degradation efficiency of DCFs increases with increasing polarization potential. In a photoelectrochemical process involving a composite obtained by combining bismuth vanadate (BiVO_4) and graphitic carbon nitride ($\text{g-C}_3\text{N}_4$), a more than fourfold increase in DCF removal rate was obtained after 2 h of treatment when the polarization potential was increased from 0 to +1 V. The increase in polarization potential to +1.5 V increased the removal degree from 29.4 to 31.2%. Similar observations were also confirmed in a review paper by McMichael et al. (2021).

A significant increase in the efficiency of photoelectrocatalysis can be achieved by combining composite materials and other oxidants, such as hydrogen peroxide, as shown in the study of McMichael et al. (2021). The authors investigated the effect of hydrogen peroxide on the degradation efficiency of diclofenac in the presence of visible light. Ten millimolars of H_2O_2 was chosen as the optimal concentration, due to the increase in the removal rate of DCF to 62.3% after 180 min of reaction. A higher concentration of H_2O_2 (15 mM) resulted in a lower removal rate due to the probable reaction of excess H_2O_2 with the generated $\bullet\text{OH}$ radicals, thus inhibiting the degradation process. Similar conclusions were postulated by Ku et al. (2005) and Ziembowicz et al. (2017).

The idea behind photoelectrocatalytic processes is to generate highly reactive oxidative radicals. It can be thought that, mainly, hydroxyl radicals ($\bullet\text{OH}$) and, to a lesser extent, $\bullet\text{O}_2^-$, H_2O_2 and h^+ radicals are responsible for the decomposition mechanism in visible light-driven photoelectrocatalysis, as shown in Cheng et al. (2015).

In the last few years (2017–2021), there have been few studies on the elimination of MB by photoelectrocatalytic processes under visible light. The Scopus database contains 29 publications for 2017–2021 containing the keywords “photoelectrocatalytic degradation of methylene blue under visible light,” with the majority (10 articles) published in 2017.

The degradation of MB in a photoelectrocatalytic process is determined by the following process parameters, among others: voltage, effective

photoelectron area, pH, type of electrolyte, and its concentration.

Light-sensitive modified catalysts (e.g., CdS , TiO_2 , ZnO , WO_3 , BiVO_4) have been used for the degradation of MB in visible light photoelectrocatalytic processes. For example, Liu et al. (2017a) modified TiO_2 with NH_4F (source of F), yielding a visible light-active material; in the presence of which, the MB removal rate was 92% compared to pure TiO_2 at 50%. The absorption band towards visible light was shifted by also using F-doped tin oxide (FTO) and $\text{WO}_3/\text{BiVO}_4$ (Thongthep et al., 2021).

Sampath et al. (2016) investigated the photoelectrocatalytic activity of the $\text{ZnO}/\text{porous silicon}$ (PS) over the applied voltage from -6 to $+6$ V. The highest photoelectrocatalytic activity (c.a. 96% of MB removal at an initial concentration of 20 mg/l after 105 min) was obtained for a negative voltage (-6 V). This was explained, among others, by the efficient separation of charge carriers by driving the photogenerated holes through an external circuit to the counter electrode during negative voltage. Increasing the voltage to 0 V systematically decreased the degradation efficiency (up to 85% at 0 V), while further increasing the voltage increased the MB removal efficiency (up to 88% at $+6$ V). Different results were presented by Zhao et al. (2019), using an indium oxide (In_2O_3)-doped ZnO catalyst for MB removal ($C_{0[\text{MB}]} = 20$ mg/l, process time = 60 min). The photodegradation efficiency depended, among others, on the amount of In_2O_3 in ZnO and the applied voltage. For the optimal In:Zn ratio of 0.05:1 (photocurrent density = $264 \mu\text{A}/\text{cm}^2$) and the applied voltage of +0.2 V, a 95% removal rate of MB was achieved. At a lower voltage (+0.1 V), an efficiency of 86% was achieved, and at the highest voltage tested (+0.4 V), the lowest MB removal rate of 79% was observed. In general, positive voltages ranging from +0.2 to +6 V are used in studies on MB removal in photoelectrocatalytic processes in the presence of visible light.

The authors of most works use photoelectrodes with an effective area between 0.0071 and 50 cm^2 (Gandamalla et al., 2021; Liu et al., 2017a; Nareejun & Ponchio, 2020). Larger photoelectrode areas can drastically reduce the process efficiency due to the possible introduction of more defects in the photoanode (cathode) materials (Li & Li, 2017).

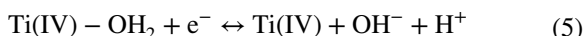
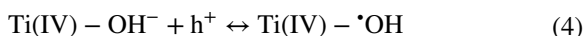
In a study by Liu et al. (2017a), the effect of solution pH on the removal rate of MB with a

concentration of 10 mg/l was tested (for conditions given in Table 2). An increase in the degradation rate of MB was observed from about 82% (at pH=3.14) to about 98% (at pH=9.94). It was shown that the MB degradation reaction occurred more efficiently at high pH due to a change in the isoelectric point (pH_{pzc}) value of the F-TiO₂ catalyst. The pH_{pzc} of the F-TiO₂ catalyst (F concentration = 15 wt%) was determined to be 6.72. Therefore, the catalyst surface at $\text{pH} > 6.72$ was negatively charged, which favored the adsorption and photodegradation of the positively charged MB molecule.

Gandamalla et al. (2021) performed an interesting study on the effect of temperature on the photoelectrocatalytic decomposition of methylene blue. Namely, an increasing temperature increased the removal rate of MB. For example, at 30 °C, the dye removal rate was 97.3%, while at 50 °C, the degradation rate was 99.09%. The authors attributed the increase in photodegradation efficiency to increased collisions between molecules at higher temperatures and more MB molecules adsorbed on the catalyst surface.

3 Overview of Visible Light-Driven AOP Mechanism and Degradation

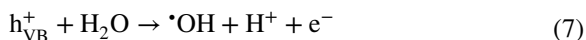
AOPs typically have complex reaction mechanisms, and more than 150 steps have been developed to describe them (Stanbury, 2020). It is also believed that the chemical mechanisms of oxidation in these systems involve multiple radical reactions (Wang et al., 2020; Ghime and Gosh 2020). The general mechanism of the photocatalysis process includes the following processes (Eqs. (3)–(5)):



When the catalyst absorbs the radiation, active transition complexes are generated on the surface of the semiconductor, resulting in the generation of $\bullet\text{OH}$ radicals, which strongly oxidize organic chemicals. The photogenerated electrons can react with H₂ and O₂ dissolved in water to form H₂O₂, which can be

photodecomposed into $\bullet\text{OH}$ radicals (Girón-Navarro et al., 2021). For the practical application of photocatalytic processes, it is important to increase the efficiency of the photocatalysis process in visible light, eliminate the agglomeration of semiconductor particles, reduce the phenomenon of blocking active sites, and increase the efficiency of separation of catalyst particles from the reaction mixture after the treatment process. Therefore, numerous semiconductor modifications are currently used to facilitate the absorption of visible light and simultaneously overcome the difficulties occurring in conventional photocatalysis (Pirhashemi et al., 2018; Wangab et al., 2016; Zawadzki et al., 2021).

As previously mentioned, photoelectrocatalysis combines photocatalytic and electrochemical oxidation processes. When light photons ($h\nu$) with an energy higher than the activation energy (E_g) reach the surface of a semiconductor (S), which is deposited on a solid surface, charge carriers are generated (Eqs. (6)–(8)). The recombination of photogenerated electrons and holes occurring in the photocatalytic process is retarded by an applied bias potential (Alulema-Pullupaxi et al., 2021; Peleyeju & Arotiba, 2018).



As shown in Eqs. (1) and (2), sulfate radicals are generated by activation of the SO₄^{•−} precursor (peroxydisulfate (PDS)) through energy transfer to the persulfate anion or reaction with an electron donor from the transition metal. In general, the essence of generating the SO₄^{•−} radical is to break the O–O bond in PDS. The O–O bond distance in PDS is 1.497 Å and must be severed in order to generate the sulfate radical (Ghanbari & Moradi, 2017). Instead of using energy-consuming UV lamps or transition metal ions that generate additional costs, materials for PDS activation under visible light, such as organic promoters, are currently being developed (Hu et al., 2021; Zawadzki, 2022).

In general, in visible light-driven AOPs, the degradation mechanism of emerging contaminants is

Table 3 Degradation mechanism of selected target pollutants

Target pollutant	Process	A brief description of the degradation mechanism	References
Methylene blue	Peroxymonosulfate (PMS) activated by surface-tailored carbon quantum dots (CQDs)	In the presence of visible light, in the CQD/PMS system, the primary reactive species for MB oxidation are $O_2^{\bullet-}$ and h^+ generated during PMS activation and excited CQDs. Under visible light irradiation, photogenerated electrons can activate PMS to generate highly reactive $O_2^{\bullet-}$. CQDs can be excited by Vis radiation, resulting in the simultaneous generation of holes and electrons. The PMS molecule decays into a HO_2^{\bullet} radical and a sulfite ion. The HO_2^{\bullet} radical breaks into a proton and superoxide ion, causing MB to degrade. The presence of MB causes the absorption of oxidation holes and limits the recombination of hole-electron pairs and further promotes the photocatalytic activation of PMS. Alkaline environment may promote the generation of more reactive species in the CQD/PMS system	Han et al. (2020a)
Methylene blue	Degradation by sodium persulfate activated by glucose (PS/G/Vis)	Degradation mechanism caused by sulfate and hydroxyl radicals Glucose and sucrose are optically active substances; i.e., they tend to rotate the light plane and are active in visible light. The activation mechanism of persulfate may be due to the generation of Krebs cycle compounds during sucrose hydrolysis. When glucose is used, persulfate activation may result from the probable electron transfer from sugar towards PS. Higher degradation efficiency is observed while sucrose is used because sucrose is hydrolyzed into glucose	Zawadzki (2019)
Methylene blue	Persulfate oxidation in the presence of photoexcited dye	The main mechanism is the radical reaction caused by the reduction of PS by photogenerated electrons of the dye; the second mechanism is a non-radical reaction involving the transfer of electrons via the dye from the pollutant to the oxidized dye	Cai et al. (2019)

Table 3 (continued)

Target pollutant	Process	A brief description of the degradation mechanism	References
Methylene blue	Graphene-decorated titanium dioxide (TiO ₂) powders	Graphene in the composite (TiO ₂ /graphene) can reduce the transfer between photogenerated electrons formed when visible light reaches the surface of graphene and TiO ₂ . The photocatalytic activity of graphene-modified TiO ₂ is much higher than that of pure TiO ₂ , confirming that there is a synergistic effect of graphene and TiO ₂ . Crystallite growth due to nucleation and growth of seed crystals were observed which may contribute to the above effect. The mechanism of MB degradation may be due to the absorption of visible light by the graphene-TiO ₂ composite and to the generation of excited photoelectrons at the Fermi level, which will tunnel into the conduction band of TiO ₂ to overcome the Schottky barrier formed by the contact between graphene and TiO ₂ . The presence of these injected electrons will then interact with the dye to start its degradation	Acosta-Esparza et al. (2020)
Chlorfenvinphos	Photocatalysis in the presence of pyruvic acid (PA)-doped TiO ₂ (TiO ₂ /PA)	The photodegradation is mainly due to O ₂ ⁻ radicals, then h ⁺ and least OH ⁻ . In the model solution at pH = 3, due to the change in hydrophobic properties of TiO ₂ modified with organic acids, the mechanism involves the adsorption of CVFP on the catalyst surface, followed by cleavage of the aromatic ring by oxidizing radicals, mainly O ₂ ⁻	Zawadzki (2020)
Chlorfenvinphos	Visible light-driven photoelectrochemical degradation in the presence of WO ₃ nanorods	Degradation in the presence of WO ₃ nanotubes occurs by cleavage of the aromatic ring (π - π^*). The time evolution of the UV absorption spectra of CFVP took values greater than 0, which means that the degradation of CFVP probably takes place by opening the aromatic ring and then generating intermediate compounds Degradation by hydroxyl radicals or directly with photodegenerated holes on the WO ₃ surface in semiconductor/electrolyte solution Further analytical work is needed to propose the full mechanism of chlorfenvinphos degradation in the presence of WO ₃ nanotubes	Fernández-Domene et al. (2019) Roselló-Márquez et al. (2019)

Table 3 (continued)

Target pollutant	Process	A brief description of the degradation mechanism	References
Chlorfenvinphos	Photodegradation by using WO ₃ nanostructures	•OH radicals are used as the main oxidizing agent for the degradation of CFVP. The photodegradation pathway of CFVP involves decomposition to a phosphate group, opening of the aromatic ring, or decomposition of the CFVP molecule by binding to phosphorus, with the formation of compounds without chlorine atoms and with longer aliphatic chains. The charge transfer mechanism for photogenerated holes in WO ₃ nanostructures occurs through the valence band	Roselló-Márquez et al. (2021)
Diclofenac	Photocatalysis in the presence of tungsten trioxide-doped TiO ₂ (TiO ₂ -WO ₃)	The TiO ₂ -WO ₃ catalyst has a higher photodegradation efficiency compared to pure TiO ₂ , which confirms that the presence of WO ₃ increases the degradation efficiency of TiO ₂ in the modified catalysts, since the addition of WO ₃ decreases the value of the bandgap of the catalyst. The DCF degradation pathway mainly proceeds through dechlorination, decarboxylation, C–N cleavage, and hydroxylation reaction. The DCF photodegradation step involves ring opening of aromatic compounds, which are then mineralized	Mugunthan et al. (2019)
Diclofenac	Photocatalysis in the presence of CQD-modified BiOCCOOH photocatalysts (CQDs/BiOCCOOH)	The CQDs greatly improved the visible light absorption by BiOCCOOH, as well as interfacial charge transfer and separation. The CQDs/BiOCCOOH contained new groups, such as CeN, NeH, and CeN/CeO, which enhanced the electron transfer ability of the material. The removal mechanism of DCFs in the presence of CQDs/BiOCCOOH was not mainly related to adsorption due to the low surface area of the samples. It was found that •OH, O ₂ ^{•-} , h ⁺ , and e ⁻ radicals were mainly involved in the degradation of DCFs during the treatment process under visible light. The main degradation pathway was via e ⁻ reduction and O ₂ ^{•-} and •OH addition reactions. The O ₂ ^{•-} radical was the most important radical in the photocatalytic degradation mechanism of DCF	Chen et al. (2018)

Table 3 (continued)

Target pollutant	Process	A brief description of the degradation mechanism	References
Diclofenac	Degradation by PMS activated by BiFeO ₃ microspheres (BFO)	The mechanism of PMS activation by BFO involves a series of reactions where a complex is formed between Fe ³⁺ and HSO ₅ ⁻ . Fe ³⁺ represents a site on the BFO surface; electron transfer from HSO ₅ ⁻ to Fe ³⁺ and the formation of a triple-bond Fe ²⁺ and the SO ₅ ⁻ radical; then, the reactions that occur lead to the formation of the SO ₄ ⁻ radical. The SO ₄ ⁻ radical can also react with H ₂ O or OH ⁻ to form the *OH radical. Thus, DCF is degraded by both sulfate and hydroxyl radicals. Visible light irradiation provides an additional way of producing the hydroxyl and sulfate radicals and supports the Fe(III)-Fe(II)-Fe(III) redox cycle. Degradation of DCF may occur by decarboxylation, methyl oxidation, hydroxylation, benzene ring cleavage, C–N bond cleavage, and dechlorination (cleavage of the C–Cl bond by the SO ₄ ⁻)	Han et al. (2020b)

similar to the conventional process. An overview of the visible light–driven AOP degradation mechanism of selected target pollutants is presented in Table 3. Free radicals, such as hydroxyl or sulfate radicals, are responsible for degradation of pollutants. O₂⁻, h⁺, and OH⁻ radicals are also involved in photodegradation. Depending on the structure of the compound, degradation may involve a number of intermediate reactions, for example dechlorination, decarboxylation, C–N bond cleavage, and hydroxylation reaction. Finally, cleavage of the aromatic ring takes place. In dye degradation, *N*-deethylation, chromophore cleavage, and ring opening can take place, leading to a series of oxidation products with smaller molecular sizes (Diao et al., 2017; Lops et al., 2019). The degradation of azo bonds has been suggested as a possible mechanism for MB decolorization (Mahdavianpour et al., 2020).

4 Conclusions

The wide range of contaminants entering surface waters with wastewater makes the application of conventional wastewater treatment technologies insufficient. Among the compounds found in water streams, there are micropollutants and substances of both natural (products of the metabolism of organisms) and anthropogenic origin can be found. In the second group, there are mainly compounds such as pharmaceuticals, pesticides, dyes, disinfection by-products (DBP), and polycyclic aromatic hydrocarbons (PAHs). Micropollutants belong to a group of chemical substances posing a particular risk to human health and life. They are the cause of the following, inter alia: cancer, mutations, poisoning, endocrine system disorders, defects in fetal development, and damage or death of embryos. These compounds are present in the environment in concentrations ranging from ng/l to µg/l.

Analysis of research in recent years has shown an increased interest in modifications of advanced oxidation processes, including those driven by visible light. As presented in this work, advanced oxidation processes driven by visible light have great potential to remove organic contaminants from water and wastewater, including diclofenac, chlorfenvinphos, and methylene blue. Undoubtedly, research into this purification technique has made considerable

progress in recent years. Visible light–active catalysts, stable over a wide pH range and capable of simultaneous degradation of organic matter and, for example, hydrogen production, have been developed. Methods for the activation of persulfates with and without catalysts have been developed, and the visible light activity of persulfates in the presence of certain materials has been documented. A combination of AOPs, e.g., photocatalysis and electrochemistry, has also been developed to immobilize the catalyst on a solid substrate and use it as an electrode, and to reduce the negative recombination phenomenon of hole-electron pairs generated in the photocatalysis.

The following specific research recommendations are suggested for the next few years:

- Further study on the degradation of chlorfenvinphos from the water and wastewater (the lowest number of studies among the three CECs analyzed).
- More research into the influence of effective electrode surface area should be performed.
- More exploration of catalyst modifications to minimize defects in photoanode (cathode) materials and reduce energy consumption must be performed.
- Focus on the development of materials that ensure high stability and durability of catalysts and photoelectrodes.
- Achieving materials capable of activating persulfates or peroxymonosulfates without the use of a catalyst (catalyst-free persulfate activation).
- Perform more studies on the removal of mixtures of dyes, pesticides, and pharmaceutical substances.
- Enhance the toxicological study of advanced oxidized solutions (e.g., MicroTox® analysis *Aliivibrio fischeri* bacteria or toxicity analyses with aquatic plant, e.g., *Lemna minor*).

Acknowledgements The presented study was performed in the framework of the research work in the Central Mining Institute in Poland.

Author Contribution PZ was responsible for the entire manuscript.

Funding This study was financially supported by the Polish Ministry of Science and Higher Education (No. 11131041–340).

Data Availability The datasets used and/or analyzed during the current study are available from the corresponding author on reasonable request.

Code Availability Not applicable.

Declarations

Ethics Approval and Consent to Participate This article does not contain any studies with human participants or animals performed by the author. Consent to participate is not applicable.

Consent for Publication Not applicable.

Competing Interests The author declares no competing interests.

Open Access This article is licensed under a Creative Commons Attribution 4.0 International License, which permits use, sharing, adaptation, distribution and reproduction in any medium or format, as long as you give appropriate credit to the original author(s) and the source, provide a link to the Creative Commons licence, and indicate if changes were made. The images or other third party material in this article are included in the article's Creative Commons licence, unless indicated otherwise in a credit line to the material. If material is not included in the article's Creative Commons licence and your intended use is not permitted by statutory regulation or exceeds the permitted use, you will need to obtain permission directly from the copyright holder. To view a copy of this licence, visit <http://creativecommons.org/licenses/by/4.0/>.

References

- Chlorfenvinfos - Compound Summary (2022) PubChem compound summary for CID 5377791. National center for biotechnology information. Retrieved February 10, 2022, from <https://pubchem.ncbi.nlm.nih.gov/compound/5377791>
- Diclofenac – Compound Summary (2022) PubChem compound summary for CID 3033. National center for biotechnology information. Retrieved February 10, 2022, from <https://pubchem.ncbi.nlm.nih.gov/compound/3033>
- Methylene Blue – Compound Summary (2022) PubChem compound summary for CID 6099. National center for biotechnology information. Retrieved February 10, 2022, from <https://pubchem.ncbi.nlm.nih.gov/compound/Methylene-blue>

- Acosta-Esparza, M. A., Rivera, L. P., Pérez-Centeno, A., Zamudio-Ojeda, A., González, D. R., Chávez-Chávez, A., Santana-Aranda, M. A., Santos-Cruz, J., & Quiñones-Galván, J. G. (2020). UV and visible light photodegradation of methylene blue with graphene decorated titanium dioxide. *Mater Res Express*, 7(3), 035504. <https://doi.org/10.1088/2053-1591/ab7ac5>
- Ahmad, M., Teel, A. L., & Watts, R. J. (2013). Mechanism of persulfate activation by phenols. *Environmental Science and Technology*, 47, 5864–5871. <https://doi.org/10.1021/es400728c>
- Ahmadi, S., Igwegbe, C. A., & Rahdar, S. (2019). The application of thermally activated persulfate for degradation of Acid Blue 92 in aqueous solution. *International Journal of Industrial Chemistry*, 10, 249–260. <https://doi.org/10.1007/s40090-019-0188-1>
- Ahmed, N., Vione, D., Rivoira, L., Carena, L., Castiglioni, M., & Bruzzoniti, M. C. (2021). A review on the degradation of pollutants by Fenton-like systems based on zero-valent iron and persulfate: Effects of reduction potentials, pH, and anions occurring in waste waters. *Molecules*, 26, 4584. <https://doi.org/10.3390/molecules26154584>
- Aissaoui, S., Ouled-Haddar, H., Sifour, M., Beggah, C., & Benhamada, F. (2017). Biological removal of the mixed pharmaceuticals: Diclofenac, ibuprofen, and sulfamethoxazole using a bacterial consortium. *Iranian Journal Biotechnology*, 15, 135–142. <https://doi.org/10.15171/ijb.1530>
- Al Hakim, S., Jaber, S., Zein Eddine, N., Baalbaki, A., & Ghauch, A. (2019). Data for persulfate activation by UV light to degrade theophylline in a water effluent. *Data in Brief*, 27, 104614. <https://doi.org/10.1016/j.dib.2019.104614>
- Almaamary, E., Abdullah, S., Hasan, H., Rahim, R., & Idris, M. (2017). Treatment of methylene blue in wastewater using *Scirpus grossus*. *Malaysian Journal of Analytical Sciences*, 21, 182–187. <https://doi.org/10.17576/mjas-2017-2101-21>
- Alulema-Pullupaxi, P., Espinoza-Montero, P. J., Sigchallo, C., Vargas, R., Fernández, L., Peralta-Hernández, J. M., & Paz, J. L. (2021). Fundamentals and applications of photoelectrocatalysis as an efficient process to remove pollutants from water: A review. *Chemosphere*, 281, 130821. <https://doi.org/10.1016/j.chemosphere.2021.130821>
- Ameta, R., Solanki, M. S., Benjamin, S., & Ameta, S. C. (2018). Chapter 6 - Photocatalysis. In S. C. Ameta & R. Ameta (Eds.), *Advanced oxidation processes for waste water treatment* (pp. 135–175). Academic Press.
- Ao, X., Liu, W., Sun, W., Cai, M., Ye, Z., Yang, C., Lu, Z., & Li, C. (2018). Medium pressure UV-activated peroxymonosulfate for ciprofloxacin degradation: Kinetics, mechanism, and genotoxicity. *Chemical Engineering Journal*, 345, 87–97. <https://doi.org/10.1016/j.cej.2018.03.133>
- Ashenurst, J. (2017). Carbohydrates. What is Mutarotation?. Master organic chemistry. Retrieved February 10, 2022, from <https://www.masterorganicchemistry.com/2017/08/17/mutarotation/>
- Bagherzadeh, M., Kaveh, R., Ozkar, S., & Akbayrak, S. (2018). Preparation and characterization of a new CdS–NiFe₂O₄/reduced graphene oxide photocatalyst and its use for degradation of methylene blue under visible light irradiation. *Research on Chemical Intermediates*. <https://doi.org/10.1007/s11164-018-3466-1>
- Ballesteros-Gómez, A., Ballesteros, J., Ortiz, X., Jonker, W., Helmus, R., Jobst, K. J., Parsons, J. R., & Reiner, E. J. (2017). Identification of novel brominated compounds in flame retarded plastics containing TBBPA by combining isotope pattern and mass defect cluster analysis. *Environmental Science and Technology*, 51, 1518–1526. <https://doi.org/10.1021/acs.est.6b03294>
- Barret, E.F., Larson T.R., & Koubek E.J. (2021). Drug excretion. Elsevier. Retrieved February 10, 2022, from <https://linkinghub.elsevier.com/retrieve/pii/B9780128204726999997>
- Bessegato, G. G., Guaraldo, T. T., de Brito, J. F., Brugnera, M. F., & Zanoni, M. V. B. (2015). Achievements and trends in photoelectrocatalysis: From environmental to energy applications. *Electrocatalysis*, 6, 415–441. <https://doi.org/10.1007/s12678-015-0259-9>
- Bessegato, G. G., Guaraldo, T. T., & Zanoni, M. B. (2014). Enhancement of Photoelectrocatalysis Efficiency by Using Nanostructured Electrodes. In: M. Aliofkha-raei (ed.), *Modern Electrochemical Methods in Nano, Surface and Corrosion Science* (1st ed., pp. 271–319). London: IntechOpen.
- Bojanowska-Czajka, A., Gałężowska, A., Marty, J.-L., & Trojanowicz, M. (2010). Decomposition of pesticide chlorfenvinphos in aqueous solutions by gamma-irradiation. *Journal of Radioanalytical and Nuclear Chemistry*, 285, 215–221. <https://doi.org/10.1007/s10967-010-0567-8>
- Bolong, N., Ismail, A. F., Salim, M. R., & Matsuura, T. (2009). A review of the effects of emerging contaminants in wastewater and options for their removal. *Desalination*, 239, 229–246. <https://doi.org/10.1016/j.desal.2008.03.020>
- Braslavsky, S. E. (2007). Glossary of terms used in photochemistry, 3rd edition (IUPAC Recommendations 2006). *Pure and Applied Chemistry*, 79, 293–465. <https://doi.org/10.1351/pac200779030293>
- Cabir, B., Yurderi, M., Caner, N., Agirtas, M. S., Zahmakiran, M., & Kaya, M. (2017). Methylene blue photocatalytic degradation under visible light irradiation on copper phthalocyanine-sensitized TiO₂ nanopowders. *Materials Science and Engineering B*, 224, 9–17. <https://doi.org/10.1016/j.mseb.2017.06.017>
- Cai, T., Liu, Y., Wang, L., Dong, W., Chen, H., Zeng, W., Xia, X., & Zeng, G. (2019). Activation of persulfate by photo-excited dye for antibiotic degradation: Radical and non-radical reactions. *Chemical Engineering Science*, 375, 122070. <https://doi.org/10.1016/j.ces.2019.122070>
- Campo, J., Masiá, A., Blasco, C., & Picó, Y. (2013). Occurrence and removal efficiency of pesticides in sewage treatment plants of four Mediterranean river basins. *J Haz Mat*, 263, 146–157. <https://doi.org/10.1016/j.jhazmat.2013.09.061>

- Ccancapa, A., Masiá, A., Navarro-Ortega, A., Picó, Y., & Barceló, D. (2016). Pesticides in the Ebro River basin: Occurrence and risk assessment. *Environmental Pollution*, 211, 414–424. <https://doi.org/10.1016/j.envpol.2015.12.059>
- Chen, W.-S., & Su, Y.-C. (2012). Removal of dinitrotoluenes in wastewater by sono-activated persulfate. *Ultrasonics Sonochemistry*, 19, 921–927. <https://doi.org/10.1016/j.ultsonch.2011.12.012>
- Chen, P., Zhang, Q., Su, Y., Shen, L., Wang, F., Liu, H., Liu, Y., Cai, Z., Lv, W., & Liu, G. (2018). Accelerated photocatalytic degradation of diclofenac by a novel CQDs/BiOCCOOH hybrid material under visible-light irradiation: Dechlorination, detoxicity, and a new superoxide radical model study. *Chemical Engineering Journal*, 332, 737–748. <https://doi.org/10.1016/j.cej.2017.09.118>
- Chen, S., Yang, F., Cao, Z., Yu, C., Wang, S., & Zhong, H. (2020). Enhanced photocatalytic activity of molybdenum disulfide by compositing ZnAl-LDH. *Colloids and Surfaces a: Physicochemical and Engineering Aspects*, 586, 124140. <https://doi.org/10.1016/j.colsurfa.2019.124140>
- Cheng, X., Wang, P., & Liu, H. (2015). Visible-light-driven photoelectrocatalytic degradation of diclofenac by N, S-TiO₂/TiO₂ NTs photoelectrode: Performance and mechanism study. *Journal of Environmental Chemical Engineering*, 3, 1713–1719. <https://doi.org/10.1016/j.jece.2015.06.015>
- Cheng, X., Guo, H., Zhang, Y., Korshin, G. V., & Yang, B. (2019). Insights into the mechanism of nonradical reactions of persulfate activated by carbon nanotubes: Activation performance and structure-function relationship. *Water Research*, 157, 406–414. <https://doi.org/10.1016/j.watres.2019.03.096>
- Chlorfenvinphos - Safety Data Sheet (2022) Santa Cruz Biotechnology - Material safety data sheet. Retrieved February 10, 2022, from <https://datasheets.scbt.com/sc-239500.pdf>
- Decision, E. C. (2015). Commission Implementing Decision (EU) 2015/495 of 20 March 2015 establishing a watch list of substances for Union-wide monitoring in the field of water policy pursuant to Directive 2008/105/EC of the European Parliament and of the Council. European Commission.
- Decision, E. C. (2020) Commission Implementing Decision (EU) 2020/1161 of 4 August 2020 establishing a watch list of substances for Union-wide monitoring in the field of water policy pursuant to Directive 2008/105/EC of the European Parliament and of the Council. European Commission.
- Criquet, J., & Karpel Vel Leitner, N. (2011). Electron beam irradiation of aqueous solution of persulfate ions. *Chemical Engineering Journal*, 169, 258–262. <https://doi.org/10.1016/j.cej.2011.02.025>
- Criquet, J., & Karpel Vel Leitner, N. (2012). Electron beam irradiation of citric acid aqueous solutions containing persulfate. *Separation and Purification Technology*, 88, 168–173. <https://doi.org/10.1016/j.seppur.2011.12.006>
- D'Amato, C. A., Giovannetti, R., Zannotti, M., Rommozzi, E., Minicucci, M., Gunnella, R., & Di Cicco, A. (2018). Band gap implications on nano-TiO₂ surface modification with ascorbic acid for visible light-active polypropylene coated photocatalyst. *Nanomaterials*, 8, 599. <https://doi.org/10.3390/nano8080599>
- da Rosa, A. P. P., Cavalcante, R. P., da Silva, T. F., Gozzi, F., Byrne, C., McGlynn, E., Casagrande, G. A., de Oliveira, S. C., & Junior, A. M. (2020). Photoelectrocatalytic degradation of methylene blue using ZnO nanorods fabricated on silicon substrates. *Journal of Nanoscience and Nanotechnology*, 20, 1177–1188. <https://doi.org/10.1166/jnn.2020.16961>
- De Gisi, S., Lofrano, G., Grassi, M., & Notarnicola, M. (2016). Characteristics and adsorption capacities of low-cost sorbents for wastewater treatment: A review. *Sustainable Materials and Technologies*, 9, 10–40. <https://doi.org/10.1016/j.susmat.2016.06.002>
- de Oliveira, L. L. D., Antunes, S. C., Gonçalves, F., Rocha, O., & Nunes, B. (2016). Acute and chronic ecotoxicological effects of four pharmaceuticals drugs on cladoceran *Daphnia magna*. *Drug and Chemical Toxicology*, 39, 13–21. <https://doi.org/10.3109/01480545.2015.1029048>
- DeLorenzo, M. E., & Fleming, J. (2008). Individual and mixture effects of selected pharmaceuticals and personal care products on the marine phytoplankton species *Dunaliella tertiolecta*. *Archives of Environmental Contamination and Toxicology*, 54, 203–210. <https://doi.org/10.1007/s00244-007-9032-2>
- Deng, Y., & Zhao, R. (2015). Advanced oxidation processes (AOPs) in wastewater treatment. *Current Pollution Reports*, 1, 167–176. <https://doi.org/10.1007/s40726-015-0015-z>
- Dhaka, S., Kumar, R., Deep, A., Kurade, M. B., Ji, S.-W., & Jeon, B.-H. (2019). Metal-organic frameworks (MOFs) for the removal of emerging contaminants from aquatic environments. *Coordination Chemistry Reviews*, 380, 330–352. <https://doi.org/10.1016/j.ccr.2018.10.003>
- Diao, Z. H., Liu, J. J., Hu, Y. X., Kong, L. J., Jiang, D., & Xu, X. R. (2017). Comparative study of rhodamine B degradation by the systems pyrite/H₂O₂ and pyrite/persulfate: Reactivity, stability, products and mechanism. *Separation and Purification Technology*, 184, 374–383. <https://doi.org/10.1016/j.seppur.2017.05.016>
- Ding, J., Bu, L., Zhao, Q., Kabutey, F. T., Wei, L., & Dionysiou, D. D. (2020). Electrochemical activation of persulfate on BDD and DSA anodes: Electrolyte influence, kinetics and mechanisms in the degradation of bisphenol A. *J Haz Mater*, 388, 121789. <https://doi.org/10.1016/j.jhazmat.2019.121789>
- Directive, E. P. (2013). Directive 2013/39/EU of the European Parliament and of the Council of 12 August 2013 amending Directives 2000/60/EC and 2008/105/EC as regards priority substances in the field of water policy. European Parliament.
- Du, X., Bai, X., Xu, L., Yang, L., & Jin, P. (2020). Visible-light activation of persulfate by TiO₂/g-C₃N₄ photocatalyst toward efficient degradation of micropollutants. *Chemical Engineering Journal*, 384, 123245. <https://doi.org/10.1016/j.cej.2019.123245>
- Dubey, M., Mohapatra, S., Tyagi, V. K., Suthar, S., & Kazmi, A. A. (2021). Occurrence, fate, and persistence of emerging micropollutants in sewage sludge treatment. *Environmental Pollution*, 273, 116515. <https://doi.org/10.1016/j.envpol.2021.116515>

- El-Katori, E. E., Ahmed, M. A., El-Bindary, A. A., & Oraby, A. M. (2020). Impact of CdS/SnO₂ heterostructured nanoparticle as visible light active photocatalyst for the removal methylene blue dye. *Journal of Photochemistry and Photobiology, a: Chemistry*, 392, 112403. <https://doi.org/10.1016/j.jphotochem.2020.112403>
- El-Sheshtawy, H. S., Ghubish, Z., Shoueir, K. R., & El-Kemary, M. (2020). Activated H₂O₂ on Ag/SiO₂-SrWO₄ surface for enhanced dark and visible-light removal of methylene blue and p-nitrophenol. *Journal of Alloys and Compounds*, 842, 155848. <https://doi.org/10.1016/j.jallcom.2020.155848>
- Esmaili, H., Kotobi, A., Sheibani, S., & Rashchi, F. (2018). Photocatalytic degradation of methylene blue by nanostructured Fe/FeS powder under visible light. *International Journal of Minerals, Metallurgy, and Materials*, 25, 244–252. <https://doi.org/10.1007/s12613-018-1567-x>
- Fantuzzi, G., Aggazzotti, G., Righi, E., Predieri, G., Castiglioni, S., Riva, F., & Zuccato, E. (2018). Illicit drugs and pharmaceuticals in swimming pool waters. *Science of the Total Environment*, 635, 956–963. <https://doi.org/10.1016/j.scitotenv.2018.04.155>
- Farhadian, N., Akbarzadeh, R., Pirsahab, M., Jen, T.-C., Fakhri, Y., & Asadi, A. (2019). Chitosan modified N, S-doped TiO₂ and N, S-doped ZnO for visible light photocatalytic degradation of tetracycline. *International Journal of Biological Macromolecules*, 132, 360–373. <https://doi.org/10.1016/j.ijbiomac.2019.03.217>
- Farner Budarz, J., Turolla, A., Piasecki, A. F., Bottero, J.-Y., Antonelli, M., & Wiesner, M. R. (2017). Influence of aqueous inorganic anions on the reactivity of nanoparticles in TiO₂ photocatalysis. *Langmuir*, 33, 2770–2779. <https://doi.org/10.1021/acs.langmuir.6b04116>
- Farré, M. J., Franch, M. I., Malato, S., Ayllón, J. A., Peral, J., & Doménech, X. (2005). Degradation of some biorecalcitrant pesticides by homogeneous and heterogeneous photocatalytic ozonation. *Chemosphere*, 58, 1127–1133. <https://doi.org/10.1016/j.chemosphere.2004.09.064>
- Fernandes, A., Nunes, M. J., Rodrigues, A. S., Pacheco, M. J., Ciriaco, L., & Lopes, A. (2021). Electro-persulfate processes for the treatment of complex wastewater matrices: Present and future. *Molecules*, 26, 4821. <https://doi.org/10.3390/molecules26164821>
- Fernández-Domene, R. M., Roselló-Márquez, G., Sánchez-Tovar, R., Lucas-Granados, B., & García-Antón, J. (2019). Photoelectrochemical removal of chlorfenvinphos by using WO₃ nanorods: Influence of annealing temperature and operation pH. *Separation and Purification Technology*, 212, 458–464. <https://doi.org/10.1016/j.seppur.2018.11.049>
- Font, C., Bregoli, F., Acuña, V., Sabater, S., & Marcé, R. (2019). GLOBAL-FATE (version 1.0.0): A geographical information system (GIS)-based model for assessing contaminants fate in the global river network. *Geoscientific Model Development*, 12, 5213–5228. <https://doi.org/10.5194/gmd-12-5213-2019>
- Gandamalla, A., Manchala, S., Anand, P., Fu, Y.-P., & Shanker, V. (2021). Development of versatile CdMoO₄/g-C₃N₄ nanocomposite for enhanced photoelectrochemical oxygen evolution reaction and photocatalytic dye degradation applications. *Materials Today Chemistry*, 19, 100392. <https://doi.org/10.1016/j.mtchem.2020.100392>
- Ge, M.-Z., Cao, C.-Y., Huang, J.-Y., Li, S.-H., Zhang, S.-N., Deng, S., Li, Q.-S., Zhang, K.-Q., & Lai, Y.-K. (2016). Synthesis, modification, and photo/photoelectrocatalytic degradation applications of TiO₂ nanotube arrays: A review. *Nanotechnology Reviews*, 5, 75–112. <https://doi.org/10.1515/ntrev-2015-0049>
- Gendrot, M., Andreani, J., Duflo, I., Boxberger, M., Le Bideau, M., Mosnier, J., Jardot, P., Fonta, I., Rolland, C., Bogreau, H., Hutter, S., La Scola, B., & Pradines, B. (2020). Methylene blue inhibits replication of SARS-CoV-2 in vitro. *International Journal of Antimicrobial Agents*, 56, 106202. <https://doi.org/10.1016/j.ijantimicag.2020.106202>
- Ghanbari, F., & Moradi, M. (2017). Application of peroxy-monosulfate and its activation methods for degradation of environmental organic pollutants: Review. *Chemical Engineering Journal*, 310, 41–62. <https://doi.org/10.1016/j.cej.2016.10.064>
- Gheraout, D., & Elboughdiri, N. (2019). Water reuse: Emerging contaminants elimination—Progress and trends. *Open Access Library Journal*, 6, 1–9. <https://doi.org/10.4236/oalib.1105981>
- Gheraout, D., & Elboughdiri, N. (2021). Advanced oxidation processes for wastewater treatment: Facts and future trends. *Open Access Library Journal*, 7, 1–15. <https://doi.org/10.4236/oalib.1106139>
- Ghime, D., & Ghosh, P. (2020). Advanced oxidation processes: A powerful treatment option for the removal of recalcitrant organic compounds. In: *Bustillo-Lecompte (Ed.) Advanced Oxidation Processes Applications, Trends, and Prospects, IntechOpen*. <https://doi.org/10.5772/intechopen.90192>
- Ghorai, K., Panda, A., Hossain, A., Bhattacharjee, M., Chakraborty, M., Bhattacharya, S. K., Bera, P., Kim, H., Seikh, Md. M., & Gayen, A. (2021). Anatase TiO₂ decorated CuCr₂O₄ nanocomposite: A versatile photocatalyst under domestic LED light irradiation. *Applied Surface Science*, 568, 150838. <https://doi.org/10.1016/j.apsusc.2021.150838>
- Girón-Navarro, R., Linares-Hernández, I., Teutli-Sequeira, E. A., Martínez-Miranda, V., & Santoyo-Tepole, F. (2021). Evaluation and comparison of advanced oxidation processes for the degradation of 2,4-dichlorophenoxyacetic acid (2,4-D): A review. *Environmental Science and Pollution Research*, 28(21), 26325–26358. <https://doi.org/10.1007/s11356-021-13730-y>
- Gogoi, A., Mazumder, P., Tyagi, V. K., Tushara Chaminda, G. G., An, A. K., & Kumar, M. (2018). Occurrence and fate of emerging contaminants in water environment: A review. *Groundwater for Sustainable Development*, 6, 169–180. <https://doi.org/10.1016/j.gsd.2017.12.009>
- Google Scholar Database (2022) Google Scholar web. Retrieved February 10, 2022, from <https://scholar.google.com/>
- Guadie, A., Tizazu, S., Melese, M., Guo, W., Ngo, H. H., & Xia, S. (2017). Biodecolorization of textile azo dye using *Bacillus* sp. strain CH12 isolated from alkaline lake. *Biotechnol Rep*, 15, 92–100. <https://doi.org/10.1016/j.btre.2017.06.007>

- Habib, I. Y., Burhan, J., Jaladi, F., Lim, C. M., Usman, A., Kumara, N. T. R. N., Tsang, S. C. E., & Mahadi, A. H. (2021). Effect of Cr doping in CeO₂ nanostructures on photocatalysis and H₂O₂ assisted methylene blue dye degradation. *Catalysis Today*, 375, 506–513. <https://doi.org/10.1016/j.cattod.2020.04.008>
- Han, W., Li, D., Zhang, M., Ximin, H., Duan, X., Liu, S., & Wang, S. (2020a). Photocatalytic activation of peroxy-monosulfate by surface-tailored carbon quantum dots. *Journal of Hazardous Materials*, 395, 122695. <https://doi.org/10.1016/j.jhazmat.2020.122695>
- Han, F., Ye, X., Chen, Q., Long, H., & Rao, Y. (2020b). The oxidative degradation of diclofenac using the activation of peroxy-monosulfate by BiFeO₃ microspheres—Kinetics, role of visible light and decay pathways. *Separation Purification Technology*, 232, 115967. <https://doi.org/10.1016/j.seppur.2019.115967>
- Hou, X., Liu, X., Han, J., Liu, H., Yao, J., Li, D., Wang, L., Liao, B., Li, J., & Zhang, R. (2020a). Enhanced photoelectrocatalytic degradation of organic pollutants using TiO₂ nanotubes implanted with nitrogen ions. *Journal of Materials Science*, 55, 5843–5860. <https://doi.org/10.1007/s10853-020-04461-5>
- Hou, X., Zhan, G., Huang, X., Wang, N., Ai, Z., & Zhang, L. (2020b). Persulfate activation induced by ascorbic acid for efficient organic pollutants oxidation. *Chemical Engineering Journal*, 382, 122355. <https://doi.org/10.1016/j.cej.2019.122355>
- Hu, Y., Li, Z., Yang, J., & Zhu, H. (2019). Degradation of methylparaben using BiOI-hydrogel composites activated peroxy-monosulfate under visible light irradiation. *Chemical Engineering Journal*, 360, 200–211. <https://doi.org/10.1016/j.cej.2018.11.217>
- Hu, J., Zeng, X., Yin, Y., Liu, Y., Li, Y., Hu, X., Zhang, L., & Zhang, X. (2020a). Accelerated alkaline activation of peroxydisulfate by reduced rubidium tungstate nanorods for enhanced degradation of bisphenol A. *Environmental Science: Nano*, 7, 3547–3556. <https://doi.org/10.1039/D0EN00840K>
- Hu, L., Wang, P., Shen, T., Wang, Q., Wang, X., Xu, P., Zheng, Q., & Zhang, G. (2020b). The application of microwaves in sulfate radical-based advanced oxidation processes for environmental remediation: A review. *Science of the Total Environment*, 722, 137831. <https://doi.org/10.1016/j.scitotenv.2020.137831>
- Hu, Z., Shi, J., Yang, H., Huang, J., & Sheng, F. (2021). How organic substances promote the chemical oxidative degradation of pollutants: A mini review. *Sustainability*, 13(19), 10993. <https://doi.org/10.3390/su131910993>
- Hussain, I., Zhang, Y., Li, M., Huang, S., Hayat, W., He, L., Du, X., Liu, G., & Du, M. (2018). Heterogeneously degradation of aniline in aqueous solution using persulfate catalyzed by magnetic BiFeO₃ nanoparticles. *Catalysis Today*, 310, 130–140. <https://doi.org/10.1016/j.cattod.2018.02.017>
- Jakab, G., Szalai, Z., Michalkó, G., Ringer, M., Filep, T., Szabó, L., Maász, G., Pirger, Z., Ferincz, Á., Staszny, Á., Dobosy, P., & Kondor, A. C. (2020). Thermal baths as sources of pharmaceutical and illicit drug contamination. *Environmental Science and Pollution Research International*, 27, 399–410. <https://doi.org/10.1007/s11356-019-06633-6>
- Ji, Y., Xie, W., Fan, Y., Shi, Y., Kong, D., & Lu, J. (2016). Degradation of trimethoprim by thermo-activated persulfate oxidation: Reaction kinetics and transformation mechanisms. *Chemical Engineering Journal*, 286, 16–24. <https://doi.org/10.1016/j.cej.2015.10.050>
- Ji, Q., Cheng, X., Wu, Y., Xiang, W., He, H., Xu, Z., Xu, C., Qi, C., Li, S., Zhang, L., & Yang, S. (2021). Visible light absorption by perylene diimide for synergistic persulfate activation towards efficient photodegradation of bisphenol A. *Applied Catalysis B: Environmental*, 282, 119579. <https://doi.org/10.1016/j.apcatb.2020.119579>
- Karickhoff, S. W., Brown, D. S., & Scott, T. A. (1979). Sorption of hydrophobic pollutants on natural sediments. *Water Research*, 13, 241–248. [https://doi.org/10.1016/0043-1354\(79\)90201-X](https://doi.org/10.1016/0043-1354(79)90201-X)
- Karim, A. V., Jiao, Y., Zhou, M., & Nidheesh, P. V. (2021). Iron-based persulfate activation process for environmental decontamination in water and soil. *Chemosphere*, 265, 129057. <https://doi.org/10.1016/j.chemosphere.2020.129057>
- Kaur, H., Kumar, S., Verma, N. K., & Singh, P. (2018). Role of pH on the photocatalytic activity of TiO₂ tailored by W/T mole ratio. *Journal of Materials Science: Materials in Electronics*, 29, 16120–16135. <https://doi.org/10.1007/s10854-018-9701-0>
- Khamparia, S., & Jaspal, D. (2018). Technologies for treatment of colored wastewater from different industries. In C. M. Hussain (Ed.), *Handbook of environmental materials management* (pp. 1–14). Springer International Publishing.
- Klamerth, N., Gernjak, W., Malato, S., Agüera, A., & Lendl, B. (2009). Photo-Fenton decomposition of chlorfenvinphos: Determination of reaction pathway. *Water Research*, 43, 441–449. <https://doi.org/10.1016/j.watres.2008.10.013>
- Koranteng, S. S., Darko, D. A., Nukpezah, D., & Ameka, G. K. (2018). Pesticides bioconcentration potential of aquatic plants in the Volta Lake. *West African Journal of Applied Ecology*, 26, 193–202. <https://doi.org/10.4314/wajae.v26i0>
- Kosmulski, M. (2011). The pH-dependent surface charging and points of zero charge: V. update. *Journal of Colloid and Interface Science*, 353, 1–15. <https://doi.org/10.1016/j.jcis.2010.08.023>
- Ku, Y., Tu, Y.-H., & Ma, C.-M. (2005). Effect of hydrogen peroxide on the decomposition of monochlorophenols by sonolysis in aqueous solution. *Water Research*, 39, 1093–1098. <https://doi.org/10.1016/j.watres.2004.11.036>
- Laws, E. A. (2013). Environmental toxicology, introduction. In E. A. Laws (Ed.), *Environmental toxicology* (pp. 1–15). Springer Nature.
- Le Coadou, L., Le Ménach, K., Labadie, P., Dévier, M.-H., Pardon, P., Augagneur, S., & Budzinski, H. (2017). Quality survey of natural mineral water and spring water sold in France: Monitoring of hormones, pharmaceuticals, pesticides, perfluoroalkyl substances, phthalates, and alkylphenols at the ultra-trace level. *Science of the Total Environment*, 603–604, 651–662. <https://doi.org/10.1016/j.scitotenv.2016.11.174>

- Lee, S. J., Jung, H. J., Koutavarapu, R., Lee, S. H., Arumugam, M., Kim, J. H., & Choi, M. Y. (2019). ZnO supported Au/Pd bimetallic nanocomposites for plasmon improved photocatalytic activity for methylene blue degradation under visible light irradiation. *Applied Surface Science*, 496, 143665. <https://doi.org/10.1016/j.apsusc.2019.143665>
- Lee, J., von Gunten, U., & Kim, J. H. (2020). Persulfate-based advanced oxidation: Critical assessment of opportunities and roadblocks. *Environmental Science and Technology*, 54(6), 3064–3081. <https://doi.org/10.1021/acs.est.9b07082>
- Lempart, A., Kudlek, E., & Dudziak, M. (2020). The potential of the organic micropollutants emission from swimming accessories into pool water. *Environment International*, 136, 105442. <https://doi.org/10.1016/j.envint.2019.105442>
- Leusch, F. D. L., Neale, P. A., Hebert, A., Scheurer, M., & Schriks, M. C. M. (2017). Analysis of the sensitivity of in vitro bioassays for androgenic, progestagenic, glucocorticoid, thyroid and estrogenic activity: Suitability for drinking and environmental waters. *Environment International*, 99, 120–130. <https://doi.org/10.1016/j.envint.2016.12.014>
- Li, R., & Li, C. (2017). Chapter One - Photocatalytic water splitting on semiconductor-based photocatalysts. In C. Song (Ed.), *Advances in catalysis* (pp. 1–57). Academic Press.
- Li, A. J., Sang, Z., Chow, C.-H., Law, J.C.-F., Guo, Y., & Leung, K.S.-Y. (2017). Environmental behavior of 12 UV filters and photocatalytic profile of ethyl-4-aminobenzoate. *Journal of Hazardous Materials*, 337, 115–125. <https://doi.org/10.1016/j.jhazmat.2017.04.067>
- Li, Z., Meng, X., & Zhang, Z. (2018). Recent development on MoS₂-based photocatalysis: A review. *Journal of Photochemistry and Photobiology, c: Photochemistry Reviews*, 35, 39–55. <https://doi.org/10.1016/j.jphotochemrev.2017.12.002>
- Li Puma, G., Bono, A., Krishnaiah, D., & Collin, J. G. (2008). Preparation of titanium dioxide photocatalyst loaded onto activated carbon support using chemical vapor deposition: A review paper. *Journal of Hazardous Materials*, 157, 209–219. <https://doi.org/10.1016/j.jhazmat.2008.01.040>
- Liao, T.-W., Verbruggen, S. W., Claes, N., Yadav, A., Grandjean, D., Bals, S., & Lievens, P. (2018). TiO₂ films modified with Au nanoclusters as self-cleaning surfaces under visible light. *Nanomaterials*, 8, 30. <https://doi.org/10.3390/nano8010030>
- Liu, D., Tian, R., Wang, J., Nie, E., Piao, X., Li, X., & Sun, Z. (2017a). Photoelectrocatalytic degradation of methylene blue using F doped TiO₂ photoelectrode under visible light irradiation. *Chemosphere*, 185, 574–581. <https://doi.org/10.1016/j.chemosphere.2017.07.071>
- Liu, S., Zhao, X., Zeng, H., Wang, Y., Qiao, M., & Guan, W. (2017b). Enhancement of photoelectrocatalytic degradation of diclofenac with persulfate activated by Cu cathode. *Chemical Engineering Journal*, 320, 168–177. <https://doi.org/10.1016/j.cej.2017.03.047>
- Liu, F., Yi, P., Wang, X., Gao, H., & Zhang, H. (2018). Degradation of Acid Orange 7 by an ultrasound/ZnO-GAC/persulfate process. *Separation and Purification Technology*, 194, 181–187. <https://doi.org/10.1016/j.seppur.2017.10.072>
- Liu, X., Li, H., Ma, J., Yu, X., Wang, Y., & Li, J. (2019). Preparation of a Bi₂WO₆ catalyst and its catalytic performance in an alpha alkylation reaction under visible light irradiation. *Mol Catal*, 466, 157–166. <https://doi.org/10.1016/j.mcat.2019.01.018>
- Lonappan, L., Brar, S. K., Das, R. K., Verma, M., & Surampalli, R. Y. (2016). Diclofenac and its transformation products: Environmental occurrence and toxicity - A review. *Environment International*, 96, 127–138. <https://doi.org/10.1016/j.envint.2016.09.014>
- Loos, R., Tavazzi, S., Mariani, G., Suurkuusk, G., Paracchini, B., & Umlauf, G. (2017). Analysis of emerging organic contaminants in water, fish and suspended particulate matter (SPM) in the Joint Danube Survey using solid-phase extraction followed by UHPLC-MS-MS and GC-MS analysis. *Science of the Total Environment*, 607–608, 1201–1212. <https://doi.org/10.1016/j.scitotenv.2017.07.039>
- Lops, C., Ancona, A., Di Cesare, K., Dumontel, B., Garino, N., Canavese, G., Hernández, S., & Cauda, V. (2019). Sono-photocatalytic degradation mechanisms of rhodamine B dye via radicals generation by micro- and nano-particles of ZnO. *Applied Catalysis B: Environmental*, 243, 629–640. <https://doi.org/10.1016/j.apcatb.2018.10.078>
- Lutz, P., Wiaderna, D., Gralewicz, S., & Kur, B. (2006). Exposure to chlorphenvinphos, an organophosphate insecticide, prevents from behavioral sensitization to amphetamine. *International Journal of Occupational Medicine and Environmental Health*, 19, 132–141. <https://doi.org/10.2478/v10001-006-0017-6>
- Ma, D., Yi, H., Lai, C., Liu, X., Huo, X., An, Z., Li, L., Fu, Y., Li, B., Zhang, M., Qin, L., Liu, S., & Yang, L. (2021). Critical review of advanced oxidation processes in organic wastewater treatment. *Chemosphere*, 275, 130104. <https://doi.org/10.1016/j.chemosphere.2021.130104>
- Mahanthappa, M., Kottam, N., & Yellappa, S. (2019). Enhanced photocatalytic degradation of methylene blue dye using CuSCdS nanocomposite under visible light irradiation. *Applied Surface Science*, 475, 828–838. <https://doi.org/10.1016/j.apsusc.2018.12.178>
- Mahdavianpour, M., Ildari, S., Ebrahimi, M., & Moslemzadeh, M. (2020). Decolorization and mineralization of methylene blue in aqueous solutions by persulfate/Fe²⁺ process. *Journal of Water Chemistry and Technology*, 42, 244–251. <https://doi.org/10.3103/S1063455X20040098>
- Mahdy, F. M., & El-Maghraby, S. I. (2010). Effect of processing on 14C-chlorfenvinphos residues in maize oil and bioavailability of its cake residues on rats. *Bulletin of Environment Contamination and Toxicology*, 84, 582–586. <https://doi.org/10.1007/s00128-010-9984-1>
- Malefane, M. E., Feleni, U., & Kuvarega, A. T. (2020). Cobalt (II/III) oxide and tungsten (VI) oxide p-n heterojunction photocatalyst for photodegradation of diclofenac sodium under visible light. *Journal of Environmental Chemical Engineering*, 8, 103560. <https://doi.org/10.1016/j.jece.2019.103560>

- Manz, K. E., Adams, T. J., & Carter, K. E. (2018). Furfural degradation through heat-activated persulfate: Impacts of simulated brine and elevated pressures. *Chemical Engineering Journal*, 353, 727–735. <https://doi.org/10.1016/j.cej.2018.07.142>
- Mazivila, S. J., Ricardo, I. A., Leitão, J. M. M., & Esteves da Silva, J. C. G. (2019). A review on advanced oxidation processes: From classical to new perspectives coupled to two- and multi-way calibration strategies to monitor degradation of contaminants in environmental samples. *Trends Environmental Analytical Chemistry*, 24, e00072. <https://doi.org/10.1016/j.teac.2019.e00072>
- McMichael, S., Fernández-Ibáñez, P., & Byrne, J. A. (2021). A review of photoelectrocatalytic reactors for water and wastewater treatment. *Water*, 13, 1198. <https://doi.org/10.3390/w13091198>
- Memmert, U., Peither, A., Burri, R., Weber, K., Schmidt, T., Sumpter, J. P., & Hartmann, A. (2013). Diclofenac: New data on chronic toxicity and bioconcentration in fish. *Environmental Toxicology and Chemistry*, 32, 442–452. <https://doi.org/10.1002/etc.2085>
- Menger, F., Ahrens, L., Wiberg, K., & Gago-Ferrero, P. (2021). Suspect screening based on market data of polar halogenated micropollutants in river water affected by wastewater. *Journal of Hazardous Materials*, 401, 123377. <https://doi.org/10.1016/j.jhazmat.2020.123377>
- Methylene Blue - Material Safety Data Sheet (2022) MSDS Number: M4381. Avantor Performance Materials, Inc. Retrieved February 10, 2022, from <http://dept.harpercoll.ace.edu/chemistry/msds/Methylene%20blue%20JTBaker.pdf>
- Miklos, D. B., Remy, C., Jekel, M., Linden, K. G., Drewes, J. E., & Hübner, U. (2018). Evaluation of advanced oxidation processes for water and wastewater treatment – A critical review. *Water Research*, 139, 118–131. <https://doi.org/10.1016/j.watres.2018.03.042>
- Montagner, C. C., Sodr e, F. F., Acayaba, R. D., Vidal, C., Campestrini, I., Locatelli, M. A., Pescara, I. C., Albuquerque, A. F., Umbuzeiro, G. A., & Jardim, W. F. (2019). Ten years-snapshot of the occurrence of emerging contaminants in drinking, surface and ground waters and wastewaters from S ao Paulo State, Brazil. *Journal of the Brazilian Chemical Society*, 30, 614–632. <https://doi.org/10.21577/0103-5053.20180232>
- Moreira, I. S., Bessa, V. S., Murgolo, S., Piccirillo, C., Mascolo, G., & Castro, P. M. L. (2018). Biodegradation of diclofenac by the bacterial strain Labrys portucalensis F11. *Ecotoxicology and Environmental Safety*, 152, 104–113. <https://doi.org/10.1016/j.ecoenv.2018.01.040>
- Mugunthan, E., Saidutta, M. B., & Jagadeeshbabu, P. E. (2018). Visible light assisted photocatalytic degradation of diclofenac using TiO₂-WO₃ mixed oxide catalysts. *Environmental Nanotechnology Monitoring and Management*, 10, 322–330. <https://doi.org/10.1016/j.enmm.2018.07.012>
- Mugunthan, E., Saidutta, M. B., & Jagadeeshbabu, P. E. (2019). Photocatalytic activity of ZnO-WO₃ for diclofenac degradation under visible light irradiation. *Journal of Photochemistry and Photobiology, a: Chemistry*, 383, 111993. <https://doi.org/10.1016/j.jphotochem.2019.111993>
- Nareejun, W., & Ponchio, C. (2020). Novel photoelectrocatalytic/solar cell improvement for organic dye degradation based on simple dip coating WO₃/BiVO₄ photoanode electrode. *Solar Energy Materials and Solar Cells*, 212, 110556. <https://doi.org/10.1016/j.solmat.2020.110556>
- Nasseri, S., Mahvi, A. H., Seyed-salehi, M., Yaghmaeian, K., Nabizadeh, R., Alimohammadi, M., & Safari, G. H. (2017). Degradation kinetics of tetracycline in aqueous solutions using peroxydisulfate activated by ultrasound irradiation: Effect of radical scavenger and water matrix. *Journal of Molecular Liquids*, 241, 704–714. <https://doi.org/10.1016/j.molliq.2017.05.137>
- Nguyen, T.-B., Huang, C. P., Doong, R., Chen, C.-W., & Dong, C.-D. (2020). Visible-light photodegradation of sulfamethoxazole (SMX) over Ag-P-codoped g-C₃N₄ (Ag-P@UCN) photocatalyst in water. *Chemical Engineering Journal*, 384, 123383. <https://doi.org/10.1016/j.cej.2019.123383>
- Ngweme, G. N., Al Salah, D. M. M., Laffite, A., Sivalingam, P., Grandjean, D., Konde, J. N., Mulaji, C. K., Breider, F., & Pot e, J. (2021). Occurrence of organic micropollutants and human health risk assessment based on consumption of *Amaranthus viridis*, Kinshasa in the Democratic Republic of the Congo. *Science of the Total Environment*, 754, 142175. <https://doi.org/10.1016/j.scitotenv.2020.142175>
- Nuengmacha, P., Porrawatkul, P., Chanthai, S., Sricharoen, P., & Limchoowong, N. (2019). Enhanced photocatalytic degradation of methylene blue using Fe₂O₃/graphene/CuO nanocomposites under visible light. *Journal Environmental Chemical Engineering*, 7(6), 103438. <https://doi.org/10.1016/j.jece.2019.103438>
- Obotey Ezugbe, E., & Rathilal, S. (2020). Membrane technologies in wastewater treatment: A review. *Membranes*, 10, 89. <https://doi.org/10.3390/membranes10050089>
- Oliveros, A. N., Pimentel, J. A. I., de Luna, M. D. G., Garcia-Segura, S., Abarca, R. R. M., & Doong, R.-A. (2021). Visible-light photocatalytic diclofenac removal by tunable vanadium pentoxide/boron-doped graphitic carbon nitride composite. *Chemical Engineering Journal*, 403, 126213. <https://doi.org/10.1016/j.cej.2020.126213>
- Ouyang, M., Li, X., Xu, Q., Tao, Z., Yao, F., Huang, X., Wu, Y., Wang, D., Yang, Q., Chen, Z., & Pi, Z. (2020). Heterogeneous activation of persulfate by Ag doped BiFeO₃ composites for tetracycline degradation. *Journal of Colloid and Interface Science*, 566, 33–45. <https://doi.org/10.1016/j.jcis.2020.01.012>
- Oveisi, M., Alinia Asli, M., & Mahmoodi, N. M. (2019). Carbon nanotube based metal-organic framework nanocomposites: Synthesis and their photocatalytic activity for decolorization of colored wastewater. *Inorganica Chimica Acta*, 487, 169–176. <https://doi.org/10.1016/j.ica.2018.12.021>
- Palit, S. (2014). Future vision of advanced oxidation process and its immediate efficacy - A deep, insightful comprehension and a far-reaching review. *International Letters of Chemistry, Physics and Astronomy*, 33, 136–145.
- Pan, L., Sun, S., Chen, Y., Wang, P., Wang, J., Zhang, X., Zou, J.-J., & Wang, Z. L. (2020). Advances in piezo-phototronic effect enhanced photocatalysis and

- photoelectrocatalysis. *Advanced Energy Materials*, 10, 2000214. <https://doi.org/10.1002/aenm.202000214>
- Parnicka, P., Mazierski, P., Grzyb, T., Wei, Z., Kowalska, E., Ohtani, B., Lisowski, W., Klimczuk, T., & Nadolna, J. (2017). Preparation and photocatalytic activity of Nd-modified TiO₂ photocatalysts: Insight into the excitation mechanism under visible light. *Journal of Catalysis*, 353, 211–222. <https://doi.org/10.1016/j.jcat.2017.07.017>
- Peleyeju, M. G., & Arotiba, O. A. (2018). Recent trend in visible-light photoelectrocatalytic systems for degradation of organic contaminants in water/wastewater. *Environmental Science: Water Research & Technology*, 4, 1389–1411. <https://doi.org/10.1039/c8ew00276b>
- Peng, H., Xu, L., Zhang, W., Liu, F., Lu, X., Lu, W., Dan-ish, M., & Lin, K. (2017). Different kinds of persulfate activation with base for the oxidation and mechanism of BDE209 in a spiked soil system. *Science of the Total Environment*, 574, 307–313. <https://doi.org/10.1016/j.scitotenv.2016.09.057>
- Pérez-Lucas, G., Vela, N., Aatik, A.E., Navarro, S. (2018). Environmental risk of groundwater pollution by pesticide leaching through the soil profile. In: M. Larramendy & S. Soloneski (Eds.), *Pesticides* (1st ed., pp. 1–27). London: IntechOpen.
- Pirhashemi, M., Habibi-Yangjeh, A., & Rahim Pouran, S. (2018). Review on the criteria anticipated for the fabrication of highly efficient ZnO-based visible-light-driven photocatalysts. *Journal of Industrial and Engineering Chemistry*, 62, 1–25. <https://doi.org/10.1016/j.jiec.2018.01.012>
- Qi, H.-P., Wang, H.-L., Zhao, D.-Y., & Jiang, W.-F. (2019). Preparation and photocatalytic activity of Ag-modified GO-TiO₂ mesocrystals under visible light irradiation. *Applied Surface Science*, 480, 105–114. <https://doi.org/10.1016/j.apsusc.2019.02.194>
- Rahman, M. A., Amin, S. M. R., & Alam, A. M. S. (2012). Removal of methylene blue from waste water using activated carbon prepared from rice husk. *Dhaka University Journal of Science*, 60, 185–189. <https://doi.org/10.3329/duj.v60i2.11491>
- Rashid, J., Karim, S., Kumar, R., Barakat, M. A., Akram, B., Hussain, N., Bin, H. B., & Xu, M. (2020). A facile synthesis of bismuth oxychloride-graphene oxide composite for visible light photocatalysis of aqueous diclofenac sodium. *Science and Reports*, 10, 14191. <https://doi.org/10.1038/s41598-020-71139-y>
- Rauf, M. A., & Ashraf, S. S. (2009). Fundamental principles and application of heterogeneous photocatalytic degradation of dyes in solution. *Chemical Engineering Journal*, 151, 10–18. <https://doi.org/10.1016/j.cej.2009.02.026>
- Ravoet, J., Reybroeck, W., & de Graaf, D. C. (2015). Pesticides for apicultural and/or agricultural application found in Belgian honey bee wax combs. *Bulletin of Environment Contamination and Toxicology*, 94, 543–548. <https://doi.org/10.1007/s00128-015-1511-y>
- Rehman, F., Ahmad, W., & Sayed, M. (2021). Mechanistic investigations on the removal of diclofenac sodium by UV/S₂O₈²⁻/Fe²⁺, UV/HSO₅⁻/Fe²⁺ and UV/H₂O₂/Fe²⁺-based advanced oxidation processes. *Environmental Technology*, 42, 3995–4005. <https://doi.org/10.1080/09593330.2020.1770869>
- Ren, W., Xiong, L., Yuan, X., Yu, Z., Zhang, H., Duan, X., & Wang, S. (2019). Activation of peroxydisulfate on carbon nanotubes: Electron-transfer mechanism. *Environmental Science and Technology*, 53, 14595–14603. <https://doi.org/10.1021/acs.est.9b05475>
- Rizal, M. Y., Saleh, R., Taufik, A., & Yin, S. (2021). Photocatalytic decomposition of methylene blue by persulfate-assisted Ag/Mn₃O₄ and Ag/Mn₃O₄/graphene composites and the inhibition effect of inorganic ions. *Environmental Nanotechnology, Monitoring & Management*, 15, 100408. <https://doi.org/10.1016/j.enmm.2020.100408>
- Rodríguez-Narvaez, O. M., Peralta-Hernandez, J. M., Goonetilleke, A., & Bandala, E. R. (2017). Treatment technologies for emerging contaminants in water: A review. *Chemical Engineering Journal*, 323, 361–380. <https://doi.org/10.1016/j.cej.2017.04.106>
- Rogowska, J., Olkowska, E., Ratajczyk, W., & Wolska, L. (2018). Gadolinium as a new emerging contaminant of aquatic environments. *Environmental Toxicology and Chemistry*, 37, 1523–1534. <https://doi.org/10.1002/etc.4116>
- Roselló-Márquez, G., Fernández-Domene, R. M., Sánchez-Tovar, R., García-Carrión, S., Lucas-Granados, B., & García-Antón, J. (2019). Photoelectrocatalyzed degradation of a pesticides mixture solution (chlorfenvinphos and bromacil) by WO₃ nanosheets. *Science of the Total Environment*, 674, 88–95. <https://doi.org/10.1016/j.scitotenv.2019.04.150>
- Roselló-Márquez, G., Fernández-Domene, R. M., & García-Antón, J. (2021). Organophosphorus pesticides (chlorfenvinphos, phosmet and fenamiphos) photoelectrodegradation by using WO₃ nanostructures as photoanode. *Journal of Electroanalytical Chemistry*, 894, 115366. <https://doi.org/10.1016/j.jelechem.2021.115366>
- Sabri, M., Habibi-Yangjeh, A., Chand, H., & Krishnan, V. (2020). Activation of persulfate by novel TiO₂/FeOCl photocatalyst under visible light: Facile synthesis and high photocatalytic performance. *Separation and Purification Technology*, 250, 117268. <https://doi.org/10.1016/j.seppur.2020.117268>
- Sampath, S., Shestakova, M., Maydannik, P., Ivanova, T., Homola, T., Bryukvin, A., Sillanpää, M., Nagumothu, R., & Alagan, V. (2016). Photoelectrocatalytic activity of ZnO coated nano-porous silicon by atomic layer deposition. *RSC Advances*, 6, 25173–25178. <https://doi.org/10.1039/C6RA01655C>
- Sathishkumar, P., Meena, R. A. A., Palanisami, T., Ashokkumar, V., Palvannan, T., & Gu, F. L. (2020). Occurrence, interactive effects and ecological risk of diclofenac in environmental compartments and biota - A review. *Science of the Total Environment*, 698, 134057. <https://doi.org/10.1016/j.scitotenv.2019.134057>
- Scheytt, T., Mersmann, P., Lindstädt, R., & Heberer, T. (2005). 1-Octanol/water partition coefficients of 5 pharmaceuticals from human medical care: Carbamazepine, clofibrac acid, diclofenac, ibuprofen, and propyphenazone. *Water, Air, and Soil Pollution*, 165, 3–11. <https://doi.org/10.1007/s11270-005-3539-9>
- Scigliano, G., & Scigliano, G. A. (2021). Methylene blue in covid-19. *Medical Hypotheses*, 146, 110455. <https://doi.org/10.1016/j.mehy.2020.110455>

- Selvaraj, S., Mohan, M. K., Navaneethan, M., Ponnusamy, S., & Muthamizhchelvan, C. (2019). Synthesis and photocatalytic activity of Gd doped ZnO nanoparticles for enhanced degradation of methylene blue under visible light. *Materials Science in Semiconductor Processing*, 103, 104622. <https://doi.org/10.1016/j.mssp.2019.104622>
- Serpone, N., Artemev, Y. M., Ryabchuk, V. K., Emeline, A. V., & Horikoshi, S. (2017). Light-driven advanced oxidation processes in the disposal of emerging pharmaceutical contaminants in aqueous media: A brief review. *Current Opinion in Green and Sustainable Chemistry*, 6, 18–33. <https://doi.org/10.1016/j.cogsc.2017.05.003>
- Serrano, R., López, F. J., Hernández, F., & Peña, J. B. (1997). Bioconcentration of chlorpyrifos, chlorfenvinphos, and methidathion in *Mytilus galloprovincialis*. *Bulletin of Environment Contamination and Toxicology*, 59, 968–975. <https://doi.org/10.1007/s001289900577>
- Shao, H., Zhao, X., Wang, Y., Mao, R., Wang, Y., Qiao, M., Zhao, S., & Zhu, Y. (2017). Synergetic activation of peroxymonosulfate by Co_3O_4 modified $\text{g-C}_3\text{N}_4$ for enhanced degradation of diclofenac sodium under visible light irradiation. *Applied Catalysis B: Environmental*, 218, 810–818. <https://doi.org/10.1016/j.apcatb.2017.07.016>
- Sharma, B. M., Bečanová, J., Scheringer, M., Sharma, A., Bharat, G. K., Whitehead, P. G., Klánová, J., & Nizzetto, L. (2019). Health and ecological risk assessment of emerging contaminants (pharmaceuticals, personal care products, and artificial sweeteners) in surface and groundwater (drinking water) in the Ganges River Basin, India. *Science of the Total Environment*, 646, 1459–1467. <https://doi.org/10.1016/j.scitotenv.2018.07.235>
- Sharma, H. K., Sharma, S. K., Vemula, K., Koirala, A. R., Yadav, H. M., & Singh, B. P. (2021). CNT facilitated interfacial charge transfer of TiO_2 nanocomposite for controlling the electron-hole recombination. *Solid State Sciences*, 112, 106492. <https://doi.org/10.1016/j.solidstatesciences.2020.106492>
- Sire, A., & Amouroux, I. (2016). Determination of thresholds in marine molluscs as an alternative to the environmental quality standards in marine water defined in the Water Framework Directive. SETAC Europe 2016 - 26th annual Meeting, 22–26 May, 2016, Nantes, France. Retrieved February 10, 2022, from <https://archimer.ifremer.fr/doc/00344/45565/45172.pdf>
- Sismeyro-Vivas, J., Abrantes, N., Pereira, J. L., Castro, B. B., & Gonçalves, F. (2007). Short-term effects of Quirlan (chlorfenvinphos) on the behavior and acetylcholinesterase activity of *Gambusia holbrooki*. *Environmental Toxicology*, 22, 194–202. <https://doi.org/10.1002/tox.20256>
- Sosnowska, B., Huras, B., Krokosz, A., & Bukowska, B. (2013). The effect of bromfenvinphos, its impurities and chlorfenvinphos on acetylcholinesterase activity. *International Journal of Biological Macromolecules*, 57, 38–44. <https://doi.org/10.1016/j.ijbiomac.2013.02.011>
- Stanbury, D. M. (2020). Mechanisms of advanced oxidation processes, the principle of detailed balancing, and specifics of the UV/chloramine process. *Environmental Science and Technology*, 54(7), 4658–4663. <https://doi.org/10.1021/acs.est.9b07484>
- Su, Y., Wang, G.-B., Kuo, D. T. F., Chang, M., & Shih, Y. (2016). Photoelectrocatalytic degradation of the antibiotic sulfamethoxazole using TiO_2/Ti photoanode. *Applied Catalysis B: Environmental*, 186, 184–192. <https://doi.org/10.1016/j.apcatb.2016.01.003>
- Sun, J., Guo, Y., Wang, Y., Cao, D., Tian, S., Xiao, K., Mao, R., & Zhao, X. (2018). H_2O_2 assisted photoelectrocatalytic degradation of diclofenac sodium at $\text{g-C}_3\text{N}_4/\text{BiVO}_4$ photoanode under visible light irradiation. *Chemical Engineering Journal*, 332, 312–320. <https://doi.org/10.1016/j.cej.2017.09.041>
- Sun, Y., Cheng, S., Lin, Z., Yang, J., Li, C., & Gu, R. (2020). Combination of plasma oxidation process with microbial fuel cell for mineralizing methylene blue with high energy efficiency. *Journal of Hazardous Materials*, 384, 121307. <https://doi.org/10.1016/j.jhazmat.2019.121307>
- Tang, S. (2020). Enhanced photocatalytic performance of BiVO_4 for degradation of methylene blue under LED visible light irradiation assisted by peroxymonosulfate. *International Journal of Electrochemical Science*, 15, 2470–2480. <https://doi.org/10.20964/2020.03.09>
- Thongthep, P., Moonmangmee, S., & Ponchio, C. (2021). Solar/photoelectrocatalytic cell development for H_2 production and simultaneous organic dye degradation. *Materials Science in Semiconductor Processing*, 124, 105597. <https://doi.org/10.1016/j.mssp.2020.105597>
- Tian, D., Zhou, H., Zhang, H., Zhou, P., You, J., Yao, G., Pan, Z., Liu, Y., & Lai, B. (2022). Heterogeneous photocatalyst-driven persulfate activation process under visible light irradiation: From basic catalyst design principles to novel enhancement strategies. *Chemical Engineering Journal*, 428, 131166. <https://doi.org/10.1016/j.cej.2021.131166>
- Tomul, F., Arslan, Y., Başoğlu, F. T., Babuçuoğlu, Y., & Tran, H. N. (2019). Efficient removal of anti-inflammatory from solution by Fe-containing activated carbon: Adsorption kinetics, isotherms, and thermodynamics. *Journal of Environmental Management*, 238, 296–306. <https://doi.org/10.1016/j.jenvman.2019.02.088>
- Tröger, R., Klöckner, P., Ahrens, L., & Wiberg, K. (2018). Micropollutants in drinking water from source to tap - Method development and application of a multiresidue screening method. *Science of the Total Environment*, 627, 1404–1432. <https://doi.org/10.1016/j.scitotenv.2018.01.277>
- Tsui, M. M. P., Lam, J. C. W., Ng, T. Y., Ang, P. O., Murphy, M. B., & Lam, P. K. S. (2017). Occurrence, distribution, and fate of organic UV filters in coral communities. *Environmental Science and Technology*, 51, 4182–4190. <https://doi.org/10.1021/acs.est.6b05211>
- Tungler, A., Szabados, E., & Hosseini, A.M. (2015). Wet air oxidation of aqueous wastes. In: M. Samer (Ed.), *Wastewater treatment engineering* (1st ed., pp. 153–178). London: IntechOpen.
- Urán-Duque, L., Saldarriaga-Molina, J. C., & Rubio-Clemente, A. (2021). Advanced oxidation processes based on sulfate radicals for wastewater treatment: Research trends. *Water*, 13, 2445. <https://doi.org/10.3390/w13172445>
- Verlicchi, P., Al Aukidy, M., & Zambello, E. (2012). Occurrence of pharmaceutical compounds in urban wastewater: Removal, mass load and environmental risk after a

- secondary treatment—A review. *Science of the Total Environment*, 429, 123–155. <https://doi.org/10.1016/j.scitotenv.2012.04.028>
- Voltaren—Prescribing Information (2022) Novartis Pharmaceuticals Corporation. Retrieved February 10, 2022, from <https://dailymed.nlm.nih.gov/dailymed/archives/fdaDrugInfo.cfm?archiveid=2884>
- Wacławek, S., Lutze, H. V., Grübel, K., Padil, V. V. T., Černík, M., & Dionysiou Dionysios, D. (2017). Chemistry of persulfates in water and wastewater treatment: A review. *Chemical Engineering Journal*, 330, 44–62. <https://doi.org/10.1016/j.cej.2017.07.132>
- Wang, W., Wang, H., Li, G., An, T., Zhao, H., & Wong, P. K. (2019). Catalyst-free activation of persulfate by visible light for water disinfection: Efficiency and mechanisms. *Water Research*, 157, 106–118. <https://doi.org/10.1016/j.watres.2019.03.071>
- Wang, C., Ran, W., Du, P., Li, W., Luo, L., & Wang, D. (2020). Enhanced visible light-driven photocatalytic activities and photoluminescence characteristics of BiOF nanoparticles determined via doping engineering. *Inorganic Chemistry*, 59(16), 11801–11813. <https://doi.org/10.1021/acs.inorgchem.0c01811>
- Wangab, Y., Ma, X., L.H. Liu, B., Li, H., Yin, S., & Sato, T. (2016). Recent advances in visible-light driven photocatalysis. In: E. Norena L & W. JA (Eds.), *Advanced catalytic materials - Photocatalysis and other current trends* (1st ed., pp. 337–357). London: IntechOpen.
- Watts, R. J., Ahmad, M., Hohner, A. K., & Teel, A. L. (2018). Persulfate activation by glucose for in situ chemical oxidation. *Water Research*, 133, 247–254. <https://doi.org/10.1016/j.watres.2018.01.050>
- Wöhler, L., Niebaum, G., Krol, M., & Hoekstra, A. Y. (2020). The grey water footprint of human and veterinary pharmaceuticals. *Water Research X*, 7, 100044. <https://doi.org/10.1016/j.wroa.2020.100044>
- Wright, S. L., & Kelly, F. J. (2017). Plastic and human health: A micro issue? *Environmental Science and Technology*, 51, 6634–6647. <https://doi.org/10.1021/acs.est.7b00423>
- Wu, Q., Wang, S., Thangavel, P., Li, Q., Zheng, H., Bai, J., & Qiu, R. (2011). Phytostabilization potential of *Jatropha curcas* L. in polymetallic acid mine tailings. *International Journal of Phytoremediation*, 13, 788–804. <https://doi.org/10.1080/15226514.2010.525562>
- Wu, Y.-H., Wu, T., & Lin, Y.-W. (2019). Photoelectrocatalytic degradation of methylene blue on cadmium sulfide-sensitized titanium dioxide film. *Materials Research Bulletin*, 118, 110500. <https://doi.org/10.1016/j.materresbull.2019.110500>
- Xia, X., Zhu, F., Li, J., Yang, H., Wei, L., Li, Q., Jiang, J., Zhang, G., & Zhao, Q. (2020). A review study on sulfate-radical-based advanced oxidation processes for domestic/industrial wastewater treatment: Degradation, efficiency, and mechanism. *Frontiers in Chemistry*, 8, 592056. <https://doi.org/10.3389/fchem.2020.592056>
- Xing, B., Shi, C., Zhang, C., Yi, G., Chen, L., Guo, H., Huang, G., & Cao, J. (2016). Preparation of TiO₂/activated carbon composites for photocatalytic degradation of RhB under UV light irradiation. *Journal of Nanomaterials*, 2016, e8393648. <https://doi.org/10.1155/2016/8393648>
- Xu, Y., Ahmed, R., Klein, D., Cap, S., Freedy, K., McDonnell, S., & Zangari, G. (2019). Improving photo-oxidation activity of water by introducing Ti³⁺ in self-ordered TiO₂ nanotube arrays treated with Ar/NH₃. *Journal of Power Sources*, 414, 242–249. <https://doi.org/10.1016/j.jpowsour.2018.12.083>
- Yang, J., Zhu, M., & Dionysiou, D. D. (2021). What is the role of light in persulfate-based advanced oxidation for water treatment? *Water Research*, 189, 116627. <https://doi.org/10.1016/j.watres.2020.116627>
- Zahn, D., Frömel, T., & Knepper, T. P. (2016). Halogenated methanesulfonic acids: A new class of organic micropollutants in the water cycle. *Water Research*, 101, 292–299. <https://doi.org/10.1016/j.watres.2016.05.082>
- Zawadzki, P. (2019). Decolorisation of methylene blue with sodium persulfate activated with visible light in the presence of glucose and sucrose. *Water, Air, and Soil Pollution*, 230, 313–313. <https://doi.org/10.1007/s11270-019-4372-x>
- Zawadzki, P. (2020). TiO₂ modified with organic acids for the decomposition of chlorfenvinphos under the influence of visible light: Activity, performance, adsorption, and kinetics. *Mater*, 13, 289. <https://doi.org/10.3390/ma13020289>
- Zawadzki, P. (2021a). Comparative studies of rhodamine B decolorization in the combined process Na₂S₂O₈/visible light/ultrasound. *Desalination and Water Treatment*, 213, 269–278. <https://doi.org/10.5004/dwt.2021.26694>
- Zawadzki, P. (2021). Eliminacja chlorfenwinfosu z oczyszczonych ścieków komunalnych w procesach zaawansowanego utleniania. *Chemical Review*, 1, 89–91. <https://doi.org/10.15199/62.2021.3.11>
- Zawadzki, P. (2022). Persulfate activation by organic compounds: Advancements and challenges. *Current Opinion in Chemical Engineering*, 37, 100837. <https://doi.org/10.1016/j.coche.2022.100837>
- Zawadzki, P., Kudlek, E., & Dudziak, M. (2020). Titanium(IV) oxide modified with activated carbon and ultrasounds for caffeine photodegradation: Adsorption isotherm and kinetics study. *Journal of Ecological Engineering*, 21, 137–145.
- Zawadzki, P., Kudlek, E., & Dudziak, M. (2021). Influence of the type of photocatalyst on photocatalytic oxidation of triclosan in the aquatic environment. *International Journal of Global Environmental Issues*, 20(1), 1–17. <https://doi.org/10.1504/IJGENVI.2021.120428>
- Zgheib, S., Moillon, R., & Chebbo, G. (2012). Priority pollutants in urban stormwater: Part 1 – Case of separate storm sewers. *Water Research*, 46, 6683–6692. <https://doi.org/10.1016/j.watres.2011.12.012>
- Zhang, Y., Geißen, S.-U., & Gal, C. (2008). Carbamazepine and diclofenac: Removal in wastewater treatment plants and occurrence in water bodies. *Chemosphere*, 73, 1151–1161. <https://doi.org/10.1016/j.chemosphere.2008.07.086>
- Zhang, R., Sun, P., Boyer, T. H., Zhao, L., & Huang, C.-H. (2015). Degradation of pharmaceuticals and metabolite in synthetic human urine by UV, UV/H₂O₂, and UV/PDS. *Environmental Science and Technology*, 49, 3056–3066. <https://doi.org/10.1021/es504799n>

- Zhang, C., Lohwacharin, J., & Takizawa, S. (2017). Properties of residual titanium dioxide nanoparticles after extended periods of mixing and settling in synthetic and natural waters. *Science and Reports*, 7, 9943. <https://doi.org/10.1038/s41598-017-09699-9>
- Zhang, Y., Zhou, J., Chen, J., Feng, X., & Cai, W. (2020). Rapid degradation of tetracycline hydrochloride by heterogeneous photocatalysis coupling persulfate oxidation with MIL-53(Fe) under visible light irradiation. *Journal of Hazardous Materials*, 392, 122315. <https://doi.org/10.1016/j.jhazmat.2020.122315>
- Zhang, J., Tian, B., Wang, L., Xing, M., & Lei, J. (2018). Mechanism of Photocatalysis. In: J. Zhang, B. Tian, L. Wang, M. Xing & J. Lei (Eds.), *Photocatalysis fundamentals, materials and applications* (1st ed., pp. 1–15). Singapore: Springer.
- Zhao, J., Ge, S., Pan, D., Pan, Y., Murugadoss, V., Li, R., Xie, W., Lu, Y., Wu, T., Wujcik, E. K., Shao, Q., Mai, X., & Guo, Z. (2019). Microwave hydrothermal synthesis of In₂O₃-ZnO nanocomposites and their enhanced photoelectrochemical properties. *Journal of the Electrochemical Society*, 166, H3074–H3083. <https://doi.org/10.1149/2.0071905jes>
- Zhong, S., Xi, Y., Chen, Q., Chen, J., & Bai, S. (2020). Bridge engineering in photocatalysis and photoelectrocatalysis. *Nanoscale*, 12, 5764–5791. <https://doi.org/10.1039/C9NR10511E>
- Zhou, Z., Liu, X., Sun, K., Lin, C., Ma, J., He, M., & Ouyang, W. (2019). Persulfate-based advanced oxidation processes (AOPs) for organic-contaminated soil remediation: A review. *Chemical Engineering Journal*, 372, 836–851. <https://doi.org/10.1016/j.cej.2019.04.213>
- Zhou, L., Zhao, Q., Yang, X., Ferronato, C., Chovelon, J.-M., Sleiman, M., & Richard, C. (2020). Sulfate radical mediated degradation of 5-halogenosalicylic acids: Phenoxy radical transformation pathways. *Chemical Engineering Journal*, 394, 124839. <https://doi.org/10.1016/j.cej.2020.124839>
- Zhu, S., Li, X., Kang, J., Duan, X., & Wang, S. (2019). Persulfate activation on crystallographic manganese oxides: Mechanism of singlet oxygen evolution for non-radical selective degradation of aqueous contaminants. *Environmental Science and Technology*, 53, 307–315. <https://doi.org/10.1021/acs.est.8b04669>
- Ziarati Saravani, A., Nadimi, M., Aroon, M. A., & Ebrahimi Pirbazari, A. (2019). Magnetic TiO₂/NiFe₂O₄/reduced graphene oxide nanocomposite as a recyclable photocatalyst for photocatalytic removal of methylene blue under visible light. *Journal of Alloys and Compounds*, 803, 291–306. <https://doi.org/10.1016/j.jallcom.2019.06.245>
- Ziembowicz, S., Kida, M., & Koszelnik, P. (2017). Sonochemical Formation of Hydrogen Peroxide. *Proceedings*, 2, 188. <https://doi.org/10.3390/ecws-2-04957>
- Zorita, S., Mårtensson, L., & Mathiasson, L. (2009). Occurrence and removal of pharmaceuticals in a municipal sewage treatment system in the south of Sweden. *Science of the Total Environment*, 407, 2760–2770. <https://doi.org/10.1016/j.scitotenv.2008.12.030>
- Zotoso, J. P., Cossich, E. S., Janeiro, V., & Tavares, C. R. G. (2017). Treatment of hospital laundry wastewater by UV/H₂O₂ process. *Environmental Science and Pollution Research International*, 24, 6278–6287. <https://doi.org/10.1007/s11356-016-6860-5>
- Zou, F., Hu, J., Miao, W., Shen, Y., Ding, J., & Jing, X. (2020). Synthesis and characterization of enhanced photocatalytic activity with Li⁺-doping nanosized TiO₂ catalyst. *ACS Omega*, 5, 28510–28516. <https://doi.org/10.1021/acsomega.0c03054>
- Zou, L., Wang, Y., Huang, C., Li, B., Lyu, J., Wang, S., Lu, H., & Li, J. (2021). Meta-cresol degradation by persulfate through UV/O₃ synergistic activation: Contribution of free radicals and degradation pathway. *Science of the Total Environment*, 754, 142219. <https://doi.org/10.1016/j.scitotenv.2020.142219>
- Zrinyi, N., & Pham, A.L.-T. (2017). Oxidation of benzoic acid by heat-activated persulfate: Effect of temperature on transformation pathway and product distribution. *Water Research*, 120, 43–51. <https://doi.org/10.1016/j.watres.2017.04.066>

Publisher's Note Springer Nature remains neutral with regard to jurisdictional claims in published maps and institutional affiliations.



Persulfates to degrade a mixture of dyes (rhodamine B, methylene blue) in the presence of glucose and visible light

Piotr Zawadzki

Laboratory of Water and Sewage Technologies, Department of Water Protection, Central Mining Institute, Plac Gwarków 1, 40-166 Katowice, Poland, Tel.: 0048 32 259-28-01; email: pzawadzki@gig.eu

Received 2 June 2022; Accepted 21 December 2022

ABSTRACT

A treatment process utilizing visible-light-activated (Vis) persulfates (PS) in the presence of an organic promoter (glucose) was developed for the simultaneous decolorization of a rhodamine B (RhB) and methylene blue (MB) mixture. Various doses of glucose, PS concentrations, pH values, initial dye concentrations and process time were tested to find out the most appropriate parameters for degrading the RhB/MB mixture in the PS/Vis/Glucose process. Under optimal conditions ($C_{0[\text{RhB/MB}]} = 5$ ppm; pH = 4; glucose dosage = 230 mM; PS concentration = 30 mM; time = 120 min), the degradation of MB and RhB in the mixture was set to 87.8% and 54.7%. The degradation process followed the pseudo-first-order kinetic model with the correlation coefficient $R^2 = 97\%–99\%$. The PS/Vis/Glucose process is more economical than other existing studies and technologies. The energy efficiency at the optimal conditions were 1.2 and 2.1 kWh m⁻³ for RhB and MB, respectively. The domination of MB degradation over RhB was confirmed and found to appear as a result of the different physico-chemical properties of the dyes and their state of charge, which enables the direct transfer of electrons from the dyes to the PS and leads to the decolorization of the dyes. This work provides an important source of information on the parameters influencing the simultaneous degradation of mixtures of dyes (rhodamine B, methylene blue). The experimental results showed that the PS/Vis/Glucose process may have a positive role in treating color solution mixtures with various dye concentrations (1–20 ppm).

Keywords: Rhodamine B; Methylene Blue; Advanced oxidation process; Sodium persulfate; Glucose; Visible light

1. Introduction

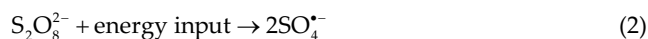
Industrial wastewater contains a broad range of various chemical compounds that can be by-products of conducted technical processes (e.g. dyes, phenols, pesticides, heavy metals). The textile, chemical, food and tanning industries generate the greatest quantities of industrial wastewater containing synthetic dyes such as methylene blue (MB) and rhodamine B (RhB) [1]. MB and RhB are heterocyclic dyes that find broad application in the industry; however, they contribute to significant environmental problems due to their high toxicity and accumulation in the environment.

Methylene blue belongs to the azo dye group. Azo dyes are histamine-releasing agents, therefore exposure to them may result, for example, in urticaria or intensified symptoms of asthma as well as uterine contractions in pregnant women, leading to miscarriage [2]. Rhodamine B is used in the chemical, textile, paper and paint industries. The negative influence of RhB on humans and animals manifests itself as skin, eye and respiratory system irritation. RhB also exhibits potential mutagenic and carcinogenic effects [3].

Due to their hazardous influence on humans and high resistance to biodegradation, it is necessary to develop a technology for eliminating dyes from water and wastewater.

Several dyes treatment methods have been developed, including physical (membrane processes, adsorption) [4,5], chemical (ozonation, chlorination) [6,7] and biological processes (aerobic, anaerobic, microbial biosorbents) [8,9] as well as combined methods (e.g., physical and chemical) [10]. The currently applied methods do not come without a drawback. For example, physical methods do not eliminate the hazard, but rather usually transfer it into a different phase (e.g., concentrate in membrane processes). On the other hand, biological methods are sensitive to high pollutant concentrations and wastewater composition variations.

Advanced oxidation processes (AOPs) are an interesting alternative to conventional treatment methods. A common feature of AOPs is the chemical reaction between oxidative radicals and organic pollutants. In recent years, significant attention has been devoted to sulfate radicals ($\text{SO}_4^{\bullet-}$) [11]. The radical precursor of $\text{SO}_4^{\bullet-}$ (persulfate (PS)) requires activation to generate sulfate radicals. The chemical structure of PS is $[\text{O}_3\text{S}-\text{O}-\text{O}-\text{SO}_3]^{2-}$. The essence of the persulfate activation mechanism is the excitation of PS, the break of the $-\text{O}-\text{O}-$ bond and the production of $\text{SO}_4^{\bullet-}$ radical with a high oxidative potential ($E^0 = 2.6\text{--}3.1\text{V}$) [12,13]. The persulfate requires activation. PS activation is often carried out by expensive, energy-consuming and complex activation methods, for example, by UV radiation, base activation ($\text{pH} > 11$), thermal methods, and low oxidation transition metal ions (e.g., Fe^0 , Fe^{2+} , Ag^+ , Co^{2+} , Cu^{2+}). Activation via transition metal ions generates a single sulfate radical [Eq. (1)]. Activation by UV or heat results in the production of two sulfate radicals [Eq. (2)].



The disadvantage of activation by UV radiation is the power of the used lamps, which often exceeds 100 W, and sometimes even 400 W [14]. Base activation requires large amounts of chemical reagents due to the high pH, then decrease of the pH to a value that is required under the applicable regulations. On the other hand, disadvantages of activation via transition metal ions include the cost of the reagents as well as iron sludge generation due to the application of ferrous ions.

A simple and economic method of activation is the combination of PS activation processes in the presence of glucose and visible light (Vis). First of all, visible light is a free source of energy. The cost of electricity in the industrial and municipal facilities (wastewater treatment plant) is one of the primary factors determining the cost-effectiveness of investments and the treatment costs of 1 m³ of wastewater. Then, glucose is an organic activator of PS, and its price might be even twice lower compared, for example, to $\text{FeSO}_4 \cdot 7\text{H}_2\text{O}$, which finds common application in PS activation. Therefore, organic promoters such as glucose decrease the operational costs, shorten the reaction time and increase the degradation efficiency [15].

Most research that assesses novel technologies evaluates the process efficiency based on a single dye [16–21]. There are few studies dedicated to the simultaneous degradation of mixtures of various compounds [22–24]. This is significant

because dyes are typically found in colored mixtures. The presence of various dyes can both intensify or weaken the pollutant degradation process. Therefore, this study presents an evaluation of the PS/Vis/Glucose process efficiency based on the simultaneous degradation of two dyes: rhodamine B and methylene blue.

The novelty of the present work lies in its simplicity by which a mixture of dyes can be degraded using non-toxic, pro-environmental reagents (glucose) and low-cost solar energy (visible light) with higher process efficiency. The dye mixture decolorization experiments with the use of PS in this study were conducted using various environmental parameters, such as different doses of glucose, PS concentrations, pH values, initial dye concentrations and process time, to find out the most appropriate parameters for degrading RhB/MB in the presence of visible light. The paper would acquaint the readers to the important source of information on the parameters influencing the simultaneous degradation of mixtures of dyes (rhodamine B, methylene blue). The novelty in the paper includes an attempt to explain the mechanism of interaction between two dyes: rhodamine B and methylene blue in mixture, proving to be a knowledge pool and helping the researchers working in the similar field to design appropriate treatment plans for real textile wastewater.

2. Materials and methods

2.1. Dyes

Rhodamine B with a purity $\geq 95.0\%$ and methylene blue with a purity $\geq 97.0\%$ were provided by Sigma-Aldrich (Poznań, Poland). The model solutions were prepared based on deionized water as well as RhB and MB standard additions. The structures of the used dyes are presented in Fig. 1.

2.2. Analyses

The decolorization effect was assessed via absorbance measurement by Jasco V-750 spectrophotometer (Kraków, Poland) over a range of 400 to 800 nm. Fig. 2 presents the absorption spectra obtained for a RhB/MB mixture with an initial concentration of 1 ppm. The RhB absorption spectrum exhibits a maximum peak at $\lambda_{\text{max}} = 554$ nm. The MB absorption spectrum exhibits a maximum peak at $\lambda_{\text{max}} = 665$ nm.

The degree of dye mixture decolorization was determined based on characteristic absorption peaks at 554 nm (RhB) and 665 nm (MB). In order to determine the decolorization efficiency, the absorption was measured before and after AOPs, as shown in Eq. (3), where: C_0 – initial concentration, C_t – concentration at time t .

$$\text{Decolorization efficiency (\%)} = \frac{C_0 - C_t}{C_0} \quad (3)$$

2.3. Experimental procedure

2.3.1. Source of visible light

A 10 W tungsten lamp emitting visible light (400–2,200 nm), model QTH10/M (Thorlabs Inc., USA), was

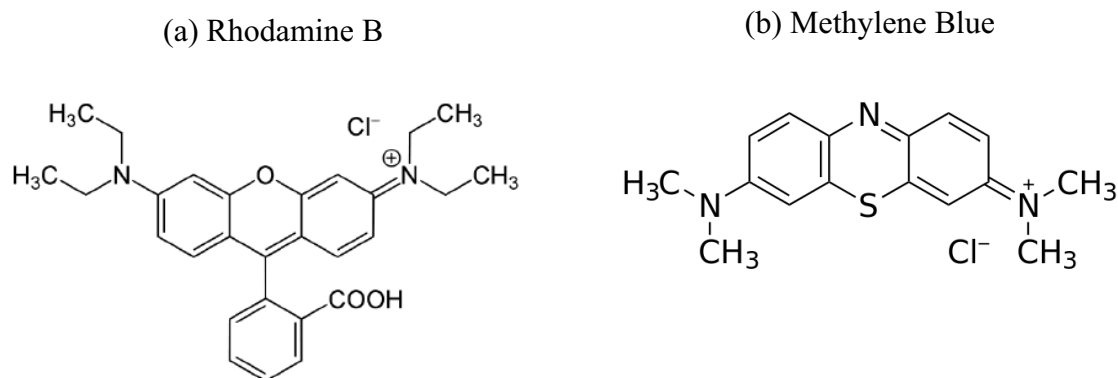


Fig. 1. Structure of Rhodamine B (a) and structure of Methylene Blue (b).

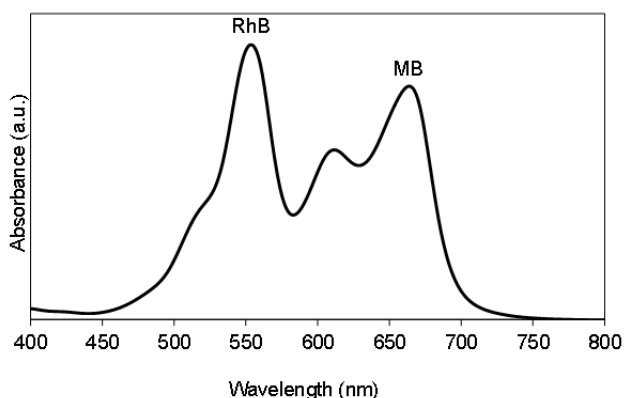


Fig. 2. Absorption spectrum of rhodamine B and methylene blue mixtures.

used for the dye mixture degradation tests. A FGS900M filter (Thorlabs Inc., USA) was applied to cut off the spectrum bands above 710 nm. All the experiments were conducted in vessels with a volume of 0.2 dm³, without the possibility of exposure to additional light sources.

2.3.2. Effect of glucose and PS

The influence of the initial glucose dosage and the initial PS concentration were examined. The following parameters were constant: RhB/MB concentration ($C_{0[\text{RhB/MB}]}$) = 1 ppm, time = 70 min, pH = 6, room temperature. The influence of the initial glucose dosage was examined at a PS concentration = 20 mM and various doses of glucose: 140, 170, 200, 230, 260 and 290 mM. The influence of the initial PS concentration was examined at a glucose concentration = 230 mM and various PS concentrations: 15, 20, 25, 30, 35 and 40 mM.

2.3.3. Effect of pH

The influence of the initial pH of the aqueous solution was studied. The following parameters were constant: $C_{0[\text{RhB/MB}]}$ = 1 ppm, time = 70 min, room temperature, dose of glucose = 230 mM, PS concentration = 30 mM. The solutions were corrected to pH values of 4, 5, 6, 7, 8, 9 and 10. The pH was corrected with 0.1 mol dm^{−3} HCl or 0.1 mol dm^{−3} NaOH

provided by Sigma-Aldrich. The pH of the model solution was measured using an Elmetron CPC-511 pH meter (Zabrze, Poland).

2.3.4. Effect of dyes concentration

The influence of the initial RhB/MB concentration was also examined. The following parameters were constant: time = 70 min, room temperature, dose of glucose = 230 mM, PS concentration = 30 mM, pH = 6. The following dye concentrations were tested: 1, 5, 10, 15 and 20 ppm.

All the experiments were conducted independently and repeated in triplicate, similarly to other studies involving persulfates [25]. The data presented in the next sections include average values.

2.4. Reaction kinetics

A pseudo-first-order kinetic model [Eq. (4)] was used to describe the kinetics, similarly to the study [26].

$$-\ln\left(\frac{C}{C_0}\right) = kt \quad (4)$$

where C_0 – RhB/MB concentration before the treatment process (ppm); C – RhB/MB concentration after the treatment process (ppm); k – reaction rate constant (−); t – reaction time (min).

2.5. Energy consumption

Electricity consumption is one of the essential criteria in the water and wastewater treatment process. To compare the cost of the current study with other existing studies and technologies, electricity consumption was estimated based on the electric energy per order indicator (E_{EO}). For the electrochemical degradation processes, the energy efficiency (E_{EO}), expressed as kWh m^{−3} of treated solution, was calculated based on the anode surface area (S , cm²), the applied current density (i , mA cm^{−2}), the applied average voltage (U , V), and the reaction volume (V , dm³), as shown in Eq. (5) [27].

$$E_{\text{EO}} (\text{kWh m}^{-3}) = \frac{S \cdot i \cdot U}{(t/V) \cdot 1000} \quad (5)$$

For the photochemical degradation, the E_{EO} was calculated with the following equation [Eq. (6)] [28,29]:

$$E_{EO} (\text{kWh m}^{-3}) = \frac{P \cdot t \cdot 1,000}{\log[C_0 / C_t] \cdot V \cdot 60} \quad (6)$$

where P – the electrical power consumed by lamp (kW); t – the process time (h); C_0 – the initial concentration of the dye (ppm); C_t – the concentration of the dye after t (ppm); V – the reaction volume (dm^{-3}).

3. Results and discussion

3.1. Effect of glucose dose on degradation of dyes mixture

As shown in Fig. 3, increasing the glucose dosage results in higher dye mixture decolorization efficiency. For further experiments, a concentration of 230 mM was selected as the optimal dose of glucose. Under optimal conditions, the decolorization degree was the highest for RhB (43.8%). Exceeding a dose of 200 mM did not result in a significant effect of MB removal. Therefore, due to the weaker decolorization effect in the case of RhB, the 230 mM dose was considered to be the most effective.

To increase the persulfate activity in visible light, sugars (e.g., glucose, sucrose) are used in the decolorization technology [30,31]. For example, glucose is an optically active substance and a donor of electrons that may activate PS. The mechanism of activation by glucose is similar to activation by phenoxides. The electron from glucose is transferred to the persulfate and activates it. On the other hand, glucose could be oxidized into products that may activate the persulfate. This is connected to organic PS activation through an external carbon source [32]. Lower doses of glucose showed unsatisfactory decolorization effect. Higher doses inhibited the decolorization effect since the glucose is also used as a free radical scavenger ($k_{OH^\cdot} = 1.5 \times 10^9$) [33].

3.2. Effect of PS dose on degradation of dyes mixture

Similarly to glucose, the PS concentration has a significant influence on the RhB/MB degradation. Therefore the influence of initial PS concentrations on the decolorization

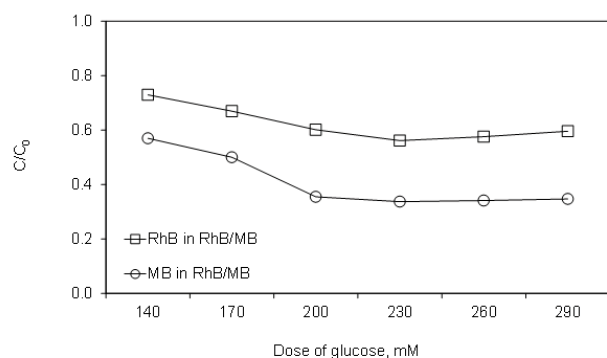


Fig. 3. The dyes mixtures decolorization effect at different glucose dose. Experimental conditions: $C_{0[\text{RhB/MB}]} = 1$ ppm; pH = 6; reaction time = 70 min; PS concentration = 20 mM.

efficiency was studied as well. Fig. 4 demonstrates that after 70 min, the initial dye mixture concentration was reduced by a range of about 12%–38% in (RhB) and by about 38% to 67% (MB). Under the operating conditions, the greatest decolorization effect for both dyes was achieved at a PS concentration of 30 mM. Similarly to the study [26], the PS concentration above 30 mM resulted in lower methylene blue decolorization efficiency. This phenomenon also occurs in the case of photocatalytic processes. Mahanthappa et al. [34] studied the influence of a different doses of the CuS-CdS catalyst ($40\text{--}240 \text{ mg dm}^{-3}$). The level of methylene blue removal ranged from 40% to nearly 100%. The highest removal degree was observed at a dose of 200 mg L^{-1} (almost 100%). Higher doses of the catalyst most likely result in nanoparticle aggregation and faster sedimentation. In this study, higher PS concentration resulted in a higher density of the generated oxidative components. After exceeding the optimal PS concentration (30 mM), the decolorization efficiency decreased, most likely due to the reaction between the sulfate anion and hydroxyl radicals [35] [Eqs. (7) and (8)].



3.3. Effect of different RhB and MB concentrations

This study shows that increasing concentrations of the dye molecules disrupt the process in which free radicals are involved. Fig. 5 confirms that the effect of the RhB/MB decolorization depends on the dye concentration. Increasing the concentration from 1 to 20 ppm resulted in a nearly twofold decrease in the decolorization efficiency. Bagherzadeh et al. [36] studied the influence of the initial MB concentration on the degradation efficiency. With the increasing MB concentration from 10 to 20 mg L^{-1} , a decrease in the degradation rate from 92% to 73% was observed. As the concentration increases, the oxidative radical consumption becomes greater, whereas the likelihood of a collision between the oxidative radicals and the dye molecules decreases. Han et al. [37] also investigated the influence of the MB concentration on the final decolorization effect and confirmed that

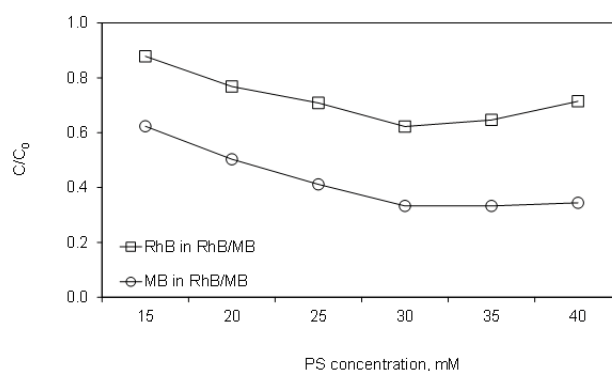


Fig. 4. The dyes mixtures decolorization effect at different PS concentration. Experimental conditions: $C_{0[\text{RhB/MB}]} = 1$ ppm; pH = 6; reaction time = 70 min; glucose dose = 230 mM.

higher dye concentrations inhibit radical reactions with the dye molecules. Chen et al. [38] also proved this relationship for RhB. Furthermore, a high molecule concentration can result in effects of competition between the dye molecules, reaction products and generated radicals.

3.4. Effect of pH on degradation of dyes mixture

The pH significantly influences the direction of radical generation, and consequently on the degradation rate. Fig. 6 shows the decolorization rate at various pH. After 70 min, the maximum decolorization efficiency of 64% and 83% for RhB and MB, respectively was achieved at pH = 4. At higher pH (6), the decolorization efficiency decreased to about 38% (RhB) and 62% (MB). At pH = 10, the decolorization efficiency decreased to about 21% (RhB) and 41% (MB). This is a result of the participation of various oxidative radical forms depending on pH. Sulfate radicals dominate at pH < 7, whereas an increase in pH results in the generation of hydroxyl radicals (OH^\cdot concentration > 10^{-7}). Thus, the removal efficiency decreases due to the scavenging of the $\text{SO}_4^{\cdot-}$ radicals by OH^\cdot [39]. Similar conclusions were presented by Oliveros et al. [40].

The degradation of methylene blue was more effective than rhodamine B. MB is a cationic dye at a pH range

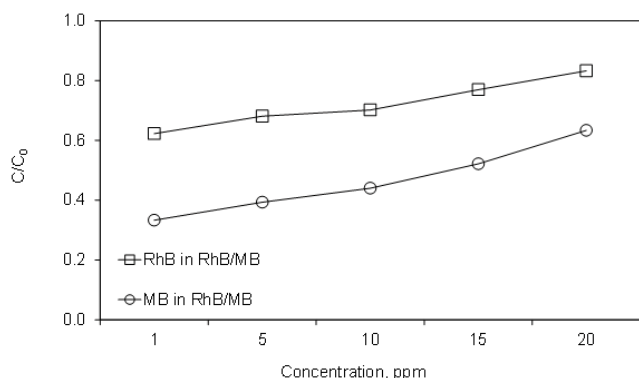


Fig. 5. Influence of different RhB and MB concentration on the decolorization effect. Experimental conditions: pH = 6; reaction time = 70 min; glucose dose = 230 ppm; PS concentration = 30 mM.

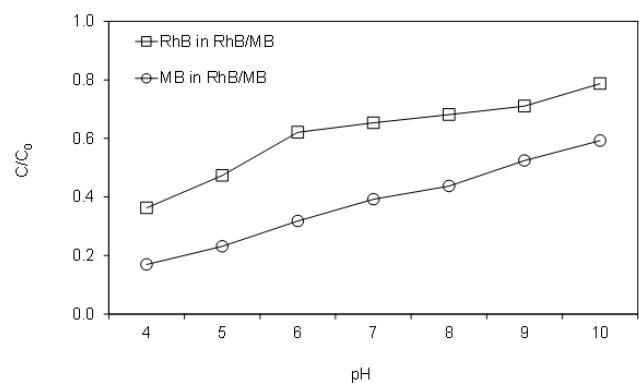


Fig. 6. RhB and MB decolorization effect at different pH. Experimental conditions: $C_{0[\text{RhB/MB}]}$ = 1 ppm; reaction time = 70 min; glucose dose = 230 ppm; PS concentration = 30 mM.

of 1.7–8.0 [41,42], whereas RhB has two molecular forms (cationic and zwitterionic) [43]. This means that a dissociated RhB molecule transfers charges from positive to neutral together with the increase in pH. Therefore a likely reason for this phenomenon may be found in the dyes' state of charge at various pH. It may result in the direct transfer of electrons from the dyes to the PS, which in turn is responsible for the dye decolorization. Sodium persulfate (a source of $\text{SO}_4^{\cdot-}$ radicals) dissociates to generate $\text{S}_2\text{O}_8^{2-}$ ion with two negative charges. MB may dissociate cations that bond with electronegative substances in an aquatic solution. Therefore the decolorization rate was higher for MB and lower for RhB [44,45]. For this reason, it is recommended to apply a pH value of 4 for the decolorization of the RhB/MB mixture in the PS/Vis/glucose process.

3.5. Degradation kinetics and efficiency

The effectiveness of the PS/Vis/Glucose technology was demonstrated by performing a degradation test for single dye (RhB and MB separately) and a dye mixture (RhB/MB). The degradation experiments were carried out at a concentration of 5 ppm, since the PS/Vis/Glucose technology was designed for this concentration range. The decolorization tests were performed under optimal conditions: pH = 4; glucose dosage = 230 mM; PS concentration = 30 mM. The process was carried out for 120 min. Fig. 7 shows the influence of time on the degree of RhB, MB and RhB/MB mixture decolorization. The decolorization degree increased together with the process duration. For example, after 20 min of the reaction, the efficiency was set to 13.1%, 44.9%, 28.3% and 10.2%, respectively for RhB (alone), MB (alone), and MB and RhB in a mixture. A satisfactory decolorization degree was obtained after 120 min. The efficiency was set to 62.8%, 95.6%, 87.8% and 54.7%, respectively for RhB (alone), MB (alone), and MB and RhB in a mixture.

As the degradation proceeds, sulfate radicals generate (Eq. (9)). Persulfate activation is the result of a synergistic reaction between the visible light and the intensified effect of electron transfer from the glucose to the persulfate. Glucose tends to rotate the plane-polarized light and is active in visible light. Glucose is also an electron donor in the PS/Vis system. It is very strongly soluble in water and facilitates

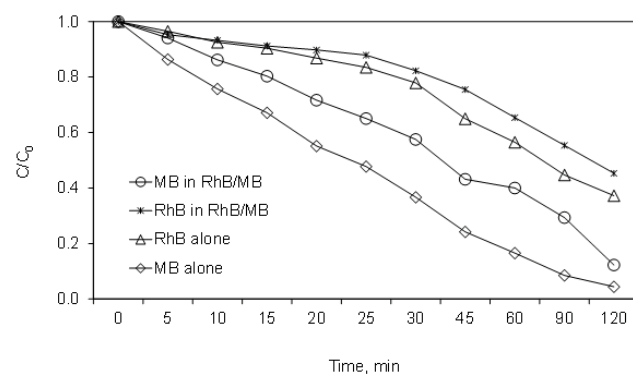
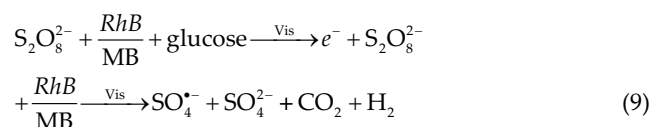


Fig. 7. Decolorization effect (C/C_0) of the RhB, MB and RhB/MB mixture. Experimental conditions: $C_{0[\text{RhB/MB}]}$ = 5 ppm; pH = 4; glucose dose = 230 mM; PS concentration = 30 mM.

persulfate activation, as its functional groups (e.g., the carbonyl group) partially receive the negative charge.



Furthermore, under operating conditions, sulfate radicals dominate at pH = 4 [39]. Sulfate ions and free hydroxyl radicals are generated as a result of the reaction of free sulfate radicals with hydroxyl ions [Eq. (10)].



Significant differences in decolorization efficiency were observed between RhB, MB and the RhB/MB mixture. It was found that the degradation efficiency was greater both in the case of the single MB dye and the RhB/MB solution compared to the RhB degradation. Furthermore, the RhB/MB degradation rate was higher than in the case of RhB, which was also confirmed by Sharma and Khare [46].

One of the possible reasons for this may be the physico-chemical characteristics of the dyes. At 25°C, RhB is less soluble in water than MB (MB = 43.6 g dm⁻³ vs RhB = 10 g dm⁻³). On the other hand, Rani et al. [47] concluded that the effective degradation of RhB requires a more basic solution compared to MB when applying catalysts such as ZnO₂.

Another reason may also arise from the lower Vis radiation absorption of the RhB dye. The Vis radiation intensity is sufficient to achieve a more significant PS activation and oxidation of MB compared to RhB [48].

The degradation of the RhB and MB mixture in the PS/Vis/Glucose process results from chemical reactions. It is briefly presented in Fig. 8. The absorbance intensity decreased during the time duration of the experiment with PS/Vis/Glucose. The primary rhodamine B degradation mechanism include the N-deethylation process, chromophore cleavage and ring opening, which result in the generation of oxidation products with smaller molecule sizes [49–51]. In turn, Mostafa Mahdavianpour et al. [52] suggested that the degradation of azo bonds is a possible mechanism of MB decolorization. On the other hand, Yang et al. [41] proposed a similar mechanism consisting of the initial formation of a complex between MB ions and a S₂O₈²⁻ ion as a result of electrostatic attraction. Afterward, this may lead to a direct transfer of electrons from MB to the PS, which is most likely the phenomenon responsible for the decolorization of methylene blue.

The decolorization rate constant is presented in Fig. 9. The correlation coefficient R² showed a very good fit of experimental data (R² = 97%–99%). Considering the low concentration of the organic molecule, the dye decolorization followed the pseudo-first-order kinetic model, as also shown in [53–55]. The mathematically calculated half-life (t/2) was set to 79.7, 26.1, 103.5 and 42.5 min, respectively for RhB (alone), MB (alone), RhB in RhB/MB and MB in RhB/MB.

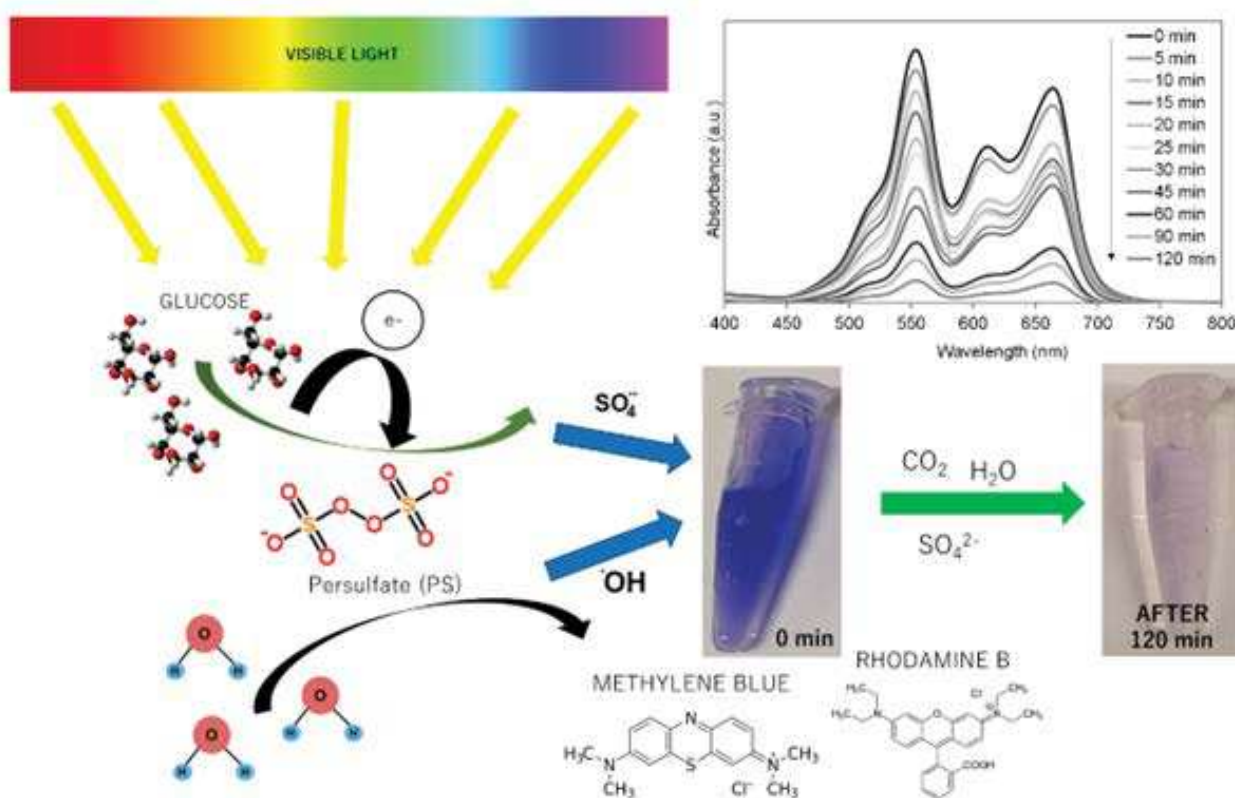


Fig. 8. Proposed summary of visible-light activation of persulfate for RhB/MB decolorization.

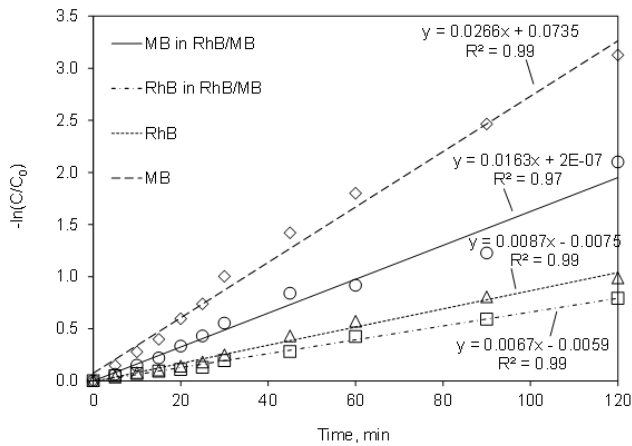


Fig. 9. Kinetic constants of the RhB, MB and RhB/MB decolorization. Conditions: $C_{0[\text{RhB/MB}]} = 5$ ppm; pH = 4; glucose dose = 230 mM; PS concentration = 30 mM.

4. Comparison with other AOPs systems

The proposed decolorization method (PS/Vis/Glucose) is a promising treatment technology for dye mixtures with concentrations of up to about 5 ppm. As presented in Table 1, the proposed technology is an interesting alternative to other methods that are commonly used to remove dyes. After 120 min of decolorization by PS/Vis/Glucose, the degradation of MB and RhB in a dye mixture was set to 87.8% and 54.7%. This time was shorter than [56], where 97.7% of RhB was removed after 180 min of reaction time. In the PS/Vis/Glucose process it is also possible to achieve a higher decolorization effect over a shorter process, time compared to the study [57], where 51% of RhB was removed after 180 min. A very important advantage of the PS/Vis/Glucose process is low energy consumption since a low-power radiation source (10 W) was used. Rokesh et al. [58] achieved 60% of RhB decolorization despite using a lamp with a power of 300W. The proposed technology is also waste-free, compared to [59], which

Table 1
Efficiency of Rhodamine B and Methylene Blue degradation in different AOPs

Process	Target pollutant	Conditions	Removal efficiency [%]	E_{EO} [kWh m ⁻³]	References
PS/Vis/Glucose	Rhodamine B	$C_{0[\text{RhB}]} = 1$ ppm Time = 70 min PS dose = 30 mM Glucose dose = 230 ppm Lamp power = 10W Reaction volume = 0.2 dm ⁻³	64	2.1	This study
PS/Vis/Glucose	Methylene Blue	$C_{0[\text{MB}]} = 1$ ppm Time = 70 min PS dose = 30 mM Glucose dose = 230 ppm Lamp power = 10W Reaction volume = 0.2 dm ⁻³	83	1.2	This study
PS/Vis/Glucose	Methylene Blue	$C_{0[\text{MB}]} = 2$ ppm Time = 90 min PS dose = 0.065 mM Glucose dose = 100 ppm Lamp power = 10W Reaction volume = 0.1 dm ⁻³	65	4.8	[15]
PS/Vis/Ultrasound	Rhodamine B	$C_{0[\text{RhB}]} = 10$ ppm Time = 60 min PS dose = 20 mM Glucose dose = 200 ppm Lamp power = 10W pH = 6.0 Reaction volume = 0.5 dm ⁻³ T = 295 K	85	0.4	[51]
Ti/SnO ₂ -Sb electrode	Rhodamine B	$C_{0[\text{RhB}]} = 50$ ppm pH = 3.0 Time = 20 min Current density = 20 mA/cm ² Applied average voltage = 8.9 V Na ₂ SO ₄ = 10 mmol/L Reaction volume = 0.03 dm ⁻³	97.8	80.1	[27]

Table 1 (Continued)

Table 1

Process	Target pollutant	Conditions	Removal efficiency [%]	E_{EO} [kWh m ⁻³]	References
Peroxide assisted photocatalytic degradation in the presence of ZnO	Rhodamine B	$C_{0[RhB]} = 5$ ppm Time = 90 min ZnO = 500 ppm Reaction volume = 0.05 dm ⁻³ Lamp power = 300W	60	326.7	[58]
Photo-Fenton processes	Methylene Blue/ Brilliant Green/ Eosin Yellow	$C_{0[dyes]} = 1$ ppm Time = 60 min pH = 3 Fe ²⁺ = 4.5 ppm H ₂ O ₂ = 13.06 mM Lamp power = 160 W Reaction volume = 0.25 dm ⁻³ Temperature = 25°C	80	15,3	[53]
Electro-Fenton	Rhodamine B	$C_{0[RhB]} = 10$ ppm pH = 2 Time = 180 min Electrode dose = 15 ppm Voltage = 8 V	97.7	n.d.	[56]
UV-LED/TiO ₂	Rhodamine B	$C_{0[RhB]} = 49$ ppm Time = 180 min pH = 3.05 TiO ₂ = 1.6 g dm ⁻³ Lamp = 5 × LED Luminous intensity = 350 mcd Radiant flux = 10–12 mW at 20 mA	51	n.d.	[57]
Fe(0)-based Fenton process with H ₂ O ₂	Rhodamine B	$C_{0[RhB]} = 49$ mg/L Time = 30 min pH = 4 Fe(0) = 1 g/L H ₂ O ₂ = 2 mM	100	n.d.	[59]
Electrochemical degradation in the presence of sulphate ions	Methylene Blue	$C_{0[MB]} = 21$ ppm Time = 180 min Room temperature Sulphate ions concentration = 0.1 ppm	73	n.d.	[60]

n.d. – no data

utilized the Fenton reagent. The main disadvantages of the Fenton reagent are the relatively high cost of H₂O₂ and the formation of iron sludge. As shown in Table 1, it can be seen, the PS/Vis/Glucose process is more economical than other existing studies and technologies. The energy efficiency at the optimal conditions were 1.2 and 2.1 kWh m⁻³ for RhB and MB, respectively. However, it should be noted that the calculated values refer only to the conversion of UV radiation. For detailed calculations, other parameters such as electricity consumption of ozone generator, chemical consumption, mixing, and other factors should be considered.

5. Conclusions

The study presented an evaluation of the PS/Vis/Glucose process efficiency based on the degradation of two dyes:

rhodamine B and methylene blue. The simultaneous degradation of dyes dissolved in an aquatic solution was investigated. The dye degradation process was modelled by testing the influence of various process parameters (different doses of glucose, PS concentrations, pH, initial dye concentrations, process durations) to find out the most optimal conditions for RhB/MB degradation in the presence of visible light and an organic promoter (glucose). Under optimal conditions ($C_{0[RhB/MB]} = 5$ ppm; pH = 4; glucose dosage = 230 mM; PS concentration = 30 mM; time = 120 min), the degradation of MB and RhB in the mixture was 87.8% and 54.7%. The dye degradation followed the pseudo-first-order kinetic model with the correlation coefficient $R^2 = 97\%–99\%$. PS/Vis/Glucose process was also the most effective process from the economic point of view comparing to other existing studies and technologies. The reaction kinetics analysis

demonstrated the dominance of MB over RhB. The most likely reason for this are the different physicochemical properties of the dyes and their state of charge. Methylene blue is a cationic dye, whereas RhB has cationic and zwitterionic forms. RhB degradation is initiated by processes of N-deethylation, chromophore cleavage and ring opening, which result in the generation of oxidation products with smaller molecule sizes. Methylene blue decolorization most likely occurs as a result of the bonding of MB ions with $S_2O_8^{2-}$ by electrostatic attraction and the subsequent transfer of electrons from MB to the PS. The designed technology is an interesting alternative for dye decolorization compared to other methods presented in literature. Particular advantages of the process include its high dye degradation, low energy consumption and lack of sludge generation.

6. Funding sources

The presented study was performed in the framework of the research work in the Central Mining Institute in Poland, financially supported by the Polish Ministry of Science and Higher Education [No. 11131032-340].

References

- [1] S. Khamparia, D. Jaspal, Technologies for Treatment of Colored Wastewater from Different Industries, C. Hussain, Ed., Handbook of Environmental Materials Management, Springer, Cham, 2018, pp. 1–14. Available at: https://doi.org/10.1007/978-3-319-58538-3_8-1
- [2] A. Lisiak, M. Miklas, Problem of harmfulness of azo-dyes, *Przełąd Włókienniczy - Włókno, Odzież, Skóra*, nr 3 (2007) 38–40.
- [3] S. Hoenke, I. Serbian, H.-P. Deigner, R. Csuk, Mitocanic di- and triterpenoid Rhodamine B conjugates, *Molecules*, 25 (2020) 5443, doi: 10.3390/molecules25225443.
- [4] W. Chen, J. Mo, X. Du, Z. Zhang, W. Zhang, Biomimetic dynamic membrane for aquatic dye removal, *Water Res.*, 151 (2019) 243–251.
- [5] A.H. Jawad, A.S. Abdulhameed, M.S. Mastuli, Acid-factonized biomass material for methylene blue dye removal: a comprehensive adsorption and mechanism study, *J. Taibah Univ. Sci.*, 14 (2020) 305–313.
- [6] J.A. Malvestiti, E. Fagnani, D. Simão, R.F. Dantas, Optimization of UV/H₂O₂ and ozone wastewater treatment by the experimental design methodology, *Environ. Technol.*, 40 (2019) 1910–1922.
- [7] W. Zhang, W. Lv, X. Li, J. Yao, Electrochemical oxidative degradation of indigo wastewater based on chlorine-containing system, *Pigm. Resin Technol.*, 49 (2019) 46–54.
- [8] R. Shoukat, S.J. Khan, Y. Jamal, Hybrid anaerobic-aerobic biological treatment for real textile wastewater, *J. Water Process Eng.*, 29 (2019) 100804, doi: 10.1016/j.jwpe.2019.100804.
- [9] U. Roy, S. Manna, S. Sengupta, P. Das, S. Datta, A. Mukhopadhyay, A. Bhowal, Dye Removal Using Microbial Biosorbents, G. Crini, E. Lichtfouse, Eds., *Green Adsorbents for Pollutant Removal: Innovative Materials*, Springer International Publishing, Cham, 2018, pp. 253–280. Available at: https://doi.org/10.1007/978-3-319-92162-4_8
- [10] R. Jain, M. Mathur, S. Sikarwar, A. Mittal, Removal of the hazardous dye rhodamine B through photocatalytic and adsorption treatments, *J. Environ. Manage.*, 85 (2007) 956–964.
- [11] D. Kiejza, U. Kotowska, W. Polińska, J. Karpińska, Peroxides - new oxidants in advanced oxidation processes: the use of peracetic acid, peroxymonosulfate, and persulfate salts in the removal of organic micropollutants of emerging concern - a review, *Sci. Total Environ.*, 790 (2021) 148195, doi: 10.1016/j.scitotenv.2021.148195.
- [12] X. Li, B. Jie, H. Lin, Z. Deng, J. Qian, Y. Yang, X. Zhang, Application of sulfate radicals-based advanced oxidation technology in degradation of trace organic contaminants (TrOCs): recent advances and prospects, *J. Environ. Manage.*, 308 (2022) 114664, doi: 10.1016/j.jenvman.2022.114664.
- [13] J. Lee, U. von Gunten, J.-H. Kim, Persulfate-based advanced oxidation: critical assessment of opportunities and roadblocks, *Environ. Sci. Technol.*, 54 (2020) 3064–3081.
- [14] H. Esmaili, A. Kotobi, S. Sheibani, F. Rashchi, Photocatalytic degradation of methylene blue by nanostructured Fe/FeS powder under visible light, *Int. J. Miner. Metall. Mater.*, 25 (2018) 244–252.
- [15] P. Zawadzki, Decolorisation of methylene blue with sodium persulfate activated with visible light in the presence of glucose and sucrose, *Water, Air, Soil Pollut.*, 230 (2019) 313–313.
- [16] M.A. Hassaan, A. El Nemr, F.F. Madkour, A.M. Idris, T.O. Said, T. Sahlabji, M.M. Alghamdi, A.A. El-Zahhar, Advanced oxidation of acid yellow 11 dye; detoxification and degradation mechanism, *Toxin Rev.*, 40 (2021) 1472–1480.
- [17] P.S. Chauhan, K. Kumar, K. Singh, S. Bhattacharya, Fast decolorization of rhodamine-B dye using novel V₂O₅-rGO photocatalyst under solar irradiation, *Synth. Met.*, 283 (2022) 116981, doi: 10.1016/j.synthmet.2021.116981.
- [18] M. Yilmaz, N. Mengelizadeh, M. khodadadi Saloot, S. Shahbaksh, D. Balarak, Facile synthesis of Fe₃O₄/ZnO/GO photocatalysts for decolorization of acid blue 113 under solar, visible and UV lights, *Mater. Sci. Semicond. Process.*, 144 (2022) 106593, doi: 10.1016/j.mssp.2022.106593.
- [19] M. Chandra, M. Nookaraju, V.K. Sharma, R. Somasekhar, Influence of Vanadium incorporated mesoporous silica on the decolorization of orange G under visible light irradiation, *Inorg. Nano-Metal Chem.*, 52 (2022) 387–396.
- [20] G. Yanagi, M. Furukawa, I. Tateishi, H. Katsumata, S. Kaneco, Electrochemical decolorization of methylene blue in solution with metal doped Ti/α,β-PbO₂ mesh electrode, *Sep. Sci. Technol.*, 57 (2022) 325–337.
- [21] A.S. Al-Shehri, Z. Zaheer, A.M. Alsudairi, S.A. Kosa, Photo-oxidative decolorization of Brilliant Blue with AgNPs as an activator in the presence of K₂S₂O₈ and NaBH₄, *ACS Omega*, 6 (2021) 27510–27526.
- [22] C. Alvarado-Camacho, C.O. Castillo-Araiza, R.S. Ruiz-Martínez, Degradation of Rhodamine B in water alone or as part of a mixture by advanced oxidation processes, *Chem. Eng. Commun.*, 209 (2022) 69–82.
- [23] J. Xie, Y. He, H. Wang, M. Duan, J. Tang, Y. Wang, M. Chamas, H. Wang, Photocatalytic degradation of binary dyes mixture over SrTiO₃ synthesized using sodium carboxymethylcellulose additive, *Russ. J. Phys. Chem.*, 92 (2018) 809–815.
- [24] F. Mahmoudian, F. Nabizadeh Chianeh, S.M. Sajjadi, Simultaneous electrochemical decolorization of Acid Red 33, Reactive Orange 7, Acid Yellow 3 and Malachite Green dyes by electrophoretically prepared Ti/nanoZnO-MWCNTs anode: experimental design, *J. Electroanal. Chem.*, 884 (2021) 115066, doi: 10.1016/j.jelechem.2021.115066.
- [25] C. Wang, Z. Yuan, A. Wang, J. Qu, Z. Fang, Y. Wen, Ultraviolet light enhanced sodium persulfate oxidation of cellulose to facilitate the preparation of cellulose nanofibers, *Cellulose*, 27 (2020) 2041–2051.
- [26] M.Y. Rizal, R. Saleh, A. Taufik, S. Yin, Photocatalytic decomposition of methylene blue by persulfate-assisted Ag/Mn₂O₄ and Ag/Mn₂O₄/graphene composites and the inhibition effect of inorganic ions, *Environ. Nanotechnol. Monit. Manage.*, 15 (2021) 100408, doi: 10.1016/j.enmm.2020.100408.
- [27] D. Maharana, J. Niu, D. Gao, Z. Xu, J. Shi, Electrochemical degradation of Rhodamine B over Ti/SnO₂-Sb electrode, *Water Environ. Res.*, 87 (2015) 304–311.
- [28] S.G. Pouloupoulos, A. Yerkinova, G. Ulykbanova, V.J. Inglezakis, Photocatalytic treatment of organic pollutants in a synthetic wastewater using UV light and combinations of TiO₂, H₂O₂ and Fe(III), *PLoS One*, 14 (2019) e0216745, doi: 10.1371/journal.pone.0216745.
- [29] P. Zawadzki, Evaluation of TiO₂/UV; O₃/UV, and PDS/Vis for improving chlorfenvinphos removal from real municipal

- treated wastewater effluent, *Int. J. Environ. Sci. Technol.*, (2022), doi: 10.1007/s13762-022-04370-x.
- [30] J.K. Laha, M.K. Hunjan, $K_2S_2O_8$ activation by glucose at room temperature for the synthesis and functionalization of heterocycles in water, *Chem. Commun. (Camb.)*, 57 (2021) 8437–8440.
- [31] L. Chu, R. Zhuan, D. Chen, J. Wang, Y. Shen, Degradation of macrolide antibiotic erythromycin and reduction of antimicrobial activity using persulfate activated by gamma radiation in different water matrices, *Chem. Eng. J.*, 361 (2019) 156–166.
- [32] R.J. Watts, M. Ahmad, A.K. Hohner, A.L. Teel, Persulfate activation by glucose for in situ chemical oxidation, *Water Res.*, 133 (2018) 247–254.
- [33] G.V. Buxton, C.L. Greenstock, W.P. Helman, A.B. Ross, Critical review of rate constants for reactions of hydrated electrons, hydrogen atoms and hydroxyl radicals ($^{\bullet}OH/^{\bullet}O$) in aqueous solution, *J. Phys. Chem. Ref. Data*, 17 (1988) 513–886.
- [34] M. Mahanthappa, N. Kottam, S. Yellappa, Enhanced photocatalytic degradation of methylene blue dye using CuScdS nanocomposite under visible light irradiation, *Appl. Surf. Sci.*, 475 (2019) 828–838.
- [35] J. Saien, F. Jafari, Chapter 1 – Methods of Persulfate Activation for the Degradation of Pollutants: Fundamentals and Influencing Parameters, M. Zhu, Z. Bian, C. Zhao, Eds., *Persulfate-based Oxidation Processes in Environmental Remediation*, 2022, 1–59. Available at: <https://doi.org/10.1039/9781839166334-00001>
- [36] M. Bagherzadeh, R. Kaveh, S. Ozkar, S. Akbayrak, Preparation and characterization of a new $CdS-NiFe_2O_4$ /reduced graphene oxide photocatalyst and its use for degradation of methylene blue under visible light irradiation, *Res. Chem. Intermed.*, 44 (2018) 5953–5979.
- [37] F. Han, X. Ye, Q. Chen, H. Long, Y. Rao, The oxidative degradation of diclofenac using the activation of peroxymonosulfate by $BiFeO_3$ microspheres—kinetics, role of visible light and decay pathways, *Sep. Purif. Technol.*, 232 (2020) 115967, doi: 10.1016/j.seppur.2019.115967.
- [38] X. Chen, Z. Xue, Y. Yao, W. Wang, F. Zhu, C. Hong, Oxidation degradation of Rhodamine B in aqueous by treatment system, *Int. J. Photoenergy*, 2012 (2012) e754691, doi: 10.1155/2012/754691.
- [39] L. Urán-Duque, J.C. Saldarriaga-Molina, A. Rubio-Clemente, Advanced oxidation processes based on sulfate radicals for wastewater treatment: research trends, *Water*, 13 (2021) 2445, doi: 10.3390/w13172445.
- [40] A.N. Oliveros, J.A.I. Pimentel, M.D.G. de Luna, S. Garcia-Segura, R.R.M. Abarca, R.-A. Doong, Visible-light photocatalytic diclofenac removal by tunable vanadium pentoxide/boron-doped graphitic carbon nitride composite, *Chem. Eng. J.*, 403 (2021) 126213, doi: 10.1016/j.cej.2020.126213.
- [41] B. Yang, Q. Luo, Q. Li, Y. Meng, L. Lingli, Y. Liu, Selective oxidation and direct decolorization of cationic dyes by persulfate without activation, *Water Sci. Technol.*, 83 (2021) 2744–2752.
- [42] N. Tripathi, Cationic and anionic dye adsorption by agricultural solid wastes: a comprehensive review, *Desalination*, 5 (2013) 91–108.
- [43] W. Li, Z. Jian, Z. Ran, L. Cong, L. Ye, Z. ChengLu, Adsorption of basic dyes on activated carbon prepared from *Polygonum orientale* Linn: equilibrium, kinetic and thermodynamic studies, *Desalination*, 254 (2010) 68–74.
- [44] W. Gao, S. Zhao, H. Wu, W. Deligeer, S. Asuha, Direct acid activation of kaolinite and its effects on the adsorption of methylene blue, *Appl. Clay Sci.*, 126 (2016) 98–106.
- [45] M. Vinuth, H.S.B. Naik, B.M. Vinoda, H. Gururaj, N. Thomas, G. Arunkumar, Enhanced removal of methylene blue dye in aqueous solution using eco-friendly Fe(III)–montmorillonite, *Mater. Today Proc.*, 4 (2017) 424–433.
- [46] S. Sharma, N. Khare, Hierarchical Bi_2S_3 nanoflowers: a novel photocatalyst for enhanced photocatalytic degradation of binary mixture of Rhodamine B and Methylene blue dyes and degradation of mixture of p-nitrophenol and p-chlorophenol, *Adv. Powder Technol.*, 29 (2018) 3336–3347.
- [47] S. Rani, M. Aggarwal, M. Kumar, S. Sharma, D. Kumar, Removal of methylene blue and rhodamine B from water by zirconium oxide/graphene, *Water Sci.*, 30 (2016), doi: 10.1016/j.wsj.2016.04.001.
- [48] D. Blažeka, J. Car, N. Klobučar, A. Jurov, J. Zavašnik, A. Jagodar, E. Kovačević, N. Krstulović, Photodegradation of Methylene Blue and Rhodamine B using laser-synthesized ZnO nanoparticles, *Materials*, 13 (2020) 4357, doi: 10.3390/ma13194357.
- [49] Z.-H. Diao, J.-J. Liu, Y.-X. Hu, L.-J. Kong, D. Jiang, X.-R. Xu, Comparative study of Rhodamine B degradation by the systems pyrite/ H_2O_2 and pyrite/persulfate: reactivity, stability, products and mechanism, *Sep. Purif. Technol.*, 184 (2017) 374–383.
- [50] C. Lops, A. Ancona, K. Di Cesare, B. Dumontel, N. Garino, G. Canavese, S. Hernández, V. Cauda, Sonophotocatalytic degradation mechanisms of Rhodamine B dye via radicals generation by micro- and nano-particles of ZnO, *Appl. Catal., B*, 243 (2019) 629–640.
- [51] P. Zawadzki, Comparative studies of Rhodamine B decolorization in the combined process $Na_2S_2O_8$ /visible light/ultrasound, *Desal. Water Treat.*, 213 (2021) 269–278.
- [52] M. Mahdavianpour, S. Ildari, M. Ebrahimi, M. Moslemzadeh, Decolorization and mineralization of methylene blue in aqueous solutions by persulfate/ Fe^{2+} process, *J. Water Chem. Technol.*, 42 (2020) 244–251.
- [53] P. Attri, S. Garg, J.K. Ratan, A.S. Giri, Comparative study using advanced oxidation processes for the degradation of model dyes mixture: reaction kinetics and biodegradability assay, *Mater. Today Proc.*, 57 (2022) 1533–1538.
- [54] H. Heidarpour, M. Padervand, M. Soltanieh, M. Vossoughi, Enhanced decolorization of rhodamine B solution through simultaneous photocatalysis and persulfate activation over Fe/C_3N_4 photocatalyst, *Chem. Eng. Res. Des.*, 153 (2020) 709–720.
- [55] Y. Pang, K. Luo, L. Tang, X. Li, Y. Song, C. Li, L. Wang, Preparation and application of magnetic nitrogen-doped rGO for persulfate activation, *Environ. Sci. Pollut. Res.*, 25 (2018) 30575–30584.
- [56] R. Jinisha, R. Gandhimathi, S.T. Ramesh, P.V. Nidheesh, S. Velmathi, Removal of rhodamine B dye from aqueous solution by electro-Fenton process using iron-doped mesoporous silica as a heterogeneous catalyst, *Chemosphere*, 200 (2018) 446–454.
- [57] T.S. Natarajan, M. Thomas, K. Natarajan, H.C. Bajaj, R.J. Tayade, Study on UV-LED/ TiO_2 process for degradation of Rhodamine B dye, *J. Chem. Eng.*, 169 (2011) 126–134.
- [58] K. Rakesh, S.C. Mohan, S. Karuppachamy, K. Jothivenkatachalam, Photo-assisted advanced oxidation processes for Rhodamine B degradation using ZnO–Ag nanocomposite materials, *J. Environ. Chem. Eng.*, 6 (2018) 3610–3620.
- [59] M.-F. Hou, L. Liao, W.-D. Zhang, X.-Y. Tang, H.-F. Wan, G.-C. Yin, Degradation of rhodamine B by Fe(0)-based Fenton process with H_2O_2 , *Chemosphere*, 83 (2011) 1279–1283.
- [60] A. Samide, B. Tutunaru, C. Tigae, R. Efreem, A. Moanță, M. Drăgoi, Removal of methylene blue and methyl blue from wastewater by electrochemical degradation, *Environ. Prot. Eng.*, 40 (2014), doi: 10.37190/epe140408.



Municipal wastewater reclamation: Reclaimed water for hydrogen production by electrolysis – A case study

Piotr Zawadzki^{*}, Beata Kończak, Adam Smoliński

Central Mining Institute, Plac Gwarków 1, 40-166 Katowice, Poland

ARTICLE INFO

Keywords:

Green hydrogen
Electrolysis
Wastewater treatment
Municipal wastewater

ABSTRACT

This paper presents an analysis of a treatment system selection for municipal wastewater stream based on the DuPont Water Solutions WAVE software. The results obtained based on an analysis of 7 different processing cases studies (ultrafiltration and reverse osmosis) confirmed that the application of 2-pass membrane systems enables the reclamation of water from municipal wastewater that fulfills the requirements concerning the quality of water intended as electrolyzer feedstock, as the obtained water exhibited a conductivity of $< 5 \mu\text{S}/\text{cm}$. Depending on the analyzed case study, the attainable level of water reclamation ranged from 68.8 to 84.1 % at an energy consumption of 606.1 – 2 694 kWh/d. The results of this work not only confirm that the selected processing solutions make it possible to reclaim water from municipal wastewater, but also confirm the necessity of using software to simulate the membrane system operation to select the most economic and cost-effective solution.

1. Introduction

With the increasing global population, water resource management should be approached unconventionally, and unused water resources should be diversified to limit the problems of deteriorating water quality and decreasing potable water reserves [1,2]. Unused water resources include e.g. wastewater, which may constitute an interesting source of drinking water as well as the water of a quality sufficient for processing purposes (process water) [3–7]. To prevent water scarcity in the European Union, the European Parliament has adopted Regulation (EU) 2020/741 of 25 May 2020 on minimum requirements for water reuse [8]. The purpose of this Regulation is to facilitate the uptake of water reuse whenever it is appropriate and cost-efficient, thereby creating an enabling framework for those member states who wish or need to practice water reuse. As per the Regulation, it is considered that the reuse of properly treated wastewater, for example from municipal wastewater treatment plants (WWTP), has a lower environmental impact than other alternative water supply methods, such as water transfers or desalination. Therefore, the necessity to identify alternative methods for water reuse or secondary wastewater treatment is justified.

The currently applied conventional methods of municipal wastewater treatment are not designed for wastewater reuse [9,10]. Conventional municipal wastewater treatment technologies include

mechanical biological methods, such as slurry removal on sieves and in settling tanks (mechanical methods) as well as through activated sludge microorganisms or biofilms (biological methods) [10,11]. In recent years, problems with access to clean and safe water as well as the global water crisis and strict legal regulations in waste management have forced municipal facilities to reconsider and implement third- and fourth-degree wastewater treatment. Examples of interest in secondary wastewater treatment processes include municipal facilities worldwide, e.g. the Waldwick wastewater treatment plant (New Jersey, USA) [12] or the Point Loma wastewater treatment plant (San Diego, USA) [13]. The Waldwick WWTP conducts secondary wastewater treatment using processes involving ultraviolet lamps to achieve the ultimate wastewater disinfection without the necessity of applying chlorine. By 2025, the Point Loma WWTP plans to produce about 129 000 m³/d of potable water from municipal waste by utilizing biological processes (biological activated carbon), membrane processes (microfiltration, reverse osmosis) and advanced oxidation (UV radiation, ozone, hydrogen peroxide). The application of secondary treatment processes depends on a WWTP's location (e.g. recreational areas, housing infrastructure, industrial areas, protected land, agricultural areas), therefore the end goals of secondary treatment may include e.g. agricultural irrigation, street and square cleaning, process water production for equipment cleaning, aquifer recharging by injection wells. The research work and

^{*} Corresponding author.

E-mail address: pzawadzki@gig.eu (P. Zawadzki).

new method investigation in this field led for example to the introduction of an installation for secondary wastewater treatment and pharmaceutical substance elimination at the Neugut WWTP in Switzerland [14,15]. The Neugut plant was the first wastewater treatment plant in Switzerland to implement full-scale ozonation. The conventional wastewater treatment system (primary settling tank, biological treatment, sand filtration) was expanded by an additional ozonation stage, which yielded a contaminant removal rate of about 80 %.

To fully close the water and wastewater circulation in a WWTP and to ensure its independence from the power supply, seeing as the price of electricity has increased drastically during the energy crisis [16], it is crucial to undertake action to enable the recovery of organic substances from wastewater and sewage sludge for energy purposes [17]. Hydrogen can be produced by a variety of processes and energy sources. The types of hydrogen depend on its production process and can be categorised as follows [18]:

- **Grey:** Grey hydrogen is mainly produced by steam reforming of natural gas or coal gasification. The use of grey hydrogen implies significant CO₂ emissions, which makes these hydrogen technologies not part of a net zero CO₂ emissions policy [19].
- **Blue:** Blue hydrogen is produced by combining natural gas steam reforming technology with Carbon Capture Storage (CCS) or Carbon Capture and Utilization (CCU) technology. In this variant, the resulting CO₂ emissions are captured using CCS or CCU technology, making the hydrogen produced nearly emission-free (emissions are reduced by up to 95 %). In contrast to green hydrogen, blue hydrogen is not a completely emission-free product, as harmful methane enters the atmosphere during the extraction and transportation of natural gas [20].
- **Green:** Green hydrogen is produced using renewable energy. Green hydrogen is part of the sustainable energy transition concept. This form of hydrogen production is the most preferable in terms of zero-emission energy and transportation [21,22].
- **Turquoise:** Turquoise hydrogen is produced by the pyrolysis of methane. The main substrate for production is natural gas. However, the process is driven not by burning fossil fuels, but by electricity (the vast majority should come from renewable energy sources to make the process CO₂-neutral). With biomethane as the feedstock, the process could be zero-emission [23].

The literature also highlights brown (or black) hydrogen. Brown (black) hydrogen is hydrogen produced by coal gasification, where during combustion, carbon dioxide is emitted into the atmosphere. Coal gasification involves heating coal to temperatures reaching over 1273 K, resulting in the release of coke gas [24].

On the other hand, the reclaimed water may be used to produce hydrogen by electrolysis, as well as for practical purposes, such as supplying technical processes, cleaning streets and equipment, watering plants, or even as a source of potable water. When considering the perspectives for technological development in the context of hydrogen production, promising directions (in the coming few years) can include anaerobic fermentation, biomass gasification, electrolysis (with renewable energy sources), and photobiological methods [25–28]. Some of these processes are already used in the context of hydrogen (electrolysis), while others still require an adjustment of the current technical solutions (anaerobic fermentation). In the public utility sector, potential can be found in biomass gasification, hydrogen recovery from biogas generated by anaerobic sewage sludge processing, and electrolysis [29–38]. Water electrolysis is the most promising direction, and in the future, it will constitute the most widely supported method of hydrogen production in the European Union. The electrolysis process consists in separating hydrogen from water using electricity through electrolyzers. The most widely recognized technical option for hydrogen production is water electrolysis powered by electricity originating from renewable sources. Hydrogen produced through systems powered by electricity

obtained from renewable sources is defined as green hydrogen [39]. The costs of green hydrogen production can be lowered by the low costs of solar and wind power as well as technical enhancements [40,41]. For these reasons, green hydrogen from water electrolysis is gaining increasingly more interest. Furthermore, it is estimated that by 2030 it will be possible to reduce green hydrogen production costs by about 60 % [18]. Currently, about 96 % of global hydrogen production originates from processes involving fossil fuels (primarily steam methane reforming and coal gasification) [42–44]. Hydrogen production using electricity (including electrolysis) constitutes about 4 % of the total production. The most popular devices for hydrogen production by electrolysis are alkaline electrolyzers. Polymer electrolyte membrane (PEM) electrolyzers are also available on the market – compared to alkaline electrolyzers, they have lower power (200–1150 kW) and similar efficiency (65 % to 78 %). Meanwhile, solid oxide electrolyzers utilizing steam at a temperature within 973 to 1173 K are currently under development, which would be characterized by high efficiency (at a level of 85 %) [45,46]. The PEM electrolyzer technology constitutes an alternative to the more conventional alkaline electrolyzers. This technology exhibits several advantages compared to the older solutions, namely increased electrolyzer efficiency (56–73 %), the possibility of obtaining ultra-pure hydrogen (purity class >=5.0, i.e. >=99.999 %), and a more compact design [47].

In theory, 8.92 L of deionized water are required to produce 1 kg of hydrogen and 8 kg of oxygen [48]. However, considering the potential water losses and the use of water for cleaning the equipment, the actual water required to produce 1 kg of hydrogen by electrolysis is estimated at 13.5–15.0 kg H₂O, and may even reach up to about 22.4 kg/kg H₂ [49]. The cost of hydrogen production depends on the applied process scale, equipment and substrates. The greater the efficiency of the equipment, the lower the investment and operating costs [36]. For example, over a short period of electrolyzer operation, the production cost may amount to about US\$10.5/kg H₂. At longer periods of equipment operation, the production costs decrease to about US\$2.05/kg H₂ [38,50]. Generally, hydrogen production by electrolysis is competitive relative to other methods, e.g. sewage sludge pyrolysis or steam methane reforming [31]. For comparison, the estimated cost of hydrogen production by sewage sludge pyrolysis may amount to about US\$1.2–2.2/kg H₂ [51]. The cost of hydrogen production by steam methane reforming ranges from about US\$1.14/kg H₂ in the case of large systems to about US\$3.19/kg H₂ for smaller systems [31,52].

Regardless of the feedstock, the water supplying an electrolyzer must first be purified and demineralized. Current research [49] indicates that water from the public water network is the most appropriate source of water for electrolysis due to the lower supply risk, lower costs, and the lack of complex processes for obtaining legal permissions. However, given the global water crisis and the dynamically changing formal and legal conditions related to the necessity for obtaining the relevant hydrological legal permits to draw water from the public water network, and considering Regulation 2020/741 of the European Parliament [8], alternative opportunities and sources of water for electrolysis should be investigated. Therefore the economic, environmental, and social factors should be considered before any final decisions are taken. Literature data indicate that treated municipal wastewater may constitute an alternative source of water for supplying electrolysis [49,53]. An advantage of the water reclaimed from municipal waste is its low hardness compared to the water drawn from the public water network (potable water quality).

The water supplying an electrolyzer should meet the requirements for deionized water and exhibit a conductivity of < 5 μS/cm; therefore depending on the quality of the treated wastewater, the following treatment processes may be necessary: accelerated filtration, chemical treatment (pre-treatment before membrane processes), ultrafiltration (UF), nanofiltration (NF), reverse osmosis (RO), ion exchange (IE), electrodeionization (EDI). Treatment by reverse osmosis and ion exchange is commonly applied before electrolysis to produce water with a

sufficiently low conductivity.

The decision to select a technology for water production from municipal wastewater must be preceded by the appropriate physico-chemical and biological analyses of the wastewater and by determining the available volume of waste as well as the water demand, and not exclusively for water production by hydrolysis. Commercial software for selecting membrane modules, provided by their producers, such as e.g. Winflows (Suez), IMSDesign (Hydranautics), or WAVE (DuPont Water Solutions), is very useful in the process of designing the appropriate membrane system for water reclamation from municipal waste for the production of water intended as an electrolyzer feedstock. This work presents the process of separation system selection for water reclamation from municipal wastewater, comprising pre-filtration, ultrafiltration, and reverse osmosis, utilizing the WAVE software by DuPont Water Solutions. This work aims to select a municipal wastewater pre-treatment technology for producing water of the quality required in the process of electrolysis using the WAVE software. Various membrane process systems (ultrafiltration, reverse osmosis) for producing water of a purity class of at least 3, i.e. with a conductivity of under 5 $\mu\text{S}/\text{cm}$, were evaluated. The WAVE software has thus far not been applied for membrane process modeling in terms of producing water from municipal waste that would fulfill the requirements for electrolysis. The primary advantage of the selected software is the user-friendly interface and the possibility of robust user panel management. Furthermore, membranes available on the market can be modeled in the WAVE software, which is unique compared to other programs.

The purpose of this paper is to present the practical aspects of applying membrane process modeling software. The demand for the results of this work arises e.g. from the Communication from the Commission to the European Parliament, the Council, the European Economic and Social Committee, and the Committee of the Regions, "A Hydrogen Strategy for a Climate-Neutral Europe" [39]. For the hydrogen economy to be implemented effectively, it is necessary to enhance the capacity for conducting and advancing research, and consequently to introduce the developed solutions and technologies for utilizing hydrogen in power generation, transport, and industry, including the conduction of research on methods for obtaining and processing water for electrolysis. The tests performed as part of this work will allow water supply and sewerage companies to implement similar technologies in municipal and industrial sites within the scope of processes enabling secondary wastewater treatment for processing purposes (water reclaimed from waste as a source for producing hydrogen by electrolysis).

2. Materials and methods

2.1. Wastewater samples

The treated wastewater was sampled in 2022 from a wastewater treatment plant located in one of the cities comprising the Silesian agglomeration (Silesian Voivodeship, Poland). The wastewater treatment plant is continuously modernized to fulfill the requirements of local law and European Union Directives for WWTP with an efficiency of > 100,000 population equivalent (PE). The last major modernization took place in 2012 and resulted in an increase in nutrient reduction by optimizing the biological wastewater treatment process. The WWTP operates in a mechanical biological system. The mechanical part comprises bar screens, sand traps, and primary settling tanks, while the biological part consists of biological reactors. The tests were carried out in 2022 at the certified laboratories of the Central Mining Institute. To inhibit any biological activity in the sample and eliminate the adsorption of compounds on the glass vessel walls, the samples were stored at a temperature of 277,15 K until the time of analysis (for no longer than 48 h), in compliance with the standard [54]. The analyses were based on composite samples (three samples mixed together, from which the average value has been obtained), as per [55]. The physicochemical

parameters of the treated municipal wastewater are presented in Table 1.

2.2. Water requirements for electrolysis

The requirements concerning water (wastewater) quality vary depending on the electrolyzer manufacturer, but typically the production of very pure hydrogen requires deionized water [49], i.e. water free of all solutes and pollutants, as pollutants may influence the reaction by deposition in the electrolyzers, on the electrode surfaces and/or in the membrane. The electrolyzer feedstock conductivity recommended by the American Society for Testing and Materials (ASTM) should amount up to about 5 $\mu\text{S}/\text{cm}$, or equal to the parameters for type I or II water per the requirements of standard D1193-06 [56], which corresponds to a conductivity of up to about 0.056 $\mu\text{S}/\text{cm}$ and 1 $\mu\text{S}/\text{cm}$ respectively. It was assumed that an optimal processing system should enable the production of water with a conductivity no > 5 $\mu\text{S}/\text{cm}$, therefore according to ASTM's specification.

2.3. Modeling in the WAVE software

2.3.1. Design parameters of the tested wastewater

The treated wastewater parameters adopted for the modeling in WAVE are presented in Table 2. The treated wastewater was characterized by increased turbidity (>10 NTU), total suspended solids (TDS), manganese, and iron. The pollutant content in the wastewater exceeded the recommended maximum pre-RO pollutant index values. The final permissible pollutant index values depend on the manufacturer's instructions and the applied membrane types. Wastewater treated by mechanical biological processes constituted the source for producing deionized water with a conductivity no > 5 $\mu\text{S}/\text{cm}$. The wastewater treated before the membrane filtration process was characterized by turbidity lower than 20 NTU, total suspended solids under 30 mg/dm^3 , and a total organic carbon content under 20 mg/dm^3 . The adopted design temperature was 19 °C. The treated wastewater was pre-treated by pre-filtration processes on a sieve with a mesh of 100 μm and by ultrafiltration to an SDI of < 2.5. The application of an antiscalant was adopted to limit scaling – sodium hexametaphosphate ($\text{Na}_6\text{P}_6\text{O}_{18}$). The efficiency of a single production process was adopted at a level of 100 m^3/h of water reclaimed from wastewater. For the analyzed processing systems, at an average water recovery of 76.3 %, the municipal wastewater flow was about 133–145 m^3/h , depending on the processing system (with or without concentrate recycling).

2.3.2. Selection of wastewater treatment processes for reclaimed water

The technology selection was based on the instructions of membrane manufacturers, including Lenntech [57,58]. The average conductivity of

Table 1
Characteristics of tested wastewater.

Parameter	Unit	Treated municipal wastewater
pH	–	7.8 ± 0.2
Temperature	°C	19.1 ± 0.1
Conductivity	$\mu\text{S}/\text{cm}$	848 ± 42
Turbidity	NTU	16.8 ± 0.12
Absorbance ($\lambda = 254 \text{ nm}$)	nm	0.196 ± 0.02
COD*	$\text{mg O}_2/\text{l}$	32 ± 4
TOC**	$\text{mg C}/\text{l}$	5.2 ± 0.8
Free chlorine	$\text{mg Cl}_2/\text{l}$	< 0.1 ± 0.03
Iron	mg/l	2.41 ± 0.2
Manganese	mg/l	0.59 ± 0.09
Chloride	mg/l	132 ± 13
Sulfate	mg/l	103 ± 10

* Chemical Oxygen Demand.

** Total Organic Carbon.

Number of samples: three samples mixed together, from which the average value has been obtained, according to [56].

Table 2
Design parameters of the tested wastewater for the modeling process.

Parameter	Unit	Design value
pH	–	7.8
Temperature	K	292.25 ± 273.15
Turbidity	NTU	16.8
Total Suspended Solids	mg/dm ³	25
TOC	mg/dm ³	5.2 ± 0.8
NH ₄ ⁺	mg/dm ³	0.020
K ⁺	mg/dm ³	14.9
Na ⁺	mg/dm ³	120
Mg ²⁺	mg/dm ³	10
Ca ²⁺	mg/dm ³	55.1
Sr ²⁺	mg/dm ³	0.019
Ba ²⁺	mg/dm ³	0.019
CO ₃ ²⁻	mg/dm ³	0.630
HCO ₃ ⁻	mg/dm ³	123
NO ₃ ⁻	mg/dm ³	13
Cl ⁻	mg/dm ³	132
F ⁻	mg/dm ³	0.13
SO ₄ ²⁻	mg/dm ³	103
Br ⁻	mg/dm ³	0.020
PO ₄ ³⁻	mg/dm ³	2.5
CO ₂	mg/dm ³	2.573
Conductivity *	µS/cm	968.93

* value corrected and calculated in the WAVE software.

the tested treated municipal wastewater samples was 848 µS/cm, therefore reverse osmosis was selected as the final process for water production for electrolysis (Table 3). Both 1- and 2-pass processes were analyzed among the selected processing systems. Pre-treatment of the wastewater is required to prepare it for deionization. The membrane filters for RO are exposed to contamination by numerous substances, including natural organic matter, solids, colloids, bacteria, viruses, etc. The above pollutants can be removed by conventional treatment processes consisting of coagulation followed by filtration (for media with low turbidity and total suspended solids – coagulants are added before filter bed entry). In the case of media with high turbidity and total suspended solids, additional stages of sedimentation are carried out before filtering the water/waste. Ultrafiltration is used with alternative pre-treatment methods (primarily for removing turbidity, suspended solids, and bacteria). In the case of membranes for reverse osmosis, antiscalant is dosed in as an addition to minimize the content of calcium carbonate and sulfates to prevent scale sedimentation (membrane fouling). Additional operations may include e.g. water chlorination or UV sterilization (eliminating bacterial flora responsible for biofouling), pH correction, free chlorine reduction, and degassing (CO₂ removal).

It was assumed that the municipal wastewater pre-treatment installation would comprise the following elements: sieve filter, ultrafiltration, and reverse osmosis.

The sieve filter is a pipeline filtering equipment element that can be applied in various branches of industry to fulfill several filtration requirements. The filter insert is located in a casing and is intended to remove solids. The sieve filter's primary purpose is the mechanical protection of downstream devices. The sieve filter offers a filtration accuracy of 100–150 µm. Using ultrafiltration in wastewater treatment typically involves the removal of various suspended solids and dissolved

Table 3
Deionized water production methods.

Wastewater quality	Required water quality	Recommended technology
< 500 µS/cm	< 5 µS/cm	Ion exchange
	< 1 µS/cm	Ion exchange and mixed bed
500–2000 µS/cm	5–20 µS/cm	Reverse osmosis
	< 5 µS/cm	2-pass reverse osmosis
	< 1 µS/cm	2-pass reverse osmosis combined with ion exchange and mixed bed

organic matter with high molecular mass, usually > 5–10 nm [59], as a result of separation by sieving. UF occurs at a pressure of 0.5 to 10 bar. A standard UF installation is typically composed of several sections, comprising: water intake and pressure pumps, initial water preparation, ultrafiltration modules, backwashing, chemical treatment, and water conditioning [60,61]. Reverse osmosis makes it possible to remove very small pollutant molecules from a solution, which concerns particularly monovalent ions. Reverse osmosis is used for water treatment and to remove salts and other pollutants to improve the color, taste, and other properties of liquids. The process makes it possible to remove bacteria, salts, sugars, proteins, dyes, and micropollutants. The RO membrane molecular weight cutoff is < 200 Da. The applied pressure ranges from 3.4 bar to 100 bar. The separation mechanism in reverse osmosis is described by the solution-diffusion model. The model assumes that the flow of specific components through the compact polymer membranes is determined by their solution in the polymer and by diffusion. The model omits the interactions between the membrane polymer and the diffusing component. The components undergo diffusion through the membrane under the influence of a thermodynamic impulse, i.e. the negative gradient of that component's chemical potential. However, reverse osmosis is significantly different from other techniques of this type, such as ultra- and microfiltration. In RO processes, solution and diffusion constitute the basic separation mechanism, whereas the sieving effect does not occur at all [62,63].

2.3.3. Modeling a membrane filtration process

The membrane filtration process modeling was conducted using the WAVE (Water Application Value Engine) software by DuPont (version 1.82.824). The WAVE software is intended for designing and simulating the operation of treatment systems involving membrane filtration. WAVE is an integrated software for expert modeling, developed for designing treatment plants, including wastewater treatment plants. The program combines leading membrane technologies: ultrafiltration (UF), reverse osmosis (RO), and ion exchange (IE), into a single, comprehensive platform. The WAVE software is based on the diffusion model and integrates the model's equations to simulate the flow of molecules through a semi-permeable membrane, and it is used to design and simulate the operation of water treatment systems involving UF, RO, and IE as constituent processes [64,65]. An attempt was undertaken to design a reverse osmosis installation for treated municipal wastewater deionization to use the wastewater as a feedstock for electrolysis. A computer simulation was carried out to verify the desired conductivity of < 5 µS/cm. Seven processing cases were subjected to analysis (Table 4).

The conductivity of the filtrate after UF/RO, which determines the applicability of the reclaimed water in the electrolysis process (max. 5 µS/cm), was the most crucial parameter on which modeling was focused. This work also involves the study of the factors determining: (a) operating costs (electricity consumption); (b) operating costs and injection of reagents (pH of the filtrate); and (c) operating costs and the negative phenomenon of limescale deposition on equipment and thus reducing the efficiency of hydrogen production (cation and anion concentration, including calcium, magnesium, and sulphate). The ultrafiltration process in all case studies was adopted to remove suspended solids and microorganisms. The elimination of suspended solids is designed to reduce the phenomenon of membrane fouling (membrane blockage due to the accumulation of contaminants on the membrane surface and inside the pores) and to protect the equipment from mechanical damage. The elimination of microorganisms is designed to reduce biofouling, i.e. biofilm growth over the membranes, which also reduces membrane permeability. For a flow rate of 133–145 m³/h, the use of 4 working UF trains and two redundant trains was adopted. UF and RO design parameters are derived from membrane suppliers' guidelines and literature data [66–70]. The 1-pass RO was adopted to test the efficiency of ion removal on a simplified technology scheme, as well as the possibility of reducing the investment and operating costs of

Table 4
Types of technological variants for membrane filtration.

Parameter	Unit	Case I	Case II	Case III	Case IV	Case V	Case VI		Case VII	
							Pass 1	Pass 2	Pass 1	Pass 2
ULTRAFILTRATION										
Feed (Wastewater) flow to UF	m ³ /h	133.3	137	137	133.3	133.3	145.4		145.4	
Permeate (product) flow	m ³ /h	100								
Type of membranes	–	Ultrafiltration SFP-2880								
Number of trains (working)	–	4								
Redundant trains	–	2								
Recovery	%	98								
TOC rejection	%	10								
REVERSE OSMOSIS										
Feed (Wastewater) flow to RO	m ³ /h	133.3	137	137	133.3	133.3	145.4	109	145.4	109
Number of passes	–	1	1	1	1	1	2		2	
Number of stages	–	1	2	1	2	2	1	1	2	2
Recovery	%	75	81.1	75	81.3	84.1	68.8		68.8	
Type of membranes	–	SW30XLE-400i								
Active area	m ²	37.2								
Pressure	bar	55.2								
Flow	m ³ /d	34.1								
Rejection	% NaCl	99.8								
Pressure vessel per stage (stage 1 / stage 2)	–	36 / 0	36 / 1	36 / 0	36 / 1	50 / 10	26	26	26 / 1	26 / 1
Elements per pressure vessel	–	6 / 0	6 / 6	6 / 0	6 / 6	6 / 6	6	6	6 / 6	6 / 6
Total elements	–	216 / 0	216 / 6	216 / 0	216 / 6	300 / 60	156	156	156 / 6	156 / 6
Flux	dm ³ /m ² × h	12.5	12.1	12.5	12.1	8.8	18.1	16.6	18.1	16.6
Concentrate recycle	%	0								

the technology. However, since the demineralization technology guidelines show that a 2-pass RO system is recommended to achieve conductivity < 5 us/cm, for this purpose this system was used to validate the data reported in the literature. The number of pressure vessels and elements per vessel was derived from the minimum and maximum recommended values of concentrate flow and recovery per element for a given membrane type, as determined by the WAVE program (based on the supplier's guidelines). The concentrate recirculation was assumed at a maximum of 10 % in order to adjust the minimum or maximum flow rate according to the membrane manufacturer's instructions. The selection of power was based on the assumed capacity, flow and heading head (geometric height, losses). In all cases, it was determined that the treated wastewater would be taken from an intermediate tank located at a distance of up to max. 10 m from the membrane installation. The parameters given in the Table 4, such as feed flow, flux, recovery rate, active area, TOC and salts rejection, etc., result from the assumed initial parameters and parameters determined by the membrane properties.

The data presented in this article is important because it allows verification and validation of the performance of the designed treatment system. The data presented is also significant because it allows to verify the assumed requirements for the quality of reclaimed water, the adopted design or operational parameters. With a very large number of parameters that can affect the final efficiency of the electrolyzer, the proper selection of a technological system for the recovery of water from municipal wastewater, which is a mix of different substances, it is often necessary to adapt a specific solution to a particular wastewater stream, which makes it very difficult to develop a uniform technological system for the water recovery as an input for the electrolyzer. To simplify the problem, the data presented in this article take into account the most important requirements for the quality of the electrolyzer feedwater to provide sufficiently low conductivity of reclaimed water and make the concentrations of problematic ions certainly lower than the requirements of electrolyzer manufacturers. To provide design support for this framework, the data presented allows for the modeling and computational analysis of membrane systems through their unique features and parameters, based on actual input data from a real municipal wastewater effluent.

3. Results and discussion

As part of the first case, the analysis involved a process comprising membrane filtration on membranes for ultrafiltration and reverse osmosis (Fig. 1). The processing system included 1-pass RO with 1-stage membrane filtration. The 1-stage filtration involved 36 pressure vessels, with 6 elements per vessel. The calculated flux was 12.5 dm³/m² × h (flow per unit of membrane surface). A pump with a power of 38.7 kW was proposed. The theoretical total energy consumption was about 929.5 kWh/d. The total water recovery was 75 %.

Fig. 2 presents the proposed design solution of the case II membrane filtration system, i.e. a processing system composed of 1-pass RO with 2-stage membrane filtration. The 1-stage filtration involved 36 pressure vessels, with 6 elements per vessel. The 2-stage filtration involved 1 pressure vessel, with 6 elements in the vessel. The calculated flux was 12.1 dm³/m² × h. A pump with a power of 36.2 kW was proposed. The theoretical total energy consumption was about 867.7 kWh/d. The total water recovery was 81.3 %.

Case III involved a membrane filtration system comprising UF and RO as part of a 1-pass RO system with 1-stage membrane filtration (Fig. 3). This case included a concentrate recycle to the membrane system entry to an amount of 3.7 m³/h (10 % of feed flow). Depending on the applied membrane types, concentrate flow modeling enables the adjustment of the minimum or maximum flow as per the membrane manufacturer's instructions. However, due to concentration, the water recovery decreases over subsequent passes (to about 73 %), and the net recovery equals 75 %. As a result of concentration, the water reclaimed from wastewater is also characterized by higher conductivity. In the first stage, the reclaimed water conductivity was 9 µS/cm, while in the second it was 48 µS/cm. The final calculated concentrate conductivity was 10 µS/cm. A pump with a power of 38.7 kW was proposed. The theoretical total energy consumption was about 929.5 kWh/d.

Case studies IV and V involved the analysis of two processing systems comprising 1-pass RO with 1-stage membrane filtration. The differences between the two analyzed cases consisted of the different total number of applied pressure vessels. A total of 212 vessels and 360 vessels was proposed for case study IV and V respectively (Fig. 4). The number of pressure vessels reduces the permeate flux – the greater it is, the lower the flux and the greater the recovery, with the simultaneous minor deterioration of the water quality. For case study IV, the recovery was

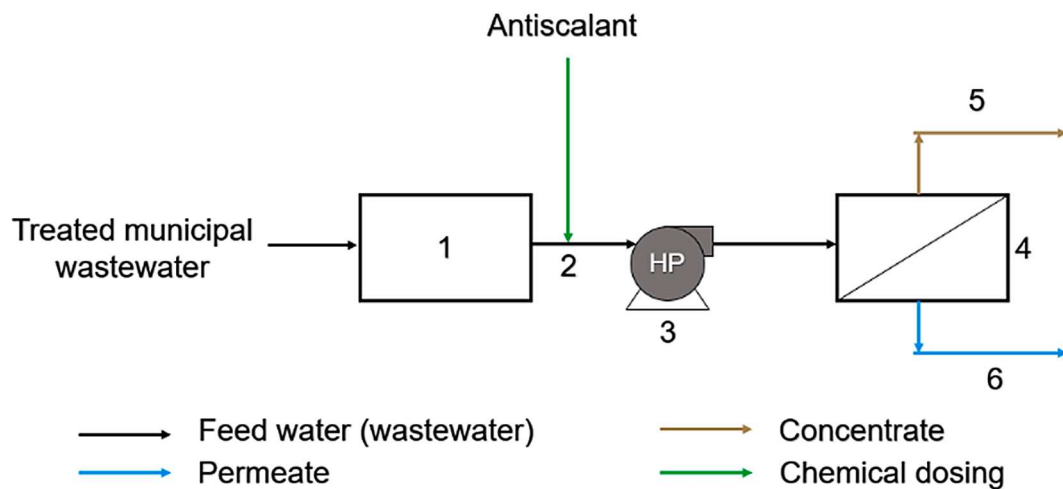


Fig. 1. Process flow – Case I 1 – Ultrafiltration unit; 2 – Antiscalant dosing; 3 – Pressure pump; 4 – 1-pass, 1-stage RO unit; 5 – Final concentrate; 6 – Permeate.

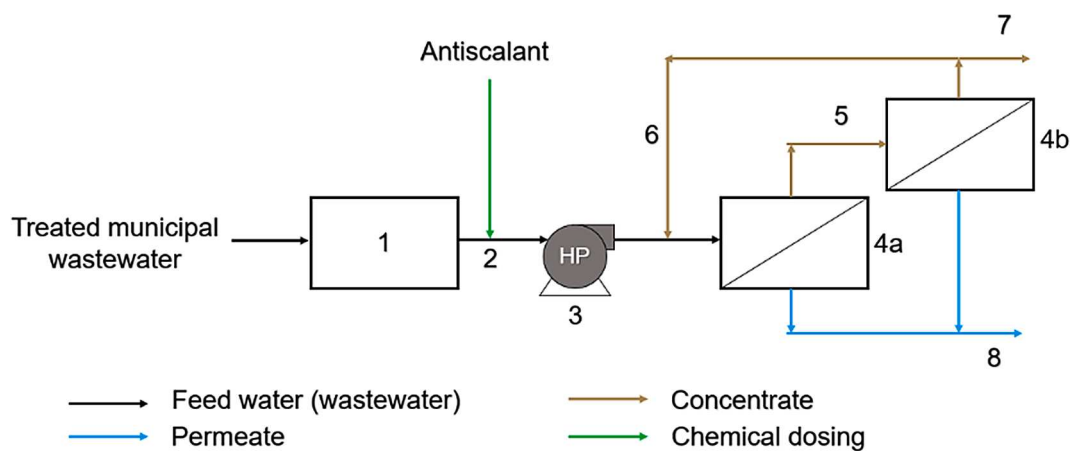


Fig. 2. Process flow – Case II 1 – Ultrafiltration unit; 2 – Antiscalant dosing; 3 – Pressure pump; 4a – 1-pass, 1-stage RO unit; 4b – 1-pass, 2-stage RO unit, 5 – Concentrate from 1-stage RO unit; 6 – Concentrate recycle; 7 – Final concentrate; 8 – Permeate.

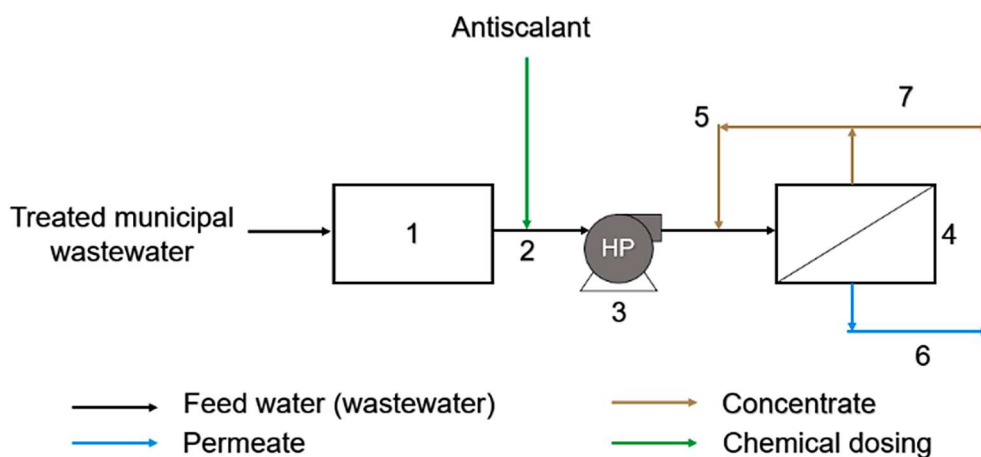


Fig. 3. Process flow – Case III 1 – Ultrafiltration unit; 2 – Antiscalant dosing; 3 – Pressure pump; 4 – 1-pass, 1-stage RO unit; 5 – Concentrate recycle; 6 – Permeate; 7 – Final concentrate.

81.3 % at a final calculated average conductivity of 10 $\mu\text{S}/\text{cm}$, whereas for case study V the values were 84.2 % and 13 $\mu\text{S}/\text{cm}$ respectively. The installation proposed as part of case study V was characterized by the lowest energy consumption (about 606.1 kWh/d) due to the application of pumps with lower power and a higher number of pressure vessels.

However, considering the unsatisfactory quality of the permeate, this processing system is not recommended.

For cases VI and VII, the proposed processing system comprised 2-pass membrane filtration. Case VI encompassed the application of 1-stage reverse osmosis as part of each pass (Fig. 5). Case VII was

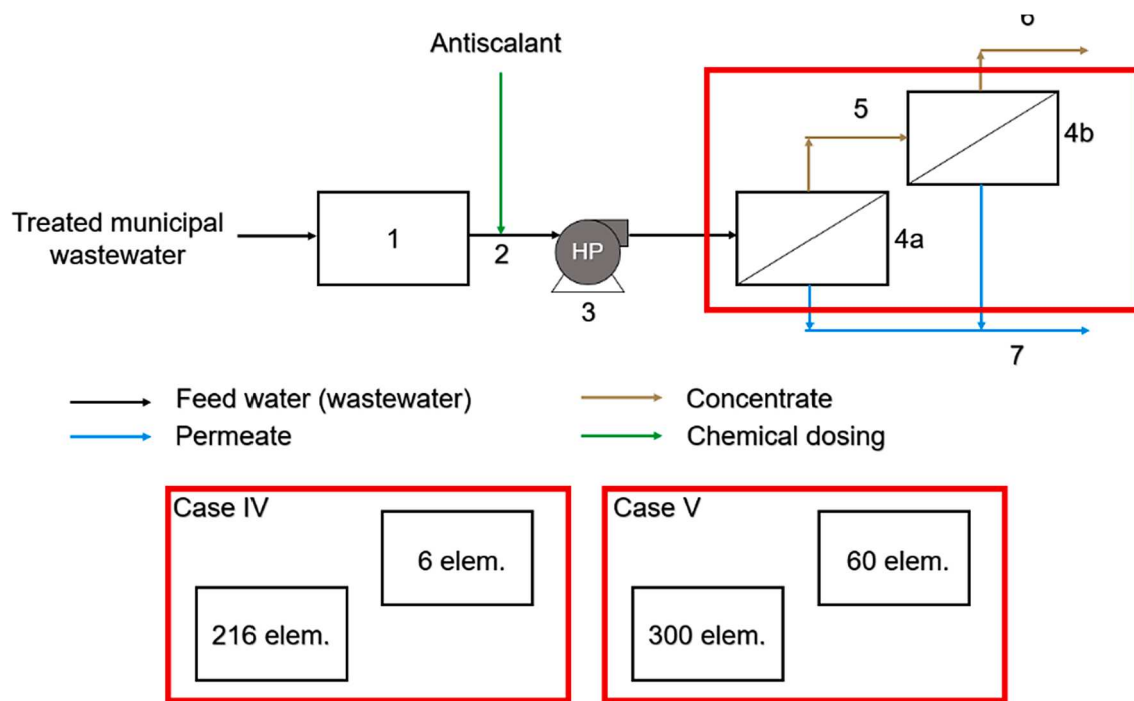


Fig. 4. Process flow – Case IV and Case V 1 – Ultrafiltration unit; 2 – Antiscalant dosing; 3 – Pressure pump; 4a – 1-pass, 1-stage RO unit; 4b – 1-pass, 2-stage RO unit, 5 – Concentrate from 1-stage RO unit; 6 – Final concentrate; 7 – Permeate.

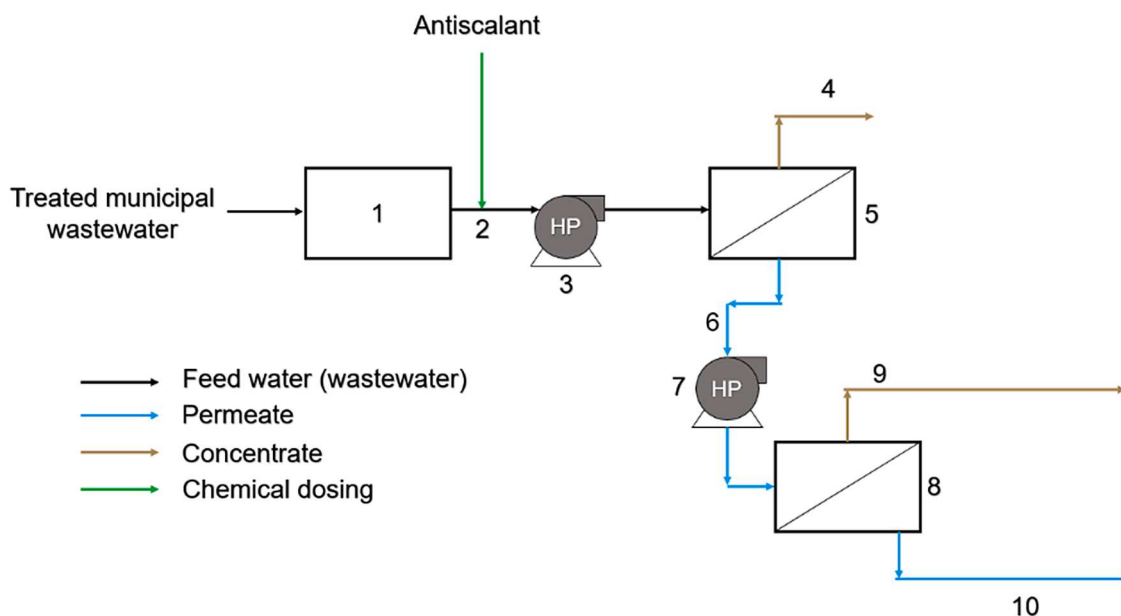


Fig. 5. Process flow – Case VI 1 – Ultrafiltration unit; 2 – Antiscalant dosing; 3, 7 – Pressure pump; 4 – Concentrate from 1-pass, 1-stage RO unit; 5 – 1-pass, 1-stage RO unit; 6 – Permeate from 1-pass, 1-stage RO unit; 8 – 2-pass, 1-stage RO unit; 9 – Concentrate from 2-pass, 1-stage RO unit; 10 – Final permeate.

expanded by 2-stage membrane filtration as part of each 2-pass process (Fig. 6). The net water recovery was similar in both cases and amounted to 68.8–71.8 %. In both cases, the application of 2-pass reverse osmosis made it possible to recover water with an average calculated conductivity of 2 $\mu\text{S}/\text{cm}$. Taking into account the conformity with the design assumptions, cases VI and VII are the recommended systems for water recovery from the analyzed municipal wastewater.

Fig. 7 shows a compilation of the conductivity of water reclaimed from municipal wastewater treated as part of the analyzed processing systems. The conductivity (an electrical conductivity of water) is defined as the capacity of the water to transmit a flow of electricity (to carry an

electrical current) [71]. The electrical conductivity of water is affected by the presence of ions that carry a negative and positive charge such as chlorides, sulphates, calcium, and magnesium [72]. As can be observed from the presented data, case VI and case VII make it possible to obtain deionized water with parameters fulfilling the requirements for electrolyzer feedstock (water conductivity < 5 $\mu\text{S}/\text{cm}$). The proposed solutions can yield about 100 m^3/h of deionized water with a conductivity of about 2 $\mu\text{S}/\text{cm}$ over 1 h of operation. Obtaining the intended product efficiency requires about 133 to 145 m^3/h of treated municipal wastewater. Low conductivity is important for several reasons. First, the higher the content of undesirable ions, the more the composition of the

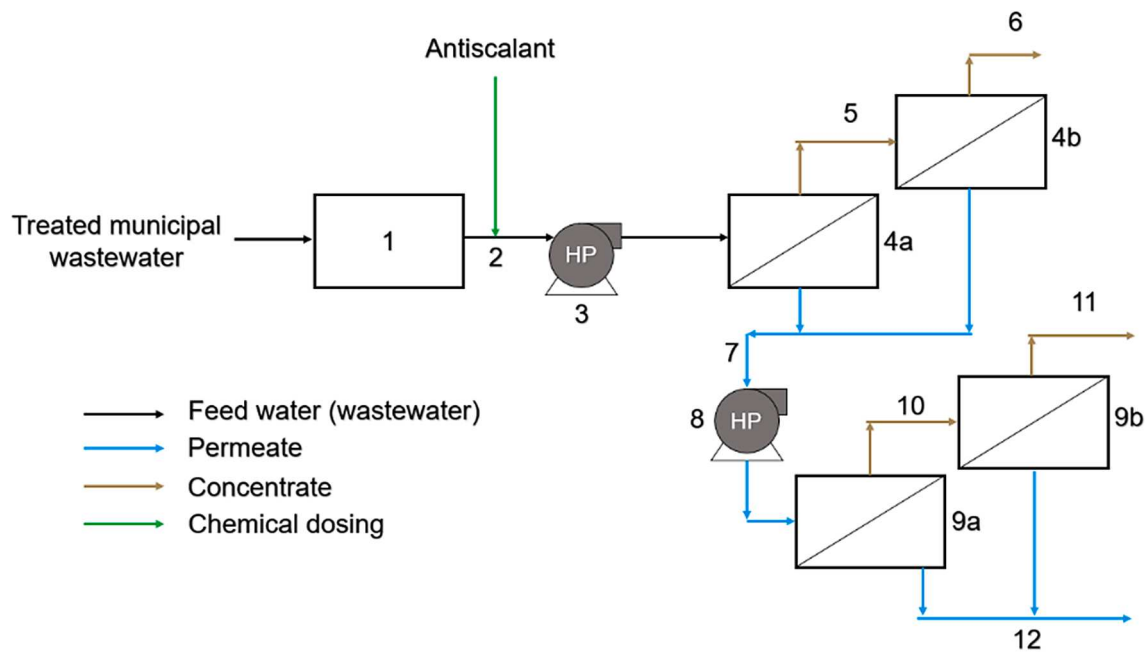


Fig. 6. Process flow – Case VII 1 – Ultrafiltration unit; 2 – Antiscalant dosing; 3, 8 – Pressure pump; 4a – 1-pass, 1-stage RO unit; 4b – 1-pass, 2-stage RO unit; 5 – Concentrate from 1-pass, 1-stage RO unit; 6 – Concentrate from 1-pass, 2-stage RO unit; 7 – Permeate from 1-pass RO units; 9a – 2-pass, 1-stage RO unit; 9b – 2-pass, 2-stage RO unit; 10 – Concentrate from 2-pass, 1-stage RO unit; 11 – Concentrate from 2-pass, 2-stage RO unit; 12 – Final permeate.

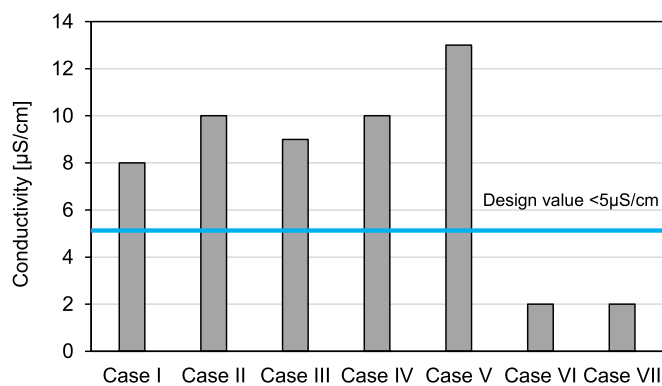


Fig. 7. Summary of conductivity values for each case study.

extracted gas changes. Due to the undesirable components contained in poorly treated water, the composition of the gas is changing. This low conductivity avoids interference of signals by ions in the water. Ions in the feed water can also interact with the electrolyzer material, which can lead to changes in electrical properties and affect results. Since municipal wastewater (even treated wastewater) is a mix of different types of substances, municipal wastewater presents technical and technological

challenges to make it possible to produce ultra-pure hydrogen (purity of $\geq 99.999\%$). Furthermore, maintaining a low conductivity (and thus a low content of undesirable ions) is expected to prevent equipment corrosion and biofouling of the electrolyzer. High water conductivity also has a major impact on the lifetime of the electrolyzer, which can in turn affect hydrogen cost by increasing the annuity of the electrolyser in the cost of hydrogen [73-77].

Table 5 presents a compilation of the analyzed case studies with the most important membrane filtration modeling results obtained. The output filtrate production (water after UF/RO) was set at $100\text{ m}^3/\text{h}$ for all cases. The water recovery rate ranged from about 69 % to up to 81 % at an effluent inflow rate of about $133\text{ m}^3/\text{h}$ to $145\text{ m}^3/\text{h}$, depending on concentrate recirculation. The results obtained based on an analysis of 7 different processing cases studies (ultrafiltration and reverse osmosis) confirmed that the application of 2-pass membrane systems enables the reclamation of water from municipal wastewater that fulfills the requirements concerning the quality of water intended as electrolyzer feedstock, as the obtained water exhibited a conductivity of $< 5\text{ }\mu\text{S}/\text{cm}$. Depending on the analyzed case study, the attainable level of water reclamation ranged from 68.8 to 84.1 % at an energy consumption of $606.1 - 2\text{ }694\text{ kWh}/\text{d}$. The results of this work not only confirm that the selected processing solutions make it possible to reclaim water from municipal wastewater, but also confirm the necessity of using software

Table 5
Specific parameters for the analyzed case studies.

Parameter	Unit	Case I	Case II	Case III	Case IV	Case V	Case VI	Case VII
Feed wastewater	m^3/h	133.3	137	137	133.3	133.3	145.4	145.4
Produced water	m^3/h	100	100	100	100	100	100	100
Recovery	%	75	81.1	75	81.3	84.1	68.8	68.8
Conductivity	$\mu\text{S}/\text{cm}$	8	10	9	10	13	2	2
Permeate TDS	mg/dm^3	4.97	6.34	4.97	5.84	7.77	3.33	3.70
Mg^{2+}	mg/dm^3	0.02	0.02	0.02	0.02	0.02	0.01	0.01
Ca^{2+}	mg/dm^3	0.08	0.10	0.08	0.10	0.12	0.05	0.06
Cl^-	mg/dm^3	0.82	1.06	0.82	0.97	1.33	0.53	0.60
SO_4^{2-}	mg/dm^3	0.08	0.10	0.08	0.09	0.12	0.05	0.06
pH	-	5.8	5.9	5.8	5.9	6.0	5.7	5.7
Energy consumption	kWh/d	929.5	867.7	929.5	858.4	606.1	2694	2569

to simulate the membrane system operation to select the most economic and cost-effective solution. The pH of the demineralized water would also need to be factored in when selecting the appropriate processing system. The reaction of the obtained water did not exceed $\text{pH} = 6$ for all the analyzed cases. After demineralization, the process water should be conditioned according to the electrolyzer manufacturer's specifications and the process water requirements. For example, the pH of the feed water to the HySTAT electrolyzers [78] should be between 5.0 and 7.0 (information obtained from the electrolyzers' supplier), so each of the streams recovered from the wastewater meets this parameter.

Furthermore, defining the optimal processing system should also factor in the risk of membrane scaling. WAVE does not provide a mechanism for estimating the antiscalant efficiency, therefore the choice of both the antiscalant and its dosage as well as its efficiency should be investigated accordingly and determined at the stage of technology selection. As presented above, among the 7 analyzed processing systems, only cases VI and VII exhibit a quality of the reclaimed water compliant with ASTM's requirements. Considering the high efficiency and the expanded processing system structure, energy consumption in these cases is higher compared to the others, but these cases exhibit the best water quality. Both the analyzed cases are characterized by similar power demands, but the energy consumption for case VII is nearly 5 % lower relative to the energy consumption for case VI at almost equivalent reclaimed water quality, therefore case VII appears to be the optimal solution from this perspective. Assuming a water consumption of 15 kg H₂O/ 1 kg H₂ for electrolysis (factoring in water loss for rinsing and cleaning as well as an electrolyzer efficiency of about 60 % [48]), at the adopted installation efficiency, the hydrogen yield over 1 h would equal about 6666 kg H₂.

In the study case appearing as the optimal (case VII), the doubtless advantages of the process include the lack of chemical dosing, since the operation of the system relies only on pressure as the driving force, and the separation takes place at room temperature, with no phase change. The proposed technology can even function as a stand-alone process system, compared, for example, to distillation which is currently not cost-effective due to high energy consumption, when used as a single reclaiming technology. Compared to distillation or evaporation processes, as the methods for wastewater treatment and water reclamation, the proposed technology is highly competitive in terms of electrical consumption (1.07 kWh/m³). Classical distillation or evaporation technologies, in addition to the electrical energy requirements (approx. 0.5 to 5.0 kWh/m³), also involve a thermal energy consumption (approx. 27–83 kWh/m³) [79-81]. Although 2-pass RO is an effective method for water reclamation, as all membrane processes has certain limitations, such as the phenomenon of membrane fouling, which forces the need for frequent membrane flushing or dosing of cleaning chemicals. The RO process also produces an additional stream of waste liquid (concentrate), which must be eliminated. Due to the recovery rate (68–84 %) of water, the RO process also produces an additional stream of waste liquid (concentrate), which must be eliminated.

Compilations of the estimated investment and operating costs are presented in Table 6 and Table 7 respectively. The appropriate indices recommended for flow processes were applied to evaluate the investment and operating costs [82-84]. The data pertains to a processing system with an efficiency of 100 m³/h of the product (water reclaimed from municipal wastewater). Direct costs (D) include the costs of purchasing equipment and machinery (E), as well as instrumentation, control systems, pipelines, electric systems, land improvement, wastewater treatment plant operation adjustments, buildings, maintenance equipment (D1), etc. The costs of equipment and machinery were adopted based on information obtained from suppliers, analyses, and own experience. Indirect costs (I) include aspects such as technical design costs and legal expenses. The economic analysis also encompasses certain risk factors and the costs of unforeseen events. The annual operating costs encompass chemicals, media, manpower, maintenance, and insurance. To calculate the annual costs, the analysis assumed the

Table 6
Estimated capital costs.

Parameter	Factor	Estimated Cost [US\$]
Equipment and devices (E)	-*	650,000
Other capital cost (D1)		
-Electrical	25 % x E	162,500
-Piping	10 % x E	65,000
-Installation	35 % x E	227,500
-Instrumentation and control	15 % x E	97,500
-Land improvement	1 % x E	6,500
-WWTP improvement	50 % x E	325,000
-Building cost	15 % x E	97,500
Other capital cost (D1)		981,500
Total direct cost (D)		1,631,500
Technical design	15 % x D	244,725
Engineering	20 % x D	326,300
Legal expenses	4 % x D	65,260
Total indirect cost (I)		636,285
Direct and indirect cost (D + I)		2,267,785
Contractor fees	5 % x (D + I)	113,389
Unforeseen expenses	10 % x (D + I)	226,779
Total investment cost		2,607,953

* Based on suppliers' information, own analyses and experience from similar implementations.

Table 7
Estimated annual operating costs.

Parameter	Factor	Estimated Cost [US\$/year]
Concentrate disposal	-*	131,900
Electricity	-*	177,217
Chemical dosing	-*	26,285
Workers (W)	2 × 1100 US\$/month	26,400
Insurance	2 % x E (Table 6)	13,000
Maintenance (M)		
-Mechanical	7 % x E (Table 6)	81,575
-Civil	3 % x D	48,945
Supervisor	25 % x W	6,600
Laboratory	10 % x W	2,640
Repairs	40 % x M	52,208
TOTAL OPERATING COSTS		566,769

* Based on WAVE calculations.

employment of 2 workers and an installation operation of about 363 days per year, factoring in technical pauses of about 4 h a month. The total investment costs for an installation with an efficiency of 100 m³/h may amount to an average of about US\$2,206,729. Meanwhile, the costs of operation and maintenance may amount to an average of about US\$536,657, factoring in the costs of concentrate management and disposal after RO.

4. Conclusions

- The paper presented an analysis of selected processing systems comprised of 1- or 2-pass membrane processes (ultrafiltration and reverse osmosis).
- Commercial software for selecting membrane modules, provided by their producers, is very useful in the process of designing the appropriate membrane system. Modeling the membrane filtration process for water reclamation from municipal wastewater to produce water intended as a feedstock for electrolyzers was conducted using the DuPont Water Solutions WAVE software for the actual conditions and parameters of a functioning public utility facility – a wastewater treatment plant with a population equivalent (PE) of > 100,000.
- 7 processing cases for treated municipal wastewater deionization were proposed to use the water as a feedstock for electrolysis, and a computer simulation was carried out to determine the desired conductivity of < 5 μS/cm. It was assumed that the municipal

wastewater pre-treatment installation would comprise the following elements: sieve filtration, ultrafiltration, and reverse osmosis.

- Two of the 7 processing cases made it possible to recover water of the expected quality (case VI and case VII). The obtained data also confirms that the instructions of membrane manufacturers in terms of technology selection were fulfilled. The analyzed 1-pass systems failed to yield water with parameters enabling its use as an electrolyzer feedstock. On the other hand, the analyzed 2-pass systems made it possible to recover water exhibiting a conductivity fulfilling the requirements of ASTM, i.e. water with a conductivity of < 5 µS/cm.
- Both the analyzed cases were characterized by nearly identical compositions of the permeate (water reclaimed from wastewater) and similar demands for electric power, though case VII exhibited a lower energy consumption. From this perspective, case VII was proposed as the recommended solution, though the final choice between cases VI and VII require more in-depth consideration, as the membrane with the highest efficiency also exhibited the highest power demand. In this regard, cost factors play a greater role.
- The work conducted as part of this paper confirmed the possibility of reclaiming water from municipal wastewater. The recovery of water with parameters fulfilling the requirements for electrolyzer feedstock was confirmed based on the modeling results.
- This work confirmed the necessity of utilizing software to simulate the operation of membrane systems to select the most economic and cost-effective solution.

Funding sources

The presented study was performed as part of the research work of the Central Mining Institute in Poland, with financial support by the Polish Ministry of Science and Higher Education [No. 11131032-340].

CRedit authorship contribution statement

Piotr Zawadzki: Conceptualization, Methodology, Investigation, Writing – original draft, Software, Data curation. **Beata Kończak:** Conceptualization, Methodology, Supervision, Writing – review & editing. **Adam Smoliński:** Conceptualization, Methodology, Supervision, Writing – review & editing.

Declaration of Competing Interest

The authors declare that they have no known competing financial interests or personal relationships that could have appeared to influence the work reported in this paper.

Data availability

Data will be made available on request.

References

- [1] K. Makanda, S. Nzama, T. Kanyerere, Assessing the Role of Water Resources Protection Practice for Sustainable Water Resources Management: A Review, *Water* 14 (19) (2022) 3153, <https://doi.org/10.3390/w14193153>.
- [2] Z. Karimidastenaie, T. Avellan, M. Sadegh, B. Kløve, A.T. Haghghi, Unconventional Water Resources: Global Opportunities and Challenges, *Sci. Total Environ.* 827 (2022), 154429, <https://doi.org/10.1016/j.scitotenv.2022.154429>.
- [3] F.-Z. Lahlou, H.R. Mackey, T. Al-Ansari, Role of Wastewater in Achieving Carbon and Water Neutral Agricultural Production, *J. Clean. Prod.* 339 (2022), 130706, <https://doi.org/10.1016/j.jclepro.2022.130706>.
- [4] X. Wei, K.T. Sanders, A.E. Childress, Reclaiming Wastewater with Increasing Salinity for Potable Water Reuse: Water Recovery and Energy Consumption during Reverse Osmosis Desalination, *Desalination* 520 (2021), 115316, <https://doi.org/10.1016/j.desal.2021.115316>.
- [5] L. Gurreri, A. Tamburini, A. Cipollina, G. Micale, Electrodialysis Applications in Wastewater Treatment for Environmental Protection and Resources Recovery: A Systematic Review on Progress and Perspectives, *Membranes* 10 (7) (2020) 146, <https://doi.org/10.3390/membranes10070146>.
- [6] P. Zawadzki, Evaluation of TiO₂/UV; O₃/UV, and PDS/Vis for Improving Chlorofenvinphos Removal from Real Municipal Treated Wastewater Effluent, *Int. J. Environ. Sci. Technol.* (2022,) 1–12, <https://doi.org/10.1007/s13762-022-04370-x>.
- [7] P. Zawadzki, Elimination of chlorofenvinphos from treated municipal wastewater in advanced oxidation processes, *Przemysł Chemiczny* T. 100, nr 3 (2021), <https://doi.org/10.15199/62.2021.3.11>.
- [8] *Regulation (EU) 2020/741 of the European Parliament and of the Council of 25 May 2020 on Minimum Requirements for Water Reuse (Text with EEA Relevance)*; 2020; Vol. 177. <http://data.europa.eu/eli/reg/2020/741/oj/eng> (accessed 2022-12-13).
- [9] P. Roccaro, Treatment Processes for Municipal Wastewater Reclamation: The Challenges of Emerging Contaminants and Direct Potable Reuse, *Curr. Opin. Environ. Sci. Health* 2 (2018) 46–54, <https://doi.org/10.1016/j.coesh.2018.02.003>.
- [10] G. Gangaraju, K. Balakrishn, R. Uma, K. Shah, Introduction to Conventional Wastewater Treatment Technologies: Limitations and Recent Advances (2021) 1–36, <https://doi.org/10.21741/9781644901144-1>.
- [11] G. Crini, E. Lichtfouse, Advantages and Disadvantages of Techniques Used for Wastewater Treatment, *Environ. Chem. Lett.* 17 (1) (2019) 145–155, <https://doi.org/10.1007/s10311-018-0785-9>.
- [12] *Northwest Bergen County Utilities Authority - Wastewater Treatment*. <http://nbcua.com/Sections-read-4.html> (accessed 2022-12-03).
- [13] Application For Renewal of NPDES CA0107409 and 301(h) Modified Secondary Treatment Requirements, POINT LOMA OCEAN OUTFALL, Volume IV Appendices A & B, 2015. https://www.sandiego.gov/sites/default/files/ploov04_15.pdf (accessed 2022-12-14).
- [14] M. Bourgin, B. Beck, M. Boehler, E. Borowska, J. Fleiner, E. Salhi, R. Teichler, U. von Gunten, H. Siegrist, C.S. McArdell, Evaluation of a Full-Scale Wastewater Treatment Plant Upgraded with Ozonation and Biological Post-Treatments: Abatement of Micropollutants, Formation of Transformation Products and Oxidation by-Products, *Water Res.* 129 (2018) 486–498, <https://doi.org/10.1016/j.watres.2017.10.036>.
- [15] C.S. McArdell, The First Full-Scale Advanced Ozonation Plant in the Dübendorf WWTP Running; the New Swiss Water Protection Act Approved, *NORMAN Bulletin* (2015) 36–37.
- [16] *The ripple effects of the energy crisis on academia*. <https://doi.org/10.15252/embr.202256287>.
- [17] A. Kiselev, E. Magaril, R. Magaril, D. Panepinto, M. Ravina, M.C. Zanetti, Towards Circular Economy: Evaluation of Sewage Sludge Biogas Solutions, *Resources* 8 (2) (2019) 91, <https://doi.org/10.3390/resources8020091>.
- [18] Making the Breakthrough: Green Hydrogen Policies and Technology Costs.
- [19] J. Gigler, M. Weeda, R. Hoogma, J. de Boer, Hydrogen for the Energy Transition.
- [20] R.W. Howarth, M.Z. Jacobson, How Green Is Blue Hydrogen? *Energy Sci. Eng.* 9 (10) (2021) 1676–1687, <https://doi.org/10.1002/ese3.956>.
- [21] Kędzierski M. Wodór – nadzieja niemieckiej polityki klimatycznej i przemysłowej.
- [22] Path-to-Hydrogen-Competitiveness Full-Study-1.Pdf. https://hydrogencouncil.com/wp-content/uploads/2020/01/Path-to-Hydrogen-Competitiveness_Full-Study-1.pdf (accessed 2023-04-05).
- [23] Hydrogen: A Renewable Energy Perspective.
- [24] *The colours of hydrogen explained | Swinburne*. <https://www.swinburne.edu.au/news/2022/05/the-colours-of-hydrogen-explained/> (accessed 2023-04-05).
- [25] A.M. Lopez-Hidalgo, A. Smoliński, A. Sanchez, A Meta-Analysis of Research Trends on Hydrogen Production via Dark Fermentation, *Int. J. Hydrogen Energy* 47 (27) (2022) 13300–13339, <https://doi.org/10.1016/j.ijhydene.2022.02.106>.
- [26] C.L. Alvarez-Guzmán, S. Cisneros-de la Cueva, V.E. Balderas-Hernández, A. Smoliński, A. De León-Rodríguez, Biohydrogen Production from Cheese Whey Powder by Enterobacter Asburiae: Effect of Operating Conditions on Hydrogen Yield and Chemometric Study of the Fermentative Metabolites, *Energy Rep.* 6 (2020) 1170–1180, <https://doi.org/10.1016/j.egyrs.2020.04.038>.
- [27] V.E. Balderas-Hernandez, K.P. Landeros Maldonado, A. Sánchez, A. Smoliński, A. De Leon Rodriguez, Improvement of Hydrogen Production by Metabolic Engineering of Escherichia Coli: Modification on Both the PTS System and Central Carbon Metabolism, *Int. J. Hydrogen Energy* 45 (9) (2020) 5687–5696, <https://doi.org/10.1016/j.ijhydene.2019.01.162>.
- [28] A. Smoliński, N. Howaniec, A. Bał, Utilization of Energy Crops and Sewage Sludge in the Process of Co-Gasification for Sustainable Hydrogen Production, *Energies* 11 (4) (2018) 809, <https://doi.org/10.3390/en11040809>.
- [29] O. Grasham, V. Dupont, T. Cockerill, M.A. Camargo-Valero, M.V. Twigg, Hydrogen via Reforming Aqueous Ammonia and Biomethane Co-Products of Wastewater Treatment: Environmental and Economic Sustainability, *Sustainable Energy Fuels* 4 (11) (2020) 5835–5850, <https://doi.org/10.1039/D0SE01335H>.
- [30] S. Rittmann, C. Herwig, A Comprehensive and Quantitative Review of Dark Fermentative Biohydrogen Production, *Microb. Cell Fact.* 11 (1) (2012) 115, <https://doi.org/10.1186/1475-2859-11-115>.
- [31] Y. Liu, R. Lin, Y. Man, J. Ren, Recent Developments of Hydrogen Production from Sewage Sludge by Biological and Thermochemical Process, *Int. J. Hydrogen Energy* 44 (36) (2019) 19676–19697, <https://doi.org/10.1016/j.ijhydene.2019.06.044>.
- [32] A. Domínguez, J.A. Menéndez, J.J. Pis, Hydrogen Rich Fuel Gas Production from the Pyrolysis of Wet Sewage Sludge at High Temperature, *J. Anal. Appl. Pyrol.* 77 (2) (2006) 127–132, <https://doi.org/10.1016/j.jaap.2006.02.003>.
- [33] P. Nikolaidis, A. Poullikkas, A Comparative Overview of Hydrogen Production Processes, *Renew. Sustain. Energy Rev.* 67 (2017) 597–611, <https://doi.org/10.1016/j.rser.2016.09.044>.
- [34] E. Koutra, P. Tsafarakidou, M. Sakarika, M. Kornaros, Chapter 11 - Microalgal Biorefinery. In *Microalgae Cultivation for Biofuels Production*; Yousef, A., Ed.;

- Academic Press, 2020; pp 163–185. <https://doi.org/10.1016/B978-0-12-817536-1.00011-4>.
- [35] D. Ucar, Y. Zhang, I. Angelidaki, An Overview of Electron Acceptors in Microbial Fuel Cells, *Front. Microbiol.* 8 (2017).
- [36] O. Schmidt, A. Gambhir, I. Staffell, A. Hawkes, J. Nelson, S. Few, Future Cost and Performance of Water Electrolysis: An Expert Elicitation Study, *Int. J. Hydrogen Energy* 42 (52) (2017) 30470–30492, <https://doi.org/10.1016/j.ijhydene.2017.10.045>.
- [37] S.M. Saba, M. Müller, M. Robinius, D. Stolten, The Investment Costs of Electrolysis – A Comparison of Cost Studies from the Past 30 Years, *Int. J. Hydrogen Energy* 43 (3) (2018) 1209–1223, <https://doi.org/10.1016/j.ijhydene.2017.11.115>.
- [38] G. Bristowe, A. Smallbone, The Key Techno-Economic and Manufacturing Drivers for Reducing the Cost of Power-to-Gas and a Hydrogen-Enabled Energy System, *Hydrogen* 2 (3) (2021) 273–300, <https://doi.org/10.3390/hydrogen2030015>.
- [39] COMMUNICATION FROM THE COMMISSION TO THE EUROPEAN PARLIAMENT, THE COUNCIL, THE EUROPEAN ECONOMIC AND SOCIAL COMMITTEE AND THE COMMITTEE OF THE REGIONS A Hydrogen Strategy for a Climate-Neutral Europe; 2020. <https://eur-lex.europa.eu/legal-content/EN/TXT/?uri=CELEX:52020DC0301> (accessed 2022-12-09).
- [40] A. Smoliński, N. Howaniec, Hydrogen Energy, Electrolyzers and Fuel Cells – The Future of Modern Energy Sector, *Int. J. Hydrogen Energy* 45 (9) (2020) 5607, <https://doi.org/10.1016/j.ijhydene.2019.11.076>.
- [41] A. Smoliński, K. Wojtacha-Rychter, M. Król, M. Magdziarczyk, J. Polański, N. Howaniec, Co-Gasification of Refuse-Derived Fuels and Bituminous Coal with Oxygen/Steam Blend to Hydrogen Rich Gas, *Energy* 254 (2022), 124210, <https://doi.org/10.1016/j.energy.2022.124210>.
- [42] P.J. Megía, A.J. Vizcaíno, J.A. Calles, A. Carrero, Hydrogen Production Technologies: From Fossil Fuels toward Renewable Sources. A Mini Review, *Energy Fuels* 35 (20) (2021) 16403–16415, <https://doi.org/10.1021/acs.energyfuels.1c02501>.
- [43] R. Pinsky, P. Sabharwal, J. Hartvigsen, J. O'Brien, Comparative Review of Hydrogen Production Technologies for Nuclear Hybrid Energy Systems, *Prog. Nucl. Energy* 123 (2020), 103317, <https://doi.org/10.1016/j.pnucene.2020.103317>.
- [44] K. Zeng, D. Zhang, Recent Progress in Alkaline Water Electrolysis for Hydrogen Production and Applications, *Prog. Energy Combust. Sci.* 36 (3) (2010) 307–326, <https://doi.org/10.1016/j.pecs.2009.11.002>.
- [45] D.S. Falção, A.M.F.R. Pinto, A Review on PEM Electrolyzer Modelling: Guidelines for Beginners, *J. Clean. Prod.* 261 (2020), 121184, <https://doi.org/10.1016/j.jclepro.2020.121184>.
- [46] M. David, C. Ocampo-Martínez, R. Sánchez-Peña, Advances in Alkaline Water Electrolyzers: A Review, *J. Storage Mater.* 23 (2019) 392–403, <https://doi.org/10.1016/j.est.2019.03.001>.
- [47] Staff, G. *Hydrogen A to Z Series: P for Purity*. Gen H2 Discover Hydrogen. <https://genh2hydrogen.com/hydrogen-a-to-z-series-p-for-purity/> (accessed 2022-12-06).
- [48] M. Newborough, Cooley, G. Green Hydrogen: Water Use Implications and Opportunities. *Fuel Cells Bulletin* 2021, 4.
- [49] S.G. Simoes, J. Catarino, A. Picado, T.F. Lopes, S. di Berardino, F. Amorim, F. Gírio, C.M. Rangel, T. Ponce de Leão, Water Availability and Water Usage Solutions for Electrolysis in Hydrogen Production, *J. Clean. Prod.* 315 (2021), 128124, <https://doi.org/10.1016/j.jclepro.2021.128124>.
- [50] M. Ball, M. Weeda, 11 - The Hydrogen Economy—Vision or Reality? In *Compendium of Hydrogen Energy*; Ball, M., Basile, A., Veziroglu, T. N., Eds.; Woodhead Publishing Series in Energy; Woodhead Publishing: Oxford, 2016; pp 237–266. <https://doi.org/10.1016/B978-1-78242-364-5.00011-7>.
- [51] M. Ni, D.Y.C. Leung, M.K.H. Leung, K. Sumathy, An Overview of Hydrogen Production from Biomass, *Fuel Process. Technol.* 87 (5) (2006) 461–472, <https://doi.org/10.1016/j.fuproc.2005.11.003>.
- [52] E. Gasafi, M.-Y. Reinecke, A. Kruse, L. Schebek, Economic Analysis of Sewage Sludge Gasification in Supercritical Water for Hydrogen Production, *Biomass Bioenergy* 32 (12) (2008) 1085–1096, <https://doi.org/10.1016/j.biombioe.2008.02.021>.
- [53] L.R. Winter, N.J. Cooper, B. Lee, S.K. Patel, L. Wang, M. Elimelech, Mining Nontraditional Water Sources for a Distributed Hydrogen Economy, *Environ. Sci. Tech.* 56 (15) (2022) 10577, <https://doi.org/10.1021/acs.est.2c02439>.
- [54] ISO 5667-3:2018 Water quality — Sampling — Part 3: Preservation and handling of water samples. ISO. <https://www.iso.org/standard/72370.html> (accessed 2022-12-08).
- [55] ISO 5667-10:2020 Water quality — Sampling — Part 10: Guidance on sampling of waste water. ISO. <https://www.iso.org/standard/70934.html> (accessed 2022-12-08).
- [56] Standard Specification for Reagent Water. <https://www.astm.org/d1193-06r18.html> (accessed 2022-12-06).
- [57] Process water production - Lenntech. <https://www.lenntech.pl/process-water.htm> (accessed 2022-12-08).
- [58] Mixed bed ion exchange demineralisation plants- Lenntech. <https://www.lenntech.com/applications/ultrapure/mixed/mixed-bed-plants.htm> (accessed 2022-12-08).
- [59] E. Obotey Ezugbe, S. Rathilal, Membrane Technologies in Wastewater Treatment: A Review, *Membranes* 10 (5) (2020) 89, <https://doi.org/10.3390/membranes10050089>.
- [60] K.N. Bourgeois, J.L. Darby, G. Tchobanoglous, Ultrafiltration of Wastewater: Effects of Particles, Mode of Operation, and Backwash Effectiveness, *Water Res* 35 (1) (2001) 77–90, [https://doi.org/10.1016/S0043-1354\(00\)00225-6](https://doi.org/10.1016/S0043-1354(00)00225-6).
- [61] D. Falsanisi, L. Liberti, M. Notarnicola, Ultrafiltration (UF) Pilot Plant for Municipal Wastewater Reuse in Agriculture: Impact of the Operation Mode on Process Performance, *Water* 2 (4) (2010) 872–885, <https://doi.org/10.3390/w2040872>.
- [62] E. Obotey Ezugbe, S. Rathilal, Membrane Technologies in Wastewater Treatment: A Review, *Membranes* 10 (5) (2020) 89, <https://doi.org/10.3390/membranes10050089>.
- [63] P. Moradiahamedani, Recent Advances in Dye Removal from Wastewater by Membrane Technology: A Review, *Polym. Bull.* 79 (4) (2022) 2603–2631, <https://doi.org/10.1007/s00289-021-03603-2>.
- [64] D. Escarabajal-Henarejos, D. Parras-Burgos, L. Ávila-Dávila, F.J. Cánovas-Rodríguez, J.M. Molina-Martínez, Study of the Influence of Temperature on Boron Concentration Estimation in Desalinated Seawater for Agricultural Irrigation, *Water* 13 (3) (2021) 322, <https://doi.org/10.3390/w13030322>.
- [65] Dupont. WAVE (Water Application Value Engine). Wave Software For Water Treatment Plant Design. <https://www.dupont.com/Wave/Default.htm> (accessed 2022-12-13).
- [66] H. Xu, K. Xiao, J. Yu, B. Huang, X. Wang, S. Liang, C. Wei, X. Wen, X. Huang, A Simple Method to Identify the Dominant Fouling Mechanisms during Membrane Filtration Based on Piecewise Multiple Linear Regression, *Membranes* (Basel) 10 (8) (2020) 171, <https://doi.org/10.3390/membranes10080171>.
- [67] J. Zhou, N. Gao, G. Peng, Y. Deng, Pilot Study of Ultrafiltration-Nanofiltration Process for the Treatment of Raw Water from Huangpu River in China, *J. Water Resour. Prot.* 1 (3) (2009) 203–209, <https://doi.org/10.4236/jwarp.2009.13025>.
- [68] DOW FILMTEC SFP-2880 Ultrafiltration Modules. Pure Aqua. Inc. <https://pureaqua.com/dow-filmtec-sfp-2880-ultrafiltration-modules/> (accessed 2023-04-06).
- [69] Filmtec Membranes SW30XLE-400i (219219). <https://www.lenntech.pl/produkty/filmtec-membranes/219219/SW30XLE-400i/index.html> (accessed 2023-04-06).
- [70] I.G. Wenten, MEMBRANE IN WATER AND WASTEWATER TREATMENT; 2008.
- [71] electrical conductivity: Water Dictionary: Water Information: Bureau of Meteorology. <http://www.bom.gov.au/water/awid/id-867.shtml> (accessed 2023-04-06).
- [72] 5.9 Conductivity | Monitoring & Assessment | US EPA. <https://archive.epa.gov/water/archive/web/html/vms59.html> (accessed 2023-04-06).
- [73] Application Of Deionized Water In Hydrogen Production Equipment - News. Cockerill Jingli Hydrogen. <https://www.jinglihydrogen.com/news/application-of-deionized-water-in-hydrogen-pro-32479464.html> (accessed 2023-04-06).
- [74] Deionised Water: it's purity and production process | ELGA LabWater. <https://www.elgalabwater.com/blog/deionisation-of-water> (accessed 2023-04-06).
- [75] Analysis of Hydrogen Production in Alkaline Electrolyzers | Journal of Power Technologies. <https://papers.itc.pw.edu.pl/index.php/JPT/article/view/888> (accessed 2023-04-06).
- [76] Matošec, M. Water treatment for green hydrogen: what you need to know. Hydrogen Tech World.com. <https://hydrogentechworld.com/water-treatment-for-green-hydrogen-what-you-need-to-know> (accessed 2023-04-06).
- [77] Green Hydrogen Cost Reduction: Scaling up Electrolysers to Meet the 1.5C Climate Goal.
- [78] Intech | Hydrogen Technology | Products | Hydrogen Generators. <http://www.intech.eu/en/hydrogen-technology/products/hydrogen-generators> (accessed 2023-04-06).
- [79] A. Deshmukh, C. Boo, V. Karanikola, S. Lin, A.P. Straub, T. Tong, D.M. Warsinger, M. Elimelech, Membrane Distillation at the Water-Energy Nexus: Limits, Opportunities, and Challenges, *Energy Environ. Sci.* 11 (5) (2018) 1177–1196, <https://doi.org/10.1039/C8EE00291F>.
- [80] F. Macedonio, E. Curcio, E. Drioli, Integrated Membrane Systems for Seawater Desalination: Energetic and Exergetic Analysis, Economic Evaluation, Experimental Study. *Desalination* 203 (1) (2007) 260–276, <https://doi.org/10.1016/j.desal.2006.02.021>.
- [81] Y. Ghalavand, M.S. Hatampour, A. Rahimi, A Review on Energy Consumption of Desalination Processes, *Desalin. Water Treat.* 54 (6) (2015) 1526–1541, <https://doi.org/10.1080/19443994.2014.892837>.
- [82] The University of Oklahoma. Capital investments and operational costs. <https://www.ou.edu/class/che-design/design1/cost-est.htm> (accessed 2022-12-13).
- [83] M.R. Shabani, R.B. Yekta, Suitable Method for Capital Cost Estimation in Chemical Processes Industries, *Cost Engineering (Morgantown, West Virginia)* 48 (2006) 22–25.
- [84] Max. S. Peters, K. D. Timmerhaus, *Plant Design and Economics for Chemical Engineers*, fourth edition.; McGraw-Hill Book Co: Singapore, 2003.